Author:
Fagnano, Marco

Title:
Development of a new microRNA-functionalized composite scaffold as a valve substitute

Author:
Fagnano, Marco

Title:
DEVELOPMENT OF A NEW MICRORNA-FUNCTIONALIZED COMPOSITE SCAFFOLD AS A VALVE SUBSTITUTE

DEVELOPMENT OF A NEW

MICRORNA-FUNCTIONALIZED COMPOSITE

SCAFFOLD AS A VALVE SUBSTITUTE

MARCO FAGNANO

A dissertation submitted to the University of Bristol in accordance with the requirements for award of the degree of Philosophiae Doctor in the Department of Translational Health Sciences, Bristol Medical School, Bristol

May 2021

59,988 words

ABSTRACT

Heart valve disease (HVD) is a growing medical issue in western countries. The majority of HVD is of degenerative etiology, the incidence of which increases along with the increase of life expectancy. When the valve function is impaired, the best solution is the implantation of either a biological or a mechanical prosthesis. Current biological prostheses have limited durability, due to degeneration, and calcification risk. The mechanical prostheses bear the risk of thromboembolism or bleeding due to the mandatory anticoagulation therapy.

Tissue engineering research aims to regenerate a native-like valve through a path in which exogenous material and self-generated tissues are progressively integrated. Eventually, the exogenous material will be completely degraded leaving a working valve made of autologous tissues only. The current challenges of this approach are the long-term duration due to leaflet retraction and general degeneration, and the formation of a complete endothelial lining in the shortest possible time.

This project aims to create a microRNA-functionalized scaffold as a potential heart valve substitute through the following steps: i) the selection of a microRNA-vector able to transfect endothelial cells (ECs) and allow the microRNA to regulate cells' gene expression, without causing toxic or immune reactions; the vector should also withstand the scaffold production process; ii) the investigation of the pro-endothelialization potential of the microRNA hsa-miR-132-3p; iii) the design and fabrication of a scaffold that can locally administer microRNA for a prolonged time, and substitute valve function until the new tissue will be mature enough to take on its duty.

Eventually, this project achieved several objectives. A lipid-based vector that can regulate ECs expression was chosen. A scaffold able to release microRNA for up to 18 days was fabricated. Also, the pro-endothelialization potential of hsa-miR-132-3p on aortic ECs was verified. Finally, aortic ECs seeded on the microRNA-functionalized scaffold were transfected for up to 6 days. The evidence shown in this thesis is a first step towards the development of the new generation of tissue-engineered heart valves that could be successful in clinical practice.

DEDICATIONS AND ACKNOWLEDGMENTS

I have a huge debt of gratitude to Prof Paolo Madeddu and Prof Gianni Angelini for having believed (more than myself) that I could carry out a Ph.D. project. During these years, I never felt a lack of support from both of them, and I still have to fully realize how much they have done for my personal and professional growth. The passion and commitment they keep putting into research are still unparalleled.

I want to thank Eva for her guidance through a world that I knew nothing about, and also for my emotional education, it may come in handy in the remote future. Since I arrived in Bristol, Michele has been always present, and he is still there ready to push me back on track every time I go sideways (honestly I would have given up long ago).

It may sound obvious, but the whole research group I am proud to be part of is something very close to a family, as well as the entire Research Floor. I would have never survived here without your help! A lot of you will never read this, mainly because you are spread in every continent of the world, but you are more meaningful than you may think to me.

Special thanks to Alessia and Michele from my family. They are really grateful that you allowed my stomach to take a break from can food once a week.

All the friends here in Bristol can claim part of this work is theirs. A simple chat in stressful moments meant a huge help to carry on with this.

Honestly, I do not what to say to my family. I know very well I left you in the worst time, but I want to believe I helped you a bit not being an additional burden myself. I hope this achievement will make you think that all the sacrifices you have done had brought something.

Well, this is it! I am sure I forgot somebody and I apologize in advance for that! After 60000 words, I feel like my fingers are dislocating, so I am going to stop it here!

Thanks!!!

AUTHOR'S DECLARATION

I declare that the work in this dissertation was carried out in accordance with the requirements of the University's Regulations and Code of Practice for Research Degree Programmes and that it has not been submitted for any other academic award. Except where indicated by specific reference in the text, the work is the candidate's own work. Work done in collaboration with, or with the assistance of, others, is indicated as such. Any views expressed in the dissertation are those of the author.

SIGNED: DATE:

PLAGIARISM DECLARATION

I declare that some of the text used in this thesis has been taken from the published review "**Jover, E**. et al. 2018. *Cell Sources for Tissue Engineering Strategies to Treat Calcific Valve Disease.* Frontiers in cardiovascular medicine 5 (155)" in which I contributed, and I declare that the text utilized was written by myself.
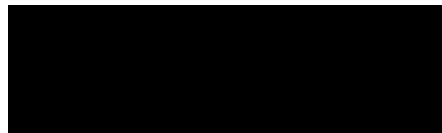
SIGNED BY FIRST AUTHORS: DATE: 31.05.2021

SIGNED BY SENIOR AUTHOR: DATE: 31.05.2021

TABLE OF CONTENTS

LIST OF FIGURES

LIST OF TABLES

LIST OF ABBREVIATION

A

AVR   Aortic Valve Replacement

AR   Aortic Regurgitation

APC   Adventitial Progenitor Cell

C

CAVD   Calcific Aortic Valve Disease

CBR   Cibacron Brilliant Red

CDKN1A   Cyclin-Dependent Kinase Inhibitor 1A

cDNA   Complementary DNA

CT   Cycle Threshold

CTAB   Cetyltrimethylammonium Bromide

$CuSO_4$ Copper sulfate

Cy5   Cyanine 5

D

Da   Dalton

DAPI   4', 6-Diamidino-2-Phenylindole, Dihydrochloride

DCM   Dichloromethane

DD   Degree of deacetylation

DLS   Dynamic Light Scattering

DMF   Dimethylformamide

DMSO   Dimethyl sulfoxide

DNA   Doxyribonucleic Acid

DOTAP   dioleoyltrimethylammoniumpropane

dNTPs   Deoxyribonucleotides Triphosphate

E

EA.hy926   Human Umbilical Vein Cell Line

EC	Endothelial Cell
ECM	Extracellular Matrix
EDTA	Ethylenediaminetetraacetic Acid
EDS	Energy Dispersive Spectroscopy
EdU	5-Ethynyl-2´-Deoxyuridine
EGM MV2	Endothelial Cell Growth Medium MV2
EMT	Endothelial to mesenchymal transition
EthD-III	Ethidium homodimer III

F

FBS	Fetal Bovine Serum
FITC	Fluorescein Isothiocyanate

G

GL	Gelatin
GPTMS	γ-Glycidoxypropyltrimethoxysilane

H

H_2SO_4	Sulfuric acid
HA	Hyaluronic Acid
HAoECs	Human Aortic Endothelial Cells
HCl	Hydrochloric Acid
HMSCs	Human mesenchymal stem cells
HVD	Heart Valve Disease
HUVECs	Human Umbilical Vein Endothelial Cells

I

IF	Immunofluorescence

K

kV	kilo Volt
kDa	kilo Dalton

L

LDH	Lactate Dehydrogenase
Lipofectamine	Lipofectamine RNAiMAX

M

miRNA	MicroRNA
MMP	Metalloproteinase
mRNA	Messenger RNA
Mw	Molecular Weight
MWCO	Molecular Weight Cut Off

N

NaCl	Sodium Chloride
ncRNA	non-coding RNA
NMP	N-Methylpyrrolidone
NO	Nitric Oxide
NP	Nanoparticle

P

PCL	Polycaprolactone
PEG	Poly(ethylene glycol)
PEI	Polyethylenimine
PEI-g-PEG	PEI-grafted PEG
PEUU	Poly(ester urethane) urea
PFA	Paraformaldehyde
PGA	Polyglycolic acid
PGS	Poly(glycerol sebacate)
PLA	Polylactic acid
PLLA	Poly L-lactic acid
PLGA	Poly(lactic-co-glycolic acid)
PP	Polypropylene
PTFE	Polytetrafluoroethylene
PVA	Polyvinyl Alcohol
PVP	Polyvinylpyrrolidone

PU	Polyurethane

R

RASA1	RAS p21 protein activator 1
RB1	RB transcriptional corepressor 1
REDV	Arg-Glu-Asp-Val
RFU	Relative fluorescence units
RISC	RNA-induced silencing complex
RM	Regenerative Medicine
RNA	Ribonucleic acid
RGD	Arginine-Glycine-Aspartic Acid
RT	Room Temperature
RT-qPCR	Quantitative Reverse Transcription Polymerase Chain Reaction

S

s	seconds
SEM	Scanning Electron Microscope
SMC	Smooth muscle cell
SPRED1	Sprouty-related EVH1 domain containing 1
S/TEM	Scanning Transmission Electron Microscope

T

TE	Tissue Engineering
TEHV	Tissue Engineered Heart Valve
TFE	2,2,2-trifluoroethanol
TEM	Transmission Electron Microscope
TMC	Trimethyl Chitosan
TPP	Tripolyphosphate
TPU	Thermoplastic polyurethane

U

U	Units
UBC	Ubiquitin C
UTR	Untranslated region

V

VEC	Valvular Endothelial Cells
VIC	Valvular Interstitial cell
VHD	Valvular Heart Disease

X

xg	multiples of gravity force

1 Introduction

1.1 The aortic valve disease

Heart valve disease (HVD), also known as valvular heart disease (VHD), has several etiologies, the prevalence of which can be correlated with the country's economic status. In low-income countries, rheumatic heart disease is the major cause of HVD, whereas in the so-called "developed countries" the majority of HVDs are of degenerative etiology, which is ultimately correlated to the increase in life expectancy. Infants and children are mainly subjected to congenital malformation-derived HVD, whereas older people have structural valve degeneration and calcification.

Here are the main categories of HVD:

- Chronic rheumatic heart disease is thought to be the outcome of repeated episodes of secondary infections originating from acute rheumatic fever. Eventually, the repetition of infectious events will lead to self-sustaining valve inflammation and valve fibrosis. Globally, mortality from rheumatic heart disease is hard to calculate, as data originate from countries where healthcare statistics practice is not well established. However, it is clear that low-income countries and low-income communities within high-income countries have the highest incidence. Rheumatic heart disease incidence is reducing along with global improvement in healthcare access. The cost of an aortic valve replacement (AVR) procedure (around $8.6 million for AVR required due to rheumatic conditions in New Zealand [1]) is hardly affordable in low-income countries. Therefore, preventive strategies to decrease bacterial infections represent a preferable strategy, with promising results already evident [2].

- Calcific aortic valve disease (CAVD) evolves from aortic sclerosis without functional impairment to severe stenosis. Severe aortic stenosis is usually an indication for surgical valve replacement, even in patients with high surgical risk, since hardly any medical therapy gives comparable life expectancy [3]. Medically treated patients with severe symptomatic AS have a mortality rate of 50% at 1 year. Calcification begins to nucleate at the base of the leaflet and then it gradually grows towards the valve orifice. The final stage of this degenerative condition is calcific AS, which causes severe blood flow restriction, risk of congestive heart failure, and sudden cardiac death. CAVD is the second most prevalent indication for heart surgery in North America. CAVD of anatomically normal valves is a slow and active process leading to degeneration and dysfunction, with a long preclinical and

asymptomatic phase. The onset of symptomatology is a general sign of advanced and severe disease associated with a high event rate, rapid valve deterioration, and malfunctioning, thus being a poor prognostic indicator.

- Congenital aortic valve stenosis is a rare form of aortic disease. Re-operation is a major issue for children with Congenital aortic valve stenosis since current prostheses are not able to grow accordingly to the natural development of pediatric patients.

- Some pharmacological and radiological treatments carry side effects on valve tissues. Pharmacological treatments for Parkinson's disease, migraine, obesity, and other disorders can induce leaflet thickening, increase in extracellular matrix (ECM) synthesis, and proliferation of myofibroblasts and smooth muscle cells (SMCs), which causes regurgitation [4].

1.1.1 Epidemiology of aortic valve disease

Degenerative VHD is a rising issue in western countries. Moderate to severe VHD affects 2.5% of the US adult population, with prevalence increasing with age – some 13% of people born before 1943 suffer from VHD [5], [6]. Aortic VHD affects 2% of people over 65 and it is the most frequent valve disease referred to hospitals [7]. In 2017, non-rheumatic VHDs were accounted as the underlying cause of 24,811 deaths by the American Centre for Disease Control and Prevention. In most cases – 61%, the aortic valve was affected [8]. In the largest UK community study conducted between 2001 and 2011, 37% of more than 70,000 suspected heart failure patients were diagnosed with mild valve pathology, whereas 14.1% suffered from moderate to severe VHD. 36.2% of all VHDs were affecting the aortic valve [9]. Moreover, VHD was detected in 51% of 2,500 people over 65 without any VHD, 12.5% of which were clinically significant. Among VHDs, the study highlighted that CAVD was the most frequent one. The fact that almost one in two people over 65 bears asymptomatic VHD suggests that valve degeneration is one of the several deteriorating processes which occurs with ageing, and that goes along with increasing prevalence in older cohorts [10]. Indeed, a Finnish study showed that aortic valve calcification has a 28% incidence in the 55-71 years cohort, which increased to 48%, 55%, and 75% in the 75-76, 80-81, and 85-86 age groups, respectively [11]. VHD is predicted to become a new cardiovascular epidemic in the next 20 years because of the increase in life expectancy in industrialized nations [12].

VHD is not only a health issue but also a not-negligible economic challenge to our healthcare systems' sustainability. The overall economic burden over EU healthcare systems of

cardiovascular disease, of which VHD is a fraction, was estimated to be €105 billion in 2009, in addition to €64 billion due to productivity loss and informal care [13]. In line with the life expectancy increase in developed countries, the economic cost of cardiovascular disease in the EU is constantly rising, and it reached €111 billion in healthcare costs, with an additional €99 billion considering productivity loss and informal care costs in 2015 [14].

1.1.2 Trends in aortic valve replacement

Patients with severe aortic stenosis have a one-year mortality rate between 30% and 50% [15]–[17]. The prognosis is less severe in the case of aortic regurgitation (AR): the mortality due to cardiac failure is 18% and 27% at 5 and 10 years, respectively [18]. As for aortic stenosis, AR has an increasing impact on life expectancy as the disease severity raises [19]. Given the grim prognosis of patients treated with conservative therapy, AVR is preferable as aortic valve function is progressively impaired.

According to the increasing prevalence of VHD, the number of annual AVR is constantly rising. In the USA, Medicare beneficiaries had their AVR rate increasing from 93 in 1999 to 112 per 100,000 person-year in 2011 [20]. The trend is even more impressive considering the period between 2009 and 2015, in which AVR procedures grew from 47.5 to 88.9 per 100,000 Medicare beneficiaries. This is partially due to new surgical procedures – e.g., transcatheter AVR, which made more patients eligible for surgery. These procedures went from 10.7 in 2012 to 41.1 in 2015 per 100,000 Medicare beneficiaries. Transcatheter AVR represents an option for patients whose health is too poor to sustain an open chest surgery [21]. Like in the USA, European countries are tallying growing numbers. Germany sees a yearly surgery increment of 4.5%, with transvascular-transcatheter aortic valve implantation increasing by 21% [22]. In the UK, 5,796 AVRs were carried out in 2015 with a trend of more than 100 additional procedures every year [23].

1.1.3 Aortic Valve replacement benefits patient's life expectancy

The increase in patients' life expectancy confirms AVR is preferable over conservative therapy when possible. As stated in the first paragraph, medically treated patients with severe symptomatic AS have a mortality rate of 50% at 1 year [24]. A 2017 National Institute for Health Research review of long-term AVR outcomes observational studies on almost 50,000 patients showed that 89.7% of people survived for more than 2 years after surgery, 24.7% of which

reached 20 years follow-up. Post-surgical life expectancy is tightly related to the patient's age at surgery. Subjects under 65 years of age had a median survival time of 16 years, which goes down to 6 years for those aged 85 or more. In the UK, the life expectancy of AVR patients aged less than 65 is 16 years as compared with 22.2 years of the general population. Interestingly, the difference between groups decreases as the age cohort increases, to reach the point at which the life expectancy is higher for AVR patients than for the general population: 6 and 3.5 years, respectively, in those aged more than 85 [25]. Reports around Europe confirm these trends. Swedish cardiac centres registered an average of 1.9 years of life expectancy loss for patients who underwent AVR; in particular, the loss was 4.4 years for patients aged 50 or less, and only 0.4 years for those older than 80 years of age [26]. Likewise, a Spanish study confirmed that AVR patients aged 75 or more have their life expectancy restored to the general population levels [27].

The Bristol Heart Institute has conducted a retrospective study on long-term outcomes of 21,515 patients, aged 65 or more, who underwent urgent AVR with or without coronary artery bypass graft between 1996 and 2011. Patients had excellent long-term survival. Indeed, the long-term mortality rate of patients who underwent AVR is comparable with the same age UK population up to eight years after surgery, disregarding subjects who experienced postoperative complications. Unfortunately, after the 8th year from AVR, the patients' mortality became increasingly higher than that of the general UK population [28].

1.2 Current surgical solutions

Current prosthetic solutions belong to two main categories: mechanical and biological. They are by far the most employed prostheses for valve replacement. Autografts and homografts are rarely used, due to insufficient availability of healthy valves and structural degeneration issues. Although AVR has dramatically increased the VHD patients' prognosis, existent devices are far from ideal. A prosthetic valve should feature the following properties:

- non-immunogenic
- non-haemolytic
- non-thrombogenic
- not release any particle
- not absorb any blood element
- non-infections
- non-inflammatory

- non-calcifying

- non-degradable

- grow accordingly to somatic development

- appropriate mechanical properties to withstand the hydrodynamic load (flexibility, durability strength, resistance to cyclic stress) without wearing or collapsing

[29].

1.2.1   Mechanical valves

Mechanical valves were the first aortic prosthesis to be introduced in 1952. Dr. Charles Hufnagel's initial design consisted of a methyl-methacrylate ball entrapped in a metallic cage [30]. The prosthesis was exploiting the drag force of the pressure pattern in the aorta. The methacrylate ball was driven to occlude a prosthesis restriction during the ventricular diastolic phase and pushed away during the systolic phase, allowing blood flow like a native aortic valve. This first attempt proved the correctness of the concept, although thromboembolism issues arose with the prosthesis implantation. Nevertheless, improved survival rates compared to conservative therapy convinced the medical community to embrace the valve replacement approach [31], [32]. From that first model, prostheses' shape and materials have dramatically evolved to improve prosthetic reliability and hemodynamic performance. Device durability was soon achieved, there are countless examples of devices explanted after up to 50-60 years of service without failure [33]–[36]. Even though some designs failed dramatically [37], [38], mechanical valve failure is not considered a major problem nowadays [39]–[41]. Unfortunately, patients receiving a mechanical valve need to take lifelong anticoagulation therapy. Usually, vitamin K antagonists are employed in such therapy [42]. The therapy requires constant coagulation monitoring, especially at the initiation phase, because of the individual's unpredictable response. In addition, there might be interactions with pre-existing pharmacological treatments, dietary restrictions, and allergies [43], [44]. Even when anticoagulation therapy is optimized, problems are not over. Indeed, several episodes of nonadherence to anticoagulant therapy are reported [45]. Most importantly, bleeding is a major side effect of anticoagulant therapy. An optimized anticoagulant therapy balances bleeding and thromboembolism risks but cannot reduce both to zero [42].

Prosthetic materials may have a key role in triggering the coagulation cascade. Blood-material interaction can trigger the intrinsic coagulation pathway beginning with protein absorption, which may create a negative surface. High-molecular-weight kininogen, prekallikrein, and Factor

XII are activated by contact with these negatively charged surfaces. Factor XII is activated by adsorption, and it converts prekallikrein into kallikrein. High-molecular-weight kininogens and kallikrein act as cofactors triggering a cascade of factors conversion which eventually leads to the conversion of prothrombin into thrombin. Thrombin is responsible for the synthesis of fibrin filaments from fibrinogen monomers. Fibrin filaments are then stabilized into an insoluble network by Factor XIII, activated by thrombin as well. The fibrin network will entangle platelets and blood components creating the blood clot [46],[47], [48]. That can lead to prosthetic valve thrombosis or systemic embolization [49]. The introduction of pyrolytic carbon was a considerable leap in the development of non-thrombolytic surfaces [50], [51]. Pyrolytic carbon shows low plasma protein absorption and weak platelet activation [52], even if not negligible [53]. Notably interesting is the case of Omni series valves (Medical Incorporated. USA). These mechanical valves have the same design but different fabrication materials. Omnicarbon is entirely made of pyrolytic carbon, whereas Omniscience has a titanium housing. Using similar anticoagulation management protocols, Omnicarbon valves had 0.5% of thrombolytic events; much less than Omniscience, which registered 1.7% of thrombolytic events [54].

1.2.2 Bioprosthetic valves

Bioprosthetic valves are manufactured from animal tissue sections, usually porcine or bovine, which can be stitched to a frame called stent. Animal-derived tissues are used because of the shortage of human valve substitutes - homografts. Geometrical, nano-structural, and material features of the bioprosthetic valve are similar to the native tissue. Stents are made out of polymers (e.g. polyester) or metals (e.g. titanium) and may be provided with a polymeric coating. If the stent is not added, the valve is called stentless, and it is constituted of animal soft tissue only [55]–[58]. As no rigid frame is implanted, the stentless prosthetic valve can follow the aortic root dilatation and contraction during the cardiac cycle. Thus, the orifice area is bigger, and a lower transvalvular pressure gradient is generated. Additional features are good consistency, reliable suture retention, easy operative handling, off-the-shelf availability, and a favorable microenvironment for cell migration and proliferation [59]. The extent of benefits from stentless valves is still under debate since the valve's performances are also influenced by the surgery type: sub-coronary or full-root replacement [60], [61]. Bioprosthetic valves are extremely appealing because they do not require lifelong anticoagulation therapy [62], reducing the bleeding risk and the activity limitations that come with it. Patients older than 60 years have a bleeding risk seven-fold the younger ones [63]. Therefore, the bleeding risk of bioprosthetic and

mechanical valves is 12% against 41% over 60 years of age [64]. Frequent use of biological prostheses, the introduction of minimally-invasive implantation techniques, and better control of risk factors and complications have considerably improved the clinical outcome of people undergoing AVR [63], [65], [66].

Unfortunately, patients who would benefit more from receiving a bioprosthetic valve than a mechanical one (younger patients with higher life expectancy and more active life) turned out to be the worst candidates to receive it [67]. The younger the patient is, the higher the failure rate, and the sooner the valve fails after implantation [68]–[70]. A major problem comes from animal tissue decellularization, which is done to make animal-derived tissues compatible with human implantation. After decellularization, a crosslinking step is usually needed to provide the prosthesis tissue with higher tensile strength, elasticity, improved non-immunogenicity, and sutures retention. Glutaraldehyde is commonly used as a crosslinking agent to create amine links with nitrogen groups of amino acids of bovine or porcine tissue. However, glutaraldehyde residues on tissue are thought to induce calcification [71]. The previous host's cell debris is also believed to act as calcification trigger points. Calcium deposits enlarge and merge, forming nodules that interfere with the bioprostheses' function. Currently, new anti-calcific treatments are being tested with promising *in-vivo* results [72].

The elimination of valvular interstitial cells (VICs), which synthesize ECM proteins and possess contractile properties, deprives the valves of their unique function in such a mechanically demanding environment and makes prostheses more susceptible to degeneration. Damages accumulate on the ECM and there are no cells available nearby to repair them[73]–[75]. These are the major hurdles along the path to exclusive use of bioprosthetic valves.
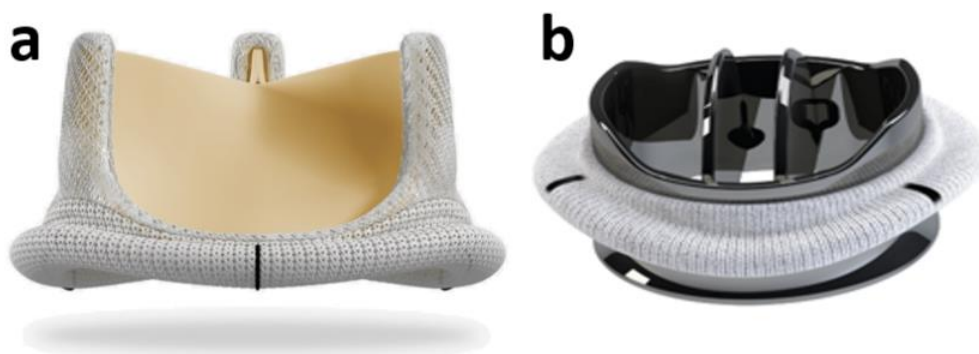
Figure 1-1: Examples of prostheses types employed in current surgical practice
a) Carpentier-Edwards PERIMOUNT Magna Ease Aortic Valve – bovine pericardium derived bioprosthetic valve (https://www.edwards.com/devices/heart-valves/aortic-pericardial/), b) On-X® Aortic Heart Valve – pyrolytic carbon mechanical prosthesis (https://www.cryolife.com/products/on-x-heart-valves/).

1.3 Application of Tissue Engineering to Aortic Valve Replacement

Tissue Engineered Heart Valves (TEHVs) have emerged as a valuable alternative for the definitive treatment of VHD. They promise to overcome both the need for chronic oral anticoagulation and the time-dependent deterioration of mechanical or biological prostheses, respectively. TEHVs would also be capable of growing and repairing themselves in a "physiologic-like" manner [76], [77]. Currently, only autografts may provide such features – e.g., the Ross procedure. However, the Ross procedure introduces a VHD, since the pulmonary valve must be replaced, and, usually, the replacement is not optimal [78]. Moreover, the pulmonary valve implanted into the aortic position must withstand the systemic pressure. This can lead to fracture of elastin fibers, matrix disorganization, root dilatation, and sometimes regurgitation [79], [80].

The next paragraph will focus on the main native valve properties needed to maintain valve function and homeostasis - ECM composition and topography, and homing cell populations. *Traditional* bioprosthetic and mechanical substitutes are not provided with these characteristics; which, on the other hand, are key features of the ideal TEHV. Then, I will introduce the two main TE strategies employed to generate TEHVs: *in-vitro* and *in-situ* maturation [12], [81].

1.3.1 Primary aspects of the native aortic valve to consider when designing a tissue-engineered valve substitute

The primary aortic valve function is to keep a unidirectional blood flow from the heart to the peripheral circulation. This is possible by blocking the flow when the local pressure tends to revert its direction. The same pressure pattern allows the valve to prevent the blood from flowing back into the heart. (figure 1-2A). At the end of the systolic phase, the pressure in the aorta becomes higher than the one in the left ventricle. As the blood begins to backflow, valve cups are opened by the blood motion, and eventually, the cups obstruct the valve lumen. In the valve wall, three sinuses of Valsava are located above each leaflet attachment point. These bulges are important to create flow turbulence that forces the cups to open and interrupt the blood flow during the diastolic phase [82]. In the close state, the leaflets meet at the center taking contact with each other at the coaptation areas (figure 1-2B) [83]. The whole aortic valve, also called the aortic root, is constituted by a crown-shaped annulus to which valve cups (or leaflets) are connected through a curved process that finds its apexes at the extremities of each cup (called commissures) (figure 1-2C). The valve microstructure is highly anisotropic. The

leaflets are made of three layers: the fibrosa, the spongiosa, and the ventricularis. The fibrosa layer presents abundant collagen type I and III bundles circumferentially orientated. The collagen orientation helps the cups to bear mechanical stress derived from the blood pressure and transmits their mechanical load to the aortic root wall. Moreover, the collagen fibers' orientation dictates the radial direction as preferential cups expansion direction, which allows an easier cups coaptation, i.e. a better valve closure during the diastolic phase [82], [84]. The spongiosa layer contains loosely packed and randomly orientated collagen fibers surrounded by a high amount of proteoglycans. Its main function is to cushion the forces applied on both valve sides. The ventricularis layer has a radial fibers arrangement, mostly elastin with some collagen fibers, which provides elasticity during the extension and retraction of the leaflets (figure 1-2D and E). The correct balance of forces' direction and intensity between the leaflet layers ensures the valve function [85], [86]. Different research groups acknowledged the importance of valve anisotropy. They tried to replicate it using manufacturing techniques with a high level of control on material orientation, such as jet-spinning [87], selective crosslinking [88], electrospinning [89], or melt electrowriting [90]. However, such a detailed microstructure has not been replicated so far [91].
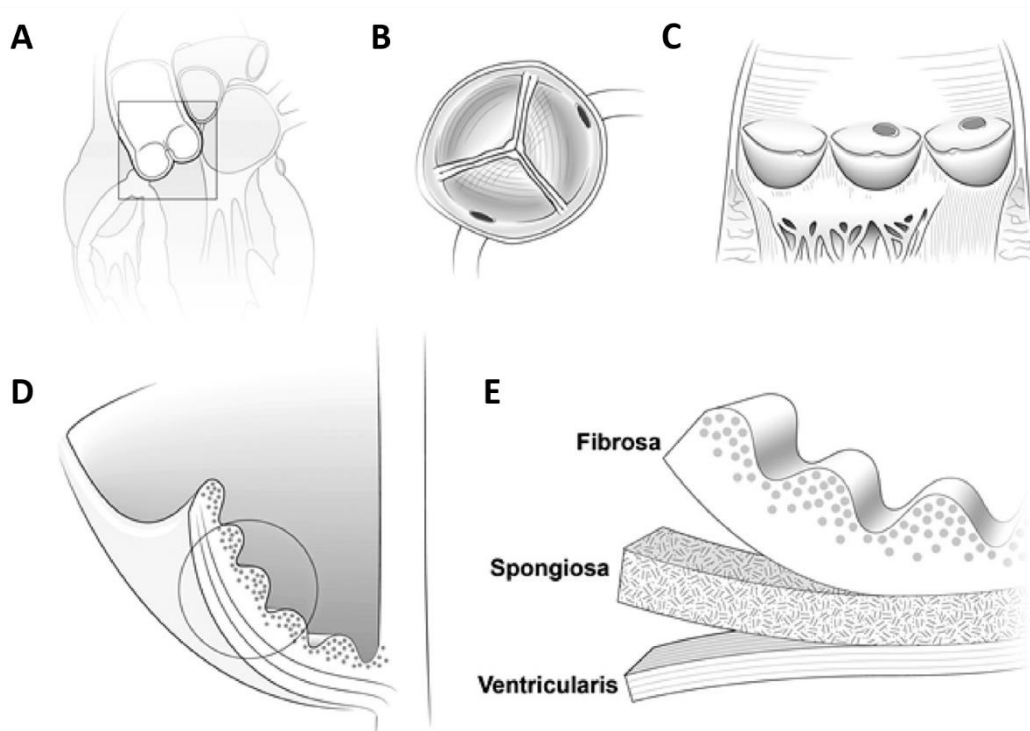
Figure 1-2: Aortic valve anatomical and microstructural details
A) Aortic valve position at the left ventricle outlet. B) View of the closed aortic valve from the aortic side. C) View of the splayed-open aortic valve that highlights the three leaflets. D) View of the cup section with the three leaflet layers in evidence. E) Three cusp layers (fibrosa, spongiosa, and ventricularis) showing their collagen fibril orientations. (From Jana et al.

Cells have an essential role in valve homeostasis. VICs are found in all three valve cups' layers. In the first steps of valvulogenesis, the valve cushions are covered by embryonic ECs. ECs migrate inside the underlying cushion bulk and undergo a phenotype transition – the endothelial to mesenchymal transition, from which the VICs originate (figure 1-3) [92]. They are a mix of mainly two distinct populations: smooth muscle α-actin (SMA)-positive – myofibroblast-like, and fibroblast-like. The former has contraction capacity; hence, it can modify the leaflet stiffness in response to mechanical and chemical stimuli, such as nitric oxide (NO) [93]. Both phenotypes are responsible for constant leaflet repair and remodeling [94]. VICs synthesize ECM components, such as collagen, elastin, proteoglycans, and glycoproteins, but also growth factors, cytokines, and chemokines. VICs control ECM remodeling by regulating metalloproteinases – enzymes able to break collagen and elastin - and their inhibitors. In particular, VICs secrete MMP-2 (gelatinase A) that cleaves gelatin type I and collagen types IV, V, VII, and X. They also produce tissue inhibitors of MMPs (TIMPs). TIMP-1 deactivates MMP-1 and MMP-2 with less efficiency, and TIMP-2 inhibits MMP-2 [95], [96]. It has been shown that VICs' collagen production can be stimulated by vasoactive mediators (such as 5-hydroxytryptamine and angiotensin II), or by mechanical force [97], [98]. Noteworthy, VICs can easily move among different phenotypes, but also degenerate in response to environmental stimuli; e.g. VICs in prolapsed leaflets became α-actin and desmin positive making them leaning towards a myofibroblast phenotype [99]–[101]. Numerous histological studies have suggested inflammation triggers ECM remodeling, fibrosis, and valve thickening leading to structural changes and the subsequent differentiation of VICs into osteoblast-like phenotypes, which start to mineralize the valve [12]. Osteoblasts secrete osteocalcin, alkaline phosphatase, and osteopontin; and organize the calcium crystals deposited on the valve [92].

Valve endothelial cells (VECs) form a coating monolayer, which separates the valve bulk from the blood. VECs have an antithrombotic function by secreting NO and prostacyclin, which reduces platelet aggregation [102]–[104]. Interruptions or lesions in the endothelial lining can lead to subendothelial thickening with lipid accumulation and ECM mineralization, eventually leading to a stenotic valve [12], [105]. VECs secretions have multiple effects on VICs. NO reduces smooth muscle α-actin activation. VECs reduce VICs proliferation and increase glycosaminoglycans synthesis in co-culture [106]. Moreover, VECs can inhibit VICs osteoblastic differentiation [102]. Finally, VECs have a key role in regulating coronary arteries contraction [103], [107].
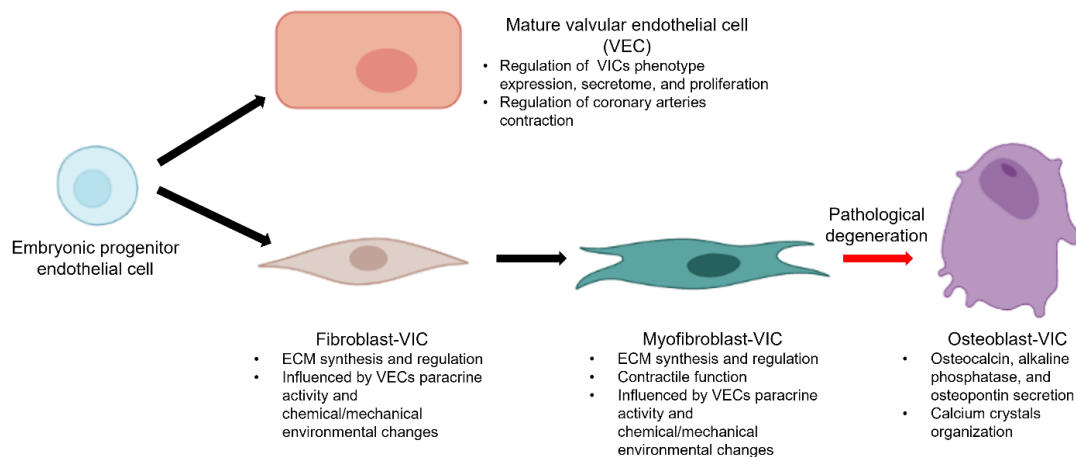
Figure 1-3: Valvular cell types and differentiation

Valvular cell types and differentiation. Embryonic ECs cover the primordial valve cushion. Part of them migrate inside the valve and differentiate mainly in two phenotypes: myofibroblast and fibroblast. In presence of a degenerative environment, VICs can differentiate into osteoblast and organize calcific deposits on the valve. The rest of the embryonic ECs remain on the valve surface and mature in VECs. They partially lose their original proliferative capacity and acquire a series of regulating functions on VICs and surrounding vessels.

1.3.2 *In-vitro* tissue-engineered heart valves

In-vitro TEHV consists of creating a living valve using TE methods and implanting it in the patient once it is fully mature and functional. Valve maturation can be carried out in a bespoke bioreactor until the valve is ready to be implanted. The underlying concept is that *in vitro* incorporation of cells shall confer the prosthetic grafts with the characteristics of living tissue. The TEHV can remodel itself physiologically and in concert with cardiac and whole-body needs, withstanding the impact of degeneration and calcification. Eventually, the regeneration process will result in a working valve made of just autologous tissue. Therefore, there will be no need for any additional intervention, as the leaving tissue valve will be able to maintain its homeostasis [81].

The main scaffold types employed for TEHV are:

- Commercially available bioprostheses (allogenic and xenogenic) (figure 1-2C). They are currently tested as a substrate to create a living valve. Bioprostheses would be ideal due to their macro and microstructure similar to the native valve[108]. However, the use of glutaraldehyde for the crosslinking of the tissue limits cell colonization[109]. Studies are being carried out to improve decellularization and crosslinking protocols. Different detergents and adjuvants are tested to grant the scaffold a mild inflammatory response and a favourable environment for cell colonization [110], [111], [112], [113].

- Biodegradable artificial scaffolds (figure 1-2B). They have the advantage of limitless supply, no risk of disease transmission, and high reproducibility. Since numerous materials can be combined with several fabrication techniques, a synthetic scaffold can be provided with a broad spectrum of mechanical, chemical, and architectural features. Synthetic scaffolds have demonstrated good cellularization, ECM deposition, and scaffold reabsorption when implanted into animal models [114],[115].

- Allogenic decellularized ECMs (figure 1-2A) are tissues grown *in vitro* by fibroblasts-like cells – i.e., cell types with a marked tendency for ECM synthesis [116]. Subsequently, the scaffold is decellularized to create a suitable substrate on which the cells chosen to be implanted are seeded (see below). This scaffold production method would grant an unlimited source of scaffolds produced by either autologous cells or homologous cells. Cells to produce the scaffold, such as dermal fibroblasts, are easily accessible [117][118]. These scaffolds must undergo decellularization, and potentially crosslinking, to become a suitable acellular substrate for colonization of autologous cells and development of the *in-vitro* TEHV. However, decellularization and crosslinking could introduce the same issues detailed in the bioprosthetic valves paragraph.
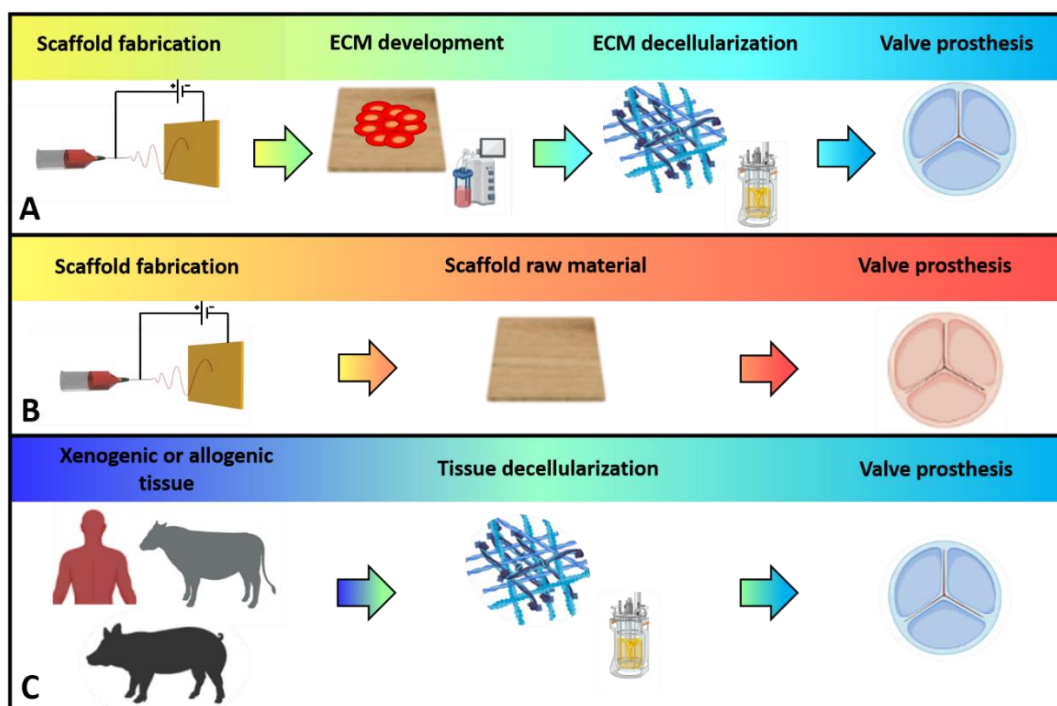
Figure 1-4: Scaffold production methods for heart valve tissue engineering
A) Allogenic decellularized ECM, B) biodegradable artificial scaffolds, C) commercially available allogenic and xenogenic bioprostheses.

Cells are supposed to confer living properties to the scaffold. The optimal cell type for valve engineering should be non-immunogenic and able to maintain its specific function or gain such specialization through differentiation. Autologous cells are the first choice, but they show significant dysfunctions if obtained from old patients or patients with cardiovascular diseases, such as osteogenic-like gene expression and low viability and proliferation [119]; while allogenic cells might be immunogenic [120]. Induced pluripotent stem cells are generated by reprogramming somatic cells and would be the ultimate solution for patient-tailored therapy, but there are still several safety concerns due to reprogramming stability and completeness, which may lead to unforeseeable mutations and potential tumorigenicity [121]. Differentiated cells or progenitor cells, including mesenchymal stem cells (MSCs), bone marrow mononuclear cells (BM-MNCs), or endothelial progenitor cells (EPCs), remain the most employed so far in research. Several cell types demonstrated good adherence to native VICs and valvular endothelial cells (VECs) expression and functions [122]–[126].

It has been demonstrated that the size of the scaffold can restrict oxygen and nutrients availability, creating areas of necrosis and degeneration [127]. Different procedures have been proposed to circumvent this problem, including mechanical compression [128] and flow perfusion [129]. The use of dynamic systems, namely bioreactors, before implantation into the recipient host is considered by several research groups as an important passage to assist TEHVs maturation and maintain the viability of the three-dimensional (3D) construct [130]–[132]. Bioreactors are built with the option of applying stimuli (i.e. fluid flow and pressure) that mimic the native valve environment [133], [134]. Pulse duplicators are used to make the TEHV develop into a structure able to withstand cardiac pressures. They simulate pressure and flow patterns of the heart. These machines can be helpful to enhance the construct's properties through *in-vitro* conditioning, but also to obverse the behaviour of a candidate TEHV [134]–[136].

Unfortunately, *in-vitro* TEHV has non-negligible issues. Leaflet retraction and thickening have been observed in scaffolds seeded with fibroblasts and myofibroblasts, or when cells with similar phenotypes were found in the explanted scaffold [132], [137]–[139]. Cells exert retraction forces on their surrounding ECM in response to mechanical stress [140]. However, stress forces promote the development of a well-organized ECM [141], [142], hence they should not be abolished entirely. The use of rigid inserts to limit leaflet contraction during the bioreactor phase (i.e. when living fibroblasts are present in the scaffold leaflets) may help to reduce leaflet retraction [143]. Nevertheless, it was shown that leaflet retraction and remodeling restart upon constraints removal due to the stress accumulated by the ECM and the cells [144], [145]. Computational predictions of *in-vivo* remodeling could help to create a scaffold adaptable to

post-implantation remodeling into a native-like shape [146]. A possible solution may be removing cells with fibroblast and myofibroblast phenotype after tissue development, and reseeding the scaffold with cells from endothelial lineage only [147]. Moreover, the production of a mature construct is time-consuming and technically complex. There is a relevant risk of contamination, cell population heterogenicity, and donor-to donor variation. Finally, the best-suited cell types for heart valve regeneration are still to be established [148], [149].

1.3.3 *In-situ* tissue-engineered heart valves

The *in-situ* valve regeneration strategy consists of using the host regeneration capacity by implanting acellular scaffolds, which recruit endogenous cells. The scaffold should guide the valve regeneration with its mechanical, topological, chemical, and biochemical features. Moreover, the scaffold should be able to attract autologous cells, favour their proliferation, and direct their differentiation to the correct phenotype. Recently, the *in-situ* regeneration strategy gained more attention since it simplifies several aspects of TEHV development compared with the *in-vitro* approach. As no living cells are supposed to be included in the final product, the complications related to isolation, cultivation, and characterization of cells are eliminated. Also, there are no concerns about adverse effects like cell-related immune reaction, malignant mutation, donor-to-donor variation, and product inconsistency. Eventually, this reflects in lower cost, less manufacturing time, and off-the-shelf availability [150], [151]. There are still several open challenges before *in-situ* TE could become a therapeutic option, such as the control of the regeneration process and synchronizing it with the scaffold degradation; making constructs compatible with minimally-invasive implantation techniques; implants long-term safety; overcoming the recipient's underlying conditions, creating scaffolds that recapitulate the complex valve microarchitecture, and achieving tissue homeostasis after the regeneration process [108], [152], [153].

The available scaffold types are the same as for the *in-vitro* approach. However, the contribution of pre-seeded cells is no longer included in this case. Hence, the focus is on designing a substrate to attract cells and direct their organization. Synthetic scaffolds lack of native-like microstructure and biochemical cues, but they offer reduced costs and complexity, no-sourcing issues, and higher control on scaffold features than decellularized homografts or xenografts [81], [108]. Short-term suitability (up to a year) of synthetic scaffolds for TEHV was shown, but their safety over the years is still to be proven [154], [155]. In the effort to amend for the synthetic scaffolds' lack of biochemical cues, they were functionalized with growth factors and other proteins or

peptides [156]. The arginine-glycine-aspartic acid peptide (RGD) was shown to enhance cell adhesion through interaction with cells' integrins and proteins involved in cell adhesion [157]. Hence, several scaffolds have been functionalized with this peptide to improve endothelial coverage [158]–[161]. Vascular endothelial growth factor (VEGF) is an endothelial cell (EC) proliferation and migration promoter, as well as an apoptosis inhibitor [162]. VEGF anchoring on scaffolds (alone or in combination with other factors) showed higher tissue endothelialization than unmodified scaffolds [163]–[165]. Basic Fibroblast Growth Factor (bFGF) has effects on various cells, including fibroblasts and ECs. BFGF increases mitogenesis and cell migration [166]. When included in vascular grafts, bFGF stimulated endothelialization and subendothelial tissue development with the recruitment of nearby SMCs and fibroblasts [167]. Stromal derived factor-1 alpha (SDF-1α) modulates local inflammation. This resulted in enhanced recruitment of mesenchymal stem cells (MSC) and less inflammatory cells to the scaffold; and reduced the fibrotic capsule thickness around the scaffold in a mice model [168]. Allogenic decellularized ECMs require a more complex developing process since they need to be grown in bioreactors. The production of this scaffold type brings back the issues regarding cell selection and the following decellularization, which were previously detailed. Nevertheless, these scaffolds have the advantage of being produced by human cells (usually produced by the recipient's cells), providing them with excellent compatibility for implantation. Studies showed that cells could repopulate such scaffolds and reorganize their matrix. Leaflet retraction is still an issue, but it can be circumvented by adapting the scaffold shape to compensate for predicted retraction [146], [169]. Xenogenic tissues were supposed to be the most suitable and immediate source for TEHV scaffolds. However, several case reports have highlighted durability issues, mainly related to the host body reaction [170]– detailed in the following section.

Cell recruitment is key for the *in-situ* approach. Native valve tissue cell populations and their functions were detailed in *paragraph 1.3.1*. Ideally, a TEHV should have a native-like cell arrangement after its maturation inside the recipient body, as the final aim is to regenerate a native tissue. Nearby tissues cells' (aortic wall), and circulating cells (EPCs) are the available sources for scaffold colonization. Circulating EPCs, which are involved in the repair of endothelial surface injury, were reportedly found on native and bioprosthetic aortic valves [171]. Moreover, EPCs have higher proliferative potential than mature ECs [172]. Therefore, they represent an optimal candidate for valve scaffold colonization. Attempts to enhance the EPCs have been made by functionalizing scaffolds with VEGF and RGD [163], and CD34 [173]. Transforming growth factor (TGF)-β1 is a polypeptide with the ability to stimulate the development of EPCs into a mesenchymal-like phenotype, thereby leading to enhanced ECM production [174], [175].

This may represent an interesting solution for the *in-situ* development of a cell population able to maintain and reshape the valve substitute. Unfortunately, as noticed for construct pre-seeded with fibroblasts and myofibroblasts in the *in-vitro* approach, there are cases of acellular scaffolds that suffered from leaflet thickening and retraction [169], [176], [177]. Cells with contractility ability were found on retracted leaflets and nearby tissues; their action is thought to be the cause of leaflet retraction [178], [179]. A construct for *in-situ* regeneration should direct the evolution of inflammatory cells' presence on the scaffold. Inflammation is considered essential for tissue regeneration, which should be achieved by modulating the classical wound healing process [180]. Just after implantation, the process begins with protein adsorption to the scaffold surface. Following, immune cells – mainly neutrophils and monocytes, concentrate on the scaffold during the so-called acute inflammation phase. If the inflammatory stimuli persist, chronic inflammation develops with macrophages and lymphocytes controlling the local environment. Ideally, scaffold colonization should happen during this phase. Locally predominant immune cells should cross-talk with fibroblasts, stem, and progenitor cells, stimulating their adhesion, proliferation, and scaffold remodeling [169]. As the newly formed tissue homeostasis is established, the inflammatory cells should leave the tissue so that inflammation is gradually resolved. Alternatively, persistent inflammation can lead to the accumulation of giant cells, fibrotic coating, calcification, valve degeneration, and implant failure [152], [181]–[184]. Most of these adverse effects are observed when decellularized xenografts are used. Thus, the unfavorable inflammatory response may be triggered by antigens of xenogenic origin [170], [185].

1.4 Biodegradable polymers for TEHV

Biodegradable materials can be of synthetic or biologically-derived origin. In TE, polymers play a major role given their multiple benefits:

- they are easy to process
- they are highly tuneable in their physical and chemical properties
- they can be functionalized with many compounds giving them different properties
- they have an unlimited supply
- their biodegradation pace can be controlled by acting on their composition

Biologically-derived polymers, such as gelatin (GL), collagen, and fibrin, are fast degrading materials produced from biological sources with good biocompatibility. However, they are hard to process in 3D structures suitable for TE with proper mechanical features tailored for each case. On the other hand, synthetic polymers, such as poly-glycolic acid (PGA) and poly-caprolactone (PCL), can be produced with the desired strength and durability and can be easily processed to obtain the required design [186]–[188]. Table 1-1 shows the most used polymers in TE.

Polymer	Biodegradable?	Origin	Examples of use
Collagen	Yes	Animal extract	Urogenital reconstruction [189] Cartilage repair [190]
Gelatin	Yes	Animal extract	Valve regeneration [191] Bone regeneration [192]
Alginate	Yes	Seaweed extract	Bone regeneration [193] Cell delivery [194]
Hyaluronic Acid	Yes	Animal extract/ Bacterial product	Cartilage regeneration [195] Skin regeneration [196]
Agarose	Yes	Seaweed extract	Cartilage regeneration [197] Neural regeneration [198]
Chitosan	Yes	Animal/Fungal extract	Wound healing [199] Cartilage regeneration [200]
Poly(glycolic acid) – PGA	Yes	Bacterial product – Synthesis from petrochemicals	Valve regeneration [201] Cornea regeneration [202]
Poly(lactic acid) - PLA	Yes	Vegetables extract– Synthesis from petrochemicals	Bone regeneration [203] Cardiovascular repair [204]
Poly(lactic-co-glycolic acid) – PLGA synthetic	Yes	Chemical synthesis from PGA and PLA	Bone regeneration [205] Drug delivery [206]
Poly(ε-caprolactone) - PCL	Yes	Chemical synthesis	Vascular graft [207] Dental regeneration [208]
Poly(ethylene terephthalate) - PET	No	Synthesis from petrochemicals	Vascular graft [209] Bone regeneration [210]
Poly(tetrafluoroethylene) - PTFE	No	Synthesis from petrochemicals	Bone regeneration [211] Vascular graft [212]

Table 1-1: Most commonly used material for scaffold fabrication and examples of their use in tissue engineering.

1.4.1 Gelatin

GL is the product of the denaturation of collagen (figure 1-5A), which can have different molecular weights (MWs) and compositions depending on its manufacturing method and the source of collagen from which it comes from. It is biodegradable, biocompatible, and non-cytotoxic. Moreover, GL can support cellular growth and can be manufactured in many shapes

and sizes. It is used in clinical medicine, especially injectable collagen for tissue defects, hemostasis, burn and wound dressing, and vascular grafts [213]. A sequence of purification steps and heating treatments, including a final ultra-heat treatment sterilization step followed by the drying phase, provide GL with a remarkably high level of viral and immunogenic safety. Moreover, GL is safer than collagen in terms of immunogenicity [214]. As an animal extract, gelatin composition is influenced by the animal breeds, genetics, feedings, and rearing; thus it is very unlikely to find identical gelatin compositions between different lots [215]. However, it is generally rich in ECM's amino acids (mainly glycine, proline, hydroxyproline, alanine, glutamic acid, arginine, aspartic acid, and serine), among which there is the RGD group, which is recognised by cell integrins [216]. While collagen degradation requires specific enzymes (collagenases like MMP-1) because it is resistant to most proteases, GL is vulnerable to many proteases. That means that scaffold recipients can degrade GL easily and in almost any body location where the scaffold may be implanted [217], [218]. GL forms physical gels in water at a concentration larger than 2% w/v. It undergoes a thermo-reversible gelation transition for temperatures under 30°C [214], [219]. However, GL hydrogels dissolve rapidly in an aqueous environment, especially at 37°C. Hence, a cross-linking treatment is mandatory to preserve the scaffold for longer periods in the tissue regeneration process. Different methods, either physical or chemical, are used to enhance the water-resistance of GL. Physical methods of cross-linking include microwave irradiations or UV treatment. Common chemical crosslinkers are aldehydes (formaldehyde, glutaraldehyde, or glyceraldehyde), polyepoxy compounds, and carbodiimides. These are well-known toxic compounds, the use of which must be carefully considered. Glutaraldehyde-crosslinked gelatin scaffolds can hold free glutaraldehyde within its bulk, and release it during scaffold degradation, causing adverse immune reactions and reducing scaffold colonization [220]. To avoid the risk of toxic chemicals release, enzymatically and naturally derived crosslinkers are under investigation [221], [222]. In the present work, γ-Glycidoxypropyltrimethoxysilane (GPTMS) was used to crosslink the GL (figure 1-5B). The GPTMS is a silane-coupling agent, in which the oxirane ring reacts with the amino groups of the GL chains. The hydration of the trimethoxy groups on the GPTMS forms pendent silanol groups (Si-OH) through an acid-catalyzed reaction. Then, Si-O-Si bonds are formed thanks to the condensation of two Si-OH during the solvent evaporation in the fabrication process (figure 1-5C). The Si-O-Si linkages provide inter-chain covalent bonds, so the result is a more stable crosslinked structure. GPTMS-crosslinked GL nanofibers have proven to support osteoblast and olfactory cells *in vitro* adhesion and proliferation; and to last around three weeks in water solution [223], [224]. GL solutions can be produced using water, N,N-Dimethylacetamide (DMA),

N,N-Dimethylformamide (DMF), 1,3-Dimethyl-2-imidazolidinone (DMI), N,N-Dimethylsulfoxide (DMSO), 1,1,1,3,3,3-Hexafluoro-2-propanol (HFP), and N-Methyl-2-pyrrolidone (NMP) [225].
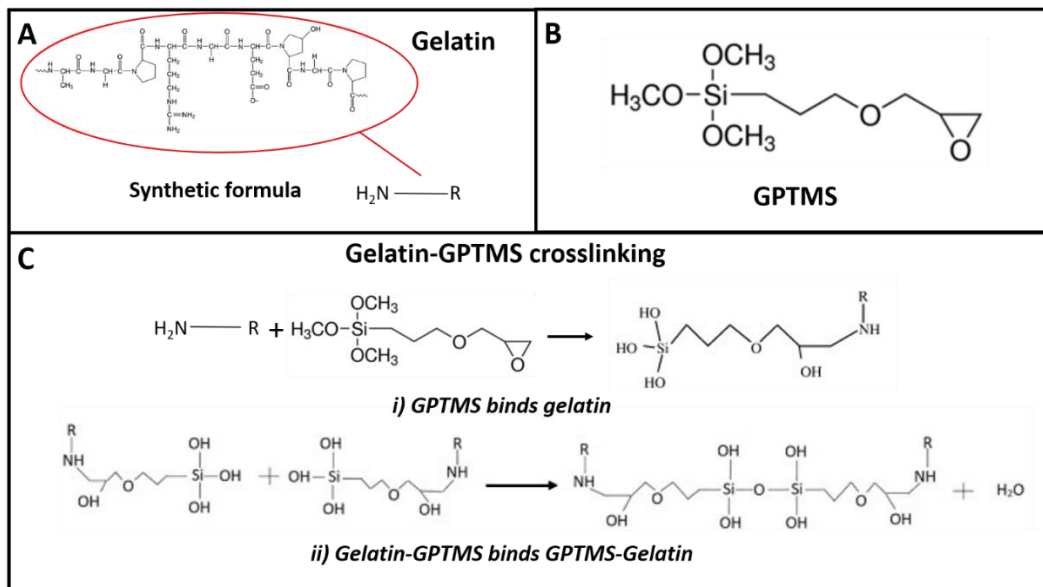
Figure 1-2: Gelatin structure and crosslinking process
A) Chemical formula of GL, B) Chemical formula of GPTMS, C) crosslinking reaction involving GL and GPTMS.

1.4.2 Polycaprolactone

PCL is an aliphatic biocompatible polyester obtained from the polymerization of the open cycle §- caprolactone (figure 1-6). PCL is an approved material by Food and Drug Administration (FDA) for implantable applications [226]. It is biodegradable but takes 2 to 4 years to vanish completely. Its aliphatic link is susceptible to enzymatic hydrolysis, which can be catalyzed by lipase and α-amylase [227], [228].

Biodegradability can be tuned by modifying the PCL scaffold production parameters. For instance, if the scaffold is produced by electrospinning – the technique used in this project, lowering the concentration of the starting polymer solution leads to a final product with thinner fibers, which are degraded quicker than thicker fibers. The same effect is obtained by increasing the production voltage or changing the solvent composition in the starting polymer solution [229]. Blending PCL with other materials is another way to tune its degradation. PCL mixed with gelatin, PLGA or PGS acquires a higher degradation rate; while a PCL blend with PU makes the product very difficult to degrade [230]. This material is widely used in the medical care industry to produce surgical sutures, deliver drug vesicles, and engineer tissue, thanks to its biocompatibility, tuneable degradation time, and mechanical characteristics (such as high

elasticity) [231]. There are PCL applications in many TE areas: dental, bone and cartilage, skin, nerve, cardiovascular regeneration, and others [232]. PCL-based scaffolds can be fabricated with several techniques: electrospinning, phase separation [233], 3D printing [234], salt leaching [235], freeze-drying [236], and gas foaming [237].

PCL is soluble in different solvents, such as chloroform, 2,2,2-trifluoroethanol (TFE), DMF, NMP, and DMSO [238].
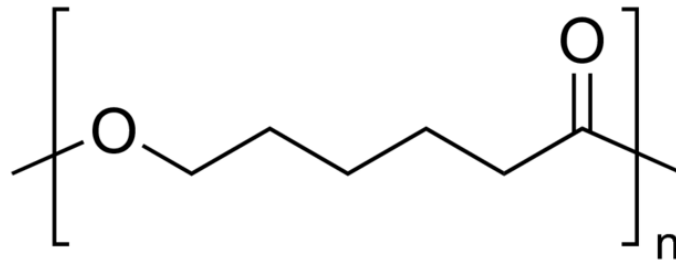
Figure 1-3: PCL chemical structure

1.5 Enhancement of tissue-engineered heart valves' regenerative properties exploiting RNA interference

1.5.1 Therapeutic potential of microRNA

Traditional pharmacology is based on chemical molecules which mainly target messenger RNA (mRNA)-expressed proteins. However, protein-coding DNA is only a minority of the human genome [239], [240]. In addition, drugs become ineffective whenever genetic mutations lead to substantial changes in the identified protein binding sites, which frequently happens in oncology [241], [242]. Even assuming the entire human proteome will be druggable in the future, around 98.5% of the human genome would not be targeted by pharmacology treatments [243], [244]. The transcribed genome has a similar distribution: only 2% of total RNA codes for proteins [245]. The remainder falls into a category called non-coding RNAs (ncRNAs).

Although the vast majority of RNAs do not code for proteins, these non-coding sequences have a tremendous impact on the regulation of cell function; as such, they are usually called regulatory ncRNAs. Long non-coding RNA (lncRNA) – more than 200 nucleotides, is active both in the nucleus and cytoplasm. It can modulate protein modifications, mRNA stability, and translation, compete with protein-coding mRNA to bind microRNAs, or act as microRNA precursors [246]. MicroRNA (or miRNA) can bind partially or fully complementary mRNA sequences to repress translation or degrade them [247]. Similar to microRNA, small interfering

RNA (siRNA) is involved in mRNA degradation, but it is able to target just the unique mRNA sequence to which it is perfectly complementary. This process is called RNA interference (RNAi). Noteworthy, microRNAs and siRNAs have a transient effect on cell mRNA expression, the cytoplasmic half-life of numerous microRNAs being between 24h to several days [248]. Once they are depleted, the cell goes back to its normal metabolism [249]. This may be an attractive feature for regenerative medicine. Indeed, after the initial regenerative phase, the newly formed tissue should go back to native-like homeostasis metabolism. Thus, the regenerative stimulus should be time-limited [250].

In the effort to develop pharmaceutical treatments which regulate cellular metabolism and functions more comprehensively, researchers took inspiration from the cell itself. RNAi is a usual occurring biologic process. As part of normal cell metabolism, small RNA sequences inhibit or reduce gene expression by targeting specific sequences [251], [252].

After pre-microRNA synthesis by the cell or in the laboratory (microRNA mimic), the sequence enters the cytoplasm, either by transfection of a synthetic microRNA or exported from the nucleus by Exportin-5. There, pre-miRNA is trimmed into a double-stranded sequence around 20 base pairs (bp) long (the microRNA) by the cytoplasmic endoribonuclease Dicer. Then, microRNA assembles in the so-called microRNA-induced silencing complex (miRISC). During this process, microRNA loses one strand, and the remaining one (mature microRNA) targets partially or perfectly complementary mRNAs [242], [253]. Silencing by the miRISC complex is triggered from a microRNA "seed" region where 2-8 perfectly complementary nucleotides bind to the correspondent mRNA sequence (figure 1-7).

MicroRNA therapeutics have reached the clinical trial stage. AS cancer therapy, antitumor activity was observed in part of the patient cohort with refractory advanced solid tumors [254]. A microRNA-based therapy against hepatitis C was also trialled. This therapy helped patients to restore an effective immune response against the hepatitis-C virus up to the point of making hepatitis-C virus RNA undetectable in several patients' plasma [255].
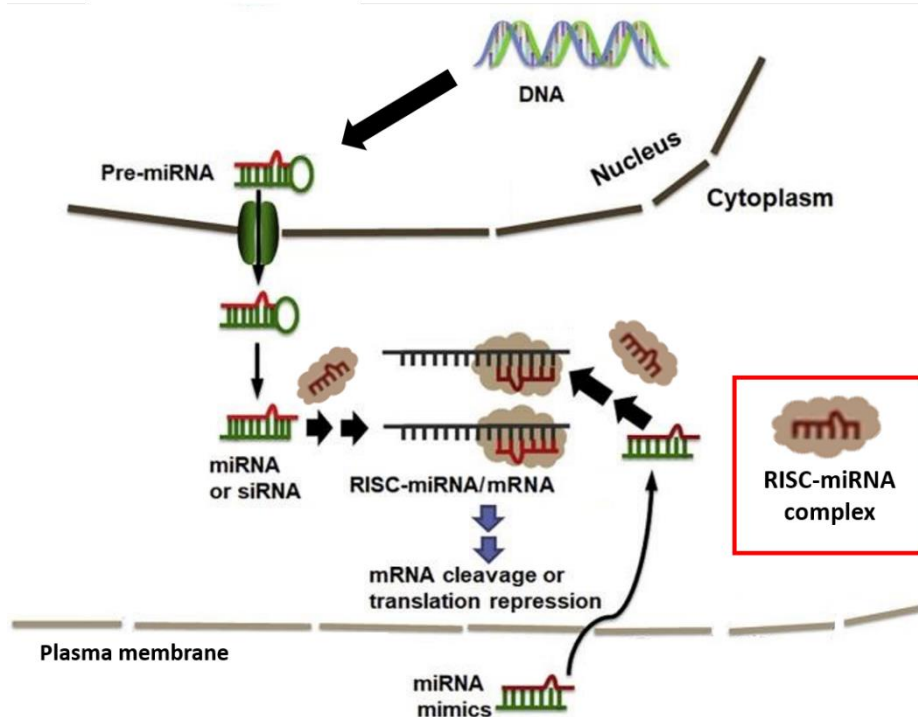
Figure 1-4: RNA interference mechanism
Figure simplified from Yu et al. "RNA Therapy: Are We Using the Right Molecules?",
Pharmacology and Therapeutics, 2019, doi: 10.1016/j.pharmthera.2018.11.011.

1.5.2 Combining RNA interference with Tissue Engineering

There are two opposite strategies to modulate microRNA function: one is to overexpress the microRNAs of interest by microRNA mimics or viral vectors. The other is to inhibit microRNA expression by genetically modifying the model to be used or administering specific antisense oligonucleotides [256], [257].

The reason that led regenerative medicine to intersect with RNAi therapeutics is that microRNAs and short interfering RNAs (siRNA) can regulate essential functions for cell repair and tissue reconstitution. For instance, it has been demonstrated that ncRNAs regulate essential functions, such as proliferation [258], migration [259], differentiation [260], viability [261], and ECM production [262]. There are several examples of microRNAs that can be used as therapeutic agents in cardiovascular regenerative medicine to influence cardiac remodelling in infarcted heart areas [263], regulate angiogenesis [264], [265], or halt EC senescence [266].

The application of microRNA therapeutics in TE raises several issues. It is hard to expect that intravenous injection of microRNA may have any effect on the site of interest. The blood continuously washes vascular cavities; hence, microRNAs would be immediately dispersed and attacked by serum nucleases. It would be difficult to reach a therapeutical effect on the site of

22

interest, and the microRNA dispersed in the circulation could be the cause of side effects to other districts of the body.

MicroRNAs should be protected, locally anchored, and driven into cells to fulfill their function in the cell cytoplasm. A scaffold loaded with microRNAs may serve as a microRNA local administration device and support tissue regeneration. Incorporation into a biodegradable scaffold makes it possible to obtain prolonged administration without the periodical need for injection or oral ingestion [267]. As the scaffold degrades, the microRNA is locally released and becomes available to nearby cells. *In-situ* microRNA delivery systems are still less developed than the scaffold seeded with pre-transfected cells, using plasmid DNA or microRNA [268].

Scaffold production may require physical and chemical conditions hard to be tolerated by a microRNA. Hydrogels are well suited to overcome this limitation, because of their ease of degradation and mild production process [269]. Also, microRNA-functionalized hydrogels can be injected and polymerize on-site, allowing a local delivery with just a minimally invasive medical procedure [270]. In the case of electrospinning, particular attention must be focused on the material solution, as some employed solvents may be aggressive on the microRNA or the vector. It is possible to circumvent the problem with post-production functionalization [271]. However, if the aim is to have a prolonged release, the microRNA should be incorporated into the material solution; thus, it is mandatory to find a compatible solvent [272], [273]. In limited cases, the material to electrospun can be dissolved in water, like GL or hyaluronic acid (HA) [274]–[276]. Finally, clinically relevant aspects must be considered when designing a microRNA-functionalized scaffold. Sterilization and implantation should not damage the microRNA, and all scaffold components should withstand long-term storage [268].

1.5.3 MicroRNA-132 as a bioactive agent to guide valve regeneration

Our team first reported that microRNA-132 secreted by human pericytes has a proangiogenic effect on ECs, stimulating EC proliferation and migration [277]. The year before, Anand et al. discovered that microRNA-132 is highly upregulated in human embryonic stem cells and endothelium of human tumors. Moreover, they proved that microRNA-132 was targeting the RAS p21 protein activator 1 (RASA1), whose expression is negatively correlated with EC proliferation and angiogenesis *in-vivo* and *in-vitro* [278]. From bioinformatic analyses, it resulted that microRNA-132 can target other genes related to cell proliferation and migration. RB transcriptional corepressor 1 (RB1) is a negative regulator of cell cycle proteins. Its inhibition facilitates cell cycle progression [279]. Paxillin (PXN) is a cell focal adhesion component. The p21-

activated kinase (PAK)-PXN pathway has a role in regulating cell protrusion and migration [280]. The repression of Sprouty-related EVH1 domain containing 1 (SPRED1) allows intracellular transmission of angiogenic signals coming from VEGF and FGF and enhances human umbilical vein endothelial cells (HUVECs) migratory activity [281]. In addition, research in our laboratory has shown that microRNA-132 has a role in contrasting calcification. High phosphate-driven osteochondrogenic induction is contained by microRNA-132 expressing APCs; whereas osteochondrogenic markers are highly expressed in microRNA-132-inhibited APCs. Moreover, APC-derived secretome prevents osteogenic differentiation of swine aortic valves through microRNA-132 signalling [282]. Indeed, microRNA reduces the expression of osteoblast markers [283]. Cyclin-dependent kinase inhibitor 1A (CDKN1A) suppression enhances EC proliferation, migration, and tube formation [284]. *Devalliere et al.* demonstrated that microRNA-132 transfection to ECs enhances their proliferation. PLGA nanoparticles (NPs) loaded with miRNA-132 and functionalized with RGD groups were administered to HUVECs. *In-vitro* proliferation and migration increased 1.8-fold and 5-fold, respectively. In addition, microRNA-132 transfection doubled the number of formed microvessels per square millimeter by HUVECs [285].

A main aim of this project is to exploit the microRNA-132 properties discussed in this paragraph to favor in-situ heart valve regeneration. Therefore, I decided to embed microRNA-132 onto a biodegradable scaffold manufactured in a bioprosthetic aortic valve shape in the effort of enhancing *in-situ* endothelialization and protecting the implant from calcification. As aforementioned, the superficial scaffold layer is made of GL, which has already been used in our lab for *in-vivo* trials [286]. GL is biodegradable and biocompatible and, as the host will degrade it, it will expose microRNA-132 carriers, which will be available for uptake from nearby cells.

1.5.4   Delivery of microRNA

Whenever a therapeutic use of ncRNA is considered, there are two main aspects to focus on: ncRNA delivery and stability. First and foremost, ncRNAs must access the cytoplasm, whichever therapeutic application is considered. However, NcRNAs have a high molecular weight (Mw) and structural stiffness. Moreover, ncRNAs and the cellular membrane are negatively charged, therefore the delivery of naked ncRNAs inside the cytosol is challenging [287]. Naked microRNA is highly unstable in body fluids. Ubiquitous nucleases degrade microRNA within minutes; microRNA is reported to have 20 minutes half-life in serum [288], [289].

There is some research showing effective naked ncRNA administration. Naked siRNA instilled in mice achieved a good antiviral activity [290], reduced the damages of lung injuries [291], or

silenced chemokine expression [292]. The feasibility of this delivery method has also been confirmed in a clinical trial to treat pulmonary viral infections [293], [294]. Perhaps, one or more components of lung surfactant are making naked ncRNA delivery possible, as demonstrated by a study in which a synthetic mimic of Surfactant Protein B was complexed with siRNA [295]. Other easily accessible tissues or organs, such as eyes and skin, can be approached with the naked ncRNA delivery [296], [297]. Yet, ncRNA needs to penetrate the plasma membrane with the preserved structure to exert biological functions. Therefore, it is preferred to use transfection agents even in the case of local administration [298]–[300].

1.5.5 Non-Viral Vectors for In-Situ Micro-RNA delivery

There are several vector types for genetic material delivery. Generally, they can be categorized into viral and non-viral vectors.

Viruses are excellent at crossing the plasma membrane. Virus-based vectors are already approved for clinical practice [301]. A couple of successful attempts to embed viral vectors into biomaterials have been already published. Recombinant Adenovirus has been incapsulated into alginate microspheres to successfully deceive specific immune reaction [302]. Also, adenovirus was integrated into the fibrin scaffold and achieved 8 days of sustained release [303]. However, some viruses modify the cell's genome permanently (retroviruses), which is not ideal for tissue regeneration. These viruses can also integrate with the host cell's genome at an undesired location - insertional mutagenesis [304]. Adenoviruses grant higher safety about mutagenesis, but they stimulate a high innate and adaptive immune response, inflammation, and are highly toxic to cells [305]. With regards to this specific project, there are specific safety concerns during the different phases of the microRNA-functionalized scaffold. The scaffold production chain should be updated to the highest safety standards required when working with viruses. Also, scaffold sterilization should be carried out without harming the virus. Above all, the main problem with using viruses is to confine them in a specific location, without allowing them to spread and cause unpredictable effects by modifying other cell types' expressions [268].

Non-viral vectors are materials able to protect RNA/DNA and facilitate its entry inside the cells. They can transfer a larger amount of genetic material than viruses; even combinations of different microRNAs in the same cargo are possible. Their transfection is always transient [306]. Liposomes are lipid-based vesicles that can carry the genetic material absorbed on their surface or in the bulk [307]. As they have the same nature as the plasma membrane, liposomes easily interact with it. Importantly, liposomes are commercially available and extensively adopted.

Concerns about liposome stability (especially in contact with blood) and their toxicity are not entirely cleared [308], [309].

Cationic polymers and polysaccharides bind genetic molecules (DNA, RNA, microRNA) by electrostatic interaction. They possess a net positive charge which binds to the negatively charged nucleotides forming complexes called polyplexes (figure 1-8). Usually, polyplexes production is less complex and cheaper than viral vectors [310]. Some polymers can create polyplexes smaller than lipoplexes, which facilitates cell entry [311]. A microRNA non-viral vector complex is likely entrapped in endosomes as it gets inside the cytoplasm. This would lead to a progression towards a more aggressive environment (lysosome) and complex degradation. Some polymers possess specific features to avoid that fate, like the one called "proton sponge". The acidification of the internal endosomal environment makes the polymer vector's amines charge positively. This attracts ions, which creates a growing osmotic pressure that is followed by water entrance. Eventually, the unbearable amount of water breaks the endosome walls releasing its content into the cytoplasm [312]. Researchers have developed a plethora of polymeric and non-polymeric vectors with different features and different available functionalization to tailor the vector to the specific application [313].
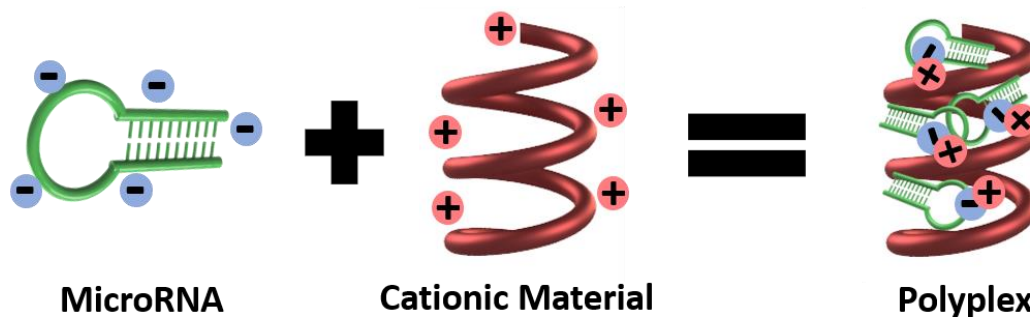
Figure 1-5: MicroRNA polyplex formation
Electrostatic attraction between the positively charged polymer/polysaccharide and the negatively charged microRNA creates a complex which protects the microRNA from the nucleases and helps it to cross the plasm membrane.

The materials studied for gene delivery are countless, the main ones are:

- Polyethylenimine (PEI)
- Poly(ethylene glycol) (PEG)
- poly(lactic-co-glycolic acid) (PLGA)
- Dextran

- Chitosan

- HA

Several co-polymers and functionalization have also been elaborated[314], [315].

PEI is one of the most studied and used non-viral vectors, and the constituent material of commercial transfection vectors, such as JetPEI (Polyplus, France) [316]. It is highly attractive for drug delivery since it possesses a dense positive charge that makes it able to easily penetrate the plasma membrane [317]. The overall charge of the microRNA-PEI complex (or nanoparticles - NPs) is positive, which establishes an electrostatic attraction between the NPs and the negatively charged cell membrane, making the transfection easier. There are different versions of PEI with different sizes and topologies. The most efficient one for transfection is the branched PEI family (figure 1-9B) [318]. Noteworthy, PEI can escape cell endosomes thanks to its proton sponge ability, as described in the previous paragraph [319]. PEI has already given good results in *in-vivo* animal models [320]–[322]. However, there are a few issues to consider. First of all, PEI has shown cytotoxicity at certain concentrations [323], [324]. As the amount of administered PEI is proportional to the size of the nucleic acids to transfect, the use of a minimal amount to transfect small RNA strands (only 21 bases) may be tolerable [325]–[327]. PEI cytotoxicity is positively correlated with its transfection efficiency [326]. There are several cytotoxic concentration thresholds in the literature, Human Embryonic Kidney 293 Cells – a cell type frequently used for cell transfection experiments, maintain >85% viability when incubated with up to 25 µg/mL of PEI [325]. To amend this, PEI was used in combination with different materials, such as PEG, chitosan, glycosaminoglycans, and polyurethanes. PEI-g-PEG (figure 1-7) is less toxic than PEI due to PEG grafting, and it has been successfully used as a transfection vector [324], [328]–[330]. PEI-g-PEG is less efficient than PEI in terms of transfection but still reaches levels that make it accepted as a constituent for transfection vectors [331], [332]. The main problem for my project is that PEI is water-soluble. Since the scaffold production process intermediates are water-based solutions, there is the risk that microRNA-PEI NPs would dissolve during the scaffold production, leaving microRNAs exposed to body nucleases.

Chitosan is a natural polysaccharide derived from the deacetylation of chitin, which can be found in crab shells for instance (figure 1-9A). At proper ratios of positively charged chitosan nitrogen to negatively charged nucleotide phosphate, chitosan will condensate genetic material into small spheroids by electrostatic attraction, making RNA/DNA available for cellular uptake (figure 1-8) [333], [334]. It also confers microRNA with efficient protection against nucleases [335]. Chitosan offers a good trade-off between biocompatibility, biodegradability, low toxicity, and

transfection efficiency. Its toxicity is comparable to sucrose by oral administration, and as much as 100 mg/kg in mice [336], [337] [338]–[341]. Chitosan safety was appreciated when used as wound-dressing material, where it also exerted antimicrobial and haemostatic properties [342]. Chitosan has been widely employed for short ncRNA delivery [333], [343]–[347]. A high chitosan concentration would lead to an excessively tight electrostatic bond, resulting in a difficult intracellular release of the nucleotides. Therefore, protection and ease of release should be balanced. In this respect, the chitosan's Mw deacetylation degree must be considered. The degree of deacetylation (DD) is the percentage of acetamido groups transformed into amino groups. It has been shown that low Mw chitosan forms smaller particles [348]. Also, chitosan with an Mw under 50 kDa creates micrometric aggregates that reduce cellular uptake [343], [349]. Generally, the higher the deacetylation degree, the more efficient is the transfection. However, it has been shown that too high DD can cause cytotoxicity [350]. Thus, it is important to find a good trade-off between DD and molecular weight. Noteworthy, the scaffold manufacturing process in this project needed non-water-soluble NPs. Chitosan NPs are only soluble at acidic pH. That is because chitosan itself is not soluble at neutral pH [351]. This should grant NPs integrity during the scaffold fabrication since it is carried out with solution at neutral pH. An interesting alternative to pure chitosan is TMC, a chitosan derivative. Two are the main differences between TMC and chitosan: TMC is water-soluble, and its positive charge is pH-independent. Its primary amine is trimethylated so the group is permanently protonated (figure 1-7). In the event of no efficacy of chitosan, choosing a material with different characteristics may be a good approach. TMC constant positive charge may help to obtain more reliable electrostatic bonds with microRNA. TMC was already tested as a transfection vector. SiRNA transfected using TMC silenced target mRNA by almost 45% in cancer cells in one study, and 30% in another study [352], [353].
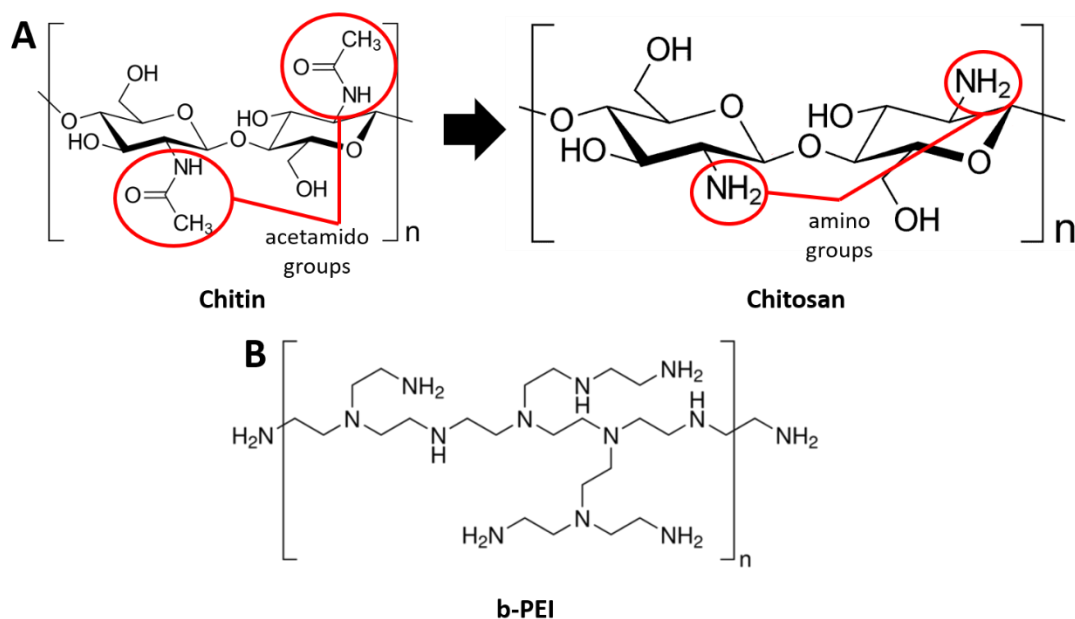
Figure 1-6: Chitosan and branched-PEI structures
A) Chitin chemical formula on the left, which is deacetylated to give chitosan on right. B) Branched-PEI chemical formula.

PLGA (figure 1-7) is biocompatible, biodegradable, hydrophobic, and not water-soluble. It is a copolymer of PGA and PLA, produced by chemical synthesis. It is FDA and European Medicine Agency-approved material for drug delivery [354]. PLGA shows good versatility. PLGA features can be regulated by tuning its molecular weight and its PGA/PLA ratio, such as degradation speed [355], [356]. PLGA-NPs have been successfully employed to deliver microRNA inhibitors to hepatocellular carcinoma cells, decreasing the target microRNA by almost 50%. Another research group managed to induce chondrogenesis in HMSCs by the administration of siRNA-loaded PLGA-NPs [357]. PLGA can be combined with other materials to increase its transfection efficiency, such as lipids. Cholesterol addition to PLGA-NPs formulations increased 2-fold the transfection efficiency compared to simple PLGA-NPs [358]. In a different study, DOTAP was used to create PLGA-hybrid NPs – PLGA/DOTAP 75/25 w/w. SiRNA delivered with these NPs was 63% more effective in its target knockout than pure PLGA-NPs [359]. PLGA-NPs can also be functionalized with peptides or other moieties to target specific membrane proteins. REDV-functionalized PLGA-NPs were produced to target ECs. Indeed, the REDV peptide is specifically recognized by the integrin α4β1 on ECs. PLGA-NPs functionalized with this peptide showed a significantly higher uptake compared with non-functionalized PLGA-NPs [360]. Octa-arginine is one of a series of peptides used to favor NPs cellular uptake, called cell-penetrating peptides.

PLGA-NPs functionalized with octa-arginine increased NPs uptake by 50-70% in canine kidney cells compared to non-functionalized PLGA-NPs after 1.5h from incubation [361].
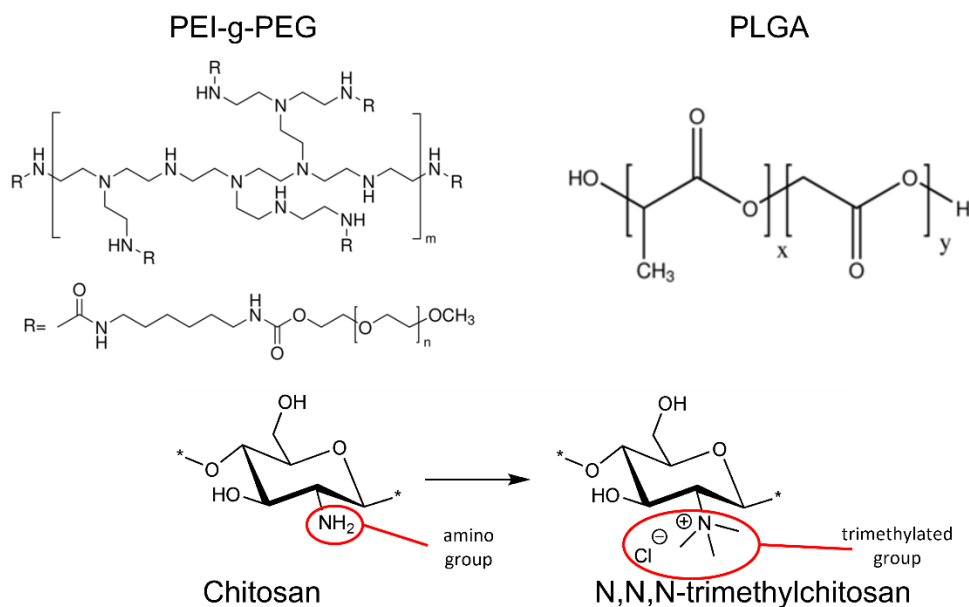
Figure 1-7: PEI-g-PEG, PLGA, TMC structures

1.6 Scaffold fabrication methods

Regenerative medicine requires biodegradable and biocompatible scaffolds. They should have high porosity with interconnected pores to favor cell colonization. In addition, each scaffold application has its own requirements in terms of mechanical properties, surface chemistry, and topology. Many fabrication techniques have been developed or adapted for TE purposes, such as particulate leaching, gas foaming, freeze-drying, membrane lamination, electrospinning, self-assembling, temperature-induced phase separation, and additive manufacturing. Table 1-2 summarized the main scaffold manufacturing techniques with their advantages and drawbacks [362], [363].

Fabrication technique	Advantages	Drawbacks
Solvent casting/ particulate leaching	Control over porosity Pore size and crystallinity	Limited mechanical property Residual solvents and porogen material

Porogen leaching	Controlled over porosity and pore geometry	Inadequate pore size and pore interconnectivity
Gas foaming	Free of harsh organic solvents Control over porosity and pore size	Limited mechanical property Inadequate pore interconnectivity
Self-assembly	Control over porosity Pore size and fiber diameter	Expensive material Complex design parameters
Electrospinning	Control over porosity Pore size and fiber diameter	Limited mechanical property Pore size decrease with fiber thickness
Phase separation	No decrease in the activity of the molecule	Difficult to control precisely scaffold morphology
Rapid prototyping	Excellent control over geometry and porosity No supporting material required	Limited polymer type Highly expensive equipment
Fiber mesh	Large surface area for cell attachment Rapid nutrient diffusion	Lack the structural stability
Fiber bonding	High surface to volume ratio High porosity	Poor mechanical property Limited applications to other polymers
Melt molding	Independent control over porosity and pore size	Required high temperature for non-amorphous polymer
Membrane lamination	Provide 3D matrix	Lack of required mechanical strength Inadequate pore interconnectivity
Freeze drying	High temperature and separate leaching steps are not required	Small pore size and long processing time

Table 1-2: Principal fabrication techniques for tissue engineering
Adapted from Subia et al "Biomaterial scaffold fabrication techniques for potential tissue engineering applications", Intechopen, 2010, doi: 10.5772/8581.

1.6.1 Electrospinning

Electrospinning is a very attractive technique since it allows to create fibers with sizes between a few nanometres to microns using a plethora of materials, mainly polymers - chitosan, collagen, gelatin, PCL, PLGA. PU, PTFE, silk fibroin, PEG, PGS, PS, PVC, PP, and many others. Indeed, this method can be employed with materials that can be reduced to the liquid state through either heat (melt electrospinning) or solvents. The material molecular weight must be enough to allow sufficient chain entanglement to create continuous fibers rather than separated droplets. In

addition, the electrospinning solution must have an appropriate dielectric constant. Perfectly insulating solutions will not allow charges to move in it and no material jet will be generated. On the other hand, if the electrospinning solution is too conductive, the material jet will not be stable enough to produce fibers. Blending and doping with different compounds allows the incorporation of materials that could not be electrospun alone, further broadening the variety of materials that can be integrated into an electrospun mat. Once optimized, electrospinning is relatively simple and multipurpose and does not require expensive machines or highly trained personnel [364]–[366].

Electrospinning allows the production of a nanofibers mat with randomly oriented or aligned fibers. Moreover, the scaffold can have high porosity (>80%) with interconnected pores, ideal for cell colonization since it resembles the ECM [367]. These properties make the method very popular in regenerative medicine. Electrospun scaffolds have a high surface-to-volume ratio, which facilitates drug absorption and delivery [368]. If the drug is absorbed on the scaffold surface, the release will be concentrated in a limited time following the implantation. The drug can also be incorporated into the electrospinning solution together with a biodegradable material, resulting in drug release that follows the material degradation dynamics [369], [370]. The mechanical properties of an electrospun scaffold can be tuned through the countless combinations of the available materials and solvents [371].

The electrospinning working principle is described in the Materials and Methods section.

2   Project aims

The study aimed to create a scaffold employable for heart valve regeneration. The scaffold should be able to take on the heart valve duty and guide a native valve regeneration at the same time. Eventually, the scaffold should degrade completely, but not before the newly generated tissue is able to function correctly. The regeneration of the native-like valve should provide an AVR solution without the flaws of the prostheses currently employed in clinical practice. Mechanical valves bear the permanent risk of thromboembolism and bleeding as a consequence of lifelong anticoagulation therapy (see paragraph 1.2.1). A construct that leads to the formation of a continuous endogenous endothelial lining (which is the most appropriate surface for blood contact known so far [372]) in the shortest time possible, should only expose the recipient to these risks for a limited time [373], [374][375]. In addition, this TEHV product should not bear the risk of degeneration and calcification that xenogenic bioprostheses are suffering from (see paragraph 1.2.2), once an endogenous endothelial lining is formed.

The addition of active biomolecules to the scaffold to accelerate the scaffold's endothelialization will be explored in this project. MicroRNAs can impact different cell functions, including migration and proliferation. My hypothesis (in accordance with my supervisors) is that a temporary enhancement of these functions can help to increase the endothelialization pace. Several TEHVs have been designed, but no one makes use of the microRNA therapeutic potential, to the best of my knowledge. However, RNA interference has already been shown to be beneficial to tissue-engineered grafts in experimental settings. For instance, a microRNA-126-functionalized electrospun scaffold showed improved endothelial cells adhesion and proliferation compared to a non-microRNA-functionalized scaffold [376]. Also, some microRNAs such as microRNA-130 or microRNA-9, are involved in EMT modulation. If appropriately used, these microRNA could induce valve interstitial cells-like phenotype from endothelial cells, allowing to generate the two main valve populations from nearby aortic ECs or circulating endothelial progenitor cells [377], [378]. Eventually, the selection of one or more microRNAs to locally administer during valve regeneration may contribute to its success, and speed up the formation of a complete endothelial coating in particular. Embedding the microRNA hsa-mir-132-3p in the TEHV may stimulate migration and proliferation of colonizing cells – details supporting this hypothesis are exposed in section 1.5.

As a proof-of-concept, this project is focused on proving that it is possible to functionalize a composite scaffold made of PCL and GL with microRNA. The microRNA should be released by the scaffold continuously for several days. ECs seeded on the scaffold should uptake the

microRNA released by the scaffold; the uptaken microRNA should have a pro-endothelialization effect on seeded cells.

This project was dived into three lines of work, each of which is described in one of the three main sections of the results and discussion chapter, to achieve three main targets:

- Select a microRNA with pro-endothelialization effects, like migration and proliferation.
- Select a vector that can protect the microRNA from blood nucleases and facilitate microRNA entrance into ECs.
- Design and fabricate a tri-layered scaffold able to substitute the native valve, host therapeutic microRNA, and make it available to colonizing ECs.

The flow chart in figure 3-1 is a graphical summary of the work done to achieve these milestones, including original plans, faced issues, and contingency actions realized to solve them.
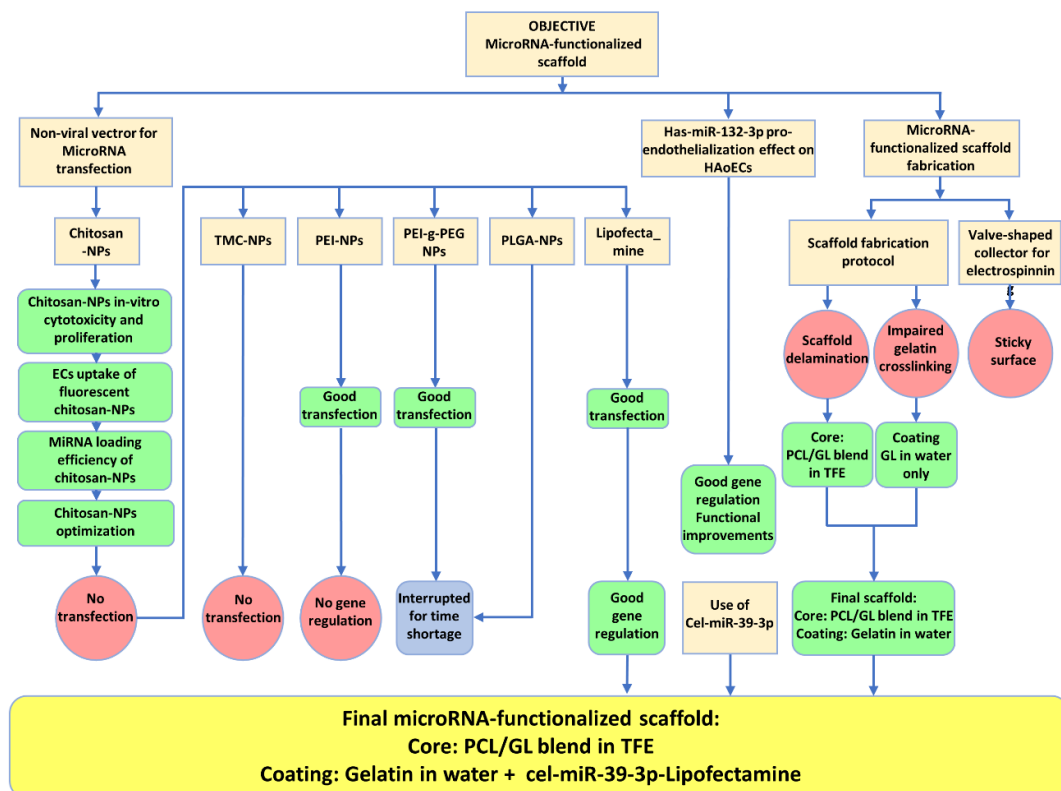
Figure 2-1: Flow-chart summarizing the development of the scaffold for heart valve reconstruction

Pale-yellow boxes represent aspects of the scaffold to develop and materials to test. Green boxes are the solutions found or the positive outcome of tested materials. Red circles represent negative outcomes. The blue box means that the employment of that solution was interrupted because of a lack of time.

A detailed outline of the path to achieve each objective is presented in the following paragraphs.

2.1 Hsa-mir-132-3p pro-endothelialization effect on aortic endothelial cells

In accordance with my supervisors, we have selected hsa-miR-132-3p as a candidate microRNA to stimulate valve endothelialization. Indeed, several publications are showing the angiogenic effect of hsa-miR-132-3p both secreted by nearby cells (paracrine effect), and administered by transfection [277], [285]. However, this is not exactly the project's aim, especially if it is considered that valves are not vascularized. Nonetheless, we hypothesized that hsa-miR-132-3p could stimulate ECs to migrate and proliferate (two functional aspects related to angiogenesis) and thereby accelerate the process of valve endothelialization. See paragraph 1.5.3 for more details.

In this part of the project, HAoECs were transfected with hsa-mir-132-3p using Lipofectamine RNAiMAX – a commercial non-viral transfection agent already successfully tested on endothelial cells [379]. The objective was to verify if hsa-mir-132-3p transfection enhances migration and proliferation.

2.2 Non-viral vector selection for microRNA transfection

Therapeutic delivery of free (naked) microRNA has limited applications - detailed in paragraph 1.5.4. Viral vectors seem not appropriate for this application due to still debate safety concerns. Also, virus confinement to a specific location (the aortic valve replacement site in the current case) has not been demonstrated yet, to the best of my knowledge – more details in paragraph 1.5.4. Thus, non-viral vectors are more appropriate for this project.

Chitosan-NPs were tested first as they seemed the most suited vector for this project. Biocompatibility and transfection efficiency of chitosan-NPs has been repeatedly demonstrated – see paragraph 1.5.5. Besides, the scaffold manufacturing process that I was planning to implement was based on GL dissolved in a water solution and electrospun to create a nanofibers mat. Therefore, non-water-soluble NPs would be appropriate to avoid the encapsulation of naked microRNA in the scaffold, which would be degraded as soon as it was getting in contact with blood nucleases [380]. Chitosan is soluble in water at acidic but not at a neutral pH; hence chitosan-NPs should not risk dissolving during scaffold production [381].

Initially, a fabrication protocol calibration was carried out. To my knowledge, there is no consensus on the best NPs diameter for microRNA transfection. In the majority of the reviewed literature on the topic, NPs diameter is ranging between 100nm and 600nm [382]–[384]. Under the hypothesis that smaller NPs - at least less than 500 nm of diameter – can be uptaken (through macropinocytosis, clathrin-mediated endocytosis, caveolae-mediated endocytosis, and clathrin- and caveolae-independent endocytosis [385]–[392]) by non-phagocytic cells like ECs, four manufacturing parameters were sequentially calibrated to obtain the smallest NPs – paragraph 4.3.2.1. These were: chitosan concentration, crosslinker (TPP) concentration, Chitosan/TPP mass ratio, and NaCl (adjuvant) concentration; which emerged to influence NPs size in the literature [393]–[395]. Other parameters could have been considered, such as stirring speed, rate of TPP/microRNA addiction to the chitosan solution, and chitosan solution pH. Tuning of additional production parameters would have been included in case an NPs' diameter of around 200 nm was not achieved with the optimization of the considered parameters. However, limiting this optimization phase was also essential. The more time would have been spent on chitosan-NPs characterization, the higher would have been the risk of running out of time before achieving all the essential goals to complete the project, especially because this was one of the first steps of a long and complex project. Following, EA.hy926 were used to test the effect of chitosan-NPs on ECs viability and proliferation in a simulated transfection – there was no microRNA loaded on chitosan-NPs, paragraph 4.3.2.2. The experiment was repeated by loading different amounts of microRNA in chitosan-NPs to test the potential impacts of the microRNA itself on proliferation and viability – paragraph 4.3.2.3. Then, the chitosan-NPs uptake by EA.hy926 was checked using fluorescent (FITC-conjugated) chitosan-NPs. Trypan Blue was employed to quench fluorescent NPs that were not internalized by ECs. Indeed, Trypan Blue is a FITC quencher and cannot penetrate live cells, thus only NPs inside live cells would have preserved their fluorescence – see paragraph 4.3.2.4 for details.

The following passage towards validation of chitosan-NPs as microRNA vector was to measure the percentage of initial microRNA loaded in NPs, namely the loading efficiency. To do so, RT-qPCR was the chosen assay as it is routinely used for microRNA quantification in cell and tissue extracts. Chitosan, the NPs' main constituent, is a cationic polysaccharide. It is renowned that polysaccharides (abundant in plants) may cause problems with RNA extraction – see details in paragraph 4.3.3.1. Thus, I compared a general-purpose RNA extraction kit (Qiagen RNA extraction kit, Qiagen, Netherlands), a plant-specific extraction buffer (CTAB-based), and a plant-specific RNA extraction kit (Plant microRNA purification kit, Norgen, Canada). In addition, I attempted to measure chitosan-NPs microRNA loading efficiency by estimating the non-

embedded fraction. The vast majority of the reviewed published works used centrifugation to concentrate the NPs, and the analyzed the micro-RNA amount in the supernatant and/or in the NPs pellet [396]–[399]. Free-non-embedded microRNA measurement in the supernatant of NPs suspension would have been a fast and cheap solution. A frequently used method is to centrifuge NPs at the bottom of a container and assay NPs-free supernatant. Another option is dialysis. It is much more gentle than centrifugation and represents an alternative to it. The dialysis principle is simple: two solutions are separated by a permeable membrane which allows passage of molecules under a certain size. Solutes or water are driven across the membrane by osmotic pressure. In this project, free microRNA should cross the dialysis membrane while chitosan-NPs should stay confined inside. Having a suitable ΔMw between the component to separate and choosing a dialysis membrane with the right MWCO is mandatory to perform dialysis properly – the relevant calculations are in paragraph 4.3.3.3. Centrifugation and dialysis were employed in the attempt to separate chitosan-NPs from free microRNA in the production solution– paragraphs 4.3.3.2 and 4.3.3.3. Since the aforementioned methods to measure chitosan-NPs microRNA loading efficiency failed, a chitosan enzymatic digestion method was chosen to degrade chitosan and make NPs-embedded microRNA available for RT-qPCR – paragraph 4.3.3.4. However, after chitosan enzymatic digestion, microRNA embedded in NPs would have been freed and mixed with non-embedded-microRNA, making it impossible to estimate the chitosan-NPs microRNA loading efficiency. Previous attempts (centrifugation and dialysis) to separate the two microRNA fractions failed. Thus, it was decided to estimate the amount of *protected microRNA*, incubating microRNA-loaded chitosan-NPs in 10% FBS for one hour before microRNA extraction. It is reasonable to assume that not only free microRNA is degraded during FBS incubation, but also that FBS can penetrate NPs and degrade microRNA strands closer to the NPs surface. However, microRNA that degrades in physiological fluids after just one hour would be hardly likely uptaken by cells during transfection. Indeed, commercial transfection protocols usually recommend a four-hour transfection. Therefore, the amount of microRNA extracted after one hour of FBS incubation is a useful estimation of the microRNA amount that would be presented to cells in a transfection experiment, even if not optimal. In this setup, it is important to neutralize serum nucleases before the chitosan enzymatic digestion starts; otherwise, all microRNA freed from chitosan-NPs would have been degraded as soon as it was getting in contact with the FBS solution. In paragraph 4.3.3.4.1, the nucleases neutralizing potential of RNAse inhibitor was tested. Then, a complete protocol including microRNA-loaded chitosan-NPs exposition to 10% FBS for 1 hour, RNAse inhibition, chitosan enzymatic extraction, and microRNA isolation was optimized - paragraph 4.3.3.4.2. Given the low amount of *protected*

microRNA, I tested additional variations on the chitosan-NPs fabrication, such as variation of chitosan concentration, microRNA concentration, and NaCl elimination, in the effort to increase the amount of protected microRNA after incubation with 10% FBS for one hour – paragraph 4.3.3.5. After the chitosan-NPs characterization and fabrication protocol tuning, the microRNA transfection efficiency using chitosan-NPs was tested – paragraph 4.3.4. EA.hy926 cells (immortalized ECs derived from HUVECs – see materials and methods) have been employed in all experiments involving cells described in sections 4.3.2 and 4.3.3. This was done to save budget and speed up the project. Indeed, EA.hy926 culture media costs 1/5 the HAoECs media. Also, EA.hy926 grow faster and in higher numbers, and can be cultured up to 100 population doublings – see paragraph 3.2.1. Promocell guarantees its HAoECs up to 15 population doublings, at the cost of £800/500000 cells. However, doubts about the transferability of my results on primary human ECs were raised. Therefore, I decided to use primary aortic ECs (HAoECs) to prevent concerns about the translationality of my work. In fact, ECs from the aortic tract are supposed to be one of the main sources of cells that could colonize the aortic valve scaffold (aortic valve scaffold colonization and potential cell sources have been discussed in paragraph 1.3.3). Therefore, the transfection efficiency experiment was carried out on commercially available primary HAoECs. Lipofectamine RNAiMAX is broadly used as a microRNA non-viral vector [379]; thus, I took it as the benchmark for the transfection efficiency of chitosan-NPs.

The negative result of microRNA transfection to HAoECs by chitosan-NPs forced us to look for an alternative transfection vector. It would have been interesting to understand why chitosan-NPs were not working, but it was imperative to progress in the project. Thus, I activated a contingency plan consisting of switching to a different transfection vector. Four non-viral vectors were considered - PEI, PEI-g-PEG, TMC, PLGA. As the time to complete the project was reducing, the vector selection process was changed. PEI, PEI-g-PEG, and TMC were immediately tested for transfection relying on published protocols without NPs characterization – paragraphs 4.3.5.1 and 4.3.5.3. PLGA required a manufacturing protocol calibration. After a first trial, PLGA-NPs development was suspended with the intention to get back to it in event that all other alternatives failed to transfect microRNA to HAoECs – paragraph 4.3.5.2. PEI gave the best transfection performances, thus PEI-mediated hsa-mir-132-3p transfection effects (in terms of viability, membrane damage, proliferation, and migration) on HAoECs were tested – paragraph 4.3.5.4. As proliferation and migration enhancements were noticed in HAoECs transfected with hsa-mir-132-3p using Lipofectamine, the expectation was to see the same effects using PEI-NPs as a microRNA vector. This would have been proof that PEI-NPs were delivering functional

microRNA, able to fulfil its RNAi duty. Thus, proliferation and migration assays on hsa-miR-132-3p-transfected HAoECs using PEI were performed and compared with HAoECs transfected with lipofectamine. Also, it was decided to test possible PEI-induced cytotoxic effects by performing membrane integrity assay (LDH assay) and viability assay. LDH assay consists of the measurement of lactate dehydrogenase released in culture media, which is an indication of membrane damage. In fact, an intact plasma membrane is LDH impermeable. If an excess of LDH is measured in the culture media, it means that the cellular membrane is damaged. This test is particularly appropriate to assess the cytocompatibility of transfection agents because when microRNA-vector complexes cross the membrane to access cell cytosol they can cause membrane perturbations. Ideally, the transfection process should not damage the cellular membrane permanently. Performed together, LDH and live & dead can give a good insight into transfection vectors' potential damages. PEI-mediated transfection of hsa-mir-132-3p did not show the expected proliferation and migration enhancement as observed with Lipofectamine-mediated one. Thus, it was decided to investigate the regulatory effect at the translational level. A panel of potential hsa-miR-132-3p potential targets involved in cell proliferation and migration was selected by bioinformatic analysis. Then, the expression of these genes was measured before and after hsa-mir-132-3p transfection using PEI and Lipofectamine as vectors – paragraph 4.3.5.5.

2.3 MicroRNA-functionalized scaffold fabrication and preliminary tests

The final and most important part of the project is the production and test of the microRNA-functionalized scaffold. The main aims of this section are to fabricate the tri-layer scaffold in which the external layers contain the microRNA-vector complex; verify the microRNA sustained release by the scaffold; and assay if HAoECs seeded on the scaffold uptake the microRNA released by the scaffold. Among all the non-viral vectors tested, Lipofectamine RNAiMAX was the only one able to ensure downregulation of the selected proliferation- and migration-related genes by hsa-miR-132-3p. This is also reflected in the enhancement of proliferation and migration of hsa-miR-132-3p-transfected HAoECs – see paragraphs 4.2, 4.3.5.4, and 4.3.3.5. Thus, it was chosen to integrate hsa-miR-132-3p-Lipofectamine lipoplexes into the GL layer of the TEHV scaffold designed in this project. Included in GL fibers, microRNA-vector complexes will not be exposed to serum nuclease from the moment of the scaffold implantation as if they were adsorbed on the surface or injected. GPTMS-crosslinked GL fibers degrade completely in

around 18-21 days from previous tests performed in my research group [400]. During GL degradation, microRNA will be continuously released on-site as if it was freshly locally injected. Ideally, first colonizing ECs (either circulating cells or cells or nearby cells from the aortic endothelial linen) would be transfected with the scaffold-embedded microRNA. That should enhance cell proliferation and mobility for a few weeks, in the effort of creating a complete endothelial layer on a wide non-cellularized area – namely the non-cellularized heart valve scaffold implanted to substitute the native heart valve. I do not know if 18-21 days are sufficient to provide the scaffold with a therapeutical advantage. However, as this is a proof-of-concept study, it is important to demonstrate the feasibility of an approach; tuning and optimization can be the subjects of following projects. In addition, the relatively short GL degradation time allowed more time to test the aforementioned hypotheses and apply protocols corrections throughout the project. GL is also an excellent substrate for cell adhesion as it has plenty of RGD groups that are recognized by cells' integrins [157].

A core of electrospun PCL will provide mechanical support. PCL has been extensively utilized to produce scaffolds in our laboratory, and electrospinning protocols were developed. TEHVs have already been developed using pure PCL, blended PCL, and composite material in which PCL is present. [401], [402]. It is a good candidate as a support material because of its mechanical support layer, biocompatibility, and durability [403]–[405]. Its degradation time is between 2 and 4 years [406], the time during which the host organism should regenerate the explanted valve. PCL-based valves have been successfully tested in pulse duplicators simulating both aortic and pulmonary valve conditions [403], [407], [408]. Therefore, PCL was selected to produce the scaffold support layer. Possible PCL blending with other materials – e.g PCL/gelatin blends [409]- may be considered to improve mechanical properties, tune degradation rate, or solve other issues that may arise during the development. Two layers of GL crosslinked with GPTMS and doped with microRNA-vector complexes will be laid on both sides of the PCL sheet by electrospinning as well. In this way, the requirement of a sufficient scaffold durability would not conflict with the tuning of the microRNA-functionalized layer degradation speed, in order to have an appropriate microRNA release dynamic for its therapeutical purpose.

The use of a valved-shaped electrospinning collector to create scaffolds in their final shape was tested. The advantage would be that no need for scaffold stitching into the proper shape should be required as it happens with decellularized animal tissue sheets. The valve scaffold would have the shape of the 3D model from which the electrospinning collectors would be created. Using medical images, the valve construct could be customizable on the patient's anatomic features, avoiding cases of size mismatch of current prostheses [410]. The development of a valve-shaped

electrospinning collector is discussed in paragraph 4.3.1. For this initial trial, a leaflet 3D model was downloaded online. The final aim is to create a patient-specific valve 3D model from medical imaging, but the customized collector fabrication pipeline was tested using available online models. Using 3D printing, the collector was printed in PLA - a plastic material. Then, an electrically conductive surface (essential for electrospinning) was laid on the surface by chemical electroplating. Scaffold production with this new collector type was tested.

Then, the focus moved to the scaffold production itself. The entire scaffold production protocol was calibrated – paragraph 4.4.2. Tests were performed using a solution of GL dissolved in different solvents mixtures of distilled water and NMP. The use of NMP was required to obtain a solution suitable for electrospinning at RT since GL in water only is solid at RT. Moreover, the GL solution must have neutral pH. MicroRNA-loaded chitosan-NPs were supposed to be incorporated in the GL solution, and chitosan is soluble at acidic pH. Thus, the preparation of pH-neutral GL solution is a prerequisite to avoid damages to the microRNA-loaded chitosan-NPs during the scaffold fabrication. For this reason, acid GL solvents, such as acetic acid, should have been avoided. NMP seemed a suitable solution as it is an organic dipolar aprotic solvent miscible with water [411]. The scaffold was dried in a custom-made vacuum oven – see paragraph 3.6.2.2. NMP boiling point is at 202°C under atmospheric pressure and it is toxic. However, a vacuum oven able to pull the pressure below 293 mbar reduces the NMP boiling temperature to 0°C.

During scaffold observation in wet conditions, fast GL layer dissolution was noticed. GPTMS crosslinking of GL has never been an issue in previous works, when water/acetic acid or water only were utilized as solvents to create GL electrospun mats. The most plausible hypothesis was that NMP was interfering with GPTMS crosslinking. Given the lack of literature reports on GPTMS-crosslinked GL scaffolds using solvents other than water and acetic acid, it was decided to use water only to produce the GL layer. Restoration of GPTMS crosslinking efficacy was mandatory to grant previously measured GL layer duration in wet conditions - 18-21 days. Thus, modifications to the GL layer manufacturing protocol were made – paragraph 4.4.2.1. To allow electrospinning of GL in water solution, the electrospinning system was fitted with a system that regulates temperature and relative humidity. An additional scaffold issue was noticed. The scaffold was delaminating, PCL and GL layers were separating. Thus, it became necessary to modify the PCL layer fabrication protocol – paragraph 4.4.2.2. PCL is hydrophobic while GL is hydrophilic. While the PCL layer tends to minimize its contact with water, the GL layer absorbs water and swells in wet conditions. The different nature of the two materials is likely to be the cause of the scaffold delamination. Delamination risk is not acceptable for this application.

Therefore, it was decided to change the core layer formulation, and substitute PCL only with a PCL/GL blend. The new hydrophilic core layer should have similar properties to the GL coatings [412], [413]. This formulation change will provide the scaffold with a stronger bond between the scaffold's layers, and hopefully avoid delamination.

The next passage in the scaffold development was to demonstrate the achieved microRNA-functionalization of the scaffold, and the sustained release of microRNA during GL layer degradation. Proofs supporting that the microRNA vector was embedded in the GL layer were shown using fluorescence microscopy (vectors were previously functionalized with FITC) and SEM – paragraph 4.4.3. The microRNA sustained release was tested by measuring the microRNA content of PBS incubated with a scaffold section and sampled periodically – paragraph 4.4.4.

The last step was showing that cells seeded on the microRNA-functionalized scaffold uptake the microRNA released by the scaffold itself during GL degradation. As a prerequisite, it was mandatory to have an efficient protocol to detach cells from the scaffold. Cell detachment from scaffolds is not an easy (usually overlooked) task like detaching cells from culture plastics. Also, it is hard to find a cell detachment protocol applicable to different scaffold types. Hence, I had to optimize a protocol suitable for the combination of cells and scaffold I have employed in my project. This passage should not be underestimated as it is not simple to detach a good number of cells without killing them from scaffolds, as I experienced in a study in which I collaborate [414]. In all protocols, EDTA incubation was intended to remove all Ca^{2+} and Mg^{2+} that may have been accumulated in the scaffold and hamper detaching enzymes' work. Its role is to chelate Ca^{2+} and Mg^{2+}, which facilitates cell adhesion on a substrate [415]. RT-qPCR was chosen to investigate the cell uptake of the microRNA released by the scaffold. However, a minimum amount of total RNA extracted from detached cells is needed to perform RT-qPCR. From reverse transcription kit guidelines (TaqMan MicroRNA Reverse Transcription Kit, Thermo Fisher, USA), a minimum of 6 ng/uL of total RNA in the extract is needed to perform reverse transcription, and produce the cDNA for RT-qPCR. The RNA extraction is performed using the miRNeasy Micro Kit (Qiagen, Germany), and it should be eluted in 14 μL of RNAse-free water. Thus, a minimal amount of cells detached from the scaffold from which extract the RNA is needed, since the elution volume and the minimal concentration are fixed. Actually, the microRNA concentration in the extract should be more than the bare minimum. This allows to assay additional targets, such as the hsa-mir-132-3p target genes, from the same samples. Therefore, different cells detachment protocols were compared, and the one which yields more live cells was selected - paragraph 4.4.5. The final experiment tests if the scaffold-released microRNA is uptaken by the ECs seeded on it using materials and protocols developed so far – paragraph 4.4.6.

3 Materials and methods

3.1 Materials

All the materials used in this project are summarized in table 3-1.

Material name	Catalogue number	Manufacturer
Cel-miR-39-3p	N/A (custom)	Eurofins, Germany
Cyanine 5 (Cy5)-functionalized cel-miR-39-3p	N/A (custom)	Eurofins, Germany
Low molecular weight chitosan	448869-50G	Merck, Germany
Chitosanase from Streptomyces Griseus	C9830	Merck, Germany
Accutase	A6964	Merck, Germany
Branched PEI Mw=25 kDa	408727	Merck, Germany
Hydroxyurea	H8627-1G	Merck, Germany
PLGA Resomer RG 503	739952	Merck, Germany
NaCl	S9888	Merck, Germany
CTAB	H6269-100G	Merck, Germany
Spermidine	85558-1G	Merck, Germany
PVA Mw= 13-23 kDa	363170-25G	Merck, Germany
PVP40	PVP40-50G	Merck, Germany
Tris-HCl pH 8.0	PPB010	Merck, Germany
EDTA pH8.0	E9884-100G	Merck, Germany
β-mercaptoethanol	444203-250ML	Merck, Germany
Glycine	G8898-500G	Merck, Germany
CuSO4	451657-10G	Merck, Germany
PEG	P2139-500G	Merck, Germany
H2SO4	4803641000	Merck, Germany
Gelatin type A from porcine skin	G1890	Merck, Germany
Amicon Ultra centrifugal filters MWCO=100 kDa	UFC910008	Merck, Germany
Sodium tripolyphosphate	238503	Merck, Germany
CBR	Sc-214719	Santa Cruz, USA
TrypLE Express Enzyme	12605010	Thermo Fisher Scientific, USA
Pierce LDH Cytotoxicity Assay kit	88953	Thermo Fisher Scientific, USA
mirVana Hsa-miR-132-3p mimic	4464066	Thermo Fisher Scientific, USA
mirVana miRNA mimic negative control	4464058	Thermo Fisher Scientific, USA
Click-iT EdU Cell Proliferation Kit	C10338	Thermo Fisher Scientific, USA
TaqMan MicroRNA Reverse Transcription Kit	4366596	Thermo Fisher Scientific, USA
High Capacity RNA-to-cDNA Kit	4387406	Thermo Fisher Scientific, USA
TaqMan Fast Universal PCR Master Mix	4364343	Thermo Fisher Scientific, USA
TaqMan MicroRNA Assays	4427975	Thermo Fisher Scientific, USA
TaqMan mRNA Assays	4331182	Thermo Fisher Scientific, USA
Ambion RNase inhibitor	AM2682	Invitrogen, USA
Lipofectamine RNAiMAX	13778075	Invitrogen, USA
MiRNeasy Micro Kit	217084	Qiagen, Germany
AllStars Negative Control siRNA	1027280	Qiagen, Germany
DCM	84534.550	Avantor, USA
Plant microRNA Purification Kit	54700	Norgen, Canada

Regenerated cellulose dialysis tubes MWCO 140 kDa	44560.01	Serva Electrophoresis, Germany
Repligen Float-A-Lyzer MWCO 50kDa	G235070	Spectrum chemicals, USA
Repligen Float-A-Lyzer MWCO 300kDa	G235060	Spectrum chemicals, USA
DMEM (low glucose, GlutaMAX(TM), pyruvate)	10567014	Gibco, USA
FBS HI	10500.064	Gibco, USA
0.5% Trypsin-EDTA	15400054	Gibco, USA
Dulbecco's PBS	14190094	Gibco, USA
Opti-MEM reduced serum medium	11058021	Gibco, USA
HAoECs	C-12271	Promocell, Germany
Cryo SFM	C-29910	Promocell, Germany
EGM MV2	C-2212	Promocell, Germany
Immortalized HUVECs	EA.hy926	Donated
Viability/Cytotoxicity Assay Kit	30002	Biotium, USA
FITC	90020	Biotium, USA

Table 3-1: List of materials used in this project

3.2 Cell biology methods

3.2.1 Immortalized endothelial cells (EA.hy926) culture

The human umbilical vein cell line (EA.hy926) is a commercial established cell line. Cells can be cultured up to 100 population doublings, maintaining several ECs' functions. They are positive for typical endothelial antigens, such as Von Willebrand factor, GMP-140, prostacyclin, platelet-activating factor, tissue plasminogen activator, and plasminogen activator inhibitor type I, thrombomodulin, vitronectin receptor. EAhy926 possess Weibel-Palade bodies in their cytoplasm and tissue-specific organelles. Finally, EAhy926 maintains differentiated endothelial cell functions such as angiogenesis, homeostasis/thrombosis, blood pressure, and inflammation regulation [416], [417]. Ea.hy926 were cultured at 37°C, 20% Oxygen, 5% carbon dioxide in 90% DMEM (with low glucose, GlutaMAX(TM) and pyruvate) and 10% fetal bovine serum (FBS).

3.2.2 Human Aortic Endothelial Cells culture

Commercial HAoECs were cultured at 37°C, 20% Oxygen, and 5% carbon dioxide in endothelial cell growth medium (EGM) MV2 culture media and used between passages 4-7.

3.2.3 Cell passage

Cells were passaged to larger culture surfaces at around 80% confluence. Cells were washed with PBS and incubated for 5 min in a solution of 0.05% (w/v) trypsin/ Ethylenediaminetetraacetic Acid (EDTA) to detach them from the culture surface. The trypsin activity was neutralized adding twice the trypsin solution volume of 10% FBS in PBS. Then, the cell suspension was centrifuged at 400 xg for 10 minutes to pellet the cells at the bottom of the tube. The supernatant was discarded and the cell pellet was re-suspended in 1 ml of culture media. Cells were counted using a Neubauer chamber and seeded in a new culturing plate at the desired density. When HAoECs were to be passaged, cells were incubated for 2 min in a solution of 0.05% (w/v) trypsin/EDTA, and the centrifuging will be at 220 xg for 2.5 minutes.

3.2.4 Cell cryopreservation and resuscitation

Cells were detached from the culture flask for the cell passage procedure. After detached cell suspension have been centrifuged, the supernatant was discarded and cells were resuspended in 0.5 or 1 mL of chilled (4°C) freezing media (Cryo SFM). Then, the cell suspension was poured into a cryotube vial and placed in a freezing container at -80°C. After 24h, the cryotube was transferred into a liquid nitrogen storage system.

To resuscitate the cells, the required aliquots were taken from the liquid nitrogen storage and rapidly thawed in a water bath at 37°C. Immediately after, the cryotube vial content was transferred to the culture container pre-filled with a proper amount of culture media.

3.2.5 MicroRNA transfection to Human Aortic Endothelial Cells

Cells were seeded in 96 well plates (culture area: 0.34 cm^2) at a density of 15000 cells/cm^2, and cultured until 80% confluence. Then, culture media was substituted with 50 μL of Opti-MEM and miRNA-NPs mix in order to reach a microRNA concentration of 25 nM. As reported in the literature, 25 nM is a common concentration for liposome-based transfection and used in several studies. MicroRNA-NPs suspension had a microRNA stock concentration of 250 nM hence this was diluted 1:10 in Optimem before adding to cells. Commercialized Lipofectamine RNAiMAX (Lipofectamine) was used as a gold standard. Lipofectamine is a lipid-based transfection vector. The RNAiMAX version of it is specific for siRNA and microRNA delivery into the cell cytoplasm, already been successfully tested with endothelial cells [379]. The

Lipofectamine's cationic lipids form a unilamellar liposomal structure that electrostatically binds the genetic material (slightly anionic) to transfect forming the transfection complex. The overall complex is positively charged and it is electrostatically attracted to the plasma membrane (negative charge). The lipid nature of Lipofectamine favors complex transport in the cytoplasm. Once in the cytoplasm, the transfection complexes move towards mRNA strands (this cytosolic trafficking phase is not clear and may be different for each lipid vector formulation) and finally interfere with mRNA translation [418], [419] (see paragraph 1.5.1). Lipofectamine transfected samples were compared with microRNA-NPs transfected samples. Liposomes with 25 nM of microRNA were created following the manufacturer's protocol and administered simultaneously to miRNA-NPs as a positive control. MicroRNA concentration of 25 nM for cell transfection is within the manufacturer's recommended concentration range, and it is also employed in several studies, as previously mentioned. After 4 hours, cells were washed with PBS and then incubated for 16 h in culture media.

3.2.6   Viability assay

Viability/Cytotoxicity Assay Kit (Biotium Inc, USA) was used to assay live and dead cells. Live cells' cytoplasm was stained in green, while dead cells' DNA was stained in red. The kit includes two components: Calcein AM and EthD-III. Calcein AM is a non-fluorescent esterase substrate that can enter the plasma membrane. Once inside viable cells, Calcein AM is cleaved by esterases to yield the green fluorescent dye Calcein, which cannot exit live cells as it is negatively charged as the plasma membrane. Consequently, viable cells with intact membranes retain green-fluorescent Calcein within their cytoplasm. EthD-III is a red-fluorescent DNA dye. It cannot cross the plasma membrane, so it does not stain viable cells' DNA with intact plasma membrane. Therefore, EthD-III stains only dead or dying cells with damaged membranes.
Reduced serum media was mixed with Calcein AM(1:2000 v/v) and EthD-III (1:500 v/v). Cells to stain were washed with PBS and incubated with Calcein AM/ EthD-III mix for 30 minutes at 37°C. Then, cells were washed with PBS and incubated with fresh reduced serum media. Cells were imaged using a fluorescence microscope.

3.2.7   Lactate dehydrogenase assay

The lactate dehydrogenase (LDH) assay was done using the Pierce LDH Cytotoxicity Assay kit (Thermo Fisher Scientific, USA). Pierce LDH Cytotoxicity Assay Kit is a colorimetric test that

estimates the amount of LDH in culture media. LDH is membrane impermeant, and not released by healthy cells. Only cells with interrupted membranes are releasing LDH. Thus, this is a method to understand whether cells have received damages to their membrane, as it may happen during transfection [420]; and a general indicator of cell health.

Cells underwent different treatments and a media sample was incubated with the LDH Assay kit reagents. The positive control is represented by cells incubated with a lysis reagent included in the assay. The LDH enzyme catalyzes a reaction cascade which eventually reduces tetrazolium salt to red formazan that can be measured at 490nm of wavelength. Briefly, 50 µL of culture media is added to 50 µL of the reaction mixture in a black-walled 96 well plate and left to react at RT for 30 min protected from light. Then, 50 µL of stop solution is added and the absorbance at 490 nm is measured using a plate reader. Cytotoxicity is calculated as follows:

$$\% \, Cytotoxicity = \frac{treated \; cells \; LDH \; activity - spontaneous \; LDH \; activity}{maximum \; LDH \; actvity - Spontaneous \; LDH \; activity} * 100$$

where spontaneous LDH activity is the activity expressed by LDH released by cells treated with 10% v/v sterile distilled water; maximum LDH activity is the activity expressed by LDH released by cells treated with 10% of included lysis buffer; treated cells LDH activity is the activity expressed by LDH released by cells treated with the compound to investigate.

3.2.8   Migration assay

A line gap in the cell monolayer was created at the center of the wells (96 well plate – 34 mm^2) by a single scratch through the monolayer with sterile 10 µL pipette tips. Then, cell monolayers were washed with PBS, and fresh culture media with 2mM hydroxyurea was added [421]. Hydroxyurea blocks cell mitosis; which ensures that the cells that closed the gap did migrate from beyond the gap border, instead of by cell proliferation. The gap closure was monitored by optical microscopy at specific time points, and the gap area was calculated using ImageJ image processing software.

3.2.9 Proliferation assay

Click-iT EdU Cell Proliferation Kit (Thermo Fisher Scientific, USA) was used to perform the proliferation assay. The kit detects proliferating cells by staining their DNA during DNA synthesis. 5-ethynyl-2´-deoxyuridine (Edu) is a nucleoside analog of thymidine, and it incorporates in replicating cells' DNA during DNA synthesis. Any replicating cell will incorporate Edu in its DNA as long as Edu is incubated in the cell culture. Once the observation window is ended, cells are fixed and Edu detection is carried out through a covalent reaction between an azide-functionalized fluorescent dye and the alkyne included in the Edu. Thus, cells that replicated during the observation window were stained by a fluorescent dye attached to Edu, which was incorporated into their DNA during their replication.

At the beginning of the observation window, half growth media was removed from the culture wells, and fresh media with Click-iT EdU Cell Proliferation Kit Component A at 20 µM was added to replace the removed volume, at the beginning of the observation period. The final Component A concentration in culture media was 10 µM. 24 and 48 hours after Component A incubation, cells were fixed with 4% Paraformaldehyde (PFA) and stained following the Click-iT EdU Cell Proliferation Kit manufacturer's protocol. Nuclei of cells that divided during the kit's Component A incubation were bound with it and became positive to the staining. In addition, 5 min incubation with 4', 6-Diamidino-2-Phenylindole, Dihydrochloride DAPI (30 nM) stained each nucleus, allowing to estimate the percentage of proliferating cells. Cell monolayers were imaged by a fluorescence microscope.

3.2.10 Cell detachment from scaffold

Colonized scaffolds were washed twice with PBS after discarding the culture media. Then, cells were incubated in 4mM EDTA in PBS (without Ca^{2+} and Mg^{2+}) for 5 min at 37°C on a plate shaker. The solution was discarded at the end of the incubation. Following, a detaching reagent was incubated at 37°C on a plate shaker:

- TrypLE for 10 minutes or 1h
- Accutase for 10 minutes or 1h
- Trypsin for 5 minutes or 15

After the incubation, the suspension was centrifuged at 220 xg for 2.5 minutes and the supernatant was discarded. Then, the cells are resuspended in fresh media and counted using a Neubauer chamber.

3.2.11 Cell count

Cells were suspended in fresh media. 20 μL of cell suspension was mixed with 20 μL of Trypan Blue. A glass coverslip was placed on top of a Neubauer chamber (figure 3-1A), and 10 μL of Trypan Blue/cells mix was injected in the gap between the top surface of the Neubauer chamber and the coverslip (figure 3-1C). Trypan blue was added to distinguish live from dead cells as it can cross only damaged plasma membranes. The cells found in the 4 large corner squares were counted, and the total was divided by four to obtain the average (figure 3-1B and D). The average was then multiplied by 20000 to obtain the number of cells per mL of suspension.
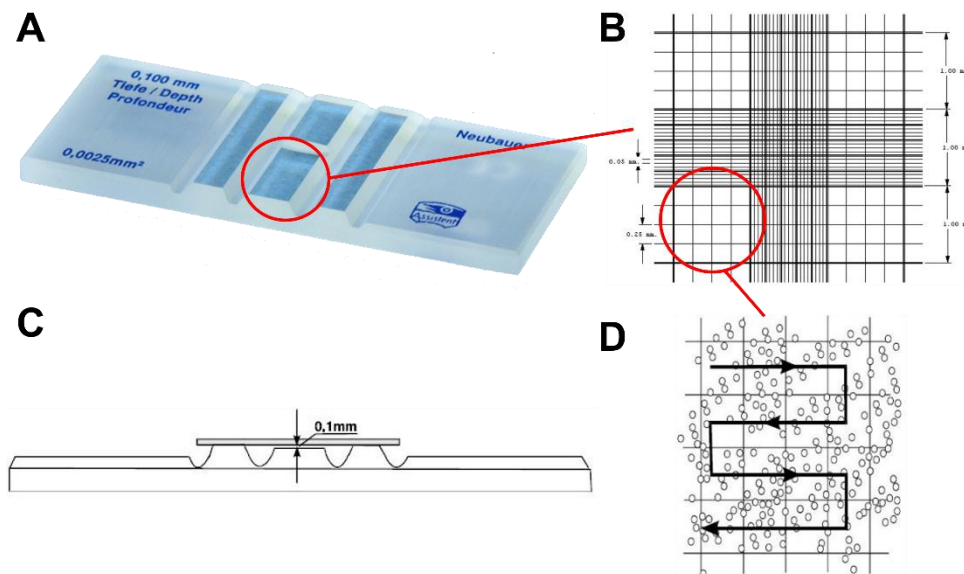
Figure 3-1: Cell manual counting
A) Image of a Neubauer chamber. B) Layout of the grid on the center of the chamber face is highlighted in figure A. C) Lateral profile of the chamber to highlight the gap in which the cells/Trypan blue mix was injected. D)Example of counting pattern in one of the four corner squares.

3.3   Molecular biology methods

3.3.1   Total RNA extraction

Total RNA was extracted using a miRNeasy micro kit from Qiagen. RNA concentration and purity were verified with the NanoDrop 2000 Spectrophotometer (Thermo Fisher Scientific). Where needed, the Cetyltrimethylammonium Bromide (CTAB) -based lysis buffer substituted the manufacturer's lysis buffer.The CTAB-based buffer was prepared mixing the following reagents in RNAse-free water: 2% w/v CTAB, 2% w/v polyvinylpyrrolidone (PVP) 40, 1.4 M NaCl, 100 mM pH=8.0 Tris-HCl, 20 mM EDTA, and 1.0 % v/v beta-mercaptoethanol [422], [423].The buffer was stored in the fridge and warmed to 65°C in a water bath before use. Norgen Plant microRNA Purification Kit was used where indicated following the manufacturer's protocol. Then, the extracted microRNA was stored at -80°C.

3.3.2   MicroRNA Reverse Transcription and Real-Time quantitative Polymerase Chain Reaction (RT-qPCR)

The TaqMan MicroRNA Reverse Transcription Kit (Life Technologies) was used with specific microRNA primers (listed below) to obtain the microRNA's complementary DNA (cDNA). MicroRNA retro transcription mix components and amounts are detailed in table 3-2, while microRNA assays are in table 3-3. MRNA retro transcription was performed using a High Capacity RNA-to-cDNA Kit Retro transcription kit. MRNA mix components and amounts are detailed in table 3-2. RT-qPCR was performed on a QuantStudio 5 (Applied Biosystems). The MicroRNA/mRNA RT-qPCR mix is detailed in table 3-4. The mRNA and microRNA expression levels were calculated using the $2^{-\Delta Ct}$ method. Each reaction was performed in triplicate. MicroRNAs expression was normalized to U6 snRNA, while the mRNA expression was normalized to Ubiquitin C (UBC).

MicroRNA retro transcription mix (µL)		MRNA retro transcription mix (µL)	
TaqMan MicroRNA Reverse Transcription Kit		High Capacity RNA-to-cDNA kit	
10x RT buffer mix	0.5	RT enzyme	0.5
dNTPs	0.05	RT buffer mix	5
Rnase inhibitor	0.063		
RT enzyme	0.33		
RNase-free water	1.33		
Taqman specific primer	1		
Sample's RNA (10 ng)	1.66	Sample's RNA (100 ng)	4.5

Total volume	5	Total volume	10

Table 3-2: Reagents included in the microRNA retro transcription mix (left) and mRNA retro transcription mix (right)

Primers and probes for mRNA/microRNA retro transcription and RT-PCR	
MicroRNA Assay Name (cat. 4427975)	Assay number
Hsa-miR-132-3p	000457
Cel-miR-39-3p	000200
Hsa-miR-26a-5p	000405
U6 snRNA	001973
MRNA Assay Name (cat. 4331182)	Assay number
Ubiquitin C	Hs00824723_m1
RAS p21 protein activator 1	Hs00243115_m1
RB transcriptional corepressor 1	Hs01078066_m1
Paxillin	Hs01104424_m1
Cyclin-dependent kinase inhibitor 1A	Hs00355782_m1
Sprouty-related EVH1 domain containing 1	Hs01084559_m1

Table 3-3: List of probes and primers employed in microRNA retro transcription and RT-qPCR and mRNA RT-qPCR.

MicroRNA/mRNA RT-qPCR mix (µL)	
Universal PCR master mix	2.5
Sample's cDNA	0.5
microRNA/mRNA Taqman probe	0.25
RNase-free water	1.75
Total volume	5

Table 3-4: Reagents included in the microRNA/mRNA RT-qPCR

3.3.3 Chitosan enzymatic digestion

Chitosanase(Merk, USA) is a chitosan-digesting enzyme. Incubated with chitosan, chitosanase breaks β-(1→4) links between chitosan monomers (figure 3-2), N-acetyl-D-glucosamine, or its deacetylated version D-glucosamine. Based on published methods [424]–[426], I tested two different enzyme concentrations – 7 Units (U)/mg of chitosan and 0.7 U/mg of chitosan. After NPs production, the NPs suspension is incubated with chitosanase at 37°C for 4h in constant agitation. Then, microRNA is extracted with an RNeasy micro kit and I perform RT-qPCR.
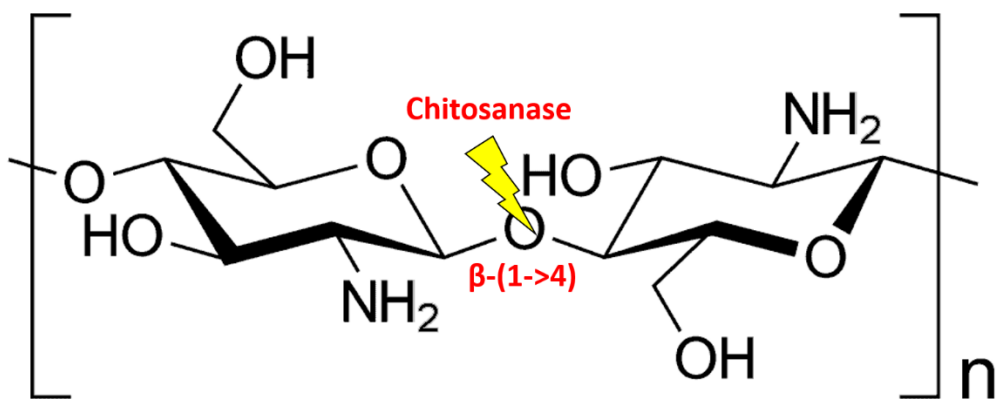
Figure 3-2: Chitosanase enzyme target bond to digest chitosan

3.3.4 RNAse inhibitor test

RNase inhibitor (Invitrogen, USA) is tested to block microRNA degradation by RNAse in FBS. RNase inhibitor is injected in microRNA-NPs dispersion or microRNA dilution in RNase-free water following the manufacturer's recommended concentration – 1 U/μL. Then, it will protect microRNA from any nucleases it should come in contact with afterward, i.e. FBS nucleases.

3.3.5 MicroRNA targets selection by bioinformatic analysis

In the cytoplasm, the double-strand microRNA (exogenously administered or internally synthetized) binds to the RISC complex, forming the miRISC. Once bound-microRNA loses its passenger strand, the miRISC complex binds with partially or totally complementary mRNA sequences - see paragraph 1.5.1. The typical microRNA/mRNA binding requires 6 complementary bases. In the microRNA, this section is called seed region and it is located in the nucleotides 2–7 of the 5' end [427]. Hsa-miR-132 target genes list was obtained from Targetscan 8.0 (https://www.targetscan.org/vert_80/). Targetscan predicts potential microRNA targets by searching for the presence of 8-mer, 7-mer, and 6-mer (sequences of 8, 7, and 6 nucleotides) on the 3' UTRs of the vertebrates mRNA pool that are matching the microRNA seed region [428]. Once the microRNA potential target list is created, it is fed to g:Profiler (https://biit.cs.ut.ee/gprofiler/gost). G:Profiler allocates any given gene to its gene ontology. A gene ontology class encompasses genes involved in the same biological process. Through this software, it is possible to select the genes of interest based on the biological process to

investigate [429]. In this project, classes involved in the regulation of cytoskeleton were selected to identify genes involved in migration, and regulation of cell cycle and programmed cell death classes for proliferation. As additional confirmation, a literature review is carried out for each chosen gene.

3.4   Nanoparticles production methods

3.4.1   Chitosan-Nanoparticles production by ionic crosslinking

I fabricated the NPs by ionic crosslinking. The NPs are produced by exploiting the electrostatic attraction between chitosan and nucleic acids, which have a positive and a negative net charge, respectively (figure 3-3B). Chitosan gains its positive charge below pH=6.5, where its amines are protonated. MicroRNA has only a mild negative charge coming from their phosphate groups. Therefore, it is thought that a negative compound is needed to enhance the electrostatic interaction and make stronger NPs. Tripolyphosphate (TPP) possesses three negatively charged phosphate groups, which increase the NPs' electrostatic bonds (figure 3-3A) [430], [431].

The polysaccharide/crosslinker weight ratio is a fundamental parameter that influences almost each NPs' property. In brief, the NPs bond is regulated by electrostatic forces. Hence, the NPs bond strength is determined by the ratio between the number of chitosan positive charged amines (N) and the number of negatively charged phosphates present in the crosslinker and microRNA (P) – N/P. Since the microRNA's phosphate groups are partially shielded, the overall microRNA negative charge is not sufficient to produce strong NPs. Thus TPP, which has a high negative charge density, is added. As a result of the addition of a material with such a high negative charge density, the microRNA contribution to P is negligible compared to TPP when the N/P ratio is calculated. Each 222 g of Chitosan (W_N) contains 1 mol of amine groups, while 122 g of TPP (W_P) contains 1 mol of phosphates. Knowing the materials' weight needed to add certain amounts of charged groups, it is possible to calculate the weights ratios required to reach specific N/Ps.

$$Needed\ chitosan\ weight\ = W_{Ch} = N * W_N; \qquad N = required\ moles\ of\ amine\ group$$

$$Needed\ TPP\ weight = W_{TPP} = P * W_P; \qquad P = required\ moles\ of\ phosphate\ group$$

$$\frac{W_{Ch}}{W_{TPP}} = \frac{N * W_N}{P * W_P} \; ; \frac{W_N}{W_P} = 1.82 \; \rightarrow \; \frac{W_{Ch}}{W_{TPP}} = \frac{N}{P} * 1.82$$

In the thesis, I will use as a convention to identify NPs with different chemical/physical properties the nomenclature N/P or Chitosan/TPP w/w, which is N/P*1.82.

In literature, N/P is variable but always larger than 1. Generally, N/P spans from 2 to 50. Following the production formula optimization (see paragraph 3.2.2), I used N/P=4 which is equal to the Chitosan/TPP weight ratio of 7. Chitosan/TPP=7 w/w was chosen since it is the highest ratio which keeps NPs size below 200nm. I chose this ratio due to the acceptable trade-off between NPs' microRNA protection and NPs' size, which directly correlated with their ability to access cellular cytoplasm. Indeed, NPs internalization by cells that cannot use the phagocytosis mechanism (mainly immune cells), is limited to a size of 500nm. However, 500nm is a very stretched limit, and the percentage of uptaken NPs with respect to available NPs decreases approaching that limit. Generally, a diameter of 200 nm allows cells to use the majority of their uptake mechanisms [432]–[434]. Zhu et al. showed an increased cellular uptake as NPS size was decreasing between 307 nm to 55 nm [435]. Lu et al. and Win et al. observed the same trend with NPS ranging from 30 to 280 nm and 1000 to 200 nm, respectively [436], [437]. On the other hand, higher Chitosan/TPP w/w improves NPs stability in water and FBS dilutions, and thus transfection efficiency [346], [395], [438]. The weight ratio between the amounts of chitosan and TPP used for NPs manufacturing is 7. The NPs are manufactured in a Class II biological safety cabinet to ensure sterility (figure 3-3C).

As example of the production process, the following is to produce chitosan-NPs with the protocol I have optimized (see paragraph 4.3.2.1) - chitosan concentration=0.25mg/mL, TPP concentration=0.1mg/mL; Chitosan/TPP weight ratio=7, NaCl concentration=50mM. A solution of 0.89mL of TPP (0.1 mg/mL) and miRNA (952.24 nM to get a final concentration of 250 nM in the dispersion) was dissolved in RNAse-free water and loaded in a sterile syringe. In a separate glass tube, 2.49 mL of chitosan (0.25 mg/mL) and 9.88 mg of NaCl in distilled water - adjusted to pH=5.5 with acetic acid, is prepared. Then, the tube is placed on a hotplate stirrer, which keeps the content in constant stirring at 1400 rpm and a temperature of 37°C. The syringe with the miRNA and TPP solution is loaded on a syringe pump, and its content is dropped inside the glass tube with the chitosan solution at a fixed flow - 0.2 mL/min.

As the two solutions meet, oppositely charged solutes are attracted to each other by electrostatic forces, and they form the NPs (figure 3-4).

The solution in the tube is kept in constant stirring to prevent the formation of bigger aggregates. In addition, NaCl (50mM) is added to both solutions since it helps to obtain a

narrower NPs' diameters distribution [395]. After the whole TPP-miRNA solution has been injected into the glass tube, the solution is left stirring for 45 min, and finally, NPs are store at 4°C before use. No washing or isolation has been performed since I could not work out a method to do so without damaging the NPs (see results). Reported concentrations refer to initial materials amounts employed at the time of NPs fabrication. NPs will be no later than one day after production.
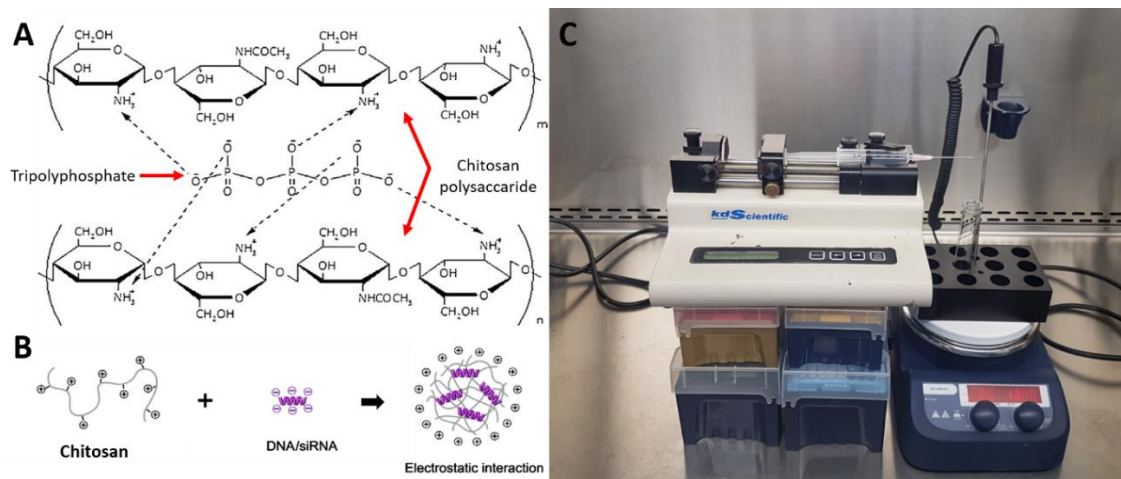
Figure 3-3: Chitosan-NPs primary bond schematic
Chitosan-TPP electrostatic interaction. B) Chitosan-nucleic acids NPs formation. C) My NPs production setup into a Class II cabinet.
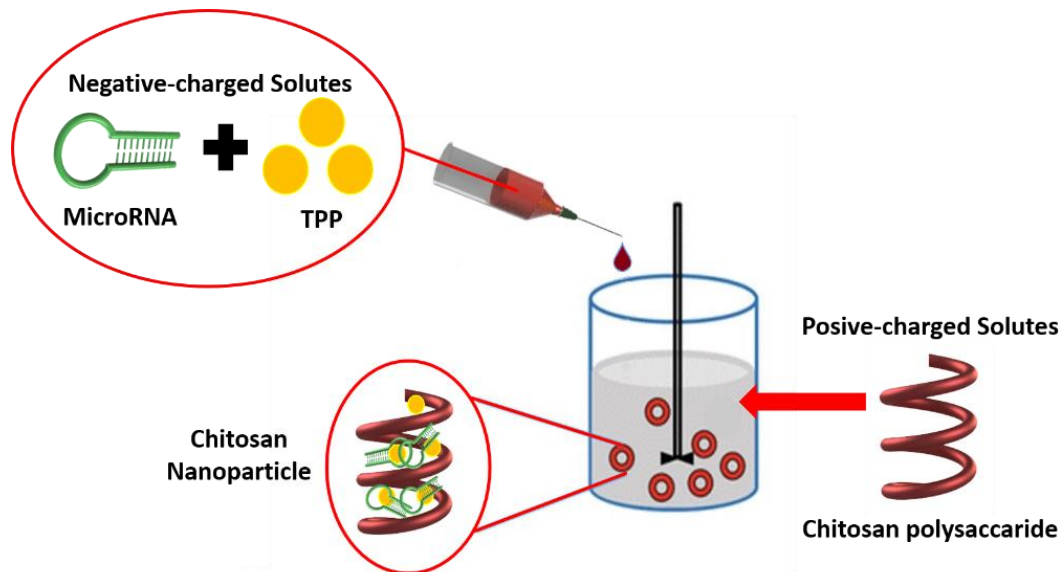
Figure 3-4: Chitosan ionic gelation process
A pH=5.5 water solution of positive-charged chitosan polysaccharides receives drops of microRNA and TPP in water (negative-charged solutes). As oppositely charged solutes meet,

they are attracted to each other and form NPs. The solution is in constant stirring to prevent the formation of large aggregates.

3.4.2   Fluorescent chitosan-NPs production

The production of fluorescent NPs allows the use of fluorescence imaging to locate NPs. FITC-conjugation of chitosan was chosen as it was deemed the most feasible in our laboratories and with our knowledge among the reviewed ones. The production protocol was replicated from a publication [439].

FITC (Biotium) was dissolved in methanol at 0.67 mg/mL. To this, 100 mL of 1% w/v of chitosan (Merck) in 0.1M acetic acid was added. The mix was left stirring in the dark for 3 hours. Then, the chitosan was precipitated adding 2M NaOH to reach a final NaOH concentration of 0.2 M. The precipitate was pelleted at 15,000 g for 1 hour and washed with methanol/water (70/30, v/v). The supernatant fluorescence was measured by the Promega Glomax fluorimeter (Promega, USA) with the following settings: excitation wavelength 475 nm and emission band 500-550 nm. The washing and pelleting were repeated until supernatant fluorescence was reduced below 1/100 of the fluorescence measured in the supernatant after the first wash. Following this, the chitosan was dissolved in 20 ml of 0.1 M HAc and dialyzed in the dark against 5 L of distilled water for 3 days. The water was replaced every 6 hours with an overnight break of 12 hours. Finally, the FITC-conjugated chitosan was freeze-dried for 3 days.

FITC-conjugated chitosan-NPs were prepared by ionic crosslinking following the protocol described in the previous paragraph.

A calibration curve was drawn to correlate the FITC-conjugated chitosan-NPs amount to the fluorimeter's fluorescence intensity. Chitosan-NPs were suspended in Optimem and EA.hy926 ECs complete media. The fluorimeter measures fluorescence in arbitrary units. In figure 3-5 fluorescence units are correlated with known amounts of FITC-NPs in suspension, expressed as fractions of the amount that will be incubated with cells (34ng/µL – see paragraphs 4.3.2.2 and 4.3.2.3 for the justification of this concentration). Linear regression equations and their relative goodness of fit coefficient R^2 were calculated with Microsoft Excel for both suspensions – Optimem- and complete media-based.
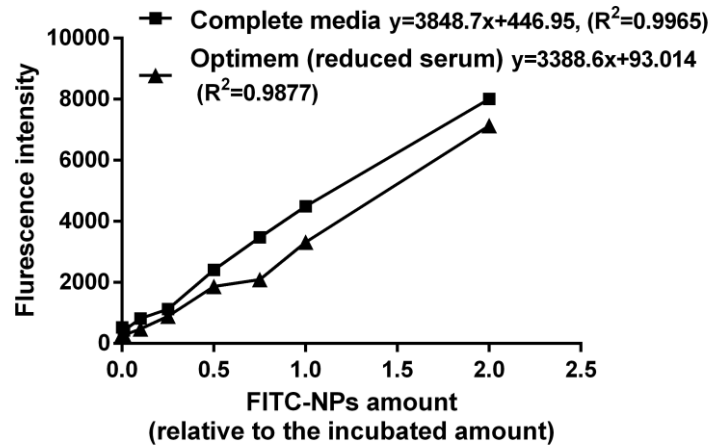
Figure 3-5: Fluorimeter calibration curve of known amounts of fluorescent chitosan-NPs
Known amounts of FITC functionalized chitosan-NPs were suspended in either Optimem or EA.hy926 ECs complete media. The suspensions fluorescence was measured by the Promega Glomax fluorimeter (Promega, USA) with the following settings: excitation wavelength 475 nm and emission band 500-550 nm. The indication of NPs quantities is expressed as fractions of the amount that will be incubated with cells - 34ng/μL. Linear regression was performed using the datasets of both media used to suspend NPs (regression equations and goodness of fit coefficient R^2 are displayed on the top of the graph).

3.4.3 PEI-NPs production

Polyethyleneimine (PEI)-based NPs are prepared with a simple mixing step before using them for transfection replicated from literature [318], concentrations included. A PEI stock solution is prepared dissolving branched PEI Mw=25 kDa (figure 3-6) in PBS at 10 mg/mL. MicroRNA stock solution is prepared in RNAse-free water at 25 μM. Since PEI-NPs bonds are electrostatic as for chitosan-NPs, the rationale to establish PEI amount involves combining compounds to reach specific electrostatic charges ratios as previously discussed. Each 39.2 g of PEI (W_N) provides 1 mol of positively charged amines, while 1 mol of negatively charged phosphates is in 325 g of microRNA (W_P). The same passages detailed for chitosan-NPs production bring to an N/P-W_{PEI}/W_{miRNA} equivalence – where W_{PEI} is the weight of PEI and W_{miRNA} s the weight of microRNA.

$Needed\ PEI\ weight\ = W_{PEI} = N * W_N;$
$N = required\ moles\ of\ amine\ group$

$Needed\ microRNA\ weight = W_{miRNA} = P * W_P;$
$P = required\ moles\ of\ phosphate\ group$

$$\frac{W_{PEI}}{W_{miRNA}} = \frac{N * W_N}{P * W_P} \; ; \frac{W_N}{W_P} = 0.121 \; \rightarrow \; \frac{W_{PEI}}{W_{miRNA}} = \frac{N}{P} * 0.121$$

$$W_{PEI} = \frac{N}{P} * 0.121 * W_{miRNA};$$

$$microRNA \; Molecular \; weigh = 7000 \; \frac{g}{mol}$$

The tested N/P molar ratios are 10 and 20 as typically used in the literature [318], [325]. Thus, the PEI stock solution is diluted to the required concentration in PBS, then, a proper amount of microRNA stock solution is added to combine. The solution is briefly mixed followed by 30 min of rest to allow NPs formation. As from published protocol, no further handling is needed before PEI-NPs use, the particle suspension is directly administered to the cultured cells in the proper volumes to reach the transfection concentration. Given the fixed microRNA concentration (25 nM) in each transfection experiment, the compounds' amount required for each mL of transfection media are:

$$W_{miRNA} = 175 \; ng$$

$$\frac{N}{P} = 20 \; \rightarrow \; W_{PEI} = \; 423 \; ng;$$

$$\frac{N}{P} = 10 \; \rightarrow \; W_{PEI} = \; 211 \; ng;$$

3.4.4 PEI-g-PEG NPs fabrication for microRNA transfection

MicroRNA-loaded polyethylenimine-grafted-poly(ethylene glycol) (PEI-g-PEG - figure 3-6) NPs production protocol is similar to the PEI-NPs one. The starting quantities were taken from a published protocol [440]. However, a higher amount of PEI-g-PEG is required since PEI-g-PEG Mw is larger than PEI to reach the same N/P molar ratios. The concentrations of required PEI-g-PEG is 347 ng/mL for N/P=5, 694 ng/mL for N/P=10, and 1.388 µg/mL for N/P=20. . As from published protocol, no further handling is needed before PEI-NPs use, the particle suspension is directly administered to the cultured cells in the proper volumes to reach the transfection concentration
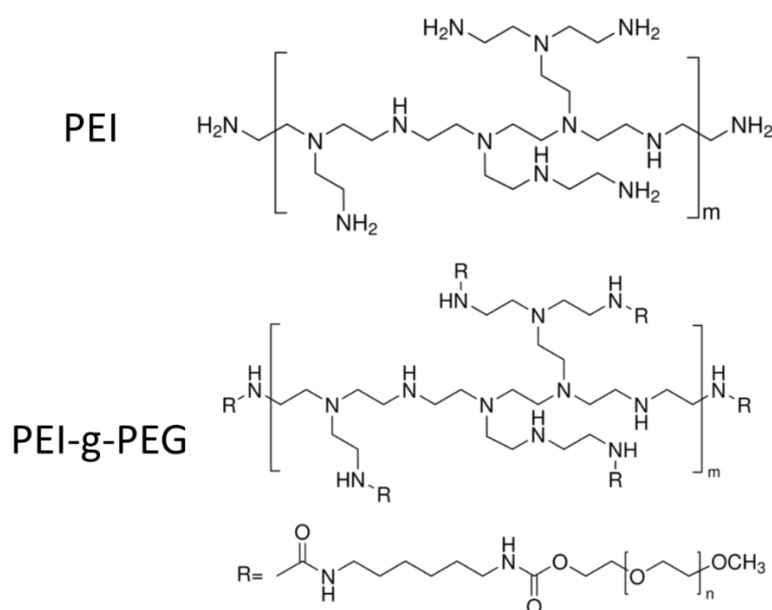
Figure 3-6: Chemical structure PEI-g-PEG compared with PEI

3.4.5 PLGA-NPs fabrication

PLGA-NPs are fabricated by emulsion-solvent evaporation, and replicated from published protocols [441]. The following procedure is carried out in a biosafety cabinet to ensure product sterility. For the production of the PLGA-NPs, a positive-charged component was needed and for this purpose, I mixed MicroRNA with Spermidine in a dichloromethane (DCM) solution. Spermidine is a natural polyamide with a positive charge. It is used to bridge between microRNA and PLGA since they are both negatively charged, therefore they would repel each other.

The fabrication procedure starts by dissolving 2.5 mg/mL PLGA in organic solvent – DCM, while 2.5 mg/mL of PVA is dissolved in RNAse-free water. Then, the spermidine-miRNA solution is prepared and the added amounts are based on the N/P ratio as seen in previous methods (figure 3-7). For this specific approach, each 85 g of spermine possesses 1 mol of amines (N) and microRNA has 1 mol of phosphates (P) each 325 g. In my experiments, N/P is 8 unless stated otherwise [442]. After 10 min of stirring at room temperature (RT), microRNA-spermidine complexes suspension is added to the PLGA solution and mixed with a blender-type homogenizer at 10000 rpm for 1 min. PLGA amount depends on the microRNA to be embedded in NPs by the PLGA/spermidine weight ratio that may vary between 200 and 1000 [443], [444]. Once homogenized, the solution is loaded on a glass syringe, which is then placed on a syringe pump. A glass vial filled with polyvinyl alcohol (PVA) solution is placed under the needle tip of the PLGA solution-loaded syringe. Then, the syringe pump drops PLGA-solution into the glass

vial at a constant flow rate – 0.2 mL/min. DMC and water are not miscible and PLGA is not water-soluble. Hence, PLGA is restrained in the organic phase (DCM). Spermidine-microRNA should stay with PLGA because of electrostatic attraction, although they are also water-soluble. PVA is employed to lower the surface tension between PLGA organic solution and water. This will allow PLGA nanodroplets to stabilize in the water continuous phase instead of aggregating in bigger drops. PVA is added following PVA/PLGA weight ratio equal to 3 [445]. While the syringe pump is functioning, the blender-type homogenizer keeps the PVA solution in constant agitation; the homogenizer shaft spins at 15000 rpm during the procedure. The homogenizer is kept on for additional 5 minutes after the PLGA solution is completely added to the PVA solution. The so-made solution is left under magnetic stirring overnight to allow the organic solvent to evaporate and PLGA-NPs to harden since PLGA does not dissolve in water. Additionally, a buffer exchange passage to substitute PVA solution with pure RNAse-free water is applied using centrifugal filters.
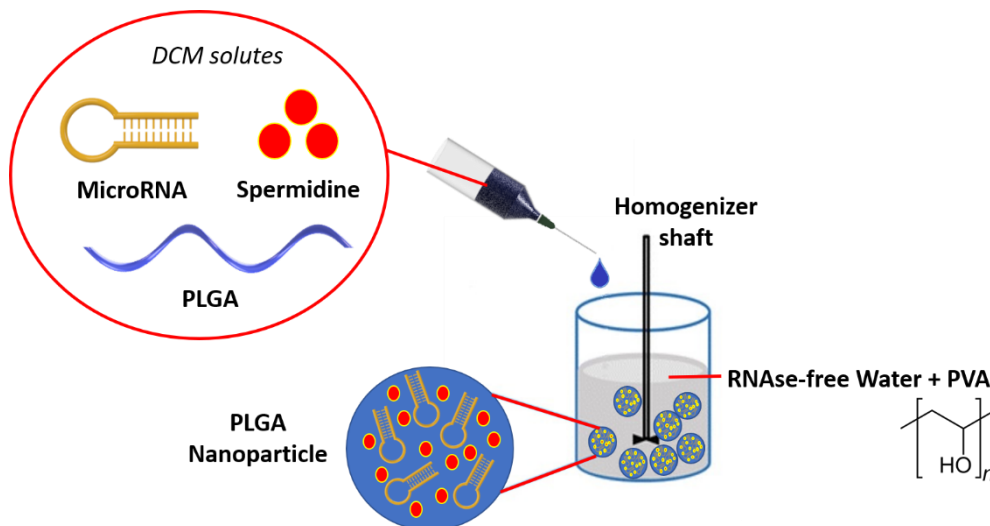
Figure 3-7: PLGA-NPs production by emulsion-solvent evaporation
A solution of microRNA, spermidine, and PLGA in DCM is slowly injected into a water-PVA mix with a syringe pump. Then, DCM evaporates and PLGA-NPs harden holding microRNA within. The solution is mixed with a homogenizer to prevent the formation of large aggregates

3.4.6   Trimethyl chitosan NPs manufacturing for microRNA transfection

Trimethyl chitosan (TMC) is a chitosan derivative. Its primary amine is trimethylated so the group becomes protonated (figure 3-8). Different from chitosan, the TMC charge is pH-independent. This should contribute to making more reliable bonds between chitosan and microRNA, and help the transfection. The test of this material was kindly suggested by Prof. Carmen Galan, who also

provided a sample for testing. The production protocol is inspired by a published simple mixing protocol, with no post-production washing or isolation [446]. In the publication, employed N/P is 6, thus I decided to test N/P equal 5, 10, 20 to explore if N/P increase increases the transfection efficiency as it happened with PEI-NPs - see results on PEI microRNA transfection.

The TMC-NPs production protocol consists of mixing the reagents in RNase-free water and allowing complex formation for 20 minutes at RT. TMC is water-soluble and possesses 1 mol of trimethyl each 649 g of TMC, assuming 100% of amine are trimethylated where it is not otherwise stated. MicroRNA concentration for transfection is set to 25 nM. The amount of TMC required is 1.75 µg/mL for N/P=5, 3.5 µg/mL for N/P=10, and 7.01 µg/mL for N/P=20.
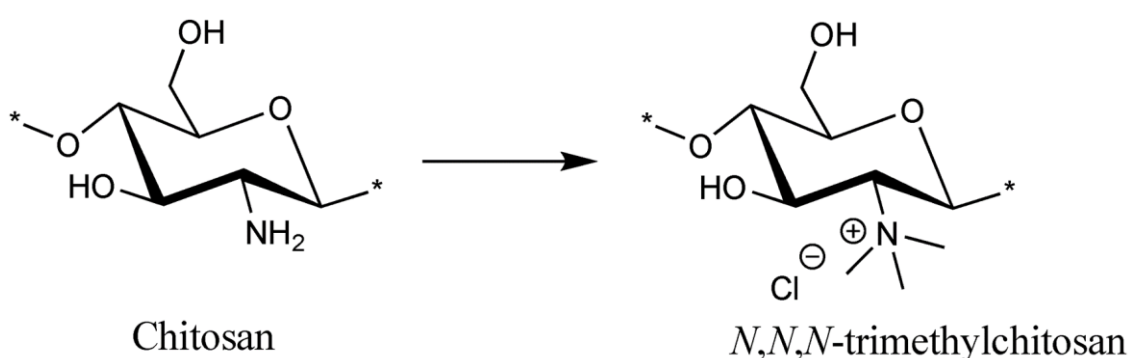
Figure 3-8: Chitosan and TMC structure
TMC is a chitosan derivative. Chitosan amine group is trimethylated, hence the nitrogen acquires a stable positive charge, independent from pH.

3.5   Nanoparticles optimization and characterization techniques

3.5.1   SEM, TEM, STEM, and back-scattered X-RAY analysis

I used scanning electron microscope (SEM – JSM-IT300, JEOL Ltd., Japan) University's services (Chemistry and Bioimaging facility) to capture images of the electrospun scaffold. The samples are precautionarily dried in a vented oven for 48 hours at 37°C, to avoid vapor eruptions during the SEM acquisition. The specimens are coated with a gold-palladium alloy with sputter coater, allowing a better electrons flow and thus images with higher resolution. After the sputtering, samples are ready to be analysed by SEM [447].

Transmission Electron Microscope (TEM) works on similar principles of SEM, but it captures transmitted electrons. Eventually, this allows a higher resolution. I used this technique through the aforementioned University's services (JEM-1400, JEOL Ltd., Japan). As described in the results chapter, I was not able to get acceptable images of chitosan-NPs with SEM. The benefits related to the use of TEM imaging are: getting rid of sample solutes that were forming a massive

coating on the sample's surface (NaCl) and have images with 0.05 nm maximum resolution – plenty to resolve the smallest NPs. Samples are drop cast on a copper grid. The grid layout lets solvent and small solutes pass through but holds the suspended NPs of interest. Once dried, the casted grids are sputtered with carbon and analysed by TEM [447], [448].

Scanning transmission electron microscope (S/TEM – integrated with JEM-1400, JEOL Ltd., Japan) is a TEM operating mode. In this mode, TEM's electron beam is focused in a very fine spot – less than 0.2 nm, which scans the specimen. In the common TEM (or CTEM – conventional transmission electron microscope), a larger beam hits the specimen's picture area at once – no scanning [449], [450]. The STEM machine gives also the opportunity to identify the nature of the sample's superficial material through energy-dispersive X-ray spectroscopy (EDS). Indeed, when the specimen is hit by an electron beam it is ionized and produces a series of secondary energy emissions, among which there are x-rays. These can be collected by specific detectors. Each elemental atom has a specific energy pattern of x-ray emission, hence it is possible to identify the atom. Moreover, it is possible to map the position of the atoms. Eventually, this technology enables the creation of an elemental map. Whether different molecules have elements that others do not possess, it is possible to draw a topological map of the sample's molecules arrangement [451].

I used Fiji ImageJ to analyse images and calculate features such as nanofibers diameter, porosity, pore size, and NPs diameters.

3.5.2   Dynamic light scattering

Dynamic light scattering (DLS) is used to characterize NPs. The technique allows calculating the NPs size distribution in a solution, though an indirect measure based on scattered fluctuations of a laser shining through the NPs suspension. When a laser hits an NP in a solution it is scattered in a different direction. NPs in water suspension are in continuous motion – Brownian motion, so the intensity of scattered light changes continuously. Noteworthy, NPs motion depends also on their size. Therefore, by analysing the scattered light intensity over time, it is possible to estimate the NPs size distribution.

This technique gives an estimation of NPs size distribution, which is closer to reality when NPs suspension is in optimal condition. However, there is always a degree of error. The positive aspects of DLS are that it is not destructive, inexpensive (apart from machine maintenance, there is just the cost of a plastic cuvette for each sample to test), quick, and does not need specimen

preparation if the sample solution contains only the NPs of interest. I used this method to screen NPs size distribution during their manufacturing protocol optimization.

3.5.3   Chitosan titration

Chitosan titration is necessary to determine if chitosan-NPs are precipitated and the supernatant is clear from them. If so, we can assume that centrifugation worked and measure the amount of free microRNA. To do so, I used a colorimetric assay method based on Cibacron Brilliant Red (CBR) [452]. Under acid pH conditions, the protonated chitosan amines can bind anionic dyes like CBR. As a result, the dye visible absorption spectrum undergoes a bathochromic shift – i.e. the spectrum moves towards longer wavelengths. A sharp peak at 575 nm is the result of the difference between free dye and bound one in the absorption spectrum. A glycine/hydrochloride acid (HCl) pH 2.8 Soerensen buffer is necessary to keep the reaction at acid pH. CBR powder is dissolved in water at 1.5% w/v. The assay requires preparing a tube for each sample to analyze with 0.1 mL of Soerensen buffer and 1 mL of dye dilution. To this, 1 mL of sample supernatant is added and the final volume is brought to 5mL adding distilled water. After 20 minutes of continuous agitation at RT, 1 mL from each tube is pipetted in a multiwell, and the absorbance is measured at 575 nm. The absorbance is then compared with a calibration curve.

3.5.4   Samples dialysis

NPs dialysis is carried out after their production and it aims to get rid of non-encapsulated microRNA. The use of dialysis tubes with a proper molecular weight cut-off (MWCO) should allow non-encapsulated microRNA to pass from the sample solution to the dialysis media while keeping the NPs inside the dialysis tube and the encapsulated microRNA with them. The final aim is to estimate the amount of encapsulated microRNA.

Once the NPs are produced, the NPs suspension is poured into a dialysis tube which is closed at both ends to form a bag. Then, the dialysis bag is placed into a 1L sterile jar filled with RNAse-free water; the water is kept in constant mild agitation on a magnetic stirrer. The dialysis lasts 8h and the water is refreshed every 1.5h. After dialysis, the samples undergo RT-qPCR to measure the microRNA amount with respect to the controls.

3.5.5 MicroRNA FBS exposition

MicroRNA-water dilution or NPs dispersion are incubated in 10% v/v FBS for 1h. After the incubation, the samples undergo microRNA extraction and RT-qPCR.

3.5.6 Chitosan-NPs protection of microRNA from FBS nucleases

I developed this protocol to extract the most possible microRNA from chitosan NPs after their incubation with 10% v/v FBS. After FBS incubation for 1h at RT, 1 U/µL RNAse inhibitor is added to NPs samples followed by 0.7 U of chitosanase per mg of chitosan. Then, samples are incubated at 37°C for 4h in constant agitation. Then, microRNA is extracted with an RNeasy micro kit and I carried out RT-qPCR.

3.5.7 NPs sedimentation by centrifugation

Ultracentrifugation is a common technique to separate particles of different sizes and weights which is extensively used to sediment NPs [398], [453], [454]. I used this method to separate chitosan-NPs and PLGA-NPs from free microRNA. The process is based on Stokes Law and Newton Law :

$$v = \frac{d^2(p - L) \times xg}{18n}; \;\; h = vt$$

where v is sedimentation speed, d is particles diameter, p is particle density, L is medium density, xg is centrifugal acceleration – typically expressed in multiples of gravity acceleration (g), n is the viscosity of the medium, h is the distance a particle at the top of the solution column has to travel to sit on the vessel bottom, t is time a particle needs to travel h [455]. Based on these equations I can calculate the proper time and centrifugal acceleration to achieve chitosan-NPs sedimentation. With regards to Chitosan, it is hard to find a broadly agreed chitosan density. Therefore, I have to find support from published sedimentation protocols, although they are not optimized specifically for my NPs.

3.6   MicroRNA-functionalized scaffold fabrication methods

3.6.1   Scaffold fabrication by Electrospinning

Electrospinning is a fabrication method that produces non-woven mats of thin fibers – usually on the scale of microns or nanometers. Tissue engineering research groups make extensive use of it.

The working principle follows the described steps: the solution of material is loaded into a syringe, positioned on a syringe pump, and the syringe needle is connected to the positive pole of a high voltage DC power generator – usually from 0 to 50 kV (figure 3-9). The power generator's negative pole (or ground) is connected to a structure called collector. When high voltage is activated, the polymer solution is positively charged and is attracted by the negative pole. This attraction force is combined with the syringe pump movement which pushes the material solution out of the needle. Electrical charges accumulated on the droplet at the tip of the needle (kept together by surface tension) cause drop-stretching into a conical structure (Taylor's cone), as a result of electrostatic repulsion. Eventually, a charged jet is ejected from the needle tip. In the first part of its journey towards the negative pole, the jet travels following a straight path while it begins to thin into a finer fiber. Then, the jet undergoes chaotic whipping motion due to bending instabilities, during which it is additionally thinned and begins to dry. Eventually, fibers accumulation creates a web on the collector. Multiple layers of fiber webs create a non-woven mat. Fibers formation requires the optimization of several parameters, including material solution viscosity, dielectric constant, solvent volatility; and production parameters like applied voltage, collector distance, flow rate, distance between the needle tip and the collector, ambient temperature and humidity. Also, the material to electrospun should have appropriate molecular weight to allow sufficient chain entanglement to create continuous fibers. Not optimized setups can lead to the solution jet breaking into charged droplets. This happens when fibers' cohesive forces are overcome (Rayleigh instability limit) by solution surface and electrostatic repulsion, which tend to increase the solution surface area. Sometimes this is a desired condition, essential to perform electrospraying instead of electrospinning. On the other hand, if solvent volatility is excessive and/or ambient temperature is too high, the solution may dry out on the needle tip, hindering electrospinning [366], [456].

In this work, electrospinning is used to produce a microRNA-functionalized scaffold based on biodegradable materials: GL and PCL. The electrospinning machines used are a custom-made machine located at Bristol Dental School (Biomeg lab. of Prof. Bo Su), and the ND-ES system from Nadetech Innovation (Spain) in our laboratory.
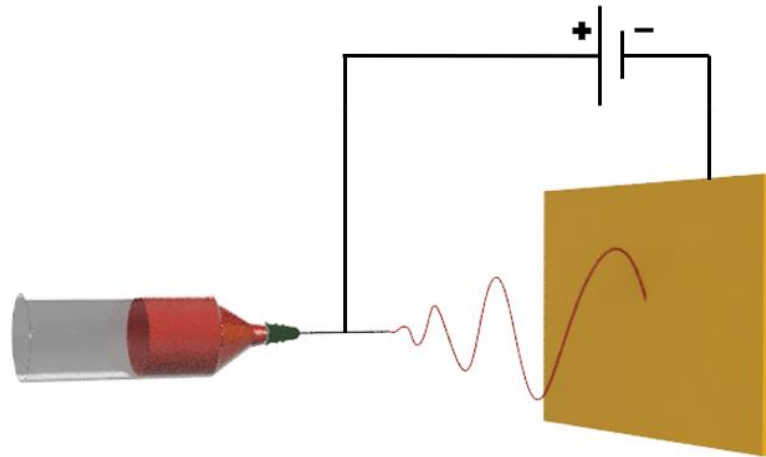
Figure 3-9: Principle of electrospinning technology
A DC power generator's negative pole is connected to a collector, while a positive pole is connected to the needle of a syringe loaded with a material solution. The high voltage charges the material solution positively and makes it attracted by the negatively charged collector. The attraction force is combined with the syringe pump movement which pushes the material solution out of the needle. Eventually, the solution's surface tension is overcome, and the solution on the tip of the needle is stretched into a thin fiber that travels towards the collector. As fibers stock on the collector, a non-woven mat starts to form.

3.6.2 Electrospinning add-ons

To address the technological challenge of the fabrication of functionalized nanofibers I developed new devices and tools. In the next paragraphs, I will introduce the collectors used to generate the scaffolds, with particular attention to the design and development of valve-shaped collectors, and I will thoroughly describe the production of the vacuum oven, temperature, and humidity control system.

3.6.2.1 Custom-made scaffold collector

As mentioned in the introduction, this project includes the fabrication of a valve-shaped scaffold for heart valve regeneration. To do so, a valve-shaped electrospinning collector is needed. During electrospinning, the scaffold fibers will coat the collector and create a scaffold with a valve shape during its fabrication.

The process begins with the acquisition of a valve 3D model on a 3D design software - Autocad Fusion 360. In this phase, the model is adapted to the 3D printing process. Ideally, the scaffold

shape should match the recipient's cardiovascular features. Thus, the valve 3D model should be generated from aortic root medical imaging. In this project, models available on the internet will be utilized since I do not have the authorization to use real medical images, and have no time to learn how to extract 3D models from medical imaging. The model is 3D printed in polylactic acid (PLA) with the 3D printer in use in our laboratory (Ultimaker 5). As the electrospinning needs a conductive collector, the printed model is not suitable since PLA is a non-conductive polymer. Therefore, I chose chemical electroplating to create a metal surface wherever we want our scaffold to be laid on.

Electroplating consists of surface coating with a metal layer – copper in this project, thanks to a driving current. Briefly, before copper deposition, the PLA model is coated with a conductive paint as a conductive surface is essential. Despite the paint being conductive, this surface is not suitable for electrospinning since the paint would transfer on the scaffold. Also, the conductive paint is water-based, so the electrospinning solutions may dissolve the paint and transfer part of it to the scaffold. After this preparatory step, the model is immersed in a 500 mL copper ion solution (copper sulfate) – the material we want to coat the PLA model with, and connected to the negative terminal of a 5V power supply. Also, the ion solution contains sulfuric acid, sodium chloride, and PEG to facilitate copper ions' movement. The exact solution composition is the following: $CuSO_4$ at 0.88 M, H_2SO_4 at 0.54 M, NaCl at 1 mM, and PEG at 25 μM [457]. The positive terminal of the power supply is connected to a copper electrode. As the power supply is switched on, copper ions will migrate to the negative terminal, namely the surface to coat (figure 3-10A). After 4 hours, a layer of solid copper is formed on the areas coated by the conductive paint (figure 3-10B).
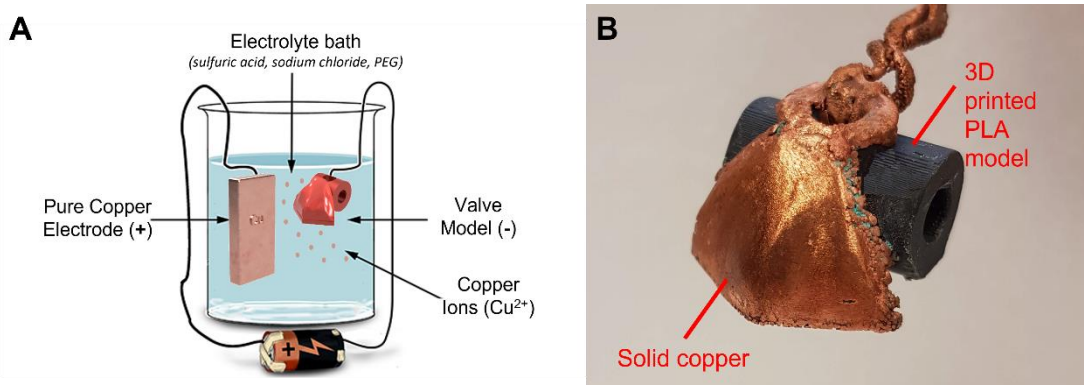
Figure 3-10: Illustration of a general electroplating set-up (A) and a picture of an electroplated valve model (B)
A) Electroplating is carried out in a water-based solution with sulfuric acid, chloride acid, and PEG. Two electrodes are immersed in the solution: a solid copper electrode (+) and the 3d model covered in conductive paint (-). The electrodes are connected to a 5 V power source,

which drives copper ions from the positive electrode to the negative electrode through the solution. B) A 3d printed model with a solid copper coating (anticipation of results).

3.6.2.2 Custom-made vacuum oven

I fabricated this machine to get rid of solvents with very high boiling temperatures, like NMP I have used for scaffold fabrication. The machine has the function of a vacuum oven. Several research groups that use toxic solvents to create electrospun scaffolds are using this technique to get rid of the solvents such as DMSO, DMF, and NMP [458]–[461].

Unfortunately, we do not possess that machine in our laboratory. Its market price was beyond our budget. Thus, I have used my electronics and mechanics knowledge and sought help from the University workshop for the work I could not carry out by myself. Eventually, I manage to replace the vacuum oven for less than £200.

High boiling points can be dramatically lowered working on the ambient pressure. The NMP boiling point is 0°C at 293 mbar on a pressure-temperature nomograph, while it is 202°C at 1 atm. Therefore, a vacuum oven is a good solution for getting rid of NMP without causing heat damages to a scaffold. This custom-made vacuum oven is a vacuum chamber that can go down to 5.5×10^{-3} mbar thanks to a vacuum pump. A copper stand, provided with a heating cartridge and a controlled in feedback with temperature probe, is in the center of the chamber (figure 3-11). The scaffold will sit on it so that the heat coming from the stand will be passed to the scaffold by thermal conduction since convection is severely limited in a vacuum. The scaffold will be exposed to a pressure of 5.5×10^{-3} mbar at 37°C.
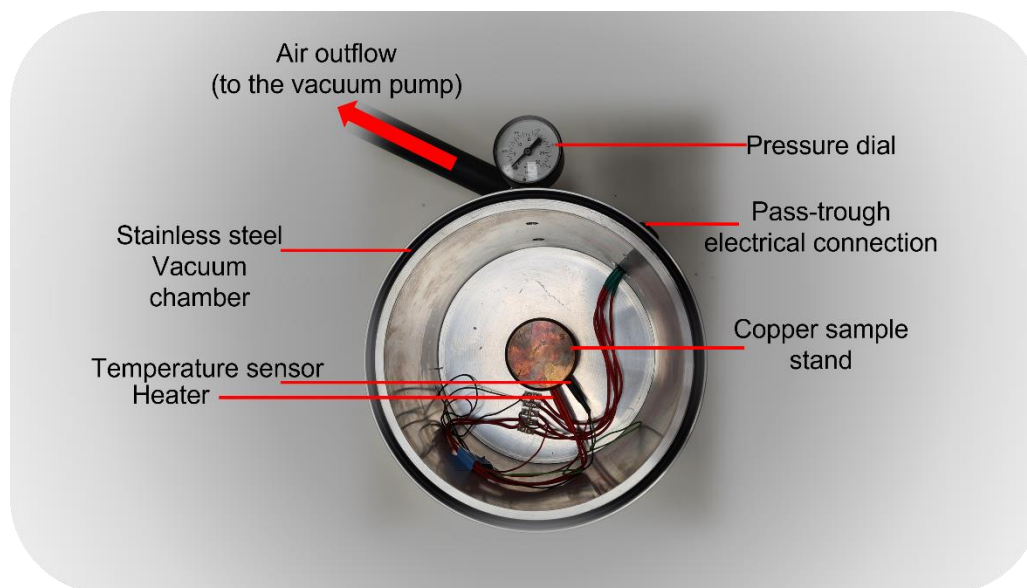
Figure 3-11: Custom-made vacuum oven
Budget in-house replacement of a vacuum oven. The stainless steel chamber was produced by the University of Bristol's workshop, made to bear the pressure of vacuum generated by a vacuum pump attached to the black hose at the top of the picture. The chamber was equipped with a pressure dial, and a heated copper stand, controlled in feedback with a temperature sensor.

3.6.2.3   Temperature and humidity control for Gelatin in water electrospinning

The first step of scaffold fabrication is the optimization of the GL electrospinning process. Acids and other organic solvents are usually mixed with water (or left pure) to allow GL electrospinning at RT. As a drawback, these strong solvents may destroy the RNA or its vector (lipid NPs soluble in alcohols [462], and some of them are also unstable at low pH [463]) loaded on the scaffold. I could not find a GL solvent that was also demonstrated compatible with lipofectamine-microRNA complexes in the literature. We usually carry out transfection in culture media, which are buffered water-based liquids. Therefore I decided to attempt the GL layer production using water as a solvent. However, this poses an additional issue. The GL-water solution is jellified at room temperature. Therefore, I have fabricated a temperature and humidity control unit. The system was able to guarantee a temperature above 35°C to be employed during the GL electrospinning (GL in water is not soluble below 35°C). Relative humidity control is important as well. When the electrospinning cabinet is heated up, the humidity decreases dramatically, and the GL solution dries on the needle tip. This creates a clot and prevents electrospinning. Thus, relative humidity must be kept under control. In my experiments, electrospinning is possible between 50 and 70% of relative humidity.

The machine is connected to the electrospinning chamber with two PTFE pipes: inlet and outlet. The fan block pumps air from the electrospinning chamber to the heater one. I have integrated three ultrasound mist makers on a water tank, and I have placed the tank in a cavity at the bottom of the heater with the mist maker facing upwards (figure 3-12B). The working principle consists of air being pumped into the heater chamber by the fans from the electrospinning chamber. The mist makers generate a jet of ultrafine water droplets that are carried away by the airflow. Then, the water-loaded air passes through a resistance heater, which brings up the air temperature and vaporizes the water droplets. Finally, the air is driven back into the electrospinning chamber by the outlet pipe. Temperature and humidity are monitored in real-time by a temperature and relative humidity sensor that provide feedback signals to the control board. The values of temperature and humidity are set up by interfacing the machine with a computer, then the control board (figure 3-12A) will regulate the heater and mist makers autonomously to keep temperature and humidity to the set values.
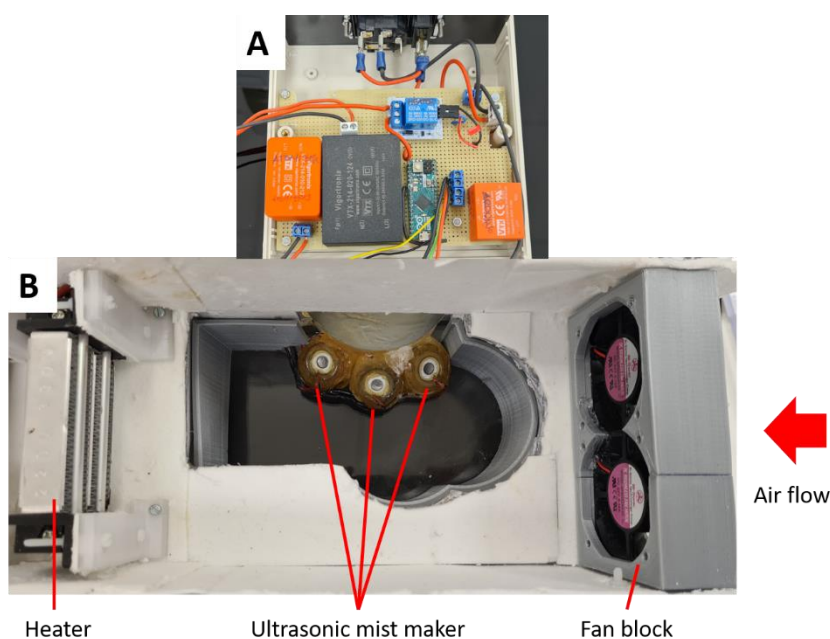
Figure 3-12: Electrospinning temperature and humidity control
A) System control board, (B)View of the machine chamber. Air sweeps in from the right end side and the fans push it towards the left. During its journey, it gets loaded with water by the ultrasonic mist generators and it is heated up when it passes through the resistance heater on the left, which also provides enough heat to turn water mist into vapor.

3.6.3 Project's Electrospinning set-ups

During my project, I explored different electrospinning protocols. The microRNA-functionalized scaffold for this project was conceived as a tri-layer composite scaffold (figure 3-13). The

composite structure derives from the necessity to find a trade-off between the need for medium-term structural integrity to support valve regeneration (and substitute the native valve duty), and shorter-term degradation for the delivery of a substantial amount of therapeutic molecules (microRNA) in the initial phases of regeneration. The external layers are made of GL. The GL is dissolved in water and microRNA-vector complexes are added to the solution prior to electrospinning. GL crosslinked with GPTMS degrades in around 14-18 days [223], [400]. Hence, there would be a window of 14-18 days for microRNA administration. The GL layers will coat a PCL core layer. PCL degrades in around 2 years. Since I could not find an example of a fully regenerated heart valve in less than a month in literature, the hypothesis is that slower degrading material should be integrated into the scaffold. The PCL layer should allow more time for valve regeneration and fulfill the heart valve duty in the meantime [464]–[466].

A post-processing passage is needed when producing GL-GPTMS nanofibers. The scaffolds are dried in an oven at 37°C to allow GPTMS to crosslink GL fibers, which makes the scaffolds water-insoluble and improves their mechanical properties (see Introduction for details on GPTMS crosslinking).

In table 3-5, I have summarized all tested protocols.
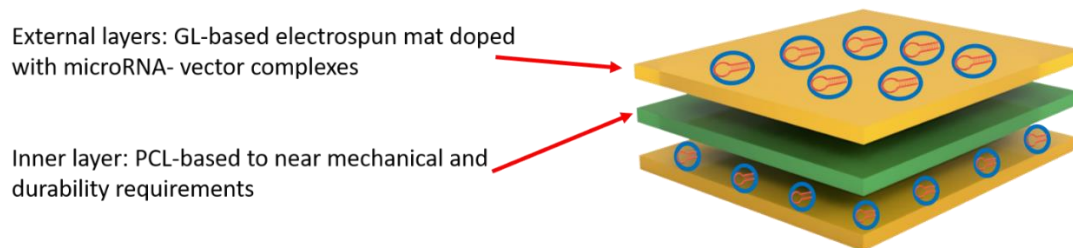
Figure 3-13: Try-layer microRNA-functionalized scaffold for valve regeneration

Protocol #	Materials	Voltage	Flow rate	Additional Features
1	GL 15% w/v in NMP/water (50/50, 60/40, or 70/30 v/v)	7, 10, 13, or 15 kV	1 or 0.5 mL/h	
2	Core: PCL 10% w/v in chloroform Coating: GL 15% w/v in NMP/water (50/50)	15 kV	1 mL/h	
3	GL 10 or 15% w/v in water	15 kV	1 or 0.5 mL/h	Heating: 35°C r. Humidity: 50-70%
4	Core: PCL 10% w/v in chloroform Coating: GL 10% w/v in water	15 kV	0.5 mL/h	Heating: 35°C r. Humidity: 50-70% (GL layer only)

5	PCL/GL (70/30) 10% w/v in TFE	15 kV	0.5 mL/h	
6	Core: PCL/GL (70/30) 10% w/v in TFE Coating: GL 10% w/v in water	15 kV	0.5 mL/h	Heating: 35°C r. Humidity: 50-70% (GL layer only)
7	Core: PCL/GL (70/30) 10% w/v in TFE Coating: GL 10% w/v in water	15 kV	0.5 mL/h	Heating: 35°C r. Humidity: 50-70% (GL layer only) microRNA-vector in GL layer

Table 3-5: Electrospinning protocols to be tested
GL: gelatin, NMP: N-Methylpyrrolidone, PCL: Polycaprolactone, TFE: 2,2,2-trifluoroethanol.

3.7 Statistical analysis of experimental data

Experimental values of continuous variables are expressed as mean ± standard deviation. Categorical variables are presented as frequencies (percentages), or as absolute numbers in a few cases. Analyses were performed using GraphPad Prism 5.0, Sigma Stat 3.1 software (San Jose, CA) statistical packages.

Where the group size allowed it – 8 or more, the D'Agostino-Pearson normality test (normality was assumed when $p > 0.05$) was performed to understand if parametric testing was applicable. Statistical analysis limited to the comparison of two groups was done using a t-test in case of data normally distributed. Otherwise, the Mann-Whitney ranks test was employed. Compared groups were assumed statistically different if $P < 0.05$.

Where data are normally distributed, the statistical analysis of three or more groups was performed by applying One-way ANOVA with Geisser-Greenhouse sphericity correction. Groups were considered from the same population if $P > 0.05$ (null hypothesis acceptance). In case of null hypothesis rejection, Tukey's multiple comparison test was performed to identify the significant differences between each group pair. Compared groups were assumed statistically different if $P < 0.05$. The analysis of three or more non-parametrical groups was carried out by the Kruskal-Wallis test. The null hypothesis was rejected (groups come from two populations at least) if $P < 0.05$. In case of null hypothesis rejection, Dunn's multiple comparison test was performed to identify the significant differences between each group pair. Compared groups were assumed statistically different if $P < 0.05$. GraphPad Prism automatically implements Bonferroni adjustment of the p-value to perform Post-Hoc analysis.

4 Results and discussion

4.1 Chapter overview

In this chapter, the results are displayed in three separate sections, which describe the development of the three main project milestones:

- The selection of a microRNA with pro-endothelialization effects, like migration and proliferation – section 4.2

- The selection of vector that can protect the microRNA from blood nucleases and facilitate microRNA entrance into ECs – section 4.3

- The design, fabrication, and test of a tri-layered scaffold able to host therapeutic microRNA, and make it available to colonizing ECs – section 4.4

4.2 Has-miR-132-3p pro-endothelialization effect on Aortic Endothelial Cells

In this experiment, I checked if hsa-mir-132-3p transfection stimulates migration and proliferation in HAoECs.

HAoECs were seeded in 96 well plates. Once they reached around 80% confluence, cells were transfected either with hsa-miR-132-3p or scramble microRNA using lipofectamine RNAiMAX transfection agent – a gold standard for microRNA transfection. After transfection, cells were left to recover for 24 hours in EGM MV2 media. Then, half samples underwent a migration assay, and the other half underwent a proliferation assay. During migration assay, cells were checked, and pictures were taken at specific time points, while cell proliferation was checked at 24 and 48 hours.

In figure 4-2E, it is displayed that transfection worked as expected. Indeed, hsa-miR-132-3p-transfected HAoECs were rich in hsa-miR-132-3p microRNA, while scramble-microRNA-transfected HAoECs did not contain any trace of hsa-miR-132-3p. Figure 4-1 shows the line gap closure evolution of migration assay at 0 (a), 8 (b and c), and 16 (d and e) hours.
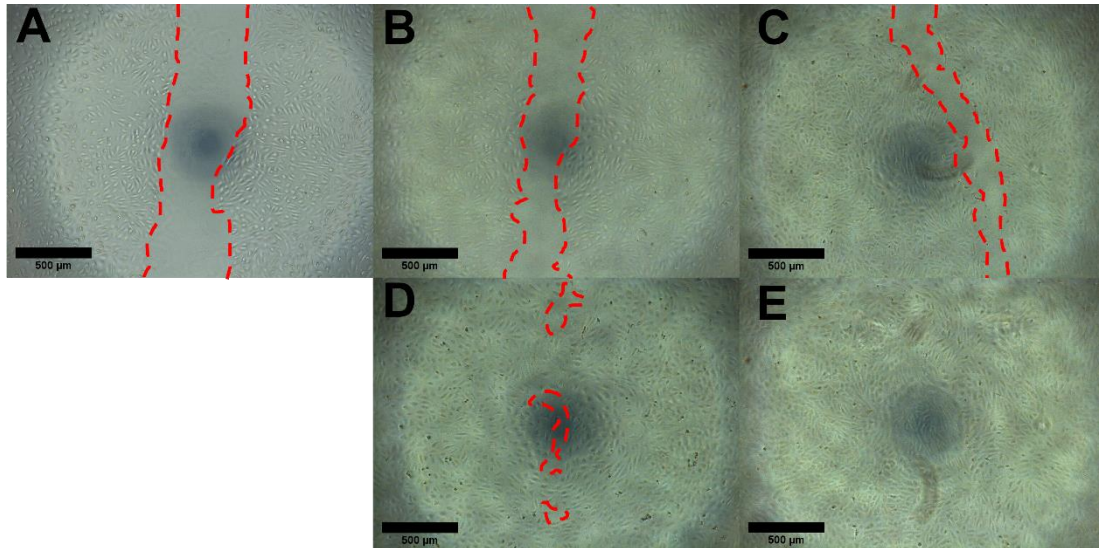
Figure 4-1: Optical microscope pictures of migration assay of transfected ECs
Cells are seeded in 96 well plates, cultured up to 80% confluence, and transfected with hsa-miR-132-3p or scramble microRNA. After 24h, a gap line is created, and the gap closure is observed at established time steps. Gap areas are highlighted by dashed red lines. A) line gap a t=0, B) line gap of scramble microRNA-transfected HAoECs at 8 hours, B) line gap of hsa-miR-132-3p-transfected HAoECs at 8 hours, D) line gap of scramble microRNA-transfected HAoECs at 16 hours, E) line gap of hsa-miR-132-3p-transfected HAoECs at 16 hours.

Data in figure 4-3A showed that hsa-miR-132-3p-transfected HAoECs had higher mobility at all time points. There are statistically significant differences between the two cell groups transfected with different microRNAs – P=0.0022 at 8 and 16 hours.

Concerning the proliferation assay, hsa-miR-132-3p enhanced HAoECs' inclination to proliferate. Figure 4-2 shows proliferation staining images of hsa-miR-132-3p-transfected (figure 4-2B and D, 24 and 48 hours window of observation) and scramble-transfected (figure 4-2A and C, 24 and 48 hours window of observation) cells.
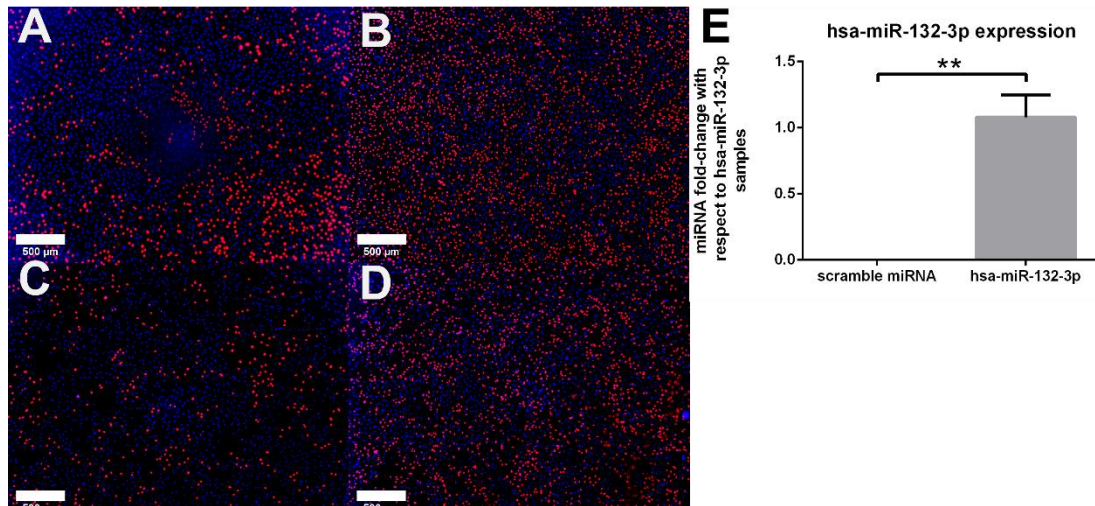
Figure 4-2: Fluorescence microscope pictures of proliferation assay of transfected ECs 24 hours after transfection, cells were incubated with component A from Click-iT EdU Cell Proliferation Kit. Cells that proliferated during component A incubation period are stained in red, while all cells are stained with DAPI (blue). A) scramble microRNA-transfected cells proliferating during 24 hours, B) hsa-miR-132-3p-transfected cells proliferating during 24 hours, C) scramble microRNA-transfected cells proliferating during 48 hours, D) hsa-miR-132-3p-transfected cells proliferating during 48 hours, E) hsa-miR-132-3p expression in scramble microRNA-transfected (scramble miRNA) and hsa-miR-132-3p-transfected (hsa-miR-132-3p) HAoECs 48 hours after transfection. Samples were tested by RT-qPCR, and fold change was calculated with respect to hsa-miR-132-3p values*P<0.05, **P<0.01, ***P<0.001, and ****P<0.0001. Values are expressed as mean ± standard deviation. Technical replicates=6. Non-parametrical test performed (Mann-Whitney).

During the 24 hours observation, 24.79±2.69% of scramble-transfected HAoECs and 46.76±4.91% of hsa-miR-132-3p-transfected HAoECs were proliferating (P=0.0022). Similarly, the proliferation rates were 25.26±3.52% and 44.74±4.68% for scramble-transfected and hsa-miR-132-3p-transfected respectively after 48 hours (P=0.0022) (figure 4-3B). These data confirm that hsa-miR-132-3p administration enhances HAoECs proliferation and migration.
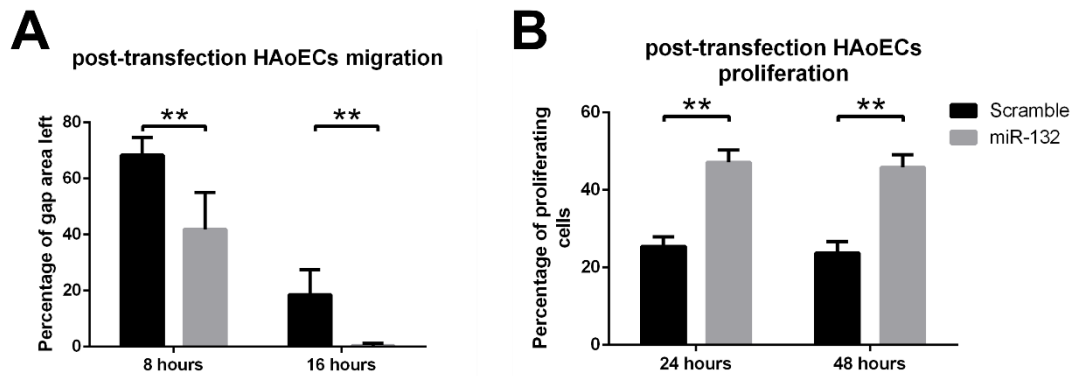
Figure 4-3: Results of post-transfection proliferation and migration assays
A) Migration assay (scratch assay): area left uncovered by cells after 8 and 16 hours from line gap creation. Black bars represent data from scramble-microRNA-transfected cells, while grey bars represent data from hsa-miR-132-3p-transfected cells. B) Proliferation assay (Click-iT EdU Cell Proliferation Kit): percentage of proliferating cells during 24 and 48 hours after one day post-transfection recovery period. Black bars represent data from scramble-microRNA-transfected cells, while grey bars represent data from hsa.miR-132-3p-transfected cells
$*P<0.05$, $**P<0.01$, $***P<0.001$, and $****P<0.0001$. Values are expressed as mean ± standard deviation. Technical replicates=6. Non-parametrical test performed (Mann-Whitney) between paired columns.

4.3   Non-viral vector selection for microRNA transfection

Due to microRNA's fast degradation in body fluids and difficulty to transfect free microRNA, it is important to select a suitable vector for purpose of this project. This section describes the path covered to select a microRNA transfection vector that allows the chosen microRNA to carry out an effective RNAi on ECs.

4.3.1   MicroRNA stability in water or FBS solution

The necessity to protect microRNA when it gets in contact with body fluids was already discussed in other parts of this manuscript – see paragraph 1.5.4. However, it was useful to test it myself as a part of training on RT-qPCR and to have a solid justification for the work undertaken in developing a microRNA vector for my specific case.
MicroRNA was not degraded in RNAse-free water at RT for up to 72h – last experimental time point (figure 4-4A). On the other hand, miRNA was completely degraded in 10% FBS from the

first experimental time point – 1h, P=0.0286 (figure 4-4B), and its expression levels remained consistently undetectable for the remaining time points - data not shown.
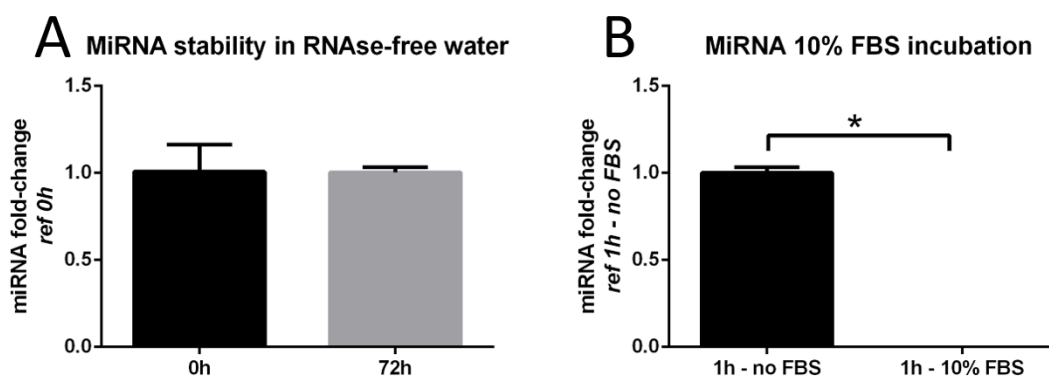
Figure 4-4: Cel-miR-39-3p expression measured by RT-qPCR after 10% FBS incubation of A) microRNA dilution in RNAse-free water incubated at RT; B) microRNA incubated in RNAse-free water at RT with (black bar)/without (grey bar) 10% v/v FBS for 1h. Since the sample is not derived from cell culture, there is no other microRNA that could be taken as housekeeping to normalize the target data; hence 25 fmol/sample of hsa-miR-26a-5p was added as spike-in.*P<0.05, **P<0.01, ***P<0.001 and ****P<0.0001. Values are expressed as mean ± standard deviation. Technical replicates=4. Non-parametrical test performed (Mann-Whitney).

10% FBS is the usual concentration added to culture media during in-vitro work. FBS is an animal-derived blood extract that contains a physiological mix of nucleases. However, the final concentration of several medium components – e.g. glucose and electrolytes - are not necessarily equal to the human organism's concentrations. Nevertheless, studies have shown that nucleic acid digestion is 2-fold quicker in in-vivo than in standard culture media, reinforcing the need of protecting genetic material for an effective administration [467], [468]. The media composition was optimized for in-vitro culture, which is the benchmark for this study which is at the *proof-of-concept* stage; thus the application of in-vitro models is compulsory. In a potential follow-up, an animal model (with its characteristics in terms of nuclease degradation dynamics) may be employed, but that is not the aim of this project.

4.3.2   Chitosan-NPs as non-viral vector for microRNA transfection

4.3.2.1   Chitosan-NPs fabrication

Chitosan seems to be one of the most suitable vectors for this project; thus, it was the first to be developed – see paragraphs 1.5.4, 1.5.5, and 2.2 for details. In this paragraph, the chitosan-NPs production protocol optimization is described. The tuning work considered four parameters,

which emerged to influence NPs size in the literature: Chitosan concentration, crosslinker (TPP) concentration, Chitosan/TPP mass ratio, and NaCl (adjuvant) concentration. The reason behind the choice of these, and these only, parameters to tune are detailed in paragraphs 2.2 and 5.2.1. Each parameter was changed singularly, starting from Chitosan concentration. The first NPs batches were closer to the upper range limit; hence I decided to choose the variant that was giving smaller NPs for each parameter tuning and carry it to the following parameter calibration (figure 4-5). The diameters were estimated by DLS as it is quick and inexpensive. The final formulation was also analyzed by SEM. DLS analysis conditions were closer to the transfection condition, i.e., the analysis was done with NPs in water solution. As chitosan-NPs are technically nanogels, their water content is relevant, even if this has not been estimated, as far as I am concerned [469]. SEM analysis is performed on dehydrated samples, which then present shrank NPs. However, DLS computes particle size from an indirect measurement using an algorithm, thus the results may have a degree of error. DLS measures the NPs' Brownian motion and relates that with NPs' size. The smaller the NPs the faster is their motion. Since we are talking about Brownian motion, the NPs' velocity is called the translational diffusion coefficient. The formula that correlates diffusion to diameter includes temperature and solvent viscosity through the Stokes-Einstein equation. Thus, it is important to have a precise measurement of solvent viscosity and temperature. Another source of error is the presence of aggregates that can mislead the estimation of diffusion. Also, as the equation assumes the NP is spherical, a non-spherical NP can lead to a wrong diameter estimation. Other influencing characteristics are the solution ionic strength and the NPs concentration. Imprecise estimation or inconsistency of these parameters can lead to diameter estimation far from reality [470]. On the other hand, SEM is more reliable even because it is much more straightforward. An SEM provides pictures of the specimen surface with a resolution of up to 3 nm. The picture derives from the sample's electron scatter pattern, which is the result of the interaction between the sample surface and the focused electron beam. However, the electrons' scatter process is influenced by the sample geometry. The resolution of objects boundaries is not always neat (shadowing effects), especially when observing tall objects with surfaces tangent to the electron beam direction. Nevertheless, in the case of NPs appropriately diluted with a spherical profile, the 2D projection of a spherical object from above corresponds to its diameter [471], [472].

Process walkthrough (figure 4-5):

- An initial formula was drawn comparing published works [395], [396], [430], [431], [473]– [475]: Ch concentration 0.5 mg/mL, TPP concentration 0.25 mg/mL, Ch/TPP mass ratio 7 mg/mg, and NaCl concentration 50mM. For each parameter, I tested a lower and a higher

concentration – I tested four points NaCl as there was a variety of concentrations in the literature:

- Ch concentration variation from 0.25mg/mL to 1 mg/mL: 0.25 mg/mL was chosen as it gives a NPs diameter of 640±25nm.

- TPP concentration variation from 0.1mg/mL to 0.5 mg/mL: 0.1 mg/mL gave NPs with smaller diameter - 466±37 nm.

- Ch/TPP weight ratio variation from 5 to 10. 7 gave NPs with smaller diameter - 172±69 nm.

- NaCl concentration variation from 0mM to 150mM: 50mM gave NPs with smaller diameter - 140±25 nm.
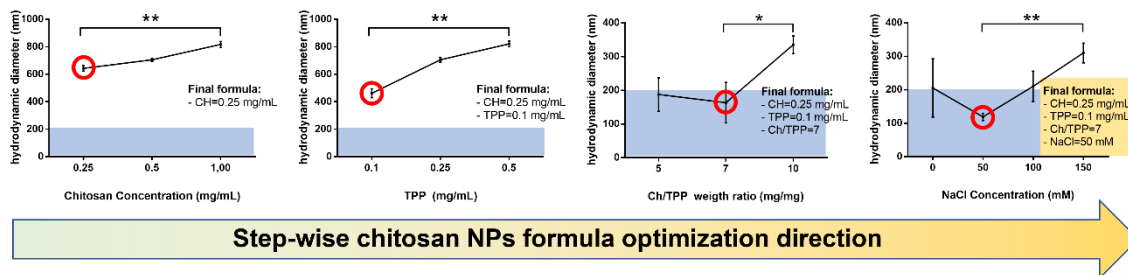
Figure 4-5: NPs fabrication protocol calibration

Chitosan-NPs were analysed in their production solution. Diameters were measured by DLS. Each graph shows the NPs' diameters evolution as a consequence of a single-parameter variation. From left to right: Chitosan concentration (0.25-1 mg/mL), TPP concentration (0.1-0.5 mg/mL), Chitosan/TPP mass ratio (5-10), and NaCl concentration (0-150 mM). Light blue areas are the acceptable NPs diameter ranges. For each step, I chose the parameter value that was giving smaller NPs (circled in red). This was carried to the following parameter calibration, so the final formula was defined in a stepwise fashion (complete formula in the yellow box). Values are expressed as mean ± standard deviation. Technical replicates=4. Non-parametrical test performed (Kruskal-Wallis ranks test and Dunn's test for multiple comparisons). *$P<0.05$, **$P<0.01$, ***$P<0.001$ and ****$P<0.0001$.

Eventually, the final formulation was Chitosan concentration=0.25mg/mL, TPP concentration=0.1mg/mL, Chitosan/TPP weight ratio=7, NaCl concentration=50mM, since it was the formulation that gave the smallest NPs among all the tested ones and below 200nm (see paragraph 2.4.1). According to DLS data, the NPs size was 140±25 nm. I also observed the final formulation with the SEM and TEM to have visual proof of NPs formation. However, I could not extrapolate any useful information from it as only a thick layer with several cracks was visible (figure 4-6A). Buffer exchange of NPs suspension was not possible as I was not able to find a centrifugation routine that avoided aggregates formation allowing to concentrate the NPs on the tube bottom at the same time (see paragraph 3.3.2). Together with the electronic

microscopy technician, we presumed that the layer was a composite of NPs and dried NaCl added to the production solution. We have also tried to drop-cast the NPs on a filter paper, but we did not obtain a good image (figure 4-6B).
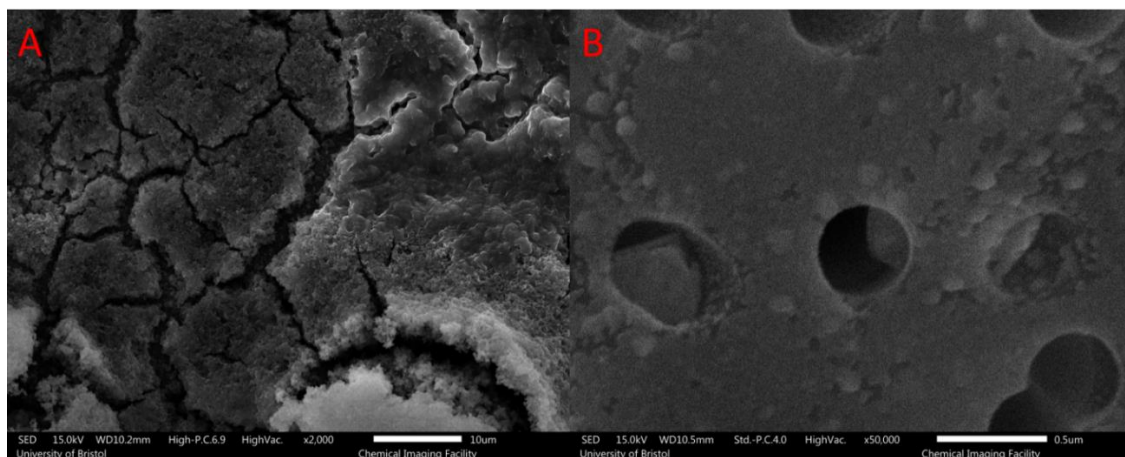
Figure 4-6: SEM images of chitosan-NPs
A) SEM image of NPs solution drop cast on an SEM stub. A layer with cracks is visible but is impossible to identify NPs. The same goes with the NPs solution cast on filter paper (B). The big-rounded circles are the filter pores, NPs are not easy to identify.

Since SEM imaging was not satisfying, we decided to try the TEM as it gives two benefits:

- higher magnification
- the possibility to drop-cast the sample on a copper grid to get rid of NaCl solution more efficiently.

TEM captures transmitted electrons through the sample, creating a topological distribution of them, similar to an x-ray scan. NPs' dimensions can be directly measured from these images that can reach astonishing resolutions – up to 0.2nm for the system used in this project. NPs can be identified if the sample is not too concentrated, and thus NPs are highly overlayed. The interpretation of TEM images of overlayed objects is complicated by the fact that TEM presents 2D images of 3D samples. In other words, as electrons interact with the whole specimen thickness, the sum of the whole interaction is projected on a 2D picture. Therefore, the specimen image will be the result of overlapped optical sections pictures for the whole machine's field of depth, added on a blurred background representing the interaction of the electrons with the rest of the unfocused specimen thickness [476]. However, the TEM pictures I have taken for

chitosan characterization seemed to show sufficiently spaced spheres with well-defined contours.

Eventually, I was able to observe the chitosan NPs (TEM mode - figure 4-7A) that have a size distribution that goes from 12 to 20 nm (figure 4-7B). I did not perform any statistical analysis on NPs diameter since I was able to analyse only two samples. The repeated attempts with SEM made this part of characterization too expensive and time-consuming. However, from the observations I carried out, the NPs size was considerably reduced compared with DLS data mainly due to the dehydration process which NPs undergo before TEM acquisition. Also, thanks to the analysis of scattered X-rays (figure 4-7D), I could obtain an additional confirmation that I was observing chitosan-NPs observing the distribution map of the crosslinker. As highlighted in figure 4-7D, the distribution of phosphorous (P) and oxygen (O) is the same as the particle distribution picture taken in STEM mode (figure 4-7C). Since P and O are the two elements of the chitosan-NPs crosslinker (TPP), P and O distribution reflects TPP distribution. Figure 4-7D shows a TPP concentration increase in correspondence to the white bodies identified in figure 4-7C. This is an additional indication of NP formation.
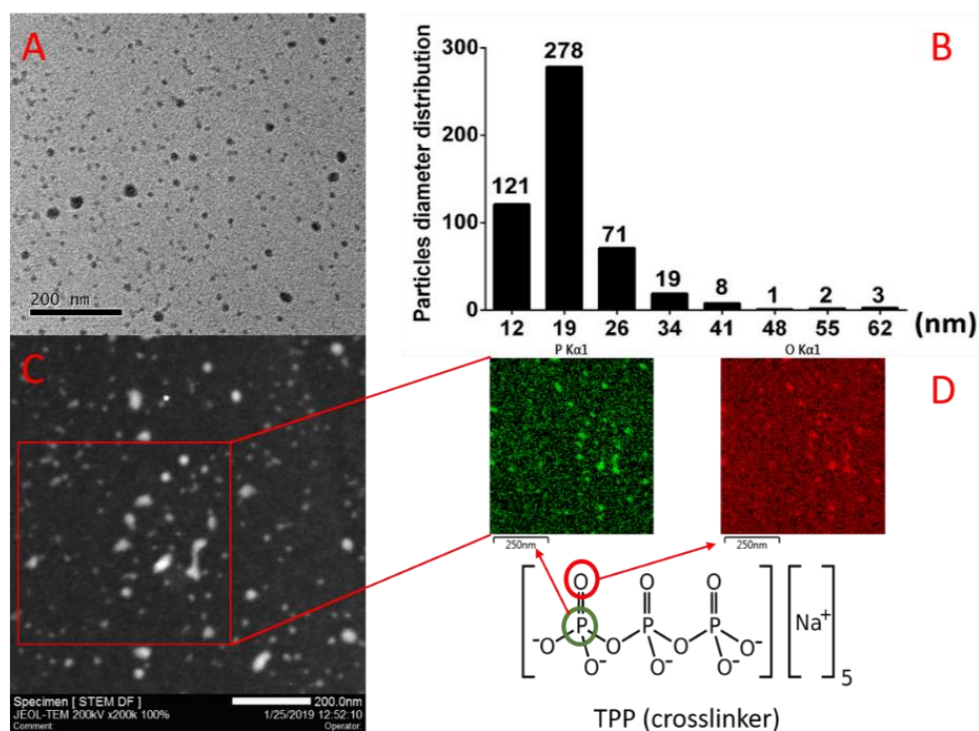
Figure 4-7: Chitosan-NPs characterization by TEM, STEM, and EDS.
A) TEM image of chitosan NPs suspension dried on a TEM sample older (copper grid). The black spots are the actual NPs. B) NPs size distribution was taken from 5 random pictures taken from two chitosan NPs samples by TEM imaging. C) STEM imaging of chitosan-NPs (white spots). In STEM mode, scattered X-rays were sampled to create elemental maps (EDS). The distribution maps of phosphorus (P - green dots on black background – figure 4-7D) and oxygen (O - red dots on black background – figure 4-7D) were obtained. The chitosan-NPs crosslinker (TPP)

formula is shown in figure 4-7D. P and O are the TPP constituent elements; thus P and O distribution correspond to TPP distribution. The TPP distribution peaks correspond to the location of the white spheroids in the STEM image, another proof supporting the achieved fabrication of chitosan-NPs. Technical replicates =2.

4.3.2.2 Chitosan-NPs in-vitro cytotoxicity and proliferation

The project aimed at developing a scaffold for cardiovascular regenerative medicine, able to stimulate valve regeneration thanks to the integration of a microRNA, which should enhance scaffold colonization. Thus, it is imperative that such product does not impair cell viability and proliferation, key features for cells supposed to repopulate an endothelial gap.

Dosing NPs in in-vitro experiments is not straightforward. As far as I am concerned, there is no easy way to count the NPs. Also, I could not find a way to calculate the average weight of each NP. Hence, I found it impossible to dose NPs in terms of NPs number per sample. In all reviewed papers (can be found in paragraphs 1.5.5, 2.2, and 5.2.1), chitosan-NPs are dosed as the weight of Chitosan and/or microRNA per sample or volume of incubated media. In addition, none of my collaborators and supervisors mentioned any NPs counting method to me. As I have not additionally manipulated the NPs production suspension (no buffer exchange, concentration, or dilution), I just dispensed the appropriate aliquot NPs production suspension considering the initial amounts of chitosan and microRNA added for NPs fabrication. Usually, chitosan-NPs concentration applied during transfections is lower than 10 ng/μL in the culture media [346], [439], [477]. Hence, in line with published work, I decided that the highest chitosan-NPs experimental concentration should have been below 10 ng/μL. I set the starting NPs concentration to 7 ng/μL per sample, halfway between the recommended maximum dosage and its half. In doing so, I hoped to avoid cell toxicity and to provide a sufficient dose for a noticeable effect. The other concentrations were around 5 and 10-fold the lower NPs concentration in the effort to explore the toxicity boundaries for my specific application. Lipofectamine RNAiMAX is a commercial transfection agent recommended for microRNA transfection. I have used it as the microRNA-transfection gold standard – i.e. the positive control.

In accordance with literature and the Lipofectamine RNAiMAX transfection protocol, ECs were transfected as follows. EA.hy926 were incubated with empty Chitosan-NPs or Lipofectamine for four hours to simulate a microRNA transfection. Then, ECs are left to rest overnight (16 hours) to recover from the stress of transfection. Finally, assay reagents are incubated [346], [396], [477](figure 4-8).
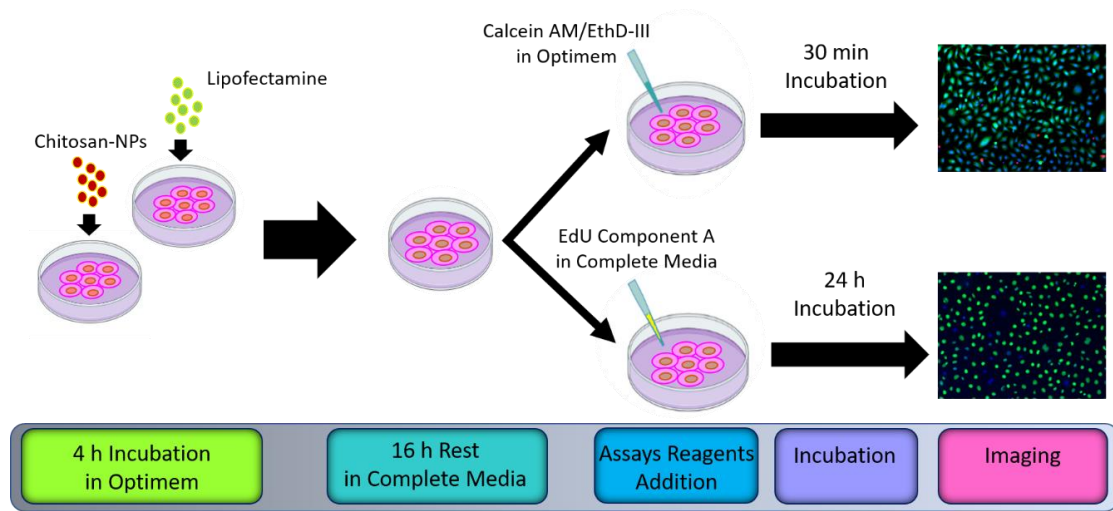
Figure 4-8: Fluorescent NPs uptake experiment walkthrough

EA.hy926 are incubated with either Chitosan-NPs or Lipofectamine for 4 hours. Then, cells are left resting to recover from incubation for 16h. At end of the rest period, cells are incubated with the assay reagents (Component A for proliferation or Calcein MA/EthD-III for viability) and imaged. Illustration created in BioRender.com

NPs cytotoxicity was tested using the Viability/Cytotoxicity Assay Kit (Biotium, USA) (figure 4-9). Live cells are in green, while the DNA of dead cells is stained in red.
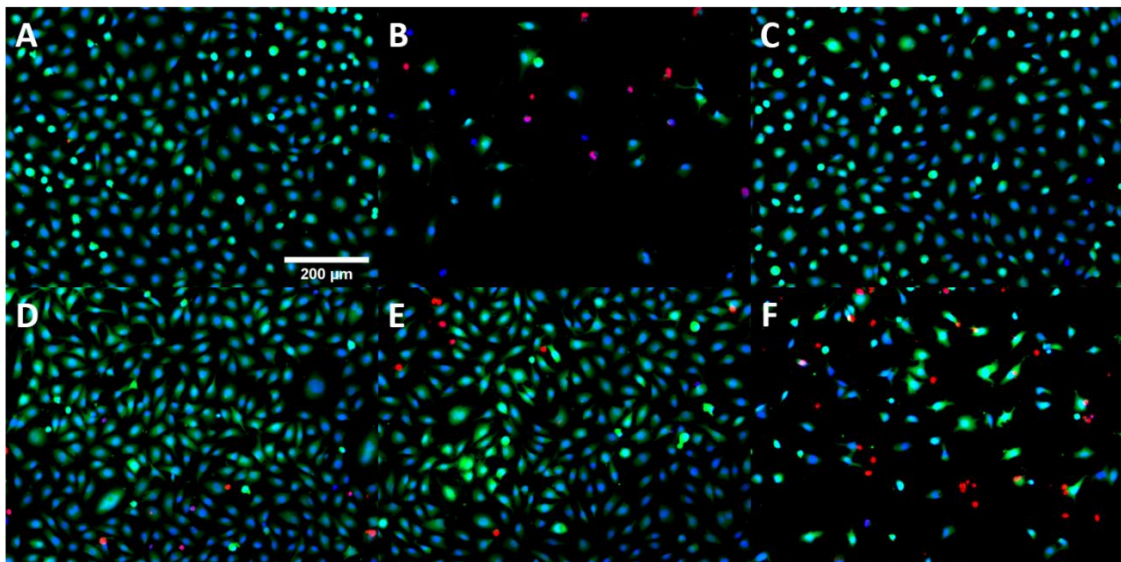
Figure 4-9: Live & dead staining of ECs incubated with different transfection vectors

A) Control – no treatment, B) Lipofectamine, C) NPs production solvent, D) Chitosan-NP at 7 ng/μL, E) Chitosan-NP at 34 ng/μL, F) Chitosan-NP at 68 ng/μL. Blue are the nuclei stained with DAPI, green is the cytoplasm of living cells stained with Calcein, and the red spots are DNA of dead cells stained with EthDIII.

Cell proliferation was evaluated using a 5-Ethynyl-2´-Deoxyuridine (EdU) kit (Click-iT® EdU Assay, Invitrogen). The nuclei of all cells were stained in blue with DAPI, and cells proliferating during the observation window had their nuclei stained in green (figure 4-10).
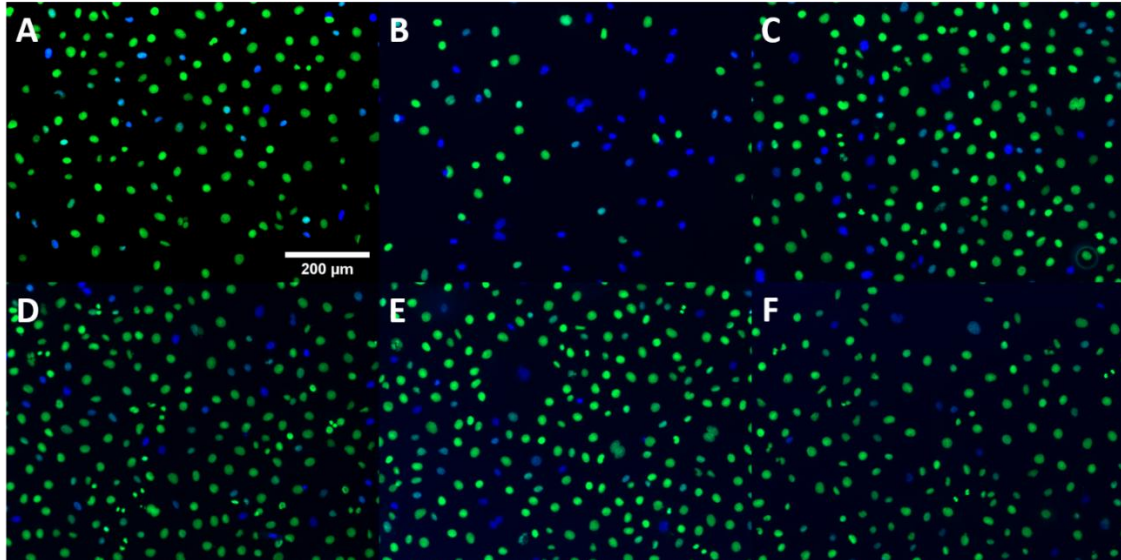
Figure 4-10: Proliferation staining of ECs incubated with different transfection vectors
A) Control – no solution incubated, B) cells incubated with Lipofectamine, C) cells incubated with NPs production solvent, D) cells incubated with chitosan-NPs 7 ng/μL, E) cells incubated with chitosan-NPs 34 ng/μL, F) cells incubated with chitosan-NPs 68 ng/μL. In green are the nuclei of cells that proliferated during the observation window, whereas in blue are nuclei of cells that did not proliferate during the observation window. All cells are stained with DAPI but proliferating cells have a brighter EdU (green) which covers DAPI.

As shown in the bar graphs (figure 4-11A and B), chitosan NPs at theoretical concentrations of 7ng/μL and 34ng/μL did not cause any significant difference in viability and proliferation compared with control, whereas Lipofectamine reduced proliferation only (P=0.048). The highest chitosan NPs dosage (68 ng/μL) significantly reduced the viability (P=0.058 vs. control) but not the proliferation ability. Also, Lipofectamine reduced significantly proliferation compared with samples administered with chitosan NPs at concentrations of 7ng/μL (P=0.0207) and the control (P=0.0048).

Noteworthy, cell density is way lower in lipofectamine-treated samples than in the other ones (data not shown). It was not possible to establish what caused that. Whether the low cell density is something to attribute to lower proliferation, higher mortality, or something else, it is not a desirable effect for an application that aims to speed-up endothelialization.
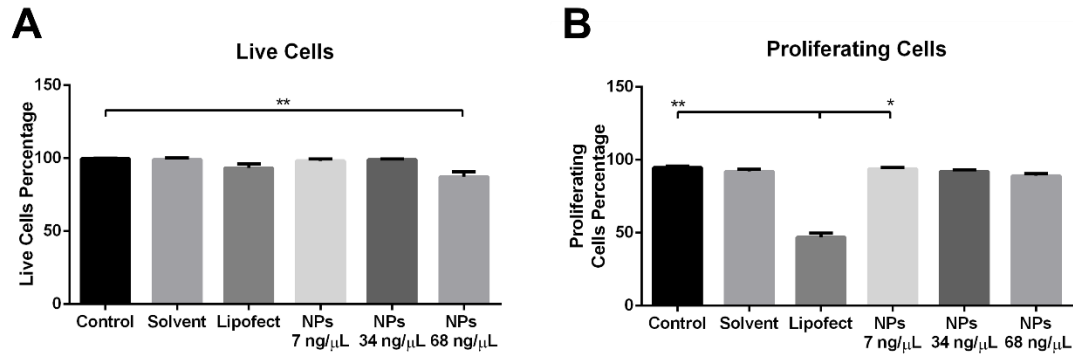
Figure 4-11: Viability and Proliferation results of ECs incubated with different transfection vectors

Percentage of alive (A) or proliferating (B) cells (EA.hy926) incubated with different solutions for four hours to simulate a microRNA transfection. Then, ECs are left to rest overnight (16 hours) to recover from the stress of transfection. Finally, assay reagents are incubated. From the left of each graph: control group with no solution incubated - Control, cells incubated with NPs production solvent - Solvent, cells incubated with Lipofectamine - Lipofect, cells incubated with chitosan-NPs at 7 ng/μL – NPs 7 ng/ μL, cells incubated with chitosan-NPs at 34 ng/μL - – NPs 7 ng/ μL, and cells incubated with chitosan-NPs 68 at ng/μL – NPs 68 ng/ μL. *P<0.05, **P<0.01, ***P<0.001 and ****P<0.0001. Values are expressed as mean ± standard deviation. Technical replicates=4. Non-parametrical test performed (Kruskal-Wallis ranks test and Dunn's test for multiple comparisons).

The results of this experiment showed that Chitosan-NPs administered to endothelial cells EAhy926 up to a concentration of 34ng/μL are non-toxic. Although there is no statistical difference between Lipofectamine and Chitosan-NPs-incubated cells in terms of viability percentage, Lipofectamine samples' cell density was visibly lower than the other samples, except for the Chitosan-NPs 68 ng/μL sample. No proliferation reduction was demonstrated for Chitosan-NPs-incubated samples compared to control, while Lipofectamine impacted negatively on that aspect (-36±11%). This experiment showed Chitosan-NPs had no negative impact up to a concentration of 34 ng/μL in terms of viability and proliferation.

4.3.2.3   Exogenous micro-RNA loaded NPs in-vitro cytotoxicity and proliferation

The highest viability- and proliferation-non-impairing chitosan-NPs concentration is 34 ng/μL – see previous paragraph. The following experiment was conceived to understand whether the incorporation of a microRNA in chitosan-NPs has an impact on cell (EA.hy926) proliferation and viability. An exogenous microRNA of nematode origin was used: cel-miR-39-3p. There is no specific purpose to use a non-human microRNA in this experiment. However, it will come useful

in future experiments when the aim will be the estimation of the amount of transfected microRNA. As human cells are not able to produce that specific microRNA, the estimation will not be altered by cell-synthetized microRNA. I decided to use cel-mir-39-3p in this experiment to give consistency to the work. The concentrations of miRNA-39-3p were 10, 20, and 30ng/µL. Control and Lipofectamine transfection samples were included. The experimental protocols remained the same as experiments with empty chitosan-NPs (4-12).
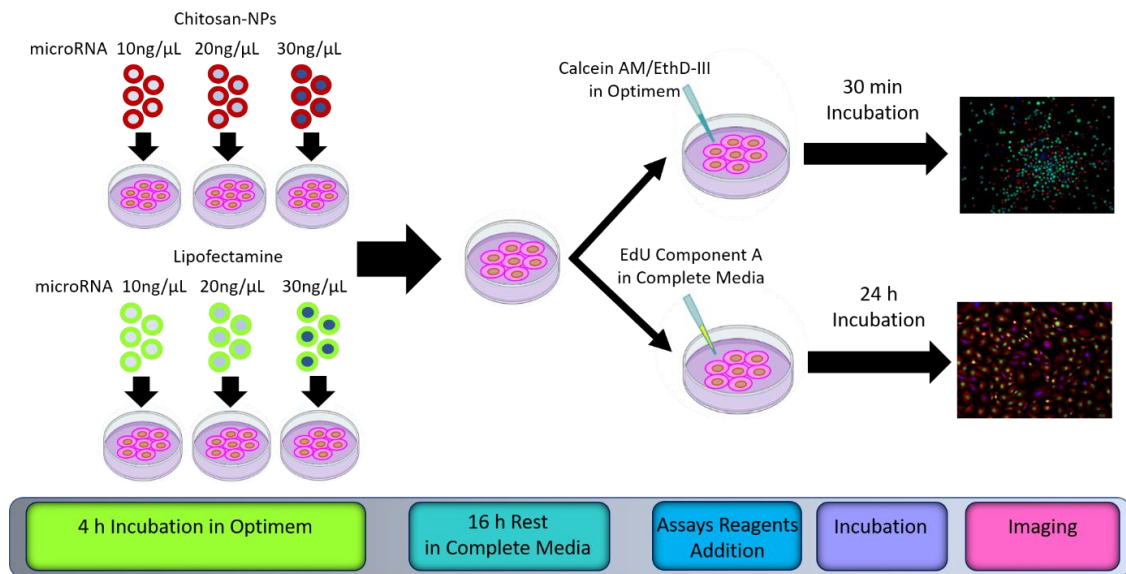
Figure 4-12: MicroRNA transfection with non-viral vectors experimental walkthrough
Cells are incubated with either Chitosan-NPs or Lipofectamine with three different microRNA concentrations (10, 20, and 30ng/µL) for 4 hours. Then, cells are left recovering from transfection for 16h. At end of the rest period, cells are incubated with the assay reagents (Component A for proliferation or Calcein AM/EthD-III for viability) and imaged. Illustration created in BioRender.com

Figure 4-13 represents viability assay (Viability/Cytotoxicity Assay Kit, Biotium, USA). Blue are the nuclei stained with DAPI, green is the cytoplasm of living cells stained with Calcein, and the red spots are DNA of dead cells stained with EthDIII. Numerical data of this assay are displayed in figure 4-15. In figure 4-13, there is a visible green dimming in several cells (identified by DAPI) of chitosan-NPs treated samples. Cells' cytoplasm becomes green when Calcein AM (administered to identify viable cells – see paragraph 3.2.6) is converted into green calcein by cells' esterases. The reduced Calcein Am conversion in chitosan-NPs-treated cells may be a sign of poor cell health [478], [479]; although this reflects in higher cell death cell rate only in samples with higher microRNA concentration - Chitosan-NP at 34 ng/µL with 30 ng/µL of cel-miR-39-3p. Another hypothesis is that chitosan-NPs may interfere with Calcein AM conversion. Unfortunately, I was not able to find a reference for this hypothesis.
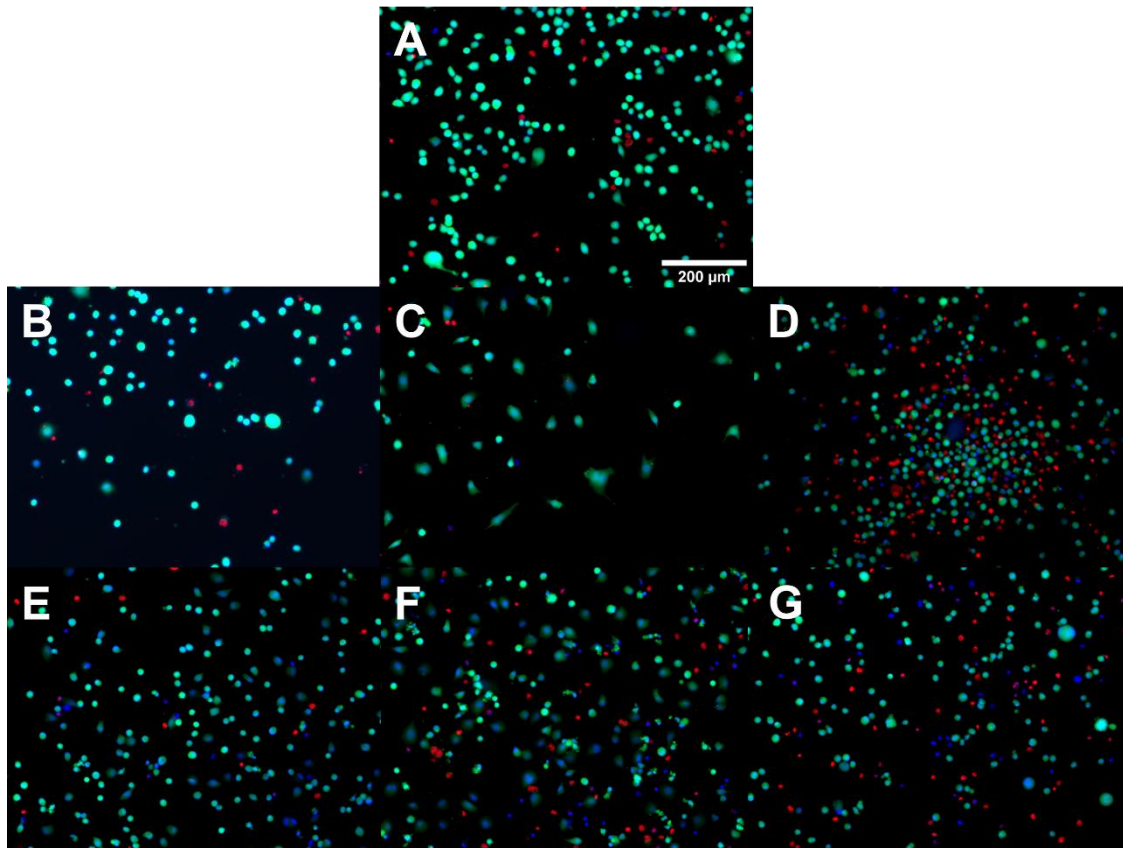
Figure 4-13: Live & dead staining of ECs after transfection with non-viral vectors
Blue are the nuclei stained with DAPI, green is the cytoplasm of living cells stained with Calcein, and the red spots are DNA of dead cells stained with EthDIII. A) Control – no treatment, B) Lipofectamine with 10 ng/µL of cel-miR-39-3p, C) Lipofectamine with 20 ng/µL of cel-miR-39-3p, D) Lipofectamine with 30 ng/µL of cel-miR-39-3p, E) Chitosan-NP at 34 ng/µL with 10 ng/µL of cel-miR-39-3p, F) Chitosan-NP at 34 ng/µL with 20 ng/µL of cel-miR-39-3p, G) Chitosan-NP at 34 ng/µL with 30 ng/µL of cel-miR-39-3p.

Figure 4-14 represents the proliferation assay (Click-iT EdU Cell Proliferation Kit, Thermo Fisher Scientific, USA). Cells' cytoskeleton was stained with β-tubulin, in green are the nuclei of cells that proliferated during the observation window, whereas in blue are nuclei of cells that did not proliferate during the observation window. Actually, all cells are stained with DAPI but proliferating cells have a brighter EdU (green) which covers DAPI. There is not much to note on the picture appearance and data derived from this assay are discussed in the next paragraph.
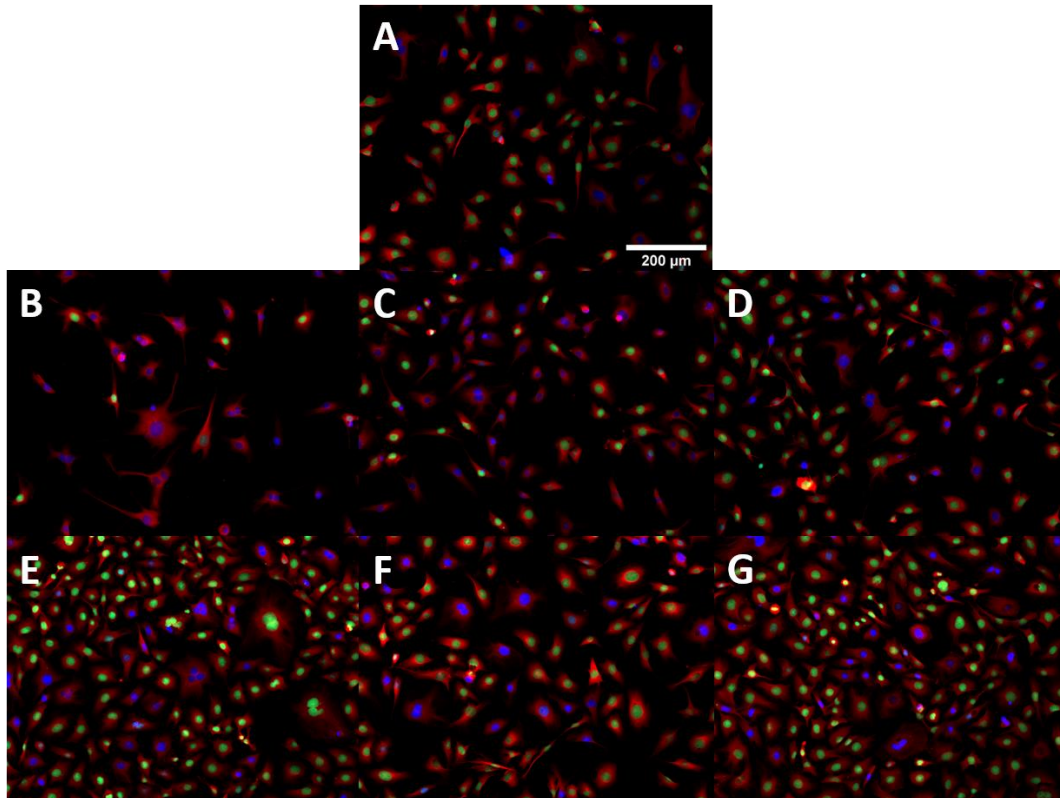
Figure 4-14: Proliferation staining of ECs after transfection with non-viral vectors
To have a clearer view of cells, I added cytoskeleton β-tubulin staining (red). Nuclei staining: in green are the nuclei of cells that proliferated during the observation window, whereas in blue are nuclei of cells that did not proliferate during the observation window (all cells are stained with DAPI but proliferating cells have a brighter EdU (green) which covers DAPI). A) Control – no treatment, B) Lipofectamine with 10 ng/μL of cel-miR-39-3p, C) Lipofectamine with 20 ng/μL of cel-miR-39-3p, D) Lipofectamine with 30 ng/μL of cel-miR-39-3p, E) Chitosan-NP at 34 ng/μL with 10 ng/μL of cel-miR-39-3p, F) Chitosan-NP at 34 ng/μL with 20 ng/μL of cel-miR-39-3p, G) Chitosan-NP at 34 ng/μL with 30 ng/μL of cel-miR-39-3p.

As the viability graph shows (figure 4-15A), chitosan-NPs were more tolerable compared with lipofectamine (P<0.001), both with a micro-RNA dosage of 10ng/μL. However, no viability difference between chitosan NPs and lipofectamine administration was observed at higher microRNA dosages. Noteworthy, chitosan-NP-transfected ECs were always above 80% viability for all the micro-RNA dosages, and no statistical difference with control arose. The proliferation results were difficult to interpret and required repetition but the experimental schedule did not allow it. Reduced proliferation was seen at the two lower infecting dosages, but not at the highest (figure 4-15B). To the best of my knowledge, there is no justification for it. Nevertheless, data from chitosan-NP-treated EA.hy926 ECs confirmed that viability and proliferation are not impaired.
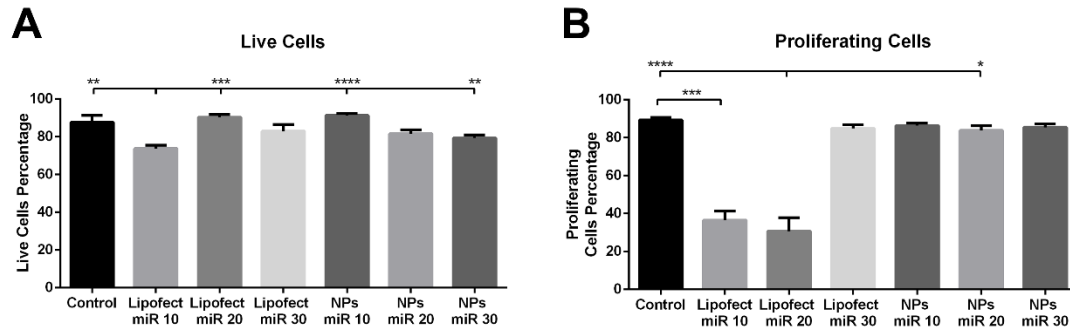
Figure 4-15: Percentage of viable and proliferating ECs after transfection with non-viral vectors Percentage of alive (A) or proliferating (B) cells (EA.hy926) incubated with different solutions. The viability assay was performed using the Viability/Cytotoxicity Assay Kit (Biotium, USA) and the proliferation assay was performed with Click-iT EdU Cell Proliferation Kit (Thermo Fisher Scientific, USA). From the left of each graph: Control (no treatment) – Control, Lipofectamine with 10 ng/µL of cel-miR-39-3p – Lipofect miR 10, Lipofectamine with 20 ng/µL of cel-miR-39-3p – Lipofect miR 20, D) Lipofectamine with 30 ng/µL of cel-miR-39-3p – Lipofect miR 30, E) Chitosan-NP at 34 ng/µL with 10 ng/µL of cel-miR-39-3p – NPs miR 10, F) Chitosan-NP at 34 ng/µL with 20 ng/µL of cel-miR-39-3p – NPs miR 20,, G) Chitosan-NP at 34 ng/µL with 30 ng/µL of cel-miR-39-3p – NPs miR 30. *P<0.05, **P<0.01, ***P<0.001 and ****P<0.0001. Values are expressed as mean ± standard deviation. Technical replicates=6. Non-parametrical test performed (Kruskal-Wallis ranks test and Dunn's test for multiple comparisons).

4.3.2.4   Endothelial Cells uptake of fluorescent chitosan-NPs

I functionalized the chitosan with fluorescein isothiocyanate FITC, to have visual proof of chitosan-NPs uptake by EA.hy926 ECs. I produced empty chitosan-NPs and applied the transfection protocol used for previous experiments. NPs concentration was set to 34ng/µL as it is the highest NPs concentration which does not impair viability and proliferation, among the tested ones. The cell monolayer was analyzed by fluorescence microscopy. In addition, it was decided to track fluorescent chitosan-NPs and establish the fraction of which ended up on the cells (illustrated experimental plan in figure 4-16). To do so, a calibration curve that correlates FITC-conjugated chitosan-NPs amount to fluorescence units was drawn - see paragraph 3.4.2.
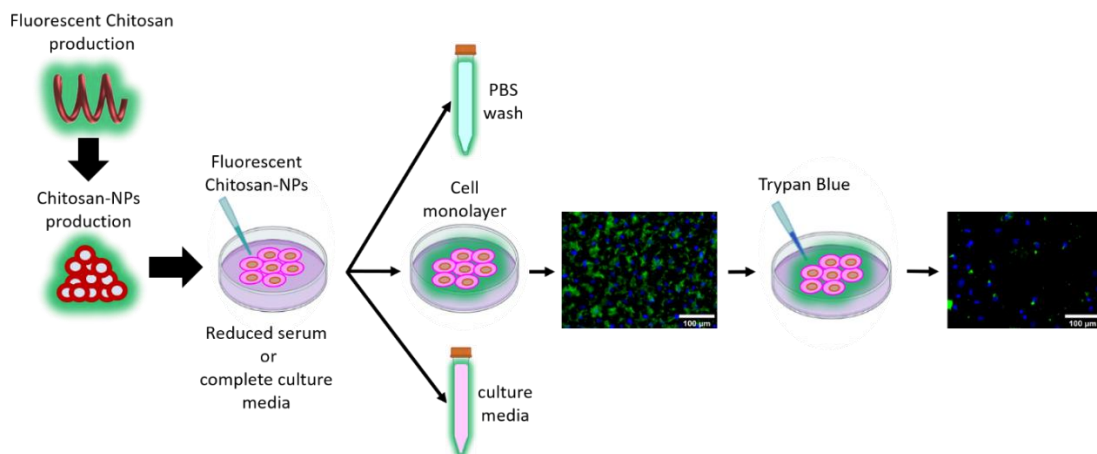
Figure 4-16: Fluorescent NPs uptake experiment walkthrough
FITC- functionalized Chitosan is produced and used to fabricate fluorescent Chitosan-NPs. Chitosan-NPs are then incubated for 4 h with ECs. After NPs incubation, fluorescence intensity is measured, and cells are imaged. Then, the cell monolayer is incubated with the Trypan Blue and imaged again. Illustration created in BioRender.com

Initially, the same NPs incubation protocol used to test viability and proliferation was applied (see paragraphs 3.2.3 and 3.2.4). This first attempt to get NPs uptake by ECs was unsuccessful. No traces of fluorescence in the FITC channel was found on the cell monolayer. After an extensive literature review, I decided to introduce two variations to the experimental protocol: incubating the cells with NPs up to 24h, and comparing normal culture media – which includes 10% serum - with reduced serum media (Optimem) for transfection [346], [480]. With these modifications, I was able to observe particle uptake (figure 4-18B and C). After 24h, cells were washed with PBS and incubated with fresh culture media. Then, fluorimeter measures were taken. Combining the fluorimeter measures with the calibration trendline equations, I calculated the NPs' relative concentration in different phases: on the cell layer, the transfection media (T media), and PBS used to wash the culture wells after the 24h incubation (figure 4-17). Chitosan-NPs amounts are expressed as fractions of the amount incubated with cells (34ng/μL). The use of Optimem reduced serum media (custom practice when doing cell transfection with liposomes) allows more NPs to be retained on the cell layer – 64.5±4.6% versus 26.1±4.1%. Chitosan-NPs that stayed suspended in the culture media were around 30% of the total for both employed media at the end of the experiment. On the other hand, around 40% more NPs were washed away with PBS when complete media was used, perhaps due to FBS proteins creating floating NPs aggregates.
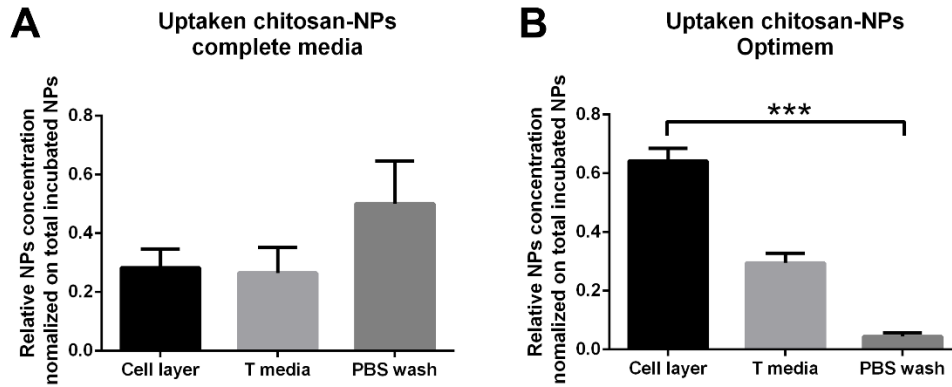
Figure 4-17: Fluorescent chitosan-NPs distribution results

Relative chitosan-NPs amount to the total incubated in the cell layer, PBS wash, and transfection media. FITC-conjugated chitosan-NPs transfection was carried out using complete EA.hy926 media (A) or Optimem (B). Data were generated before incubating Trypan Blue to quench extracellular FITC-NPs. NPs were incubated with complete media (10% FBS – 4-17A) and reduced serum media (Optimem – 4-17B) for 24h. Cells were washed with PBS and incubated with fresh culture media. Then, the fluorescence of the cell layers, the transfection media (T media), and the PBS used to wash the cells (PBS wash) was measured by Promega Glomax fluorimeter (excitation wavelength 475 nm and emission band 500-550 nm). The amounts of chitosan-NPs were calculated by correlating the fluorescence values to the amount of chitosan-NPs using the calibration curves calculated in paragraph 3.4.2. *$P<0.05$, **$P<0.01$, ***$P<0.001$ and ****$P<0.0001$. Values are expressed as mean ± standard deviation. Technical replicates=6. Non-parametrical test performed (Kruskal-Wallis ranks test and Dunn's test for multiple comparisons).

Cell monolayer fluorescence microscopy images gave visual confirmation of previous data (figure 4-18). Figures 4-18B and 4-18C show the cell monolayer after NPs incubation with complete media and Optimem, respectively. The difference in favour of the latter is clear. However, detecting the FITC signal on the cell monolayer does not necessarily mean that the NPs have been internalized in the ECs, rather they can be either inside cells or externally attached to cell membranes. To exclude the extracellular NPs, half of the samples were incubated with Trypan Blue after fluorescent fluorimeter measurement. Trypan Blue has two favourable qualities: it quenches fluorescent signals in the FITC wavelength and does not penetrate live cells [481]. Following a published protocol, cells were incubated with a solution of trypan blue in PBS (1.2 mg/mL) at 4°C for 30'. Then, the cell monolayer was washed trice with PBS, fixed, stained with DAPI, and then imaged. The small dots that can be seen in Figures 4-18E and 4-18F can only come from NPs inside live cells – magnified versions of the cell layers after Trypan Blue incubation are shown in figure 4-19. Noteworthy, I have used a 20x lens – the highest magnification in our laboratory's microscope, and chitosan-NPs are on average almost 1000-fold smaller than the scale bar, as measured by DLS. Thus, it is highly likely that I have not

been able to detect the fluorescence of all internalized NPs, since the microscope was not able to resolve the smallest ones.
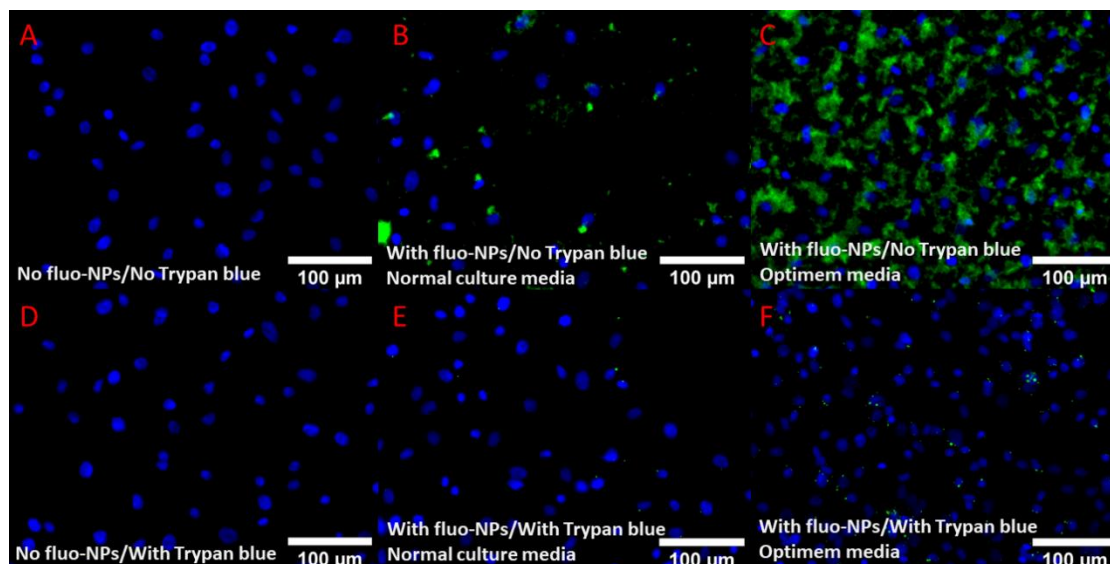
Figure 4-18: Fluorescent chitosan-NPs uptake images
In blue are nuclei stained with DAPI and in green are the chitosan-NPs functionalized with FITC. Pictures were taken after the FITC-conjugated chitosan-NPs transfection. Then, part of them was incubated with Trypan Blue (protocol outlined in this paragraph). A and D) Control samples (no NPs incubation) with (A) and without (D) the incubation with Trypan Blue. B and E) Samples with NPs incubated in complete media with (B) and without (E) the incubation with Trypan Blue. C and F) Samples with NPs incubated in reduced serum media (Optimem) with (C) and without (F) the incubation with Trypan Blue.

Figure 4-19 are 2 magnified fields of cells incubated with fluorescent NPs in normal culture media (4-19 A and B), and 2 magnified fields of cells incubated with fluorescent NPs in Optimem media (4-19 A and B). Pictures were taken after the application of the aforementioned Trypan Blue incubation protocol. Cells with at least one visible fluorescent NP around or on the nucleus were marked positive. Cells without any fluorescent NP around or on the nucleus fell in the negative group. Keeping in mind that only NPs inside live cells are not quenched by trypan blue (see above), this can be a metric that contributes to evaluate the chitosan-NPs ability to cross the plasma membrane, a necessary requisite of a good transfection vector. From each of the 3 technical replicates for each condition, 5 random pictures (imaged at 20x) were analysed. The positive cells were 49.4±12.5% in samples incubated with normal culture media (figures 4-18E, magnified version in 4-19 A and B), and 82.4±9.2% in samples incubated with Optimem (figures 4-18F, magnified version in 4-19 C and D).
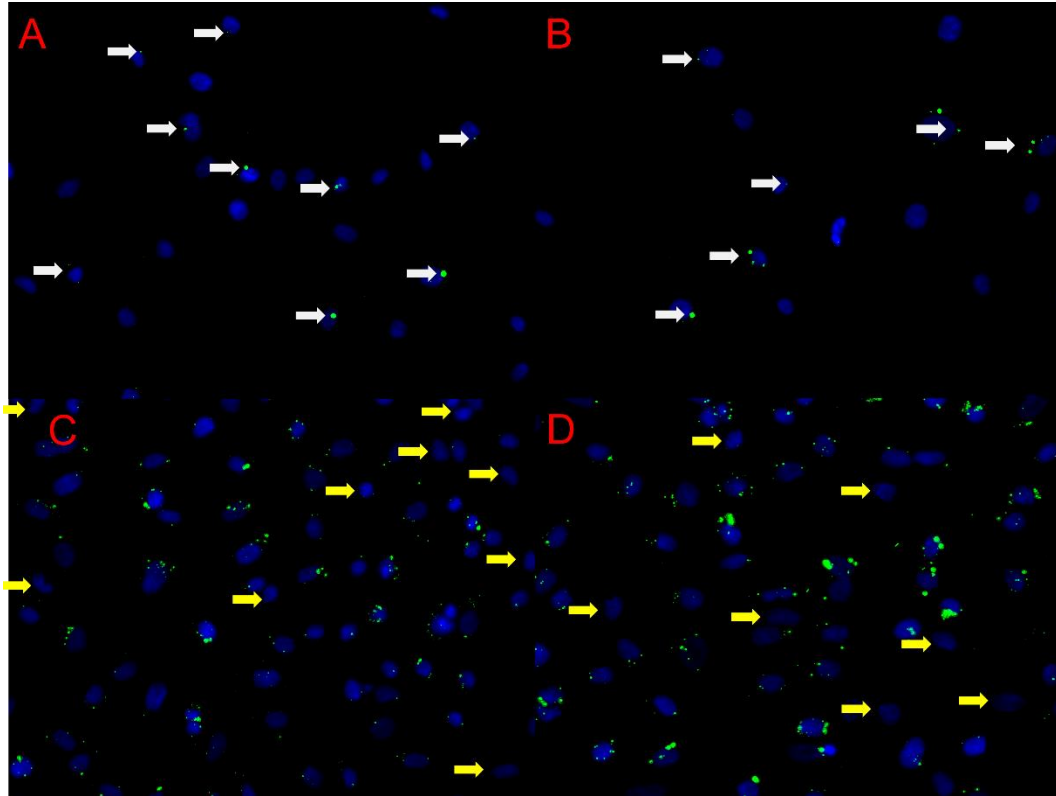
Figure 4-19: Magnified fluorescence images of EA.hy926 ECs after FITC-conjugated chitosan-NPs uptake and Trypan Blue incubation.
Pictures were taken after FITC-conjugated chitosan-NPs transfection and Trypan Blue incubation (protocol outlined in this paragraph). Cells with at least one visible fluorescent NP around or on the nucleus after incubation with Trypan Blue were counted positive (white arrows). Cells without any fluorescent NP around or on the nucleus fell in the negative group (yellow arrows). In the pictures, only the arrows of the smaller group are drawn for clarity purposes. A and B) Picture of cells incubated with fluorescent NPs in normal culture media (only positive cells pointed by white arrows). C and D) Picture of cells incubated with fluorescent NPs in Optimem media (only negative cells pointed by yellow arrows).

4.3.3   MicroRNA loading efficiency of chitosan-NPs

RT-qPCR is a very sensitive technique that allows the detection of minimal amounts of RNA. I have used this assay to measure microRNA during the development of my project. The ability to determine the quantity of microRNA incorporated in the NPs (loading efficiency) is crucial to the success of the project itself. Additionally, RT-qPCR will be used on transfected cells to correlate the amount of microRNA incubated in cell culture with the effect on cells. Section 4.3.3 is focused on the development of a protocol to assay microRNA loading efficiency on chitosan-NPs.

4.3.3.1   RT-qPCR efficacy in detecting microRNA embedded in chitosan-NPs

This experiment is designed to evaluate the precision of RT-qPCR in measuring the amount of microRNA encapsulated in chitosan-NPs. As aforementioned, I selected a non-human microRNA (cel-miR-39-3p) because I wanted to estimate the exact amount of microRNA uptaken by cells in following transfection experiments without the interference of endogenous production. This is not the case in this experiment, but I used cel-miR-39-3p here to give consistency to my work. In this experiment, I focused on testing different chitosan-NPs components to understand if any of them interferes with RT-qPCR. One may be the abundance of polysaccharides like chitosan. From the literature, polysaccharides-rich samples (e.g., plant samples) pose additional problems during the extraction phase [482]. Thus, I decided to test a CTAB-based extraction buffer, which is specific for polysaccharides-rich samples RNA extraction [483], as a possible alternative Qiazol – a phenol-based extraction buffer, which is included in the Qiagen RNA extraction kit (Qiagen, Netherlands). Also, a Norgen RNA extraction kit specific to plant samples was tested (Plant microRNA purification kit, Norgen, Canada). Moreover, chitosan-NPs are made of different materials in addition to chitosan: microRNA, TPP, and NaCl. Any of them, or even a combination of them, could be responsible for microRNA detection by RT-qPCR impairment. Therefore, I decided to analyse a series of intermediate solutions employed during chitosan-NPs fabrication, in addition to using different RNA extraction methods. The sample choice allowed me to break down the problem and increase the likelihood of identifying the responsible for a potential RT-qPCR sensitivity decrease. Hence, I measured the cel-miR-39-3p levels of:

- chitosan-NPs without encapsulated microRNA to understand if any NPs component could give microRNA-unspecific background signal.
- NPs with encapsulated microRNA, which is the target of my investigation.
- a microRNA dilution in RNAse-free water as a positive control.
- a TPP and NaCl dilution in RNAse-free water at the same concentration used for NPs production to understand if these compounds can influence RT-qPCR giving false positives.
- a solution of microRNA, NaCl, TPP identical to the solution loaded on the syringe during NPs production to understand if the interaction of these compounds (which are mixed around one hour before NPs production) could affect RT-qPCR.

Each sample was divided into three and total RNA was extracted with the three different methods outlined before: Qiagen RNeasy micro kit, Qiagen RNeasy micro kit with CTAB-based extraction buffer instead of the manufacturer's one, and the Norgen Plant microRNA Purification

Kit (figure 4-20). Since samples did not include live cells, a spike-in microRNA was added immediately after the lysis buffer addition to replace the missing housekeeping microRNA – 25 fmol/sample of hsa-miR-26a-5p. This allowed me to normalize RT-qPCR results on the amount of samples added, preventing potential dosage errors and losses; and also to identify possible Retro-Transcription and RT-qPCR malfunctions.
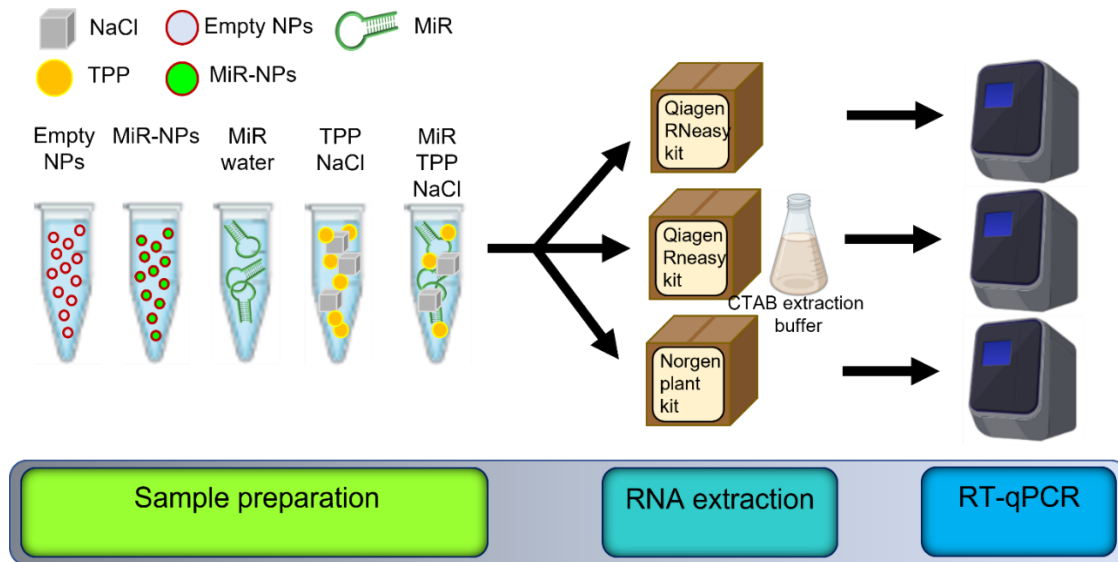
Figure 4-20: RT-qPCR efficacy test experimental walkthrough
Different solutions are prepared: Empty NPs (Empty-NPs), microRNA-loaded NPs (MiR-NPs), microRNA in RNAse-free water(MiR/water), TPP and NaCl in RNAse-free water (TPP/NaCl), and microRNA, TPP, and NaCl in RNAse-free water (MiR/TPP/NaCl). Then, the samples are split into three aliquots and the microRNA is extracted with either Qiagen RNeasy micro kit, Qiagen RNeasy micro kit with CTAB-based extraction buffer instead of the manufacturer's one, or Norgen Plant microRNA Purification kit. Finally, the microRNA levels are analysed by RT-qPCR.

The use of CTAB-based lysis buffer resulted in less microRNA extraction from all samples, both the spike-in and the target microRNA. In table 4-1, CT values and microRNA fold-change (normalized by the Qiagen kit values) of microRNA diluted in RNAse-free water – theoretically the easiest sample to extract – are shown. The CT values of samples extracted with CTAB-based buffer were sensibly higher. Since the spike-in is added just before RNA extraction, it is likely that the extraction with a CTAB-based buffer was less efficient. MicroRNA extracted with Plant microRNA Purification Kit from Norgen expression gave similar results. Both cel-mir-39-3p and hsa-miR-26a-5p (spike-in) CT values were higher compared with samples extracted with the Qiagen kit. As for CTAB-based buffer, this indicated less RNA extraction efficiency. Considering this, samples subjected to microRNA extraction with CTAB-based buffer and with Norgen Plant microRNA Purification Kit were excluded from the analysis.

Sample id	Spyke-in CT number (hsa-miR-26a-5p)	Target CT number (cel-mir-39-3p)	microRNA fold change (ref Qiagen kit)
Qiagen kit	13.134	4.944	1
	13.157	4.835	
	13.092	4.918	
Qiagen kit with CTAB buffer	35.559	27.676	0.822
	35.318	27.665	
	35.861	27.563	
Norgen kit	33.662	25.633	0.901
	33.675	25.584	
	33.879	25.771	

Table 4-1: RT-qPCR data of microRNA dilution (cel-miR-39-3p) in water extracted using different methods.
MicroRNA was diluted in RNAse-free water and microRNA was extracted with three different kits: Qiagen RNeasy micro kit, Qiagen RNeasy micro kit with CTAB-based extraction buffer instead of the manufacturer's one, and the Norgen Plant microRNA Purification Kit. CT values are shown to highlight the lower amount of both target and spike-in in the Qiagen kit with CTAB buffer and Norgen kit compared to the Qiagen kit used as per the manufacturer's indication.

The results of the samples isolated with Qiazol lysis buffer are displayed in figure 4-21 and are normalized by the microRNA signal found in the cel-miR-39-3p dilution in RNAse-free water. As expected, there was no trace of cel-miR-39-3p in the samples in which it has not been added (figure 4-21A) - TPP and NaCl dilution and chitosan-NPs without encapsulated microRNA. MiR/TPP/NaCl/water resulted in higher microRNA concentration, with a statistically relevant difference only with MiR/NPs (P=0.043 – figure 4-21B). The most relevant information was the low amount of microRNA detected in the NPs with encapsulated microRNA – around 24% of the initially added amount.
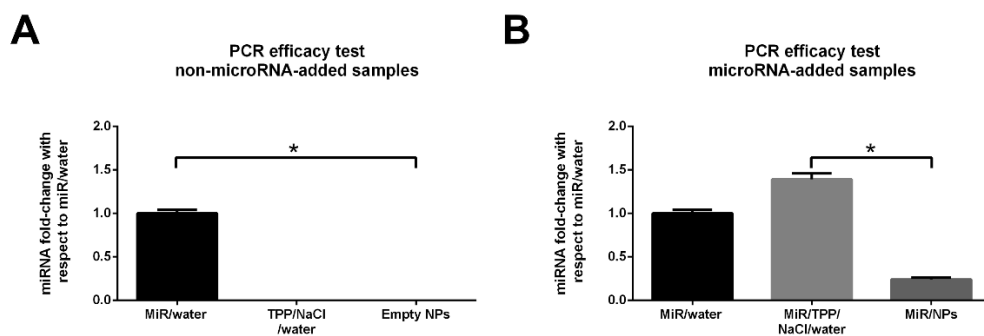
Figure 4-21: Cel-miR-39-3p expression measured by RT-qPCR of different suspension A) microRNA diluted in RNAse-free water compared to samples without microRNA (TPP/NaCl/water and Empty NPs). B) microRNA diluted in RNAse-free water compared to samples with microRNA (miR/TPP/NaCl/water and miR/NPs). MiR/water is a microRNA dilution

in RNAse-free water, miR/TPP/NaCl/water and TPP/NaCl/water are solutions of NaCl, TPP (identical to the solution loaded on the syringe during NPs production) with and without microRNA. MiR/NPs is an NPs suspension with encapsulated microRNA. Empty NPs is an NPs suspension without encapsulated microRNA. Since the samples are not extracted from cell cultures or tissues, there is no other microRNA that could be taken as housekeeping to normalize the target data, hence 25 fmol/sample of hsa-miR-26a-5p was added as spike-in. *P<0.05, **P<0.01, ***P<0.001 and ****P<0.0001. Values are expressed as mean ± standard deviation. Technical replicates=3. Non-parametrical test performed (Kruskal-Wallis ranks test and Dunn's test for multiple comparisons).

From RT-qPCR raw data, I have also noticed that spike-in expression was also dimmed. Most likely, the presence of chitosan in suspension was causing problems to the RNA extraction, even if microRNA is not bound in NPs, as is the case of the spike-in (table 4-2). Thus, the effect of chitosan did not depend on whether microRNA was embedded in NPs or simply added after NPs production. However, it cannot be excluded that the problems were coming from RT-qPCR or retro-transcription.

microRNA/water Spyke-in CT number	Empty NPs Spyke-in CT number	miR/NPs Spyke-in CT number
13.134	18.934	21.978
13.157	19.185	22.133
13.092	18.962	22,243

Table 4-2: Spike-in (hsa-miR-26a-5p) CT values of samples with chitosan.
Samples were prepared as from protocol. Before total RNA extraction, the spike-in is added to the suspension (25 fmol/sample). Then, RNA is extracted with a Qiagen RNeasy micro kit. RT-qPCR spike-in CT values are higher in samples with chitosan - empty NPs and miR/NPs, which means that less microRNA has been detected in those samples.

4.3.3.2   Extraction of non-embedded Micro-RNA by centrifugation

From the previous experiment, it is clear that detecting microRNA in chitosan-NPs by RT-qPCR presents hurdles. Measurement of non-embedded microRNA floating in the NPs suspension supernatant would have been a way to circumvent the problem. The centrifugation of the NPs suspension should concentrate NPs at the bottom of the container, and allow to measure the amount of microRNA in the NPs-free supernatant. To properly set a centrifugation routine, I would have needed the NPs and the media density. As mentioned in the methods section, it is

hard to device chitosan-NPs density from literature, so I had to use published protocols [484]–[486]– with NPs centrifuged at around 12000 x g for 30 minutes - and adapt them by attempts. Unfortunately, I was not able to pellet the NPs without crushing or aggregating them. Indeed, DLS analyses showed poor quality data. The DLS (Zetasizer Nano ZS, Malvern Panalytical, UK) output was "measurement error due to out-of-boundaries polydispersity". That means that it was not possible to measure NPs sizes because of the presence of bodies with sizes in a range of several magnitudes. It is worth nothing the presence of eye-visible agglomerates, which were not present in pre-centrifuge samples, suggests that NPs have been excessively compressed and aggregated and/or broken. I also tried to apply very low accelerations for a longer time – 3000 x g for 7 hours. The amount of chitosan in the supernatant was estimated by a colorimetric assay using a published protocol [487] - see paragraph 3.5.3. The colorimetric titration measures chitosan concentration in ppm. The chitosan amount initially added to chitosan-NPs preparation was 148 ppm. The theoretic concentration of a chitosan homogeneous solution at 148 ppm in the colorimetric solution is 29.6 ppm, since from protocol 1 mL of chitosan solution should be diluted in 5 mL. All results I got (5 samples) were above 15 ppm, which means that there was plenty of chitosan in the post-centrifugation supernatant, more than 50% of what would be present in a homogeneous chitosan solution. That means that more than 50% of chitosan used to produce NPs was still floating instead of being on the bottom of the vial. Assuming chitosan all NPs to have a narrow size distribution (from paragraph 3.2.2, I estimated them to have a diameter of 140±25nm), around 50% of NPs were floating in the supernatant. Thus, centrifugation at low speed was inefficient. The estimation of free-floating microRNA was difficult to carry out with a sensible share of NPs-bonded microRNA mixed with the amount of not-bonded microRNA I wished to estimate.

4.3.3.3   Extraction of non-embedded Micro-RNA by dialysis

Centrifugation did not allow to sediment NPs and collect NPs-free supernatant. The use of dialysis is an additional approach analyzed in this project. The idea was to get rid of free-microRNA from the chitosan-NPs manufacturing solution. Then, microRNA would be extracted from NPs. Obviously, I must have an efficient method to quantify microRNA embedded in chitosan-NPs, which is not so easy given the issues I had with RT-qPCR efficiency. However, this issue is faced in the following experiments – section 4.3.3.4.x.

The dialysis principle is simple: two solutions are separated by a permeable membrane which allows passage of molecules under a certain size. Solutes or water are driven across the membrane by osmotic pressure. In my experiment, I poured the chitosan-NPs manufacturing solution into a dialysis bag which was fitted in a jar filled up with RNAse-free water. If the dialysis membrane is chosen properly, free microRNA should cross the membrane to end up in RNAse-free water. Usually, a dialysis membrane MWCO should be 3-fold the bigger compound it is wished to pass freely through the membrane. I chose dialysis tubes with MWCO equal to 50 kDa, since micro-RNA Mw nears 9 kDa, and a single chain of chitosan polysaccharides has Mw≥ 50 kDa. It should be almost impossible for chitosan-NPs (being 140±25nm large) to get across a membrane with MWCO 50 kDa. Indeed, a 100 nm pore diameter corresponds to an MWCO of several million [488].

In the first experiment, dialysis was applied to a solution of microRNA (cel-miR-39-3p), NaCl, and TPP, identical to the solution loaded on the syringe during NPs production; NPs without encapsulated microRNA; and NPs with encapsulated microRNA. In figure 4-22, it comes manifest that there was no microRNA decrease after dialysis. Disappointingly, the microRNA amount did not diminish in the dialyzed samples, even when simply diluted in water (figure 4-22A). These results pose severe doubts about the efficacy of dialysis in separating non-encapsulated microRNA from the encapsulated one.
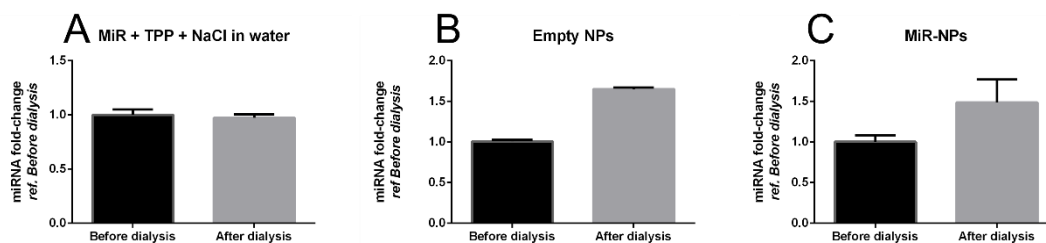
Figure 4-22: Cel-miR-39-3p expression measured by RT-qPCR before and after dialysis
The dialysis membrane had MWCO equal to 50 kDa. A) Mix of microRNA, TPP, and NaCl in water. This mix is identical to the solution loaded on the syringe during NPs production; B) Empty NPs is an NPs suspension without encapsulated microRNA, and C) MiR/NPs is an NPs suspension with encapsulated microRNA. The samples were analysed before and after dialysis. Since the sample is not derived from cellular, there is no other microRNA that could be taken as housekeeping to normalize the target data, hence 25 fmol/sample of hsa-miR-26a-5p was added as spike-in. *P<0.05, **P<0.01, ***P<0.001 and ****P<0.0001. Values are expressed as mean ± standard deviation. Technical replicates=3. Non-parametrical test performed (Mann-Whitney).

I hypothesized that either the dialysis membrane MWCO was not large enough, or the dialysis was too short. Therefore, I repeated the dialysis experiment using a simple microRNA dilution

in RNAse-free water to assess the dialysis membrane compatibility with microRNA. In this experiment, I chose two different dialysis tubes with MWCO of 140 and 300 kDa – among the largest pore sizes on the market. Considering the microRNA size, the Mw of cel-miR-39-3p synthetized by Eurofins is around 9.3 kDa, an MWCO of 300 kDa should be 20-fold larger than needed.

Figure 4-23 clearly shows dialysis is not appropriate to pursue my aim. Indeed, microRNA concentration remained stable after 8h and 24h of dialysis with the 140 kDa MWCO dialysis membrane, if not slightly rising (figure 4-23A). When using a 300 kDa MWCO dialysis membrane, the microRNA concentration nearly doubles after 8h and goes down to around 79.7±1.6% of the initial amount after 24h (figure 4-23B). Given these results, dialysis was deemed not suitable to separate free microRNA for chitosan-NPs and abandoned.
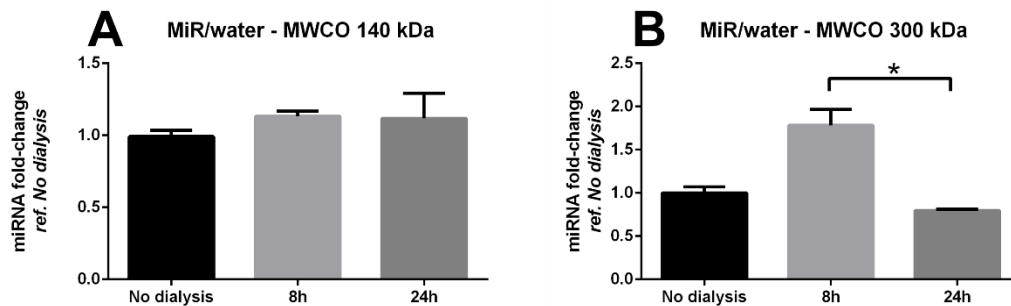
Figure 4-23: Water-diluted Cel-miR-39-3p expression measured by RT-qPCR before and after dialysis
A) miR/water – MWCO 140kDa shows data about a microRNA dilution in RNAse-free water dialysed in dialysis bags with MWCO of 140 kDa for either 8 or 24 h; B) miR/water – MWCO 300kDa shows data about a microRNA dilution in RNAse-free water dialysed in dialysis bags with MWCO of 300 kDa for either 8 or 24 h. Samples are compared with no-dialysis controls. Since the sample is not derived from cellular, there is no other microRNA that could be taken as housekeeping to normalize the target data, hence 25 fmol/sample of hsa-miR-26a-5p was added as spike-in. *P<0.05, **P<0.01, ***P<0.001 and ****P<0.0001. Values are expressed as mean ± standard deviation. Technical replicates=3. Non-parametrical test performed (Kruskal-Wallis ranks test and Dunn's test for multiple comparisons).

4.3.3.4 Chitosan enzymatic digestion

Since I could not optimize an assay to detect microRNA not embedded in the chitosan-NPs suspension, I focused on finding a way to extract and detect a significant fraction of NPs-embedded microRNA, larger than the one previously obtained, which was around 24% - see

paragraph 4.3.3.1. Chitosan digestion (using the specific enzyme chitosanase) before the RNA extraction should allow a more efficient microRNA detection [346].

N/P is the ratio between TPP and microRNA phosphate groups (P) and chitosan amine groups (N). N/P and weight ratio between components are inversely proportional – see chitosan-NPs production in Materials and Methods for details. Usually, a higher N/P grants more protection to microRNA, since it is bound to chitosan more strongly [489]–[491]. MicroRNA negative phosphate groups offer a marginal contribution to the strength of NPs electrostatic bonds because their number is negligible compared to TPP ones. Therefore, microRNA concentration in chitosan-NPs and N/P is assumed to be independent. In other words, N/P can be changed independently from microRNA concentration. These two observations gave me leverage to increase microRNA protection without the limitation of sticking to the desired microRNA concentration in NPs. In the foreseeable event that microRNA would need protection enhancement, I included NPs formulations with a higher chitosan/TPP weight ratio - 17.5 (N/P=10).

Following the literature, I decided to compare two different chitosanase concentrations for chitosan enzymatic digestion, 0.7 and 7 U per mg of chitosan [346], [425], [426].

Chitosanase effectively made microRNA available for RT-qPCR (figure 4-24). The microRNA concentration read was 9.45±1% (Ch/TPP=7) and 10.4±3.6% (Ch/TPP=17.5) in non-digested samples, which increased to 61.1±5.6% (Ch/TPP=7) and 74.4±5.5% (Ch/TPP=17.5) in samples digested with 0.7U/mg of chitosan (P=0.0082 and P=0.0011, respectively). Data are normalized by the same microRNA amount in RNAse-free water. Chitosanase concentration increase did not increase the amount of detected microRNA. The chitosanase digestion was accomplished at the best of its potential because a 10-fold increase in enzyme concentration did not statistically increase microRNA estimation – no difference in samples prepared with Ch/TPP=7 and an actual decrease in samples prepared with Ch/TPP=17.5 (P=0.0295). A concentration of 0.7 U of chitosanase per mg of chitosan was enough to digest NPs produced with both protocols. The result of this experiment convinced me to apply chitosanase digestion before RNA extraction from chitosan-NPs.
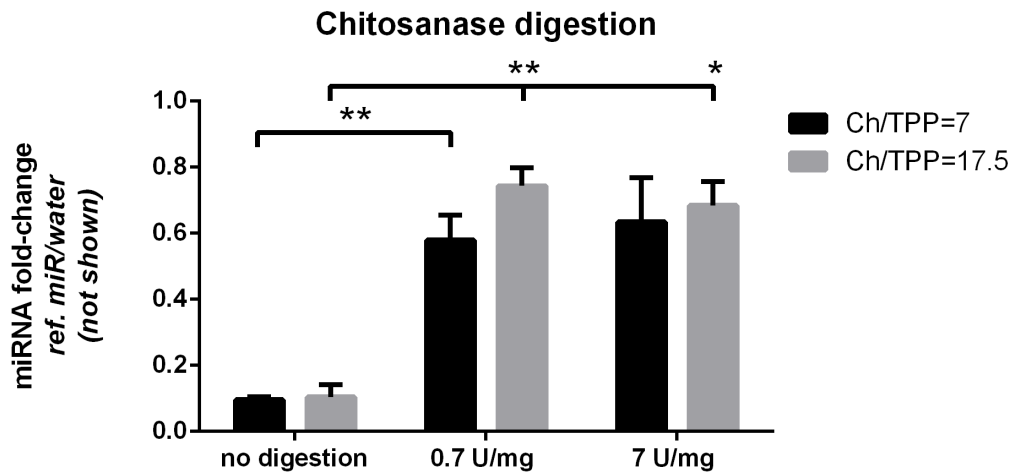
Figure 4-24: Cel-miR-39-3p expression measured by RT-qPCR after chitosan enzymatic digestion.
Cel-miR-39-3p levels were measured in samples of microRNA-embedded chitosan-NPs produced with two different Chitosan/TPP weight ratios, 7 and 17.5. After production, NPs were digested with 0.7 or 7 U of chitosanase per mg of chitosan, and assayed by RT-qPCR. Since the sample is not derived from cellular, there is no other microRNA that could be taken as housekeeping to normalize the target values, hence 25 fmol/sample of hsa-miR-26a-5p was added as spike-in. *P<0.05, **P<0.01, ***P<0.001 and ****P<0.0001. Values are expressed as mean ± standard deviation. Technical replicates=4. Non-parametrical test performed (Kruskal-Wallis ranks test and Dunn's test for multiple comparisons).

4.3.3.4.1 FBS nuclease inhibitor test

Following the failure in estimating the chitosan-NPs microRNA loading efficiency, the focus moved to estimate the amount of *protected microRNA* – namely the survived microRNA after incubation of microRNA-loaded chitosan-NPs in 10% FBS for one hour. However, FBS nucleases should be neutralized after 1-hour FBS exposition and before chitosan digestion by chitosanase – demonstrated in the previous paragraph. If FBS nucleases are not blocked before NPs digestion, all microRNA freed from within NPs would be degraded as soon as it gets in contact with the FBS solution. RNAse inhibitor could help in that regard.

In this experiment, I incubated a microRNA (Cel-miR-39-3p) dilution in RNAse-free water with 10% v/v FBS for 1h. Before FBS addition, I added RNAse inhibitor to half samples and performed RT-qPCR after incubation. The control was a simple microRNA dilution in RNAse-free water. Figure 4-25 shows experimental results. There was a striking difference between samples incubated with 10% FBS only and the other conditions (P<0.0001). The RNAse inhibitor was able to preserve the microRNA from degradation by FBS nuclease, not fully though. The microRNA concentration in samples that received RNAse inhibitor was 77.1±3% of control. Therefore, I

added RNase inhibitor in the next experiments which involved miRNA-NPs enzymatic digestion after FBS incubation.
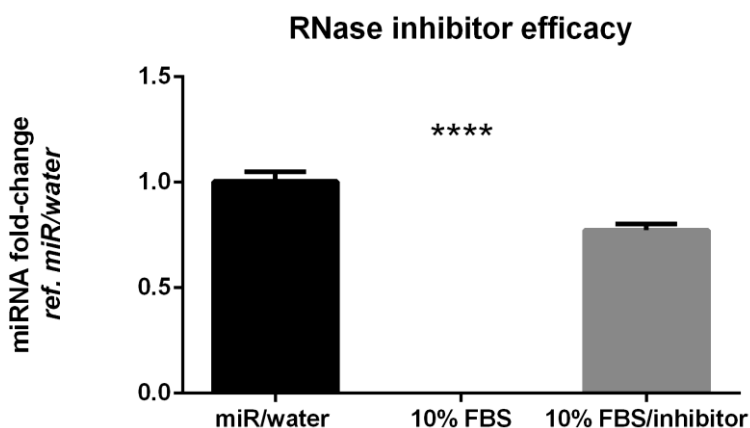
Figure 4-25: Cel-miR-39-3p expression measured by RT-qPCR after 10% FBS incubation with/without RNAse inhibitor
RT-qPCR readings were normalized by control (miR/water). MiR/water is a microRNA dilution in RNAse-free water, 10% FBS is the same amount of microRNA of miR/water incubated with 10% v/v FBS for 1h, 10% FBS/inhibitor is the same amount of microRNA of miR/water with the addition of 1 U/µL of RNAse inhibitor and incubated with 10% v/v FBS for 1h. The samples were incubated for 1h at RT and then analysed through RT-qPCR. Since the sample is not derived from cellular, there is no other microRNA that could be taken as housekeeping to normalize the target data, hence 25 fmol/sample of hsa-miR-26a-5p was added as spike-in. *$P<0.05$, **$P<0.01$, ***$P<0.001$ and ****$P<0.0001$. Values are expressed as mean ± standard deviation. Technical replicates=5. Non-parametrical test performed (Kruskal-Wallis ranks test and Dunn's test for multiple comparisons).

4.3.3.4.2 MicroRNA extraction from chitosan-NPs using chitosanase and nuclease inhibitor

In the light of previous experiments, I combined chitosanase with the RNAse inhibitor to obtain the most precise estimation of preserved microRNA from NPs incubated with 10% v/v FBS in this experiment. The experiment was split into two parts. Initially, I focused on understanding the impact of the digestion process on microRNA. Then, I estimated the amount of microRNA left after miRNA-NPs have been incubated with 10% FBS for one hour at RT. I also included an NPs formulation with a higher chitosan/TPP weight ratio - 17.5 (N/P=10) as I did before – paragraph 4.3.3.4. This let me understand if there was better microRNA protection with the increase of chitosan in the NPs formulation.

The outcomes of the first part are outlined in figure 4-26A. The digestion process (sample incubation with Chitosanase and RNAse inhibitor for four hours at 37°C – right column of graph

4-26A) did not affect the levels of detectable microRNA. The microRNA amount detected in the miRNA solution in RNAse-free water after four hours at 37°C (miR/water 4h-37°C) was aligned with control, which is the same amount of miRNA solution in RNAse-free water analyzed by RT-qPCR as soon as it was mixed (miR/water).
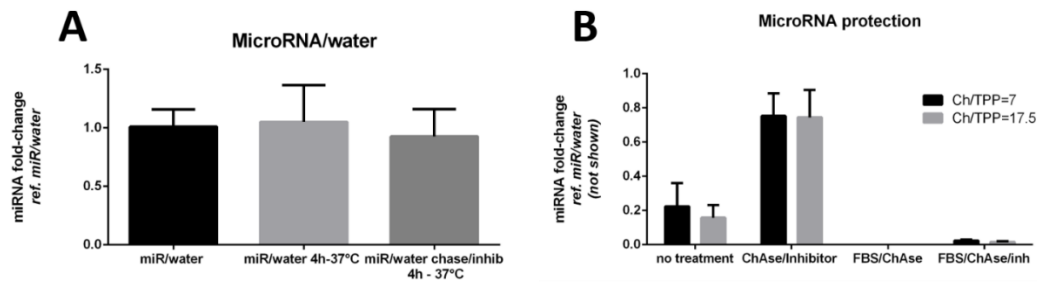
Figure 4-26: Cel-miR-39-3p expression measured by RT-qPCR after 10% FBS incubation applying the digestion protocol completely
A) microRNA in RNAse-free water solutions which readily underwent RT-qPCR (miR/water) or underwent RT-qPCR after four hours at 37°C (miR/water 4h-37°C) or underwent RT-qPCR after receiving chitosanase and RNA inhibitor and incubated at 37°C for four hours (miR/water chase/inhib 4h-37°C). B) microRNA-embedded NPs which received no further treatment (no treatment) or incubated with chitosanase and RNAse-inhibitor for four hours at 37°C (ChAse/Inhibitor) or incubated with chitosanase for four hours at 37°C following one-hour incubation in 10% FBS at RT (FBS/ChAse) or incubated with chitosanase and RNAse inhibitor for four hours at 37°C following one-hour incubation in 10% FBS at RT (FBS/ChAse). All microRNA levels are normalized by the same amount of microRNA in RNAse-free water solution samples (not shown). Since the sample is not derived from cellular, there is no other microRNA that could be taken as housekeeping to normalize the target data, hence 25 fmol/sample of hsa-miR-26a-5p was added as spike-in*P<0.05, **P<0.01, ***P<0.001, and ****P<0.0001. Values are expressed as mean ± standard deviation. Technical replicates=6. Non-parametrical test performed (Kruskal-Wallis ranks test and Dunn's test for multiple comparisons).

Figure 4-26B shows the microRNA concentration of NPs suspensions after different protocols; microRNA levels are normalized by the same amount of miRNA solution in RNAse-free water (not shown). Statistical significance is not indicated in the graph since it would have been too crowded. No statistical differences were observed between the two Chitosan/TPP weight ratios which underwent the same procedure. Hence, the following analysis is limited to samples in different conditions. The no-treatment samples are miRNA-NPs suspensions analyzed by RT-qPCR after no additional treatments: the detected microRNA was 23.2±13.1% of the, while after complete digestion (ChAse/Inhibitor) the microRNA level was 78.3±10.1% - P<0.0001 with FBS/ChAse and P=0.008 with FBS/ChAse/inh. FBS/ChAse stands for the samples incubated with 10% FBS and then digested with chitosanase without the addition of RNAse inhibitor. As from

the hypothesis, the absence of RNAse inhibitor allowed FBS nucleases to degrade all microRNA freed by NP digestion, leaving no detectable traces - $P<0.0001$ with ChAse/Inhibitor, $P=0.0087$ with no treatment samples, and no statistical difference with FBS/ChAse/inh. ChAse/Inhibitor are samples digested with chitosanase in presence of RNAse inhibitor. They display the maximum amount of microRNA detectable by RT-qPCR from these chitosan-NPs using this extraction method – 78.3±10.1%. Indeed, chitosanase degrades chitosan, whereas microRNA receives the maximum protection thanks to the incubation of RNAse inhibitor and the absence of RNAses since no FBS was incubated.

FBS/ChAse/inh identifies NPs incubated with 10% FBS for one hour and digested with chitosanase in the presence of RNAse inhibitor. These samples underwent complete digestion and the microRNA released from NPs was protected from FBS RNAse by the RNAse inhibitor. Eventually, the detected microRNA was the preserved amount after one-hour incubation with FBS nucleases. It is the value I would like to be as high as possible, as it measures the amount of microRNA that could be transfected to cells. Unfortunately, the remaining microRNA amount was not satisfying since it was only 3.2±0.62%. Besides, no statistical difference was observed with FBS/ChAse procedure, in which no microRNA was found.

4.3.3.5   Chitosan-NPs optimization: microRNA and chitosan concentration variation

In the previous experiment, I verified that only 3.2±0.62% of the original microRNA amount loaded in chitosan-NPs remains after 1-hour exposition to FBS nucleases. This experiment was designed to understand if increasing chitosan concentration in NPs composition allows a higher amount of microRNA to withstand RNAse degradation. In the second part, I also varied the microRNA concentration to understand if degraded microRNA is proportional to the microRNA added during NPs manufacturing, and if adding more microRNAs can be beneficial for transfection.

The chitosan-NPs manufacturing protocol requires the addition of NaCl as an adjuvant of NPs formation. However, NaCl splits into Na^+ and Cl^- ions in water solution. Free-floating ions could bind to their counterparts: microRNA negative charges and chitosan positive charges. This could prevent microRNA and chitosan from attracting each other and generating well-packed microRNA-loaded chitosan-NPs. Therefore, I avoided adding NaCl to produce NPs for this experiment to see if this idea had some grounds.

I used to produce NPs with N/P=4 which is equal to Chitosan/TPP weight ratio equal to 7. In this experiment, I also tested N/P=10 (chitosan/TPP=17.5 w/w), and N/P=30 (chitosan/TPP=52.6 w/w).
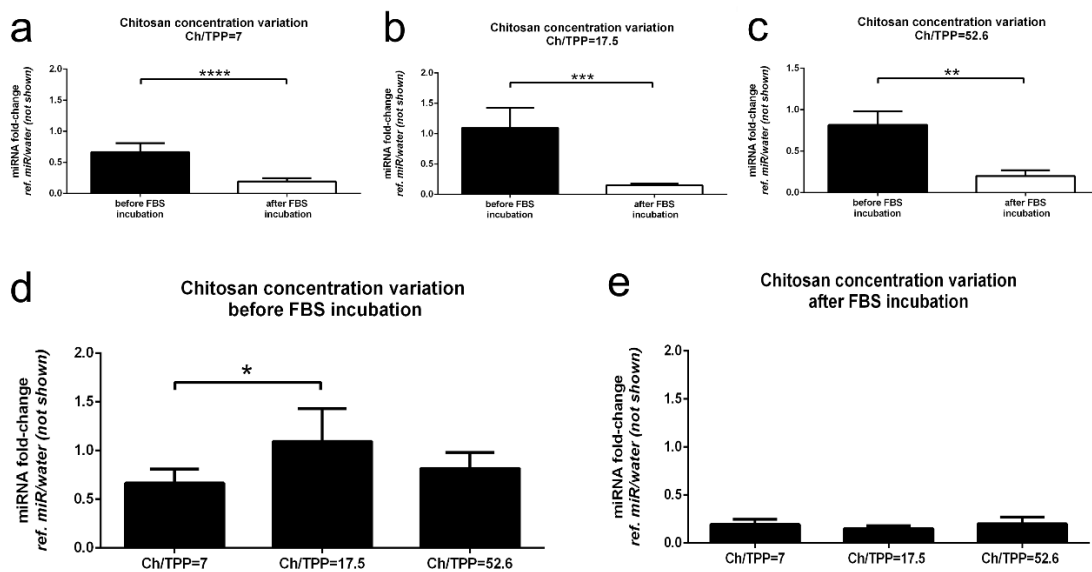
Figure 4-27: Cel-miR-39-3p expression measured by RT-qPCR of chitosan-NPs produced with different chitosan concentrations.
Cel-miR-39-3p concentrations measured by RT-qPCR. Ch/TPP=7 are microRNA-loaded chitosan-NPs produced with chitosan/TPP=7 w/w, Ch/TPP=17.5 are microRNA-loaded chitosan-NPs produced with chitosan/TPP =17.5 w/w, Ch/TPP=52.6 are microRNA-loaded chitosan-NPs produced with chitosan/TPP =52.6 w/w. MicroRNA was extracted right after production from the *before FBS incubation* samples. Instead, microRNA was extracted after incubation with 10% FBS for 1h from the *after FBS incubation* samples. The microRNA levels are normalized by miR/water samples (not shown). a) microRNA levels of samples produced with Ch/TPP=7 w/w before and after 10% FBS incubation. b) microRNA levels of samples produced with Ch/TPP=17.5 w/w before and after 10% FBS incubation. c) microRNA levels of samples produced with Ch/TPP=52.6 w/w before and after 10% FBS incubation. d) microRNA levels of samples (all tested weight ratios) before 10% FBS incubation. e) microRNA levels of samples (all tested weight ratios) after 10% FBS incubation. Since the sample is not derived from cellular, there is no other microRNA that could be taken as housekeeping to normalize the target data, hence 25 fmol/sample of hsa-miR-26a-5p was added as spike-in. *$P<0.05$, **$P<0.01$, ***$P<0.001$, and ****$P<0.0001$. Values are expressed as mean ± standard deviation. Technical replicates=6. Non-parametrical test performed (Kruskal-Wallis ranks test and Dunn's test for multiple comparisons).

After incubation with 10% FBS at RT for one hour, there was no statistical difference between the three different Chitosan/TPP w/w in their detectable microRNA amount (figure 4-27e). The microRNA levels were around 18.3±3%. That means that higher chitosan concentration does not enhance microRNA protection from FBS nucleases. The absence of NaCl addition during NPs fabrication seems responsible for the increase of detected microRNA from around 3% to 18%, as it is the only parameter changed in the Ch/TPP=7 w/w samples. The effect of the FBS

incubation is still well present and statistically significant (figures 4.27a, b, and c)– P<0.0001 for

NPs produced with Ch/TPP= 7 w/w, P=0.007 for NPs produced with Ch/TPP= 17.5 w/w, P=0.004

for NPs produced with Ch/TPP= 52.6 w/w. Pre-FBS exposition microRNA levels were higher in

Ch/TPP= 17.5 samples than in Ch/TPP= 7 ones (P=0.0462).
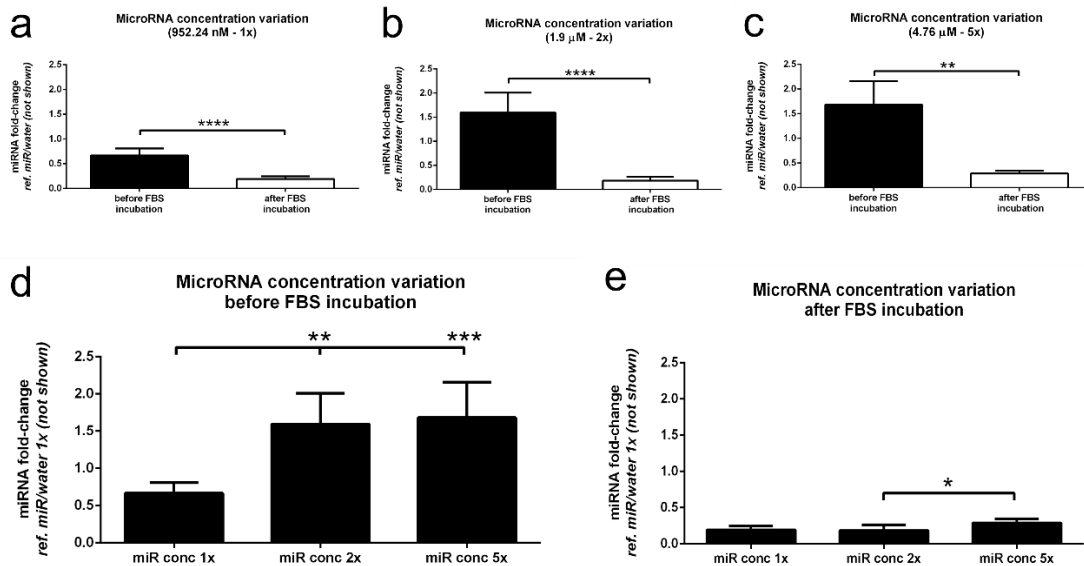
Figure 4-28: Cel-miR-39-3p expression measured by RT-qPCR of chitosan-NPs produced with
different microRNA concentrations
MiR conc 1x is microRNA-loaded chitosan-NPs produced with microRNA concentration=952.24
nM, miR conc 2x is microRNA-loaded chitosan-NPs produced with microRNA
concentration=1.9 µM, miR conc 5x is microRNA-loaded chitosan-NPs produced with
microRNA concentration=4.76 µM. MicroRNA was extracted right after production from the
before FBS incubation samples. Instead, microRNA was extracted after incubation with 10%
FBS for 1h from the *after FBS incubation* samples. The microRNA levels are normalized by
miR/water samples (not shown). a) microRNA levels of samples loaded with a microRNA
concentration of 952.24 nM before and after 10% FBS incubation. b) microRNA levels of
samples loaded with a microRNA concentration of 1.9 µM before and after 10% FBS
incubation. c) microRNA levels of samples loaded with a microRNA concentration of 4.76 µM
before and after 10% FBS incubation. d) microRNA levels of samples (all tested microRNA
concentrations) before 10% FBS incubation. e) microRNA levels of samples (all tested
microRNA concentrations) after 10% FBS incubation. Since the sample is not derived from
cellular, there is no other microRNA that could be taken as housekeeping to normalize the
target data, hence 25 fmol/sample of hsa-miR-26a-5p was added as spike-in. *P<0.05,
**P<0.01, ***P<0.001, and ****P<0.0001. Values are expressed as mean ± standard
deviation. Technical replicates=6. Non-parametrical test performed (Kruskal-Wallis ranks test
and Dunn's test for multiple comparisons).

In the second part of the experiment, I increased the microRNA amount from the usual 952.24

nM (1x) to 1.9 µM (2x) and 4.76 µM (5x). 952.24 nM is the microRNA concentration in the initial

mix (microRNA and TPP in RNAse-free water) that is then added to the chitosan suspension to

produce chitosan-NPs. Eventually, the concentration would be 25 nM during transfection to cells (see Materials and Methods). I applied microRNA concentration increments to understand if chitosan-NPs can retain more microRNA than 30 nM after FBS incubation; 30 nM is the 3.2% of 952.24 nM (1x), which is the concentration of extracted microRNA from NPs after exposure to FBS nucleases for one hour - i.e. the amount measured in the previous experiment.

As for chitosan variation, the effect of the FBS incubation on NPs loaded with different amounts of microRNA is evident and statistically significant (figures 4.28a, b, and c) – P<0.0001 for *miR conc 1x*, P<0.0001 for *miR conc 2x*, and P=0.0016 for *miR conc 5x.* Samples analyzed before the FBS exposition showed almost a doubling of detected microRNA between *miR conc 1x* and *miR conc 2x*, in line with the respective added amounts (P=0.0028 - figure 4-28d). Disappointingly, *MiR conc 5x* did not show the 5-fold microRNA amount detected in *miR conc 1x* as I was expecting. Perhaps, NPs could not host more microRNA. Most importantly, it appears that the microRNA concentrations after FBS treatment were equal in all three formulations (figure 3-26e). Although I have added 2-fold and 5-fold the usual microRNA quantity during NPs fabrication, the after-treatment amount was always around 30 nM. That means that only 3.68±3% and 5.78±1.1% of initially added microRNA in *miR conc 2x* and *miR conc 5x* survived nucleases. MicroRNA amounts left after exposure to FBS were aligned with what was found in samples with lower initial microRNA concentrations.

4.3.4   Chitosan-NPs transfection efficiency on Aortic Endothelial Cells

The optimized chitosan-NPs production protocol I developed consisted of a mix of 0.89mL of TPP (0.1 mg/mL) and miRNA (952.24 nM) in RNAse-free water loaded in a syringe. The solution is dropped in a 15 mL glass tube (filled up with 2.49 mL of chitosan (0.25 mg/mL) in RNAse-free water and adjusted to pH=5.5 with acetic acid) at a fixed flow (0.2 mL/min) by a syringe pump. The tube sits on a hotplate stirrer that keeps it in constant stirring (1400 rpm) at 37°C. The N/P is equal to 10 (chitosan/TPP=17.5 w/w) – see previous paragraphs, and paragraph 4.3.2.1.

Here, I tested the chitosan-NPs transfection efficiency. I used primary aortic ECs (HAoECs) to prevent concerns about the translationality of my work – see paragraph 2.2 for the motivation. As it is broadly used as a microRNA non-viral vector, Lipofectamine RNAiMAX was chosen as a benchmark for the transfection efficiency of chitosan-NPs. All transfected cells underwent the Lipofectamine RNAiMAX transfection protocol – outlined in paragraph 3.2.5, which consists of five hours of incubation of microRNA-vector suspension in reduced serum media - Optimem.

Chitosan-NPs were produced with N/P=10. Since the collected samples included endogenous cellular microRNA, there was no need for spike-in addition for CT values normalization this time. U6 snRNA was used as housekeeping microRNA.

Regrettably, the results are clearly showing that cel-miR-39-3p was not transfected using chitosan-NPs as a transfection vector (figure 4-29). MiR39-NPs samples have 0.3±0.3% cel-miR-39-3p amount of lipofectamine samples (P=0.0009), which means almost nothing. In addition, the same samples' miR39-NPs values are aligned with values from empty NPs (empty-NPs) and NPs loaded with scramble microRNA (scramble-NPs) – a random and non-significant microRNA sequence, which was not added with cel-miR-39-3p whatsoever. Given these results, it was clear that the NPs that I designed are not suitable for microRNA transfection to HAoECs.
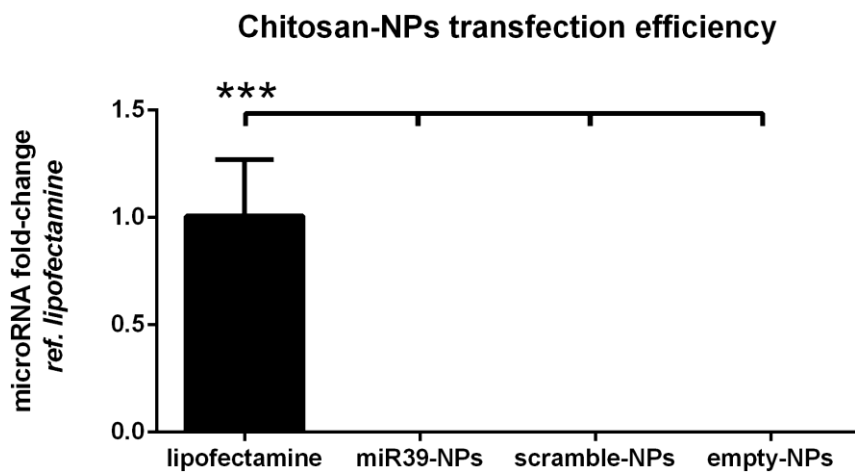
Figure 4-29: Cel-miR-39-3p levels in transfected HAoECs measured by RT-qPCR
Cells were transfected by applying the Lipofectamine transfection protocol. Total RNA extraction and RT-qPCR analysis were carried out 64 hours after transfection – 16h overnight recovery plus 2 days as recommended by the manufacturer. Readings were normalized by the lipofectamine samples value. Lipofectamine is samples transfected with commercial lipofectamine RNAiMAX, miR39-NPs are samples transfected with cel-miR-39-3p-loaded chitosan-NPs, scramble-NPs are samples transfected with scramble microRNA-loaded chitosan-NPs, empty-NPs are samples transfected with no microRNA loaded in chitosan-NPs. Lipofectamine, miR39-NPs, and scramble-NPs samples contained an equal microRNA amount – 25 nM. As samples come from cell monolayers and U6 snRNA was used as housekeeping microRNA. *P<0.05, **P<0.01, ***P<0.001, and ****P<0.0001. Values are expressed as mean ± standard deviation. Technical replicates=6. Non-parametrical test performed (Kruskal-Wallis ranks test and Dunn's test for multiple comparisons).

4.3.5 Contingency plan to select a non-viral vector for microRNA transfection

In this section, the additional materials (PEI, PEI-g-PEI, PLGA, TMC) were considered as potential microRNA non-viral vectors, after chitosan-NPs failure. Then, proliferation, migration, and viability were tested on hsa-miR-132-3p-trasfected cells to assay changes inducted by its transfection. In addition, potential hsa-mir-132-3p mRNA targets expression levels were measured to asses the downregulation effect of the transfected microRNA.

4.3.5.1 Polyethylenimine-NPs transfection efficiency

In this experiment, PEI is tested as a potential microRNA transfection vector to HAoECs. PEI is cytotoxic at high concentrations [323], [324]. However, PEI concentration in transfection media is proportional to the weight of genetic material to transfect through the N/P ratio. Since microRNA is way smaller than long ncRNA or plasmid DNA, a fixed molar concentration means way fewer phosphates in case microRNA is administered. Therefore, less PEI amount is needed to achieve the required N/P. Human Embryonic Kidney 293 Cells – a cell type frequently used for cell transfection experiments, maintain >85% viability when incubated with up to 25 µg/mL of PEI [325]. As I add a microRNA concentration of 25nM in my experiments, the incubated PEI concentrations were 211 ng/mL and 423 ng/mL to achieve N/P=10 and N/P=20, respectively – 850-fold less than the toxicity threshold just mentioned. Thus, there should not have been cytotoxicity – see paragraphs 1.5.5 and 3.4.3 for details.

PEI-NPs fabrication and transfection were conducted as outlined in the material and methods section. U6 snRNA was used as housekeeping microRNA. As expected, PEI-NPs were extremely efficient in transfecting microRNA (figure 4-30). PEI-NPs were 70±14% (N/P=10) and 160±35% (N/P=20) more efficient than lipofectamine – P=0.0029 and P<0.0001, respectively. From these results, PEI seems a good candidate for microRNA transfection.

PEI-NPs transfection efficiency
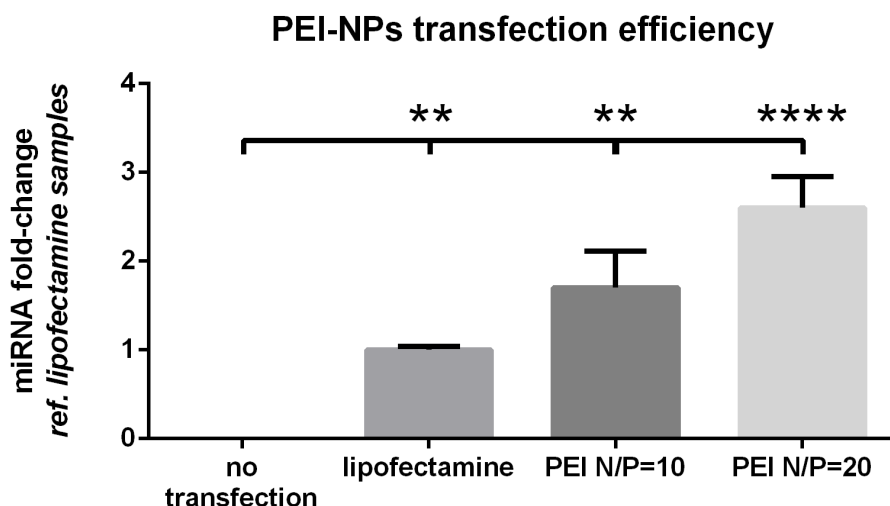
Figure 4-30: Cel-miR-39-3p expression of PEI-NPs-transfected HAoECs measured by RT-qPCR Cel-miR-39-3p levels from cell monolayer samples transfected with different vectors. RT-qPCR readings were normalized by lipofectamine value. No transfection are samples that did not undergo any transfection, lipofectamine are samples transfected with commercial lipofectamine RNAiMAX, PEI N/P=10 are samples transfected with cel-miR-39-3p-loaded PEI-NPs at an N/P=10, PEI N/P=20 are samples transfected with cel-miR-39-3p-loaded PEI-NPs at an N/P=20. All samples contained an equal microRNA amount – 25 nM, except for no transfection samples. As samples come from cell monolayers and U6 snRNA was used as housekeeping microRNA. *P<0.05, **P<0.01, ***P<0.001, and ****P<0.0001. Values are expressed as mean ± standard deviation. Technical replicates=6. Non-parametrical test performed (Kruskal-Wallis ranks test and Dunn's test for multiple comparisons).

4.3.5.2   PLGA-NPs manufacturing

PLGA-NPs development is part of the contingency plan to select a suitable non-viral vector for microRNA transfection. I considered PLGA-NPs as an alternative to PEI-NPs in the event that PEI's cytotoxicity, or its water-solubility, may be hampering microRNA transfection from the microRNA-functionalized scaffold.

First trials on empty-NPs – no microRNA embedded, have given morphologically satisfying results (figure 4-31). Three technical replicates were prepared and imaged by TEM. From each replicate, 5 random fields were captured and the NPs' diameter was measured. NPs diameter is 17.6±5.3 nm, and their rounded shape suggests particles have properly hardened. NPs size is way underneath 200nm; the threshold I do not want to go above because it makes cellular uptake more difficult and less likely [432]–[434]. Since the tested NPs were empty, I am expecting microRNA-loaded NPs to be bigger, but not to a great extent. PLGA-NPs fabrication outcomes were satisfying enough to make a transfection trial.
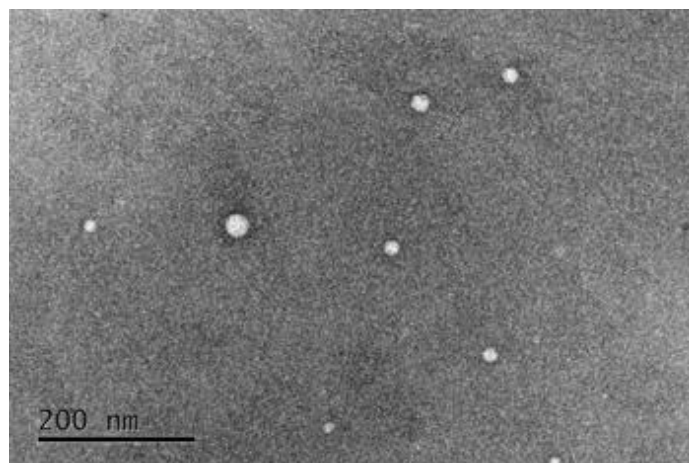
Figure 4-31: PLGA-NPs characterization
TEM picture of PLGA-NPs (rounded clear spots). Technical replicates=3.

4.3.5.3   PEI-g-PEG and TMC based NPs transfection efficiency

As done for PLGA-NPs, I tested PEI-g-PEG and TMC as potential candidates for microRNA transfection – see paragraph 1.5.5 for the description of the material and use in gene delivery examples.

As outlined in Material and Methods, the NPs production protocol using both PEI-g-PEG and TMC consists in simply mixing the proper amount of reagents in RNAse-free water. As no buffer exchange or washing is employed between fabrication and cell transfection phases, the final concentrations are easily calculated from the initial amounts mixed. The reagents amounts derive from the N/P number since even in this case the force which should keep NPs together is electrostatic. MicroRNA final concentration for transfection was set to 25 nM (this concentration is motivated in paragraph 2.2.5). HAoECs were transfected following Lipofectamine RNAiMAX transfection protocol - paragraph 3.2.5. The amount of TMC required was 1.75 µg/mL for N/P=5, 3.5 µg/mL for N/P=10, and 7.01 µg/mL for N/P=20; while 347 ng/mL for N/P=5, 694 ng/mL for N/P=10, and 1.388 µg/mL for N/P=20 are required for PEI-g-PEG NPs.

TMC transfection efficiency
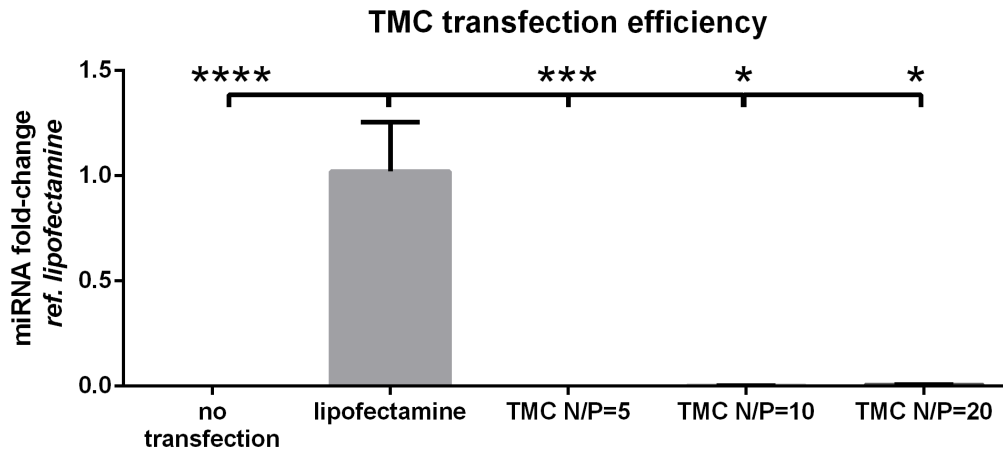
Figure 4-32: Cel-miR-39-3p expression of TMC-NPs-transfected HAoECs measured by RT-qPCR RT-qPCR readings were normalized by lipofectamine value. No transfection are HAoECs which did not undergo any transfection, lipofectamine are HAoECs transfected with commercial lipofectamine RNAiMAX, TMC N/P=5 are HAoECs transfected with cel-miR-39-3p-loaded TMC-NPs at N/P=5, TMC N/P=10 are HAoECs transfected with cel-miR-39-3p-loaded TMC-NPs at N/P=10, TMC N/P=20 are HAoECs transfected with cel-miR-39-3p-loaded TMC-NPs at N/P=20. All samples contained an equal microRNA amount – 25 nM, except for no transfection samples. U6 snRNA was used as housekeeping microRNA. *P<0.05, **P<0.01, ***P<0.001, and ****P<0.0001. Values are expressed as mean ± standard deviation. Technical replicates=3. Non-parametrical test performed (Kruskal-Wallis ranks test and Dunn's test for multiple comparisons).

TMC-aided transfection did not work (figure 4-32). The average fold-change went from 0.055±0.052% for *TMC N/P=5* to 0.049±0.02% for *TMC N/P=20*. There was no statistically significant difference between TMC samples and control – i.e. no transfection.

PEI-g-PEG transfection efficiency
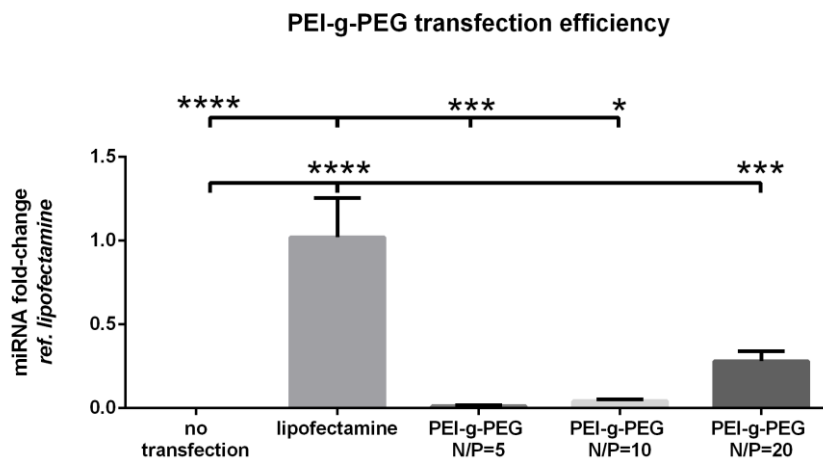
Figure 4-33: Cel-miR-39-3p expression of PEI-g-PEG NPs-transfected HAoECs measured by RT-qPCR (1)

RT-qPCR readings were normalized by lipofectamine value. No transfection are HAoECs that did not undergo any transfection, lipofectamine are HAoECs transfected with commercial lipofectamine RNAiMAX, PEI-g-PEG N/P=5 are HAoECs transfected with cel-miR-39-3p-loaded PEI-g-PEG at N/P=5, PEI-g-PEG N/P=10 are HAoECs transfected with cel-miR-39-3p-loaded PEI-g-PEG at N/P=10, PEI-g-PEG N/P=20 are HAoECs transfected with cel-miR-39-3p-loaded PEI-g-PEG at N/P=20. All samples contained an equal microRNA amount – 25 nM, except for no transfection samples. U6 snRNA was used as housekeeping microRNA. *P<0.05, **P<0.01, ***P<0.001, and ****P<0.0001. Values are expressed as mean ± standard deviation. Technical replicates=3. Non-parametrical test performed (Kruskal-Wallis ranks test and Dunn's test for multiple comparisons).

PEG-g-PEI-based transfection gave mixed results (figure 4-33). *PEI-g-PEG N/P=5* and *PEI-g-PEG N/P=10* cel-mir-39-3p expression levels were not different from no transfection samples, but *PEI-g-PEG N/P=20* showed sensibly higher expression levels (P=0.002) - 28±6% of lipofectamine expression. However, *PEI-g-PEG N/P=20* resulted in less than a third of lipofectamine expression levels.

PEI-g-PEG transfection efficiency
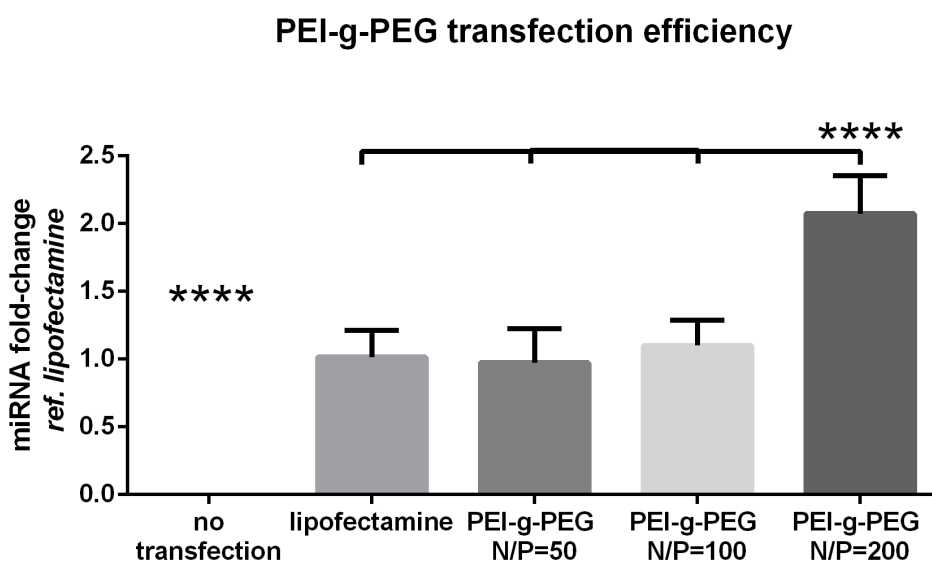
Figure 4-34: Cel-miR-39-3p expression of PEI-g-PEG-NPs-transfected HAoECs measured by RT-qPCR (2)

RT-qPCR readings were normalized by lipofectamine value. No transfection are HAoECs that did not undergo any transfection, lipofectamine is HAoECs transfected with commercial lipofectamine RNAiMAX, PEI-g-PEG N/P=50 are HAoECs transfected with cel-miR-39-3p-loaded PEI-g-PEG at N/P=50, PEI-g-PEG N/P=100 are HAoECs transfected with cel-miR-39-3p-loaded PEI-g-PEG at N/P=100, PEI-g-PEG N/P=200 are HAoECs transfected with cel-miR-39-3p-loaded PEI-g-PEG at N/P=200. All samples contained an equal microRNA amount – 25 nM, except for no transfection samples. U6 snRNA was used as housekeeping microRNA. *P<0.05, **P<0.01, ***P<0.001, and ****P<0.0001. Values are expressed as mean ± standard deviation. Technical replicates=6. Non-parametrical test performed (Kruskal-Wallis ranks test and Dunn's test for multiple comparisons).

I repeated the PEI-g-PEG-based transfection experiment to understand if increasing N/P could benefit transfected microRNA expression levels. *PEI-g-PEG N/P=50* and *PEI-g-PEG N/P=100* cel-mir-39-3p expression levels were aligned to lipofectamine samples (figure 4-34). Moreover, *PEI-g-PEG N/P=200* outperformed lipofectamine samples expressing by 2-fold ($P < 0.0001$). However, cytotoxicity concerns arose after transfection with high amounts of *PEI-g-PEG*. Optical microscope pictures show gaps on cell monolayer in cells transfected with PEI-g-PEG at N/P=100 and N/P=200 (figure 4-35C and D). Also, there is an increase of rounded-shaped cells in those samples, a sign of poor cell health.
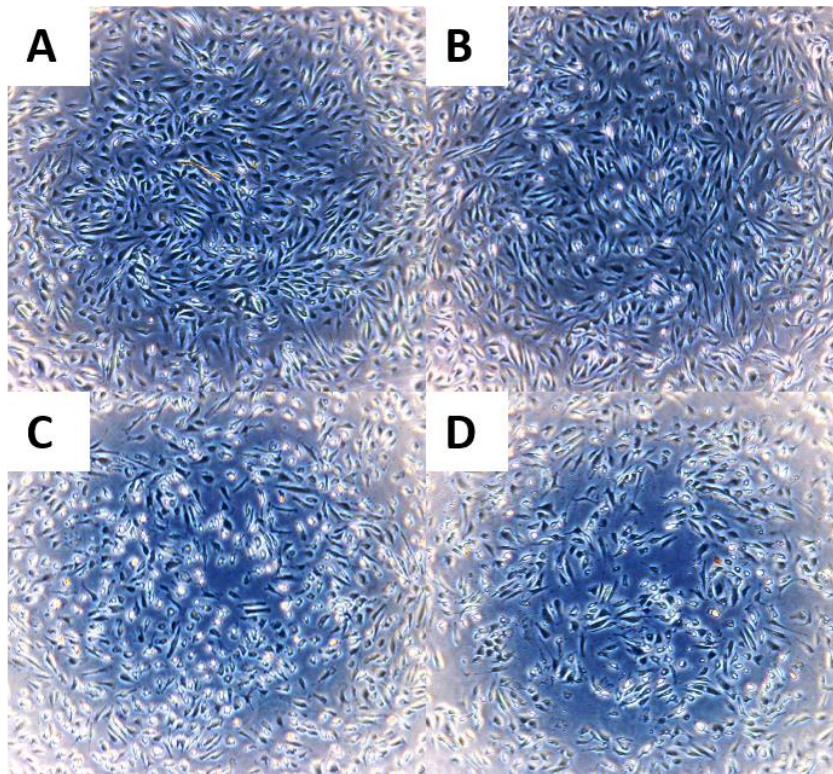
Figure 4-35: Optical microscope pictures of cel-mir-39-3p transfected ECs with PEI-g-PEG vector at high concentration

Cells are seeded in 96 well plates, cultured up to 80% confluence, and samples transfected with different vectors. After 24h, pictures of samples were taken to roughly evaluate the cells' health status. A) Control - no transfection, B) cells transfected with Lipofectamine RNAiMAX, C) cells transfected with PEI-g-PEG NPs at N/P=100, D) cells transfected with PEI-g-PEG NPs at N/P=200.

4.3.5.4 Proliferation, migration, and viability of cells transfected with hsa-miR-132-3p loaded PEI-NPs

Once PEI-NPs transfection efficiency was verified, it was important to understand if hsa-miR-132-3p transfected to HAoECs had a similar effect using PEI-NPs or Lipofectamine RNAiMAX (see paragraph 4.2) as a vector – i.e. enhanced proliferation and migration as previously shown. In this experiment, hsa-miR-132-3p is compared with scramble microRNA - a microRNA sequence with the weakest (or no) match with any mRNA in the mRNA pool of homo sapiens, to separate the potential effects of the vector and the specific microRNA. I have also included membrane integrity (also known as LDH assay) and live & dead assay to investigate possible PEI-NPs cytotoxicity – see paragraphs 2.2, 3.2.6, and 3.2.7 for details. Following the PEI-NPs transfection efficiency test in paragraph 4.3.5.1, two PEI concentrations were tested, N/P=10 and N/P=20. MicroRNA transfection was effective (figure 4-36). Hsa-miR-132-3p-transfected cells using PEI-NPs overexpressed it.

Hsa-miR-132-3p Expression
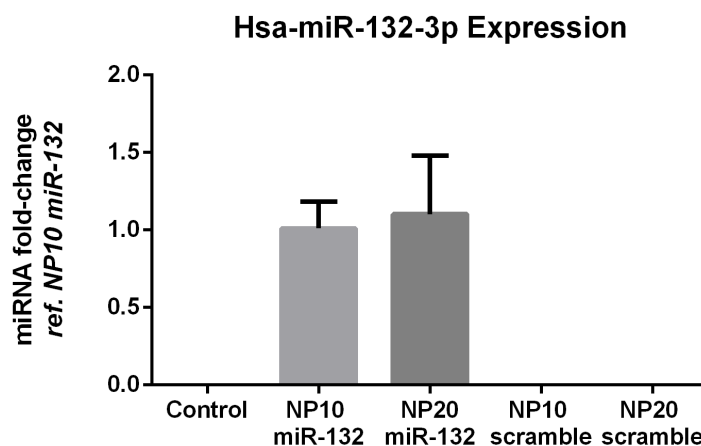
Figure 4-36: Hsa-miR-132-3p expression of PEI-NPs-transfected HAoECs
RNA was extracted 48h past transfection recovery time. RT-qPCR readings were normalized by the NP10 miR-132 level. From the left: Control – no transfection, NP10 mir-132 are HAoECs transfected with hsa-miR-132-3p-loaded PEI-NPs at N/P=10, NP20 mir-132 are HAoECs transfected with hsa-miR-132-3p-loaded PEI-NPs at N/P=20, NP10 scramble are HAoECs transfected with scramble-microRNA-loaded PEI-NPs at N/P=10, NP20 scramble are HAoECs transfected with scramble-microRNA-loaded PEI-NPs at N/P=20. All samples contained an equal microRNA amount – 25 nM, except for no transfection samples. U6 snRNA was used as housekeeping microRNA. *P<0.05, **P<0.01, ***P<0.001, and ****P<0.0001. Values are expressed as mean ± standard deviation. Technical replicates=3. Non-parametrical test performed (Kruskal-Wallis ranks test and Dunn's test for multiple comparisons).

Live & dead assay did not show significantly lower viability for PEI-NPs-treated cells. Cells were cultured in 96 well plates, with 6 technical replicates for each condition. From each replicate, 5 random fields were imaged, and live, dead, and total cells were counted. The total cell number per replicate is variable but never below 900 cells. Dead cells were below 6% in all samples for both time points: 24 and 48 hours (figure 4-37A and B).
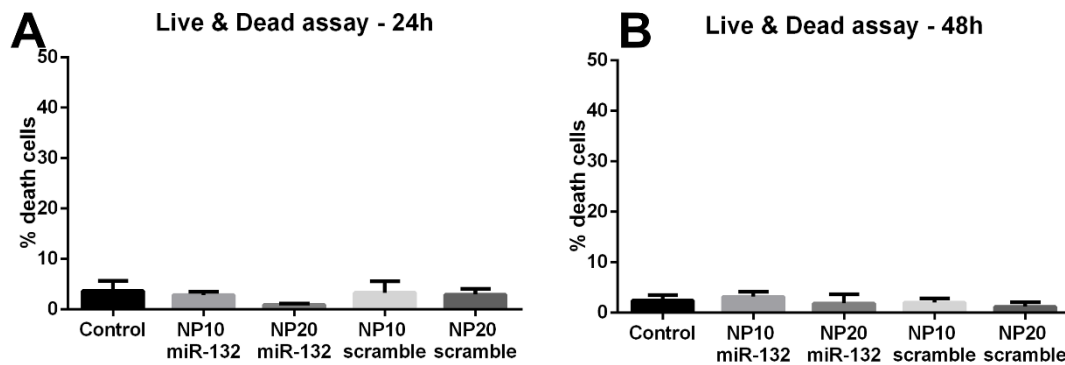
Figure 4-37: Percentage of dead hsa-miR-132-3p-transfected HAoECs
Percentage of dead cells 24 (A) and 48 (B) hours past transfection recovery time. From the left of each graph: Control (no treatment) , HAoECs transfected with 25 nM of hsa-miR-132-3p loaded on PEI-NPs at N/P=10 – NP10 mir-132, HAoECs transfected with 25 nM of hsa-miR-132-3p loaded on PEI-NPs at N/P=20 – NP20 mir-132, HAoECs transfected with 25 nM of scramble microRNA loaded on PEI-NPs at N/P=10 – NP10 scramble, HAoECs transfected with 25 nM of scramble microRNA loaded on PEI-NPs at N/P=20 – NP20 scramble. Cells were cultured in 96 well plates. From each replicate, 5 random fields were imaged, and live, dead, and total cells were counted. *P<0.05, **P<0.01, ***P<0.001, and ****P<0.0001. Values are expressed as mean ± standard deviation. Technical replicates=6. Non-parametrical test performed (Kruskal-Wallis ranks test and Dunn's test for multiple comparisons).

Also, the membrane integrity assay did not highlight any membrane damage problems (figure 4-38). All treatments' cytotoxicity was around zero.
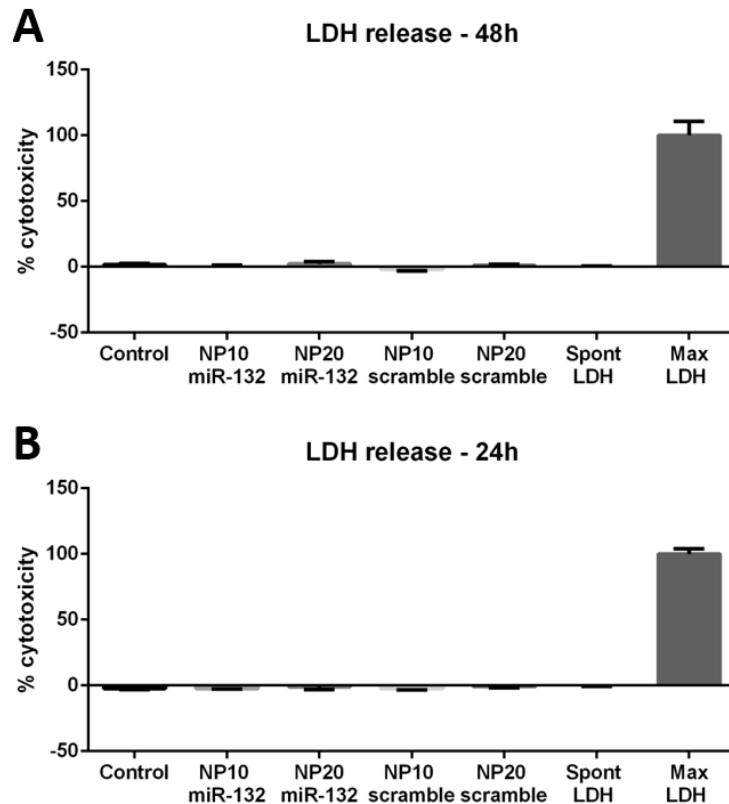
Figure 4-38: Cytotoxicity percentage of hsa-miR-132-3p-transfected HAoECs
The assay was performed 24h and 48h past transfection recovery time. From the left of each
graph: Control (no treatment), HAoECs transfected with 25 nM of hsa-miR-132-3p loaded on
PEI-NPs at N/P=10 – NP10 mir-132, HAoECs transfected with 25 nM of hsa-miR-132-3p loaded
on PEI-NPs at N/P=20 – NP20 mir-132, HAoECs transfected with 25 nM of scramble microRNA
loaded on PEI-NPs at N/P=10 – NP10 scramble, HAoECs transfected with 25 nM of scramble
microRNA loaded on PEI-NPs at N/P=20 – NP20 scramble, spontaneous LDH release, and
maximum LDH release (see Materials and Methods). *$P<0.05$, **$P<0.01$, ***$P<0.001$, and
****$P<0.0001$. Values are expressed as mean ± standard deviation. Technical replicates=6.
Non-parametrical test performed (Kruskal-Wallis ranks test and Dunn's test for multiple
comparisons).

Concerning the functional assays (proliferation and migration), the situation does not appear
clear. At both time points, cells from the control seemed to migrate less than any other sample
(figure 4-39A and B). Surprisingly, cells that received scramble microRNA were the fastest ones.
I have no explanation for that behaviour, only that scramble microRNA could have had an
unexpected interference effect on cells' RNA expression. A similar pattern was noticeable in the
proliferation assay, only that now there was a single statistically significant difference
($P=0.0141$): cells transfected with 25 nM of scramble microRNA loaded on PEI-NPs at N/P=20 at
48 hours (figure 4-40A and B).
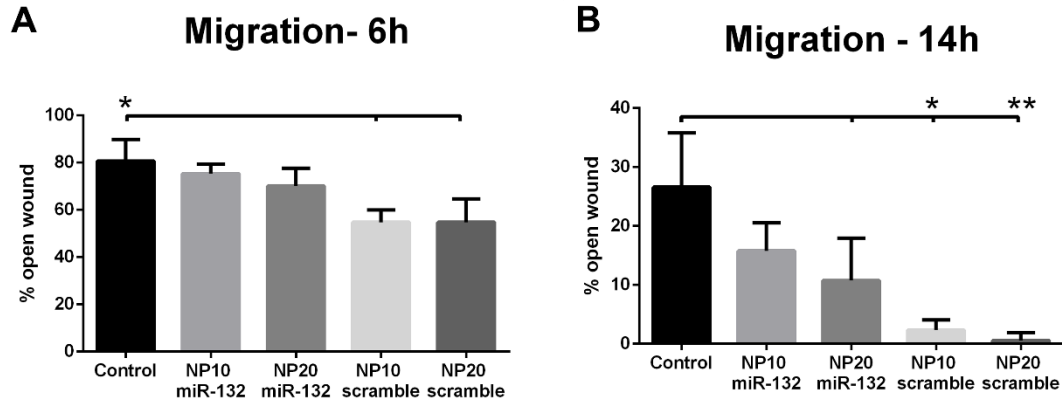
Figure 4-39: Migration inclination of hsa-miR-132-3p-transfected HAoECs
Percentage of the open wound at 6 (A) and 14 (B) hours. The assay was initiated 48h past transfection recovery time. From the left of each graph: Control (no treatment) , HAoECs transfected with 25 nM of hsa-miR-132-3p loaded on PEI-NPs at N/P=10 – NP10 mir-132, HAoECs transfected with 25 nM of hsa-miR-132-3p loaded on PEI-NPs at N/P=20 – NP20 mir-132, HAoECs transfected with 25 nM of scramble microRNA loaded on PEI-NPs at N/P=10 – NP10 scramble, HAoECs transfected with 25 nM of scramble microRNA loaded on PEI-NPs at N/P=20 – NP20 scramble. *P<0.05, **P<0.01, ***P<0.001, and ****P<0.0001. Values are expressed as mean ± standard deviation. Technical replicates=6. Non-parametrical test performed (Kruskal-Wallis ranks test and Dunn's test for multiple comparisons).

Figure 4-40: Proliferating percentage of hsa-miR-132-3p-transfected HAoECs
Percentage of proliferating at 24 (A) and 48 (B) hours. The assay was initiated 48h past transfection recovery time. From the left of each graph: Control (no treatment) , HAoECs transfected with 25 nM of hsa-miR-132-3p loaded on PEI-NPs at N/P=10 – NP10 mir-132, HAoECs transfected with 25 nM of hsa-miR-132-3p loaded on PEI-NPs at N/P=20 – NP20 mir-132, HAoECs transfected with 25 nM of scramble microRNA loaded on PEI-NPs at N/P=10 – NP10 scramble, HAoECs transfected with 25 nM of scramble microRNA loaded on PEI-NPs at N/P=20 – NP20 scramble. *P<0.05, **P<0.01, ***P<0.001 and ****P<0.0001. Values are expressed as mean ± standard deviation. Technical replicates=6. Non-parametrical test performed (Kruskal-Wallis ranks test and Dunn's test for multiple comparisons).

In the light of such unexpected results from the functional assays, I repeated the experiment using a different scramble microRNA from Qiagen to understand if the scramble microRNA (Thermo Fisher) used in the previous experiment had a specific effect. Moreover, I decided to compare PEI-NPs vectors with Lipofectamine. I have previously demonstrated that the Lipofectamine-hsa-miR-132-3p complex enhances migration and proliferation. In this experiment, I wanted to understand if the PEI-based vector had a comparable effect. Thus, I added Lipofectamine-transfected samples for a direct comparison in the same experiment. A sample incubated with an equal amount of PEI to the one used for PEI-NPs was also included to investigate the potential effects of the vector material.

As before, I analysed microRNA expression and I verified that the transfection took place, as overexpressed hsa-mir-132-3p levels in hsa-mir-132-3p-transfected cells show (figure 4-41).
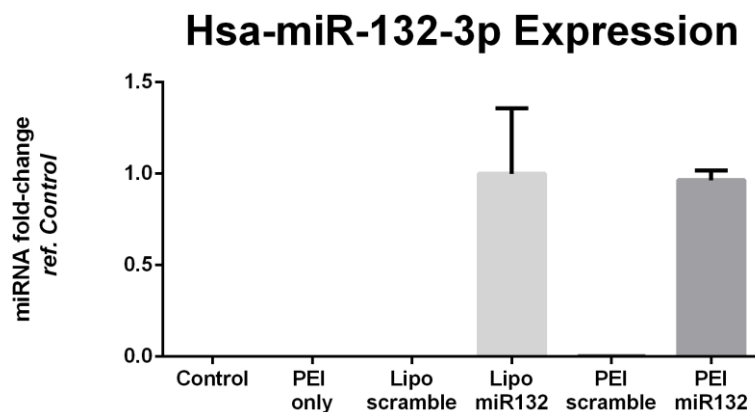
Figure 4-41: Hsa-miR-132-3p expression of HAoECs transfected with different vectors
RT-qPCR readings were normalized by Lipo miR-132 level. RNA was extracted 48h past transfection recovery time. From the left: Control – no transfection, PEI only are HAoECs incubate with PEI without any microRNA, Lipo scramble are HAoECs transfected with scramble-microRNA-loaded Lipofectamine, Lipo miR132 are HAoECs transfected with hsa-miR-132-3p-loaded Lipofectamine, PEI scramble are HAoECs transfected with scramble-microRNA-loaded PEI-NPs at N/P=10, PEI mir132 are HAoECs transfected with hsa-miR-132-3p-loaded PEI-NPs at N/P=10. All samples contained an equal microRNA amount – 25 nM, except for no transfection samples. U6 snRNA was used as housekeeping microRNA. *P<0.05, **P<0.01, ***P<0.001 and ****P<0.0001. Values are expressed as mean ± standard deviation. Technical replicates=3. Non-parametrical test performed (Kruskal-Wallis ranks test and Dunn's test for multiple comparisons).

It seemed PEI-NPs/hsa-miR-132-3p-transfected cells were the only samples having a faster migration at the first time point (8h) (figure 4-42A), but only compared to cells incubated with PEI (P=0.0204) and lipofectamine/scramble microRNA (P=0.005). There is no statistically significant difference between PEI-NPs/hsa-miR-132-3p-transfected cells and non-transfected cells (control). At 17 hours, the control cells are slower compared with *PEI scramble* and *PEI*

mir132 (P=0.008 and P=0.003, respectively - figure 4-42B). Also, *Lipo miR132* seems to be migrating faster than control, but there is no statical significance. While it would be easy to conclude that hsa-miR-132-3p enhances migration, it is hard to understand why samples transfected with scramble-microRNA-loaded PEI-NPs are also moving faster. Hence, scramble itself should not be responsible for increased migration - *Lipo scramble* samples did not show increased mobility, nor *PEI only* did. Therefore, it is the combined effect of PEI with a random microRNA that seems to increase the cells' migratory attitude.

On the other hand, proliferation assay outcomes were clearer. Samples transfected with hsa-miR-132-3p-loaded Lipofectamine were proliferating around 20% more than any other samples at all time points (figure 4-43). Data variance, low replicates number, and the use of a non-parametric statistical method do not allow a statistically significant difference to emerge at 24h (figure 4-43A). At 48h, data variability is reduced and *Lipo miR132* has statistically confirmed increased proliferation (P=0.0259 – figure 4-43B). PEI-transfected cells (*PEI scramble* and *PEI mir132*) had performances aligned with control samples.

These results, especially the proliferation ones, showed a potential problem with PEI-NPs transfection. It has been shown - in this paragraph and in 3.5 - that hsa-mir-132-3p transfected with lipofectamine enhances HAoECs proliferation and migration (only in experiments discussed in paragraph 3.5). When lipofectamine is substituted for PEI, these enhancements are lost.
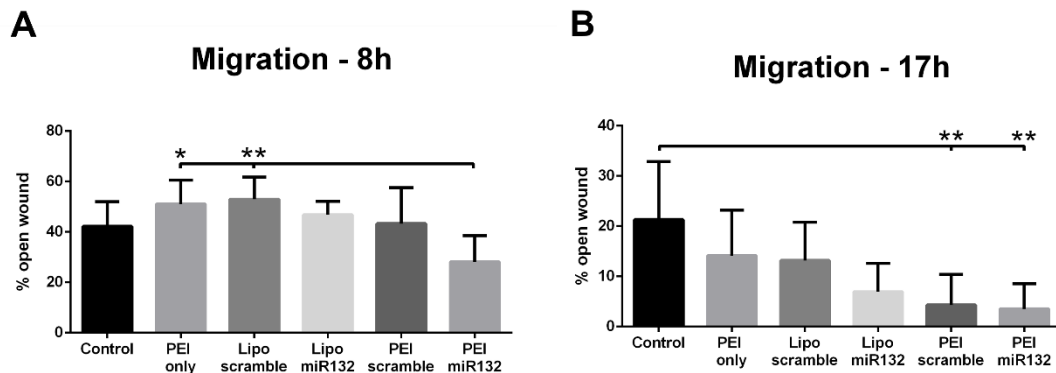
Figure 4-42: Migration inclination of hsa-miR-132-3p-transfected HAoECs using different vectors

Percentage of the open wound at 6 (A) and 14 (B) hours. The assay was initiated 48h past transfection recovery time. From the left of each graph: Control – no transfection, PEI only are HAoECs incubate with PEI without any microRNA, Lipo scramble are HAoECs transfected with scramble-microRNA-loaded Lipofectamine, Lipo miR132 are HAoECs transfected with hsa-miR-132-3p-loaded Lipofectamine, PEI scramble are HAoECs transfected with scramble-microRNA-loaded PEI-NPs at N/P=10, PEI mir132 are HAoECs transfected with hsa-miR-132-3p-loaded PEI-NPs at N/P=10*P<0.05, **P<0.01, ***P<0.001 and ****P<0.0001. Values are expressed as mean ± standard deviation. Technical replicates=3. Non-parametrical test performed (Kruskal-Wallis ranks test and Dunn's test for multiple comparisons).

A

Proliferation - 24h

B

Proliferation - 48h

Figure 4-43: Proliferating percentage of hsa-miR-132-3p-transfected HAoECs using different vectors

Percentage of proliferating at 24 (A) and 48 (B) hours. The assay was initiated 48h past transfection recovery time. From the left of each graph: Control – no transfection, PEI only are HAoECs incubate with PEI without any microRNA, Lipo scramble are HAoECs transfected with scramble-microRNA-loaded Lipofectamine, Lipo miR132 are HAoECs transfected with hsa-miR-132-3p-loaded Lipofectamine, PEI scramble are HAoECs transfected with scramble-microRNA-loaded PEI-NPs at N/P=10, PEI mir132 are HAoECs transfected with hsa-miR-132-3p-loaded PEI-NPs at N/P=10. *$P<0.05$, **$P<0.01$, ***$P<0.001$ and ****$P<0.0001$. Values are expressed as mean ± standard deviation. Technical replicates=3. Non-parametrical test performed (Kruskal-Wallis ranks test and Dunn's test for multiple comparisons).

4.3.5.5   Regulation of hsa-miR132-3p targets

Proliferation and migration assays on hsa-miR-132-3p-transfected HAoECs showed that proliferation was enhanced only when Lipofectamine was employed as a transfection vector, but not when PEI was employed. To investigate this discrepancy, it was decided to measure expression levels of hsa-miR132-3p gene targets involved in cell proliferation and migration. Based on published work and bioinformatic analysis performed by a collaborator (Dr. Andrea Caporali, University of Edinburgh, UK) (see paragraph 3.3.5), we selected a genes panel:

- RAS p21 protein activator 1 (RASA1). It was shown that hsa-miR-132-3p downregulates RASA1 expression and increases endothelial proliferation [492]–[494]
- RB transcriptional corepressor 1 (RB1): this gene encodes for a negative regulator of cell cycle protein. Its inhibition facilitates cell cycle progression [495]
- Paxillin (PXN) is a cell focal adhesion component. The PAK-paxillin signal pathway is involved in the regulation of cell protrusion and migration [496]
- Sprouty-related EVH1 domain containing 1 (SPRED1) is a negative regulator of MAP kinase signalling. If repressed, SPRED1 allows intracellular transmission of angiogenic signals coming from VEGF and FGF and enhances HUVECs' migratory activity [497].

- Cyclin-dependent kinase inhibitor 1A (CDKN1A). When suppressed, EC proliferation, migration, and tube formation are enhanced [498]

Bioinformatics analysis predicted binding regions for hsa-miR132-3p for mRNA encoding these proteins. UBC was used as the housekeeping gene. The gene expression analysis was carried out on previous experiment samples. The bioinformatics prediction was fairly accurate, only CDKN1A did not show any statistically significant difference between hsa-miR132-3p and scramble transfected samples (figure 4-44) when Lipofectamine was the transfection vector.
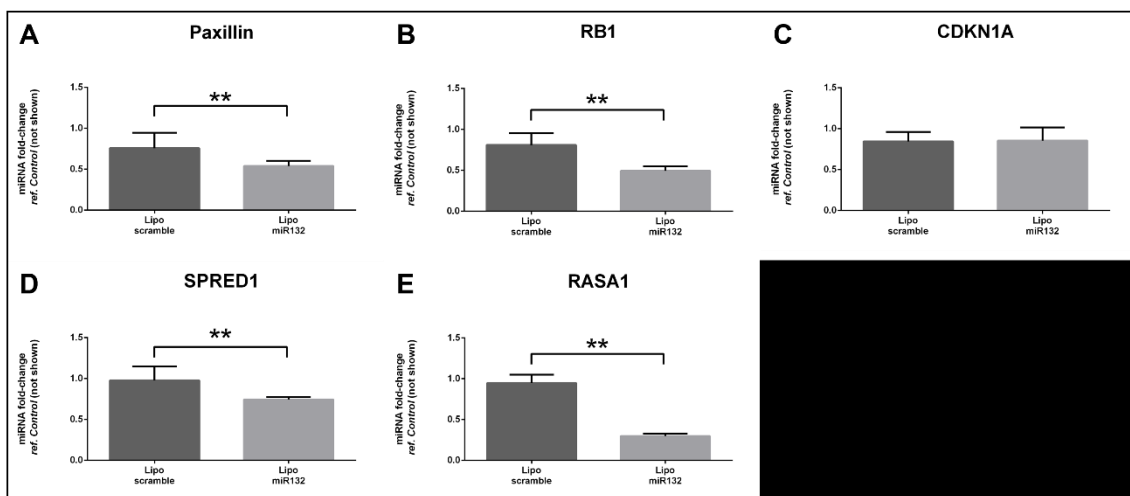
Figure 4-44: Hsa-miR-132-3p-target genes panel expression by hsa-miR-132-3p- and scramble microRNA-transfected HAoECs with Lipofectamine.
Cells were transfected using Lipofectamine RNAiMAX. Each graph compares a single gene expression (name on the title) from HAoECs transfected either with hsa-miR-132-3p or scramble microRNA. A: PXN, B: RB1, C: CDKN1A, D: SPRED1, and E: RASA1. *P<0.05, **P<0.01, ***P<0.001 and ****P<0.0001. Values are expressed as mean ± standard deviation. Technical replicates=6 Non-parametrical test performed (Mann-Whitney).

Regrettably, this experiment showed the ineffectiveness of the PEI-NPs vector on downregulating target genes (figure 4-45). RNA interference effect on transfected HAoECs using PEI was not sufficient to give a statistically significant difference between scramble- and hsa-miR-132-3p-transfected samples.
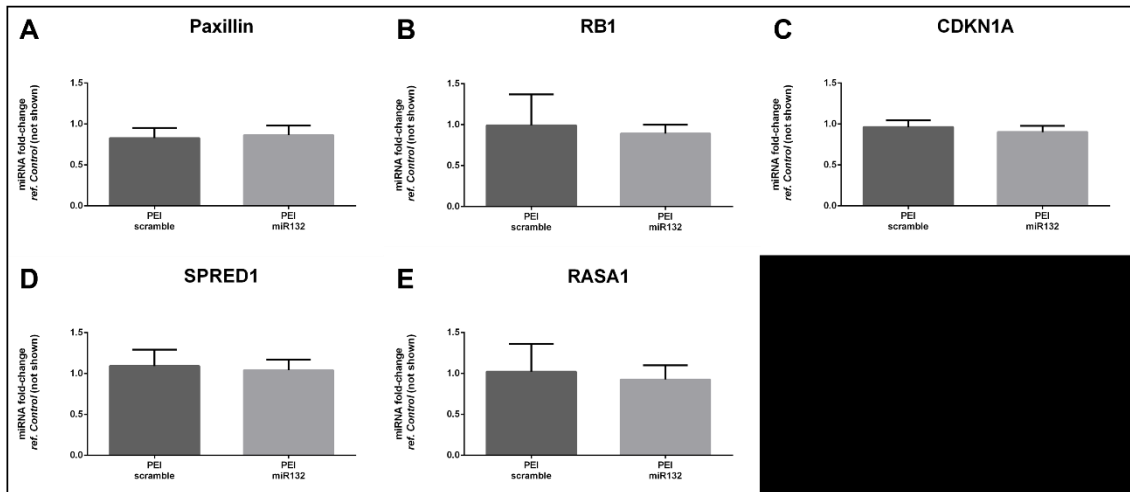
Figure 4-45: Hsa-miR-132-3p-target genes panel expression by hsa-miR-132-3p- and scramble-transfected HAoECs with PEI.
Cells were transfected using PEI-NPs. Each graph compares a single gene expression (name on the title) from HAoECs transfected either with hsa-miR-132-3p or scramble microRNA. A: PXN, B: RB1, C: CDKN1A, D: SPRED1, and E: RASA1. *$P<0.05$, **$P<0.01$, ***$P<0.001$ and ****$P<0.0001$. Values are expressed as mean ± standard deviation. Technical replicates=6 Non-parametrical test performed (Mann-Whitney).

The gene regulation outcomes match with the proliferation and migrations assays obtained in the previous paragraph. The absence of downregulation of genes that reduce migration and proliferation speed by PEI-mediated transfection is likely a cause of no downstream effect – i.e. the lack of migration and proliferation acceleration in PEI-mediated hsa-mir-132-3p-transfected HAoECs. On the other hand, hsa-miR-132-3p-transfected HAoECs using Lipofectamine showed downregulation of genes that are known to slow down migration and proliferation.

4.4 MicroRNA-functionalized scaffold fabrication and preliminary tests

In the following paragraphs, I describe the optimization of the scaffold manufacturing process and composition (figure 4.46). Then, the release of microRNA embedded in the scaffold is tested. Finally, HAoECs are seeded on the microRNA-functionalized, and their uptake of the microRNA released by the scaffold is assayed.
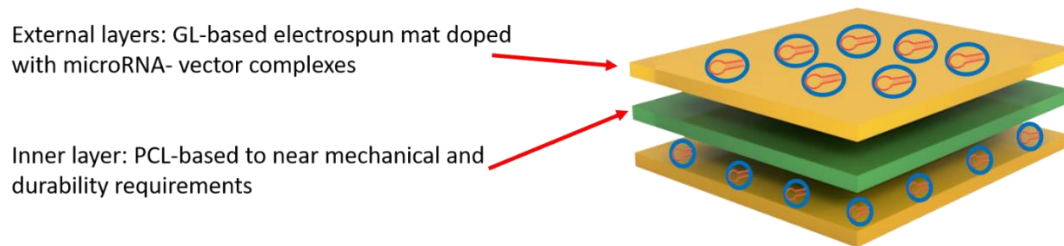
Figure 4-46: Tri-layered microRNA-functionalized scaffold for valve regeneration designed in this project

The illustration describes the scaffold design concept. The PCL-based core layer should provide the mechanical and durability requirements for the implantation of the scaffold in the valvular position. The GL coatings integrate the microRNA-vector complexes, which are released as the GL degrades.

4.4.1 Fabrication of a valve shaped collector for electrospinning

One of my project aims was to investigate the possibility to manufacture a valve-shaped scaffold directly during the electrospinning phase, without committing the surgeon to create a valve on the surgical theatre from flat sheets. To do so, I had to build an electrospinning collector with a valve shape, so that the scaffold will take its final morphology as the fibers are laid on the collector.

The final collector would be fabricated from 3D models of bioprosthetic valves or patients from CT scans. The 3D image is imported in a 3D design software (Autodesk Fusion 360, USA). In this phase, the model is adapted to the 3D printer that will print the model. Then, the model is 3D printed in polylactic acid. The electrospinning needs a conductive collector on which it attracts the polymer fibers, but the printed model is made of PLA - a non-conductive polymer. Therefore, chemical electroplating was employed to create a metal coating on the surface on which the scaffold should be laid on (see paragraph 2.6.2.1). In this project, the scaffold deposition surface was provided with a copper coating. The production pipeline was tested using a 3D model of the aortic valve found on the internet (figure 4-47). Electrospinning trials on the so-made collectors were carried out applying the scaffold production protocol adopted in this project - see paragraph 2.6.3. Unfortunately, the electrospun nanofibers used to stick firmly on the collector and it was not possible to remove the scaffold without tearing it. I sought help from Chemistry and Engineering Departments at the University of Bristol, but nobody was able to help. Therefore, this approach was abandoned in favor of the production of a simpler flat sheet scaffold in order to complete the project on time. Like other materials employed in

128

cardiovascular surgery, scaffold sheets can be sewed in the required shape before surgery, even by surgeons in the surgical theatre.
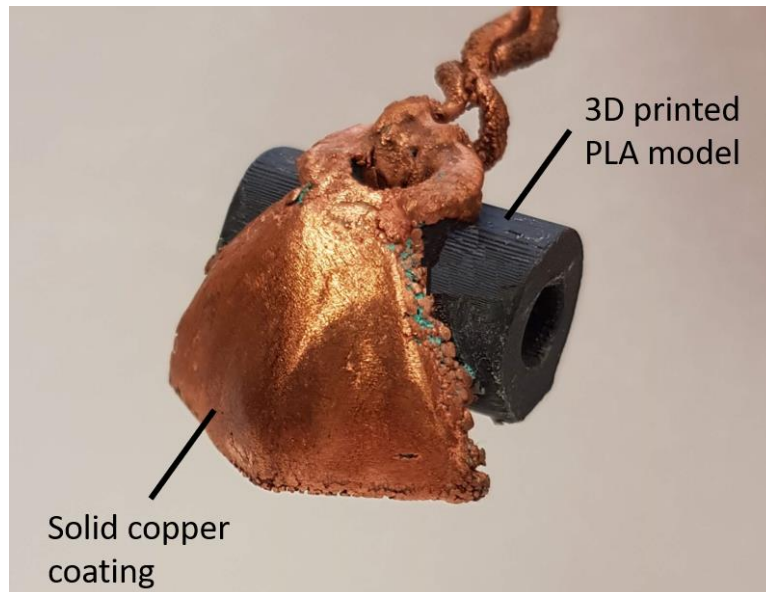
Figure 4-47: A 3D printed leaflet model with copper plating that makes it suitable as an electrospinning collector.

4.4.2 Scaffold fabrication protocol

Initially, preliminary scaffold production protocol tuning was carried out.

For the coating layers tests were performed using a solution of GL dissolved in different solvents mixtures of distilled water and NMP – see paragraph 2.3. GL concentration was kept fixed to 15% (w/v), and the crosslinker GPTMS (200 µL/g of added gelatin) was added 1h before electrospinning. The solution was then stirred at 37 °C for 60 min. The distance between the needle tip and the collector was fixed to 20 cm, and the parameters to tune were:

- Voltage: 7, 10, 13, and 15 kV
- Feed/Flow rate: 1 and 0.5 ml/h
- NMP/water v/v ratio: 50/50, 60/40, and 70/30

Since the NMP boiling point is at 202°C under atmospheric pressure, the scaffold was dried under a pressure of 5.5x10-3 mbar and a temperature of 37°C in a custom-made vacuum oven for 48h.

SEM images indicate that NMP is a good solvent to produce GL nanofibers. Fibers' diameter and pore size tend to increase with the growth of NMP proportion in the solvent mix (figure 4-48D and E). The 70:30 v/v NMP/water proportion creates deformed fibers with beads and large clots of fused fibers. The final protocol (table 4-3) was: 50:50 NMP/dH$_2$O, a voltage of 15kV, and a flow rate of 1ml/hr, which produces well-defined and thin fibers (figure 4-48A). The resultant GL nanofibers had an average diameter of 336.7±56.4nm and an average pore dimension of 290±23nm (figures 4-48D and E).
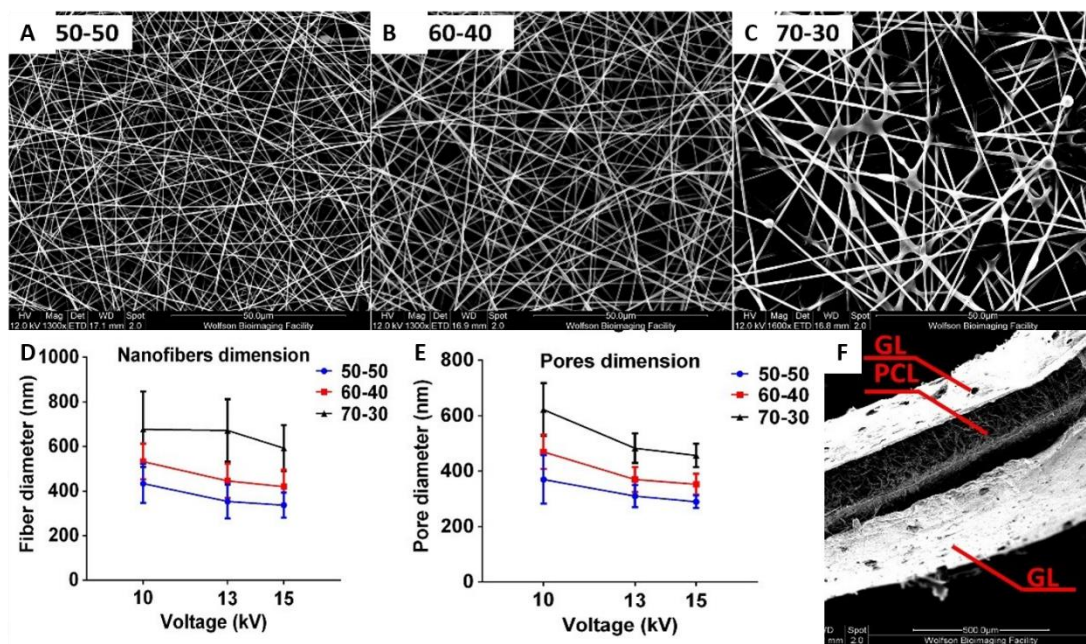
Figure 4-48: Sem imaging and characterization of the electrospun scaffold
A-C) SEM pictures of the GL nanofibers produced with a solvent mix at different NMP-water v/v ratios. D-E) Graphs showing nanofiber diameters and porosity. F) SEM picture of the triple layer of GL-PCL-GL electrospun scaffold.

After the design of the GL nanofibers layer manufacturing process, I focused on creating a three-layered scaffold GL-PCL-GL (figure 4-48F). I have verified that the overall PCL-GL scaffold thickness is 369±131 μm, which is in line with the measured leaflet thickness (460 μm) of a bovine pericardium-based commercial bioprosthetic valve (PERI-GUARD SUPPLE, Bovine Pericardium with Apex processing).

Protocol #	Materials	Voltage	Flow rate	Additional Features	Outcome
1	GL 15% w/v in NMP/water (50/50 v/v)	15 kV	1 mL/h		Good spinnability

| 2 | Core: PCL 10% w/v in chloroform Coating: GL 15% w/v in NMP/water (50/50) | 15 kV | 1 mL/h | | Good spinnability |

Table 4-3: Tested electrospinning protocols (1)
In line 1 are the parameters of the optimal GL layer fabrication protocol. In line 2 are the parameters of the optimal PCL layer fabrication protocol. GL: gelatin, NMP: N-Methylpyrrolidone, PCL: Polycaprolactone.

4.4.2.1 Mandatory changes in the gelatin coating fabrication: Gelatin in water only

After the calibration, it appeared that the GL layer was soft and easy to dissolve in water. After 2 scaffold fabrication repetitions, the problem was still present (table 4-4, Protocol 2). I did not have this problem when I used water/acetic acid 40/60 v/v as a solvent. Thus, the hypothesis was that NMP was interfering with the GL crosslinker – GPTMS. It was decided that the GL layer would have been produced with water only as solvent To allow it, the electrospinning chamber was fitted with a custom-made temperature and humidity control system – see paragraph 3.6.2.3. The temperature must be kept above 35°C to have GL in the liquid state. To avoid GL drying around the needle tip hampering the electrospinning, relative humidity must also be controlled and kept between 50 and 70% (Table 4-4, Protocol 3) [224].

Protocol #	Materials	Voltage	Flow rate	Additional Features	Outcome
1	GL 15% w/v in NMP/water (50/50, 60/40, or 70/30 v/V)	7, 10, 13, or 15 kV	1 or 0.5 mL/h		Good spinnability
2	Core: PCL 10% w/v in chloroform Coating: GL 15% w/v in NMP/water (50/50)	15 kV	1 mL/h		Good spinnability The gelatin layer dissolves upon scaffold wetting
3	GL 10 or 15% w/v in water	15 kV	1 or 0.5 mL/h	Heating: 35°C r. Humidity: 50-70%	Good Spinnability No issues in the fabrication stage

Table 4-4: Tested electrospinning protocols (2)
In red: previously developed protocol with its problems outlined in the Outcome column and discussed in the paragraph. In green: the newly developed protocol that allows the electrospinning of GL coatings with only water as the solvent. GL: gelatin, NMP: N-Methylpyrrolidone, PCL: Polycaprolactone.

4.4.2.2   Mandatory changes in the PCL core fabrication: PCL/GL blend in TFE

The scaffold as designed so far - PCL core and GL form water-only solution coating – suffered from delamination. PCL layer was detaching from the GL one in wet conditions (figure 4-49A). This is likely due to the different properties of GL and PCL – see paragraphs 2.3 and 5.4. PCL tends to minimize its contact with water, and it wraps around itself when it is in water (figure 3-50D). On the other hand, GL fibers swell as soon as they get in contact with water, they become thicker and much more packed. In the SEM pictures, it is possible to note that the fibers are thicker, and the pores are hardly visible (and fewer) in the wet electrospun GL mat (figure 4-49B and C). This causes a dimension rearrangement at the macro scale – lateral length -14,8% and thickness +90,8% [499]. I could not take SEM images of wet PCL. However, PCL does not change its macroscopic dimensions. This different behavior may be the cause of the delamination. To avoid it, the scaffold manufacturing protocol was changed. After literature research, I tested a GL/PCL blend in TFE to create a hydrophilic core layer [412], [413]. The electrospinning set-up remained the as used before. The changes were all in the material solution:

- GL in TFE 10% w/v.
- PCL in TFE 10% w/v.
- The above solutions are mixed with a ratio of 70% PCL solution and 30% GL solution.
- 0.2% v/v of acetic acid is added to the final solution to enhance miscibility.

As stated in paragraph 3.7.2, the scaffold was left in the vacuum oven for 48h after the electrospinning. Eventually, I obtained a hydrophilic core layer (PCL/GL blend) with similar behavior to the GL-only layer in wet conditions (figure 4-49E). With these last adjustments (Table 4-5), the tri-layer scaffold was not affected by delamination anymore (figure 4-49F).
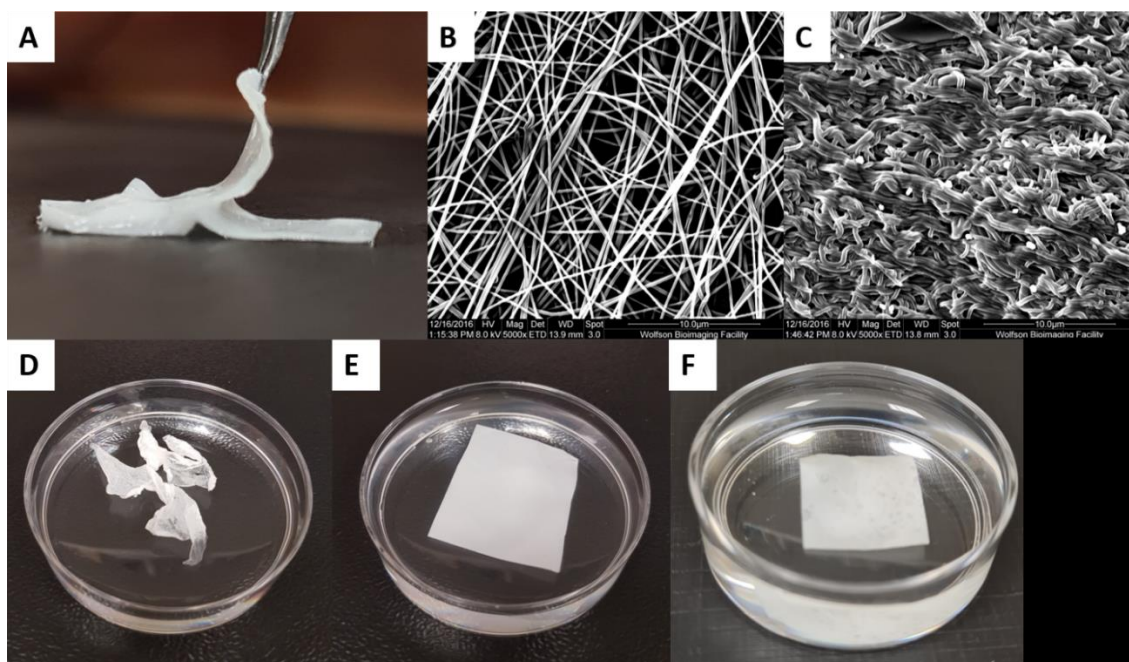
Figure 4-49: Outcomes of the initial and the adjusted scaffold production protocols
(A) PCL core and GL coating original scaffold delamination, (B) SEM image of dry GL-only electrospun scaffold, (C) SEM image of wet GL electrospun scaffold, (D) PCL-only electrospun scaffold in water, (E) PCL/GL blend core layer in water, (F) Complete tri-layer scaffold (GL in water – PCL/GL blend in TFE – GL in water) in water.

Protocol #	Materials	Voltage	Flow rate	Additional Features	Outcome
1	GL 15% w/v in NMP/water (50/50, 60/40, or 70/30 v/V)	7, 10, 13, or 15 kV	1 or 0.5 mL/h		Good spinnability
2	Core: PCL 10% w/v in chloroform Coating: GL 15% w/v in NMP/water (50/50)	15 kV	1 mL/h		Good spinnability Impaired GPTMS crosslinking
3	GL 10 or 15% w/v in water	15 kV	1 or 0.5 mL/h	Heating: 35°C r. Humidity: 50-70%	Good Spinnability
4	Core: PCL 10% w/v in chloroform Coating: GL 10% w/v in water	15 kV	0.5 mL/h	Heating: 35°C r. Humidity: 50-70% (GL layer only)	Good Spinnability Delamination
5	PCL/GL (70/30) 10% w/v in TFE	15 kV	0.5 mL/h		Good spinnability Hydrophilic mat
6	Core: PCL/GL (70/30) 10% w/v in TFE Coating: GL 10% w/v in water	15 kV	0.5 mL/h	Heating: 35°C r. Humidity: 50-70% (GL layer only)	Good spinnability No delamination

Table 4-5: Tested electrospinning protocols (3)
In red: previously developed protocol with its problems outlined in the Outcome column. In green: the newly developed protocol that mends the previous issue. GL: gelatin, NMP: N-Methylpyrrolidone, PCL: Polycaprolactone, TFE: 2,2,2-trifluoroethanol.

4.4.3 Encapsulation of chitosan NPs in gelatin scaffold

To give visual proof of NPs embedding in the scaffold, scaffolds with fluorescent chitosan-NPs were fabricated. The amount of embedded NPs was the same used for transfection with microRNA-vector complex suspended in culture media. For the scaffold manufacturing, the NPs preparation solution was added to dissolve the GL instead of pure distilled water. The solvent of the NPs production solution is essentially water with traces of unreacted reagents from the NPs fabrication process. Therefore, the scaffold fabrication procedure was unaltered.

The result was a nanofibers mat with visible spherical bodies. The SEM picture (figure 4-50B) shows some spherical structures (within yellow circles), which are not present in the GL nanofibers mat without NPs incorporation (negative control - figure 4-50A). Obviously, SEM does not allow to look into the fibers' bulk, but only the surfaces. Thus, it is not possible to understand the proportion of NPs embedded inside the fibers.

Examining the fluoresce pictures, the FITC signal – supposed to come from the fluorescent NPs - appears in a dotted pattern distributed throughout the scaffold (figure 4-50D), while it is completely absent in the negative control image (figure 4-50C). Even in this case, it is hard to discriminate which NPs are inside the fibers or on the surface. However, this experiment confirms that NPs were immobilized on the scaffold.
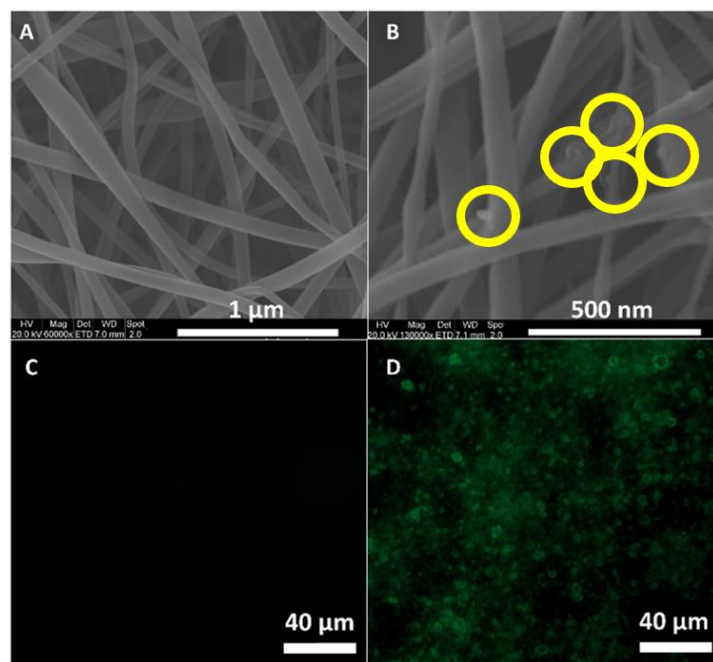
Figure 4-50: SEM and fluorescence images of chitosan-NPs-functionalized and non-functionalized scaffolds

A-B) SEM pictures of GL nanofibers without (A) and with (B) embedded chitosan NPs (within yellow circles). C-D) Fluorescent images of GL scaffold without fluorescent NPs (C) and with fluorescent NPs (D). NPs were fabricated using FITC-conjugated NPs. Then the fluorescent NPs suspension was used to dissolve GL for the electrospinning solution.

4.4.4   MicroRNA release from the functionalized scaffold

In this experiment, a microRNA release curve from a functionalized scaffold was drawn to understand the dosage dynamics of microRNA to cells seeded on the scaffold. Lipofectamine will be the microRNA vector.

The embedded microRNA is functionalized with Cy5 (cel-miR-39-3p-Cy5), thus the release curve was drawn using a fluorimeter (Promega Glomax), λ_{ex}= 627nm and λ_{em}= 660nm. I realized a calibration curve to associate the microRNA amount in solution to the measured RFU (figure 4-51A). To draw the release curve, scaffold strips were incubated with PBS in an incubator, PBS was collected, and fluorescence was measured by fluorimeter, while the scaffold was incubated with fresh PBS. I added 3.75 pmol (26.25 ng) of microRNA for each cm^2 of seeded surface, which is equal to microRNA incubated in culture media for the same surface during a standard transfection. That is the same amount I should embed in the scaffold to have the amount of microRNA per cell of a standard transfection. The difference is that the scaffold will release microRNA during its GL layer degradation - 18 days, not in a single bolus incubation. Hence, I decided to add 2-fold the amount incubated usually based on the following considerations. A GL scaffold degrades in around 18 days, which means that I should get 52 ng/18=3ng of released microRNA each day, assuming a constant release, which is the most sensible hypothesis for the first trial. That means that every three days the scaffold should lose 9 ng of microRNA. Calibration data show around 10-fold RFU units between 0.1 ng (smallest data point) and 10 ng. Therefore, I want to have a 10% sensitivity of the microRNA amount that the scaffold should theoretically release.
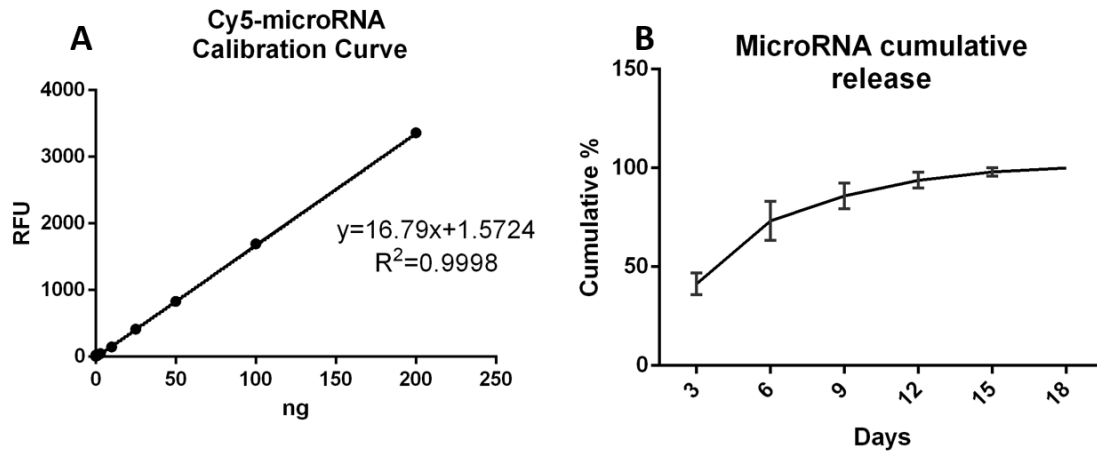
Figure 4-51: MicroRNA release curve
(A) Calibration curve of Cy5-functionalized cel-miR-39-3p drawn adding known amounts of microRNA, and read by a fluorimeter with the following parameters: λ_{ex}= 627nm and λ_{em}= 660nm. (B) Scaffold cumulative release is expressed in the percentage of the total released microRNA. Values are expressed as mean ± standard deviation. Technical replicates=3.

Results show an initial burst release of some 40% in the first three days, and definitely not a linear curve (figure 4-51B). Then, microRNA loss diminishes each time point: 30% between the 3rd and 6th day, 12% between the 6th and 9th day, 8% between the 9th and 12th day, 5% between the 12th and 15th day, and 2% between the 15th and 18th day. Data suggest that the majority of microRNA was on the surface or nearby as it was released in the early stages of gelatin degradation.

4.4.5 Cell detachment from scaffold

Cells seeded on the microRNA-functionalized scaffold need to be detached before verifying if the transfection was successful by RT-qPCR. It is important to detach a sufficient number of cells from the scaffold to then extract enough RNA for RT-qPCR analysis. Thus, several cell detachments protocols were tested on blank scaffolds prior to seeding cells on microRNA-functionalized scaffolds.

I tested different dislodging agents: Trypsin, Accutase, and TrypLE. These agents are usually in combination with EDTA. Its role is to chelate Ca^{2+} and Mg^{2+}, which facilitates cell adhesion on a substrate [415]. The scaffold can absorb substantial amounts of Ca^{2+} and Mg^{2+} and release them during displacing agents incubation. Hence, I decided to include an initial step consisting of the incubation of an EDTA solution. The tested dislodging protocols were:

- Scaffold incubation with 4mM EDTA in PBS for 5 minutes at 37°C on a plate shaker, followed by incubation with TrypLE for 10 minutes or 1h at 37°C on a plate shaker (*TrypLE 10 min* or *TrypLE 1h* in the results graph 4-52).

- Scaffold incubation with 4mM EDTA in PBS for 5 minutes at 37°C on a plate shaker, followed by incubation with Accutase for 10 minutes or 1h at 37°C on a plate shaker (*Accutase 10 min* or *Accutase 1h* in the results graph 4-52).

- Scaffold incubation with 4mM EDTA in PBS for 5 minutes at 37°C on a plate shaker, followed by incubation with Trypsin-EDTA for 5 minutes or 15 at 37°C on a plate shaker (*Trypsin 5 min* or *Trypsin 15 min* in the results graph 4-52).

EDTA solution was used to wash cellularized scaffold and discarded since there were no cells suspended. Then, the scaffold was incubated with a dislodging enzyme. This solution is supposed to contain cells after incubation. Cells were seeded at a density of 15,000 cells/cm^2 with a growing surface of 3.9 cm^2. After 3 days, cells were detached.
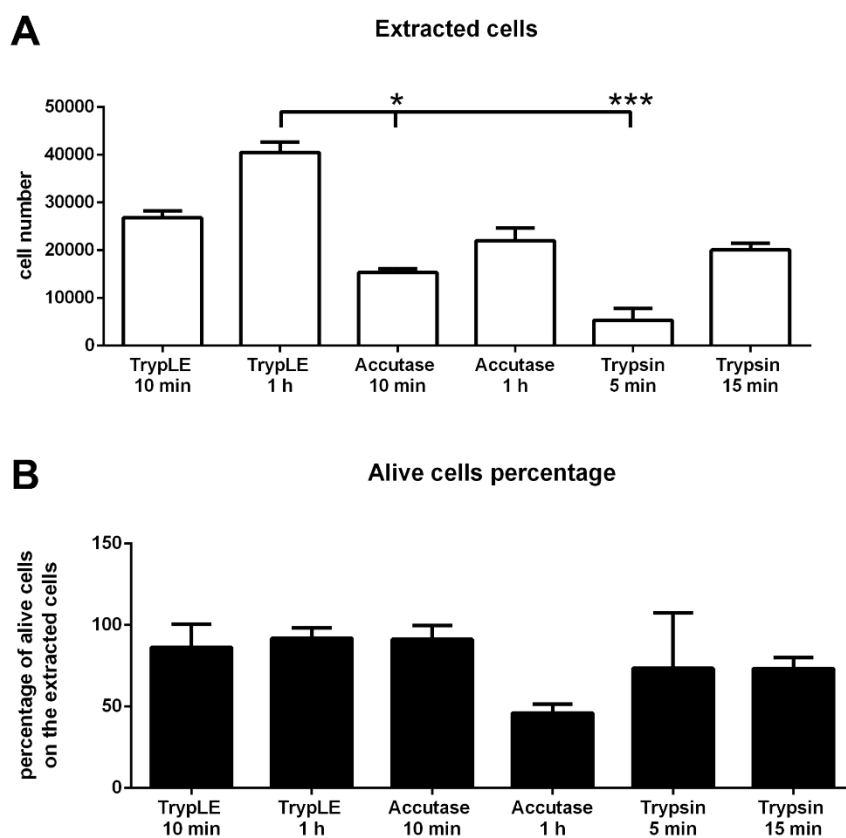
Figure 4-52: Dislodged HAoECs from the seeded scaffold using different detaching protocols A) Total detached cells, B) Alive cells percentage of detached cells (checked with Trypan Blue staining). 15,000 cells/cm2 were seeded on a growing surface of 3.9 cm^2 and detached after 3

days. From the left (in both graphs): cells detached after incubation with TripLE for 10 minutes, cells detached after incubation with TripLE for 1 hour, cells detached after incubation with Accutase for 10 minutes, cells detached after incubation with Accutase for 1 hour, cells detached after incubation with Trypsin for 5 minutes, cells detached after incubation with Trypsin for 15 minutes. *$P<0.05$, **$P<0.01$, ***$P<0.001$ and ****$P<0.0001$. Values are expressed as mean ± standard deviation. Technical replicates=3. Non-parametrical test performed (Kruskal-Wallis ranks test and Dunn's test for multiple comparisons).

Results are displayed in figure 4-52. The highest number of extracted cells was from *TrypLE 1h* samples – 40529±2135 (figure 4-52A). Statistically significant difference is only with *Trypsin 5 min* ($P<0.001$) and *Accutase 10 min* ($P=0.0207$). The numbers of extracted cells are less than the initially seeded ones – 60000 per sample. Noteworthy, the counting method (manual count of cells with Neubauer chamber) is prone to errors when cell number is low. Since all samples have been counted with the same method, similar errors apply to each sample. There is no statistically justified difference in the analysis of the percentage of survived cells among the extracted ones. However, *TrypLE 1h* comes first in this metric as well – 91.95±6.30%.

Calcein staining on a sample treated with TrypLE for 1 hour shows that there are just a few cells after the detachment (figure 4-53). In terms of RNA yield, putting together three samples I obtained 30 ng of RNA each μL, sufficient for RT-PCR analysis. Thus, the best performing detaching protocol for future experiments is: incubation of the scaffold with 4mM EDTA in PBS for 5 minutes at 37°C on a plate shaker, followed by incubation with TrypLE for 1h at 37°C on a plate shaker.
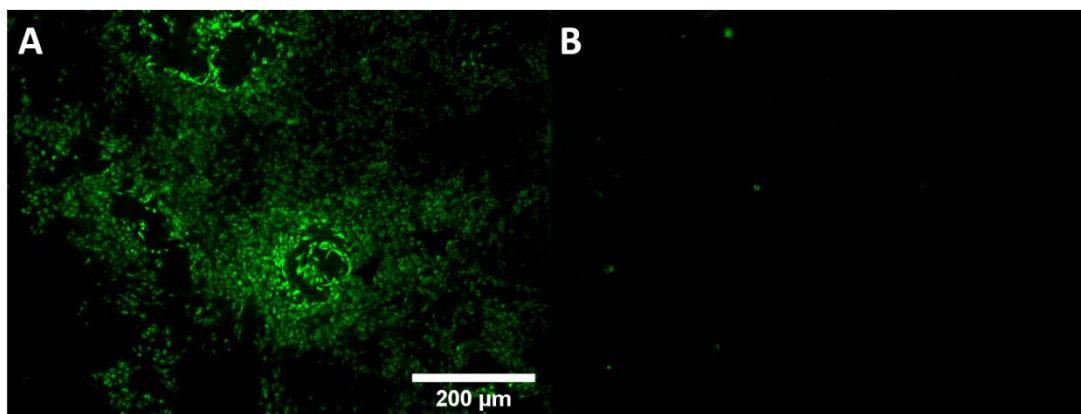
Figure 4-53: Fluorescence images of the seeded scaffold before and after the application of the dislodging protocol

HAoECs were seeded on the scaffold. Then, cells were stained with Calcein before (A) and after (B) applying the TrypLE detachment protocol (4mM EDTA in PBS for 5 minutes, followed by incubation with TrypLE for 10 minutes or 1h at 37°C on a plate shaker).

4.4.6 MicroRNA transfection to ECs by microRNA-functionalized scaffold

The last experiment of this project consisted of transfecting microRNA to HAoECs using the microRNA-functionalized scaffold designed in this project (protocol on table 4-6).

Protocol #	Materials	Voltage	Flow rate	Additional Features	Outcome
1	GL 15% w/v in NMP/water (50/50, 60/40, or 70/30 v/V)	7, 10, 13, or 15 kV	1 or 0.5 mL/h		Good spinnability
2	Core: PCL 10% w/v in chloroform Coating: GL 15% w/v in NMP/water (50/50)	15 kV	1 mL/h		Good spinnability Impaired GPTMS crosslinking
3	GL 10 or 15% w/v in water	15 kV	1 or 0.5 mL/h	Heating: 35°C r. Humidity: 50-70%	Good Spinnability
4	Core: PCL 10% w/v in chloroform Coating: GL 10% w/v in water	15 kV	0.5 mL/h	Heating: 35°C r. Humidity: 50-70%(GL layer only)	Good Spinnability Delamination
5	PCL/GL (70/30) 10% w/v in TFE	15 kV	0.5 mL/h		Good spinnability Hydrophilic mat
6	Core: PCL/GL (70/30) 10% w/v in TFE Coating: GL 10% w/v in water	15 kV	0.5 mL/h	Heating: 35°C r. Humidity: 50-70% (GL layer only)	Good spinnability No delamination
7	Core: PCL/GL (70/30) 10% w/v in TFE Coating: GL 10% w/v in water	15 kV	0.5 mL/h	Heating: 35°C r. Humidity: 50-70% (GL layer only) microRNA-vector in GL layer	Cells transfected with microRNA on the scaffold

Table 4-6: Tested electrospinning protocols (4-FINAL)
In yellow: the definitive protocol to produce the microRNA-functionalized scaffold for heart valve regeneration. GL: gelatin, NMP: N-Methylpyrrolidone, PCL: Polycaprolactone, TFE: 2,2,2-trifluoroethanol.

Cells were seeded at 10,000 cells/cm^2 (recommended by Promocell – the HAoECs provider) on a growing surface of 5.8 cm^2. After three and six days, I applied the detachment protocol previously optimized: incubation with 4mM EDTA in PBS for 5 minutes at 37°C on a plate shaker, followed by incubation with TrypLE for 1h at 37°C on a plate shaker. Total RNA was extracted and analyzed by RT-qPCR. Cel-miR-39-3p expression is noticeable in all microRNA extract from cells seeded on the cel-miR-39-3p functionalized scaffold (figure 4-54). However, variability was quite high, so much so that a statically significant difference is achieved only for cells collected after 6 days on a cel-mirR-39-3p functionalized scaffold compared to control – cells seeded on scaffolds without embedded cel-mir-39-3p. This shows that microRNA is released by the scaffold and picked up by the cells seeded on top of it.
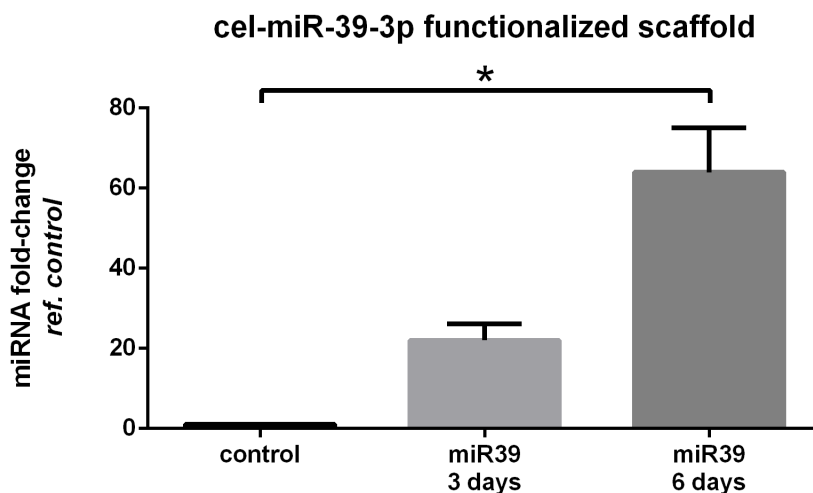
Figure 4-54: Cel-miR-39-3p expression levels of HAoECs seeded on the cel-miR-39-3p-functionalized scaffold.
RT-qPCR readings were normalized by control samples. From the left: control – no transfection, miR39 3days are samples in which cells were seeded on a cel-mirR-39-3p-functionalized scaffold and collected three days after seeding, miR39 6days are samples in which cells were seeded on a cel-mirR-39-3p-functionalized scaffold and collected six days after seeding. The total RNA was extracted from the detached HAoECs and analysed by RT-qPCR to find cel-miR-39-3p. As samples come from cell monolayers and U6 snRNA was used as housekeeping microRNA. *P<0.05, **P<0.01, ***P<0.001 and ****P<0.0001. Values are expressed as mean ± standard deviation. Technical replicates=3. Non-parametrical test performed (Kruskal-Wallis ranks test and Dunn's test for multiple comparisons).

5   Final discussion

The main issues of currently available aortic valve prosthesis are thrombogenicity, progressive degeneration, and immunogenicity [500][501]. Many of these problems are triggered by the initial interaction between the blood and the prosthesis surface. So far, no better valve prosthesis surface than an ECs lining was discovered despite several signs of progress in material finishing [373][375]. The hurdles of an *in-vitro* valve regeneration convinced researchers to adopt a simpler acellular approach. In-situ tissue engineering research is focused on the design of heart valve constructs able to guide the regeneration of native-like valves inside the recipient's body. The newly formed valve should possess all the native valves' functions, including not being thrombogenic and being able to repair and remodel itself [148]. Decellularized valves may struggle to be endothelialized without biochemical functionalization [502][503]. Moreover, recellularization results obtained in animal models may not be repeatable in clinical practice [504]. Given the usual thrombogenicity of prosthetic surfaces, ECs should form a continuous coating in less time possible. To achieve this, different types of scaffold functionalization were proposed, such as antibodies [505] and growth factors [506]. MicroRNA has great therapeutic potential and can influence all aspects of cell function, including the ones concerning regenerative medicine, like proliferation, migration, differentiation, protein synthesis, and others.

This thesis was focused on the design of a microRNA-functionalized scaffold for aortic valve regeneration. The project considered three main aspects to develop:

- The fabrication of a non-cellularized scaffold able to support in-situ aortic valve regeneration and release a therapeutic microRNA to colonize cells at the same time.
- The selection of a microRNA able to stimulate the formation of an endothelial lining on the scaffold.
- The selection of a vector suitable for delivery of a functional microRNA to aortic ECs.

5.1   Micro-132 regenerative potential

Hsa-miR-132-3p transfection to aortic valve ECs should favor scaffold endothelialization. If the implanted scaffold will locally release hsa-miR-132-3p in the injury site, colonizing cells should receive a proliferation and migration boost; so that the endothelialization may be quicker.

Correlation between ECs' migration and proliferation enhancement and hsa-miR-132-3p transfection was already reported [277] [278]. Accordingly, I observed a doubling of proliferative cells after the microRNA transfection. Also, migration was enhanced – paragraph 4.2.

I investigated proliferation- and migration-correlated gene expression – paragraph 4.3.5.5. The RASA1 downregulation was shown to increase ECs' proliferation [278]. Moreover, our group demonstrated that the implantation of hsa-miR-132-3p-secreting cells stimulated ECs' proliferation and migration and downregulated RASA1 [277]. Bioinformatics prediction identified other hsa-miR-132-3p target genes involved in migration and proliferation. Paxillin is a cell focal adhesion component involved in the migration of ECs [280]. Paxillin gene downregulation is correlated with the reduction of proliferation and migration in cancer cells [507]. SPRED1 allows intracellular transmission of angiogenic signals coming from VEGF and FGF and enhances HUVECs' migratory activity [281]. RB1 reduces cell proliferation in tumor cells [279]. Its inhibition facilitates cell cycle progression. To the best of my knowledge, this gene has not been reported to influence ECs' proliferation and migration so far.

All the aforementioned genes were downregulated by hsa-miR-132-3p transfection to aortic ECs while their proliferation and migration inclinations were higher than the control. Bioinformatics analysis also suggested that CDKN1A could be a target of hsa-miR-132-3p. When it is suppressed, angiogenesis is increased, and ECs' proliferation, migration, and tube formation are enhanced [508]. However, I did not observe its regulation after HAoECs were transfected with hsa-miR-132-3p.

In addition, research in our laboratory has shown that microRNA-132 has a role in contrasting calcification [282]. Indeed, microRNA-132 reduces the expression of osteoblast markers [283]. This is not relevant to valve endothelialization. However, native and bioprosthetic valves are subjected to calcification and the protection from calcification could be beneficial to the newly regenerated valve.

Hsa-miR-132-3p is a good candidate to enhance in-situ endothelialization and to protect the implant from calcification. Clearly, has-miR-132-3p is not the only microRNA studied to enhance endothelialization. MicroRNA-126 seems promising and tissue-engineered constructs functionalized with it have already been tested. Wen et al. realized an in-situ vascular regeneration application that promoted endothelialization and nitric oxide synthesis by local transfection of microRNA-126, which downregulates Sprouty-related EVH1 domain-containing protein 1 [509]. Zhou et al. produced another vascular scaffold that exploited the regulatory mechanisms; they demonstrated that prolonged release of microRNA-126 was highly beneficial for ECs proliferation [510]. There is a lack of re-endothelialization publication specific to the

valve tissue in which microRNAs were employed. Nevertheless, inspiration can be provided mainly from the abundant number of vascular regenerative studies. The environment is far from similar, and the ECs are not the same, but they share similarities.

5.2   Selection of a microRNA vector compatible with scaffold embedding

MicroRNA influences cell expression via RNA interference at the post-transcriptional level, reducing or repressing the translation of mRNA with perfectly or partially complementary sequences [511]. To do so, microRNA must enter the cytoplasm in an intact and functional state. However, all RNA types are prone to enzymatic degradation by ubiquitous RNA-specific and generic nucleases [512], [513]. Unmodified short interfering RNA has an average half-life of 20 min in serum [289]. My experiments confirmed the total microRNA degradation after one-hour incubation in 10% FBS. 10% FBS is the usual concentration added to culture media during in-vitro work. FBS is an animal-derived blood extract that contains a physiological mix of nucleases. I am not sure if culture media nucleases concentration and composition are equal to the human organism's concentrations. However, it was shown that nucleic acid digestion is 2-fold quicker in in-vivo setups than in in-vitro cultures, reinforcing the need of protecting genetic material for an effective administration [467], [468]. The media composition was optimized for in-vitro culture, which is the benchmark for this study which is at the *proof-of-concept* stage; thus the application of in-vitro models is compulsory. In a potential follow-up, an animal model (with its characteristics in terms of nuclease degradation dynamics) may be employed, but that is not the aim of this project. In addition, *naked*-microRNA has a reduced capacity to cross the plasma membrane due to its excessive size and its negative polarity. The cell membrane is negatively charged as well, hence it naturally repels RNA sequences [287]. The selection of a safe and efficient vector for microRNA delivery in the cytoplasm is a prerequisite for the application of RNA interference in clinical practice.

Chitosan was repeatedly proven to be suitable for short ncRNA delivery. *Liu et al.* demonstrated a knockdown of enhanced green fluorescent protein expression between 45% and 65% with chitosan NPs [343]. This data was in accordance with *Howard et al.* who reached almost 78% of knockout in human lung carcinoma cells [345]. Also, chitosan has low cytotoxicity [514], [515]. Chitosan-NPs were used to transfect microRNA and plasmid RNA [516][517]. Regarding the specific application of this project, chitosan was particularly attractive since is soluble only in acidic solutions. MicroRNA-NPs were supposed to be embedded in the scaffold for heart valve

regeneration. This entailed that the NPs were to be added to water-based solutions used to produce the scaffold itself. As long as the solution was having a neutral pH (as was planned), the likelihood of chitosan-NPs dissolution and microRNA release during the scaffold production was reduced. These reasons were behind the decision not to use polyethyleneimine in the first place. Indeed, it raised cytotoxicity concerns and it is water-soluble [325][323].

5.2.1 Optimization of the chitosan vector fabrication protocol

Chitosan-NPs production is realized with just a single mixing passage, with no need for specific chemical expertise and machines. Optimization of a chitosan-NPs production protocol is relatively simple. The NPs' physical properties can be changed by variating their composing material, concentrations, and relative ratios. The results of formula optimization often lead to the creation of NPs with a diameter smaller than 500 nm [343][345][518]. The transfection suitability of such-sized NPs has a cytological motivation. Cell types that do not possess phagocytosis capacity (the main cell types with phagocytic ability are macrophages, monocytes, and osteoclasts) struggle to internalize particles larger than 500 nm [432], [519]. Also, the smaller are the NPs, the more likely is the NPs' internalization because more cell endocytic pathways are available, like macropinocytosis, clathrin-mediated endocytosis, caveolae-mediated endocytosis, and clathrin- and caveolae-independent endocytosis [520]–[523]. All these endocytic pathways are available in endothelial cells [385], [387]–[392], [521], whereas no phagocytosis activity has been observed by them, to the best of my knowledge.

I used Sigma low molecular weight chitosan. The material was successfully employed in short ncRNA transfection, and it allows the production of properly sized NPs – around 200 nm or 350 nm [343][345]. I attempted the optimization of the NPs production protocol, starting from an initial formula and variating one parameter at a time. I considered four parameters to be tuned: chitosan concentration, TPP concentration, chitosan-TPP mass ratio, and NaCl concentration. Generally, the reduction of chitosan concentration is correlated with NPs' size reduction [524], which was confirmed in my study. Indeed, the lowest chitosan concentration (0.25 mg/mL) gave the smallest NPs (640±25nm). I then fixed the chitosan concentration at 0.25 mg/mL and changed the other three parameters sequentially to obtain the smallest particles possible. The TPP concentration had the same trend as the chitosan concentration. The lowest one (0.1 mg/mL) produced the smallest NPs (466±37 nm). The variation of the chitosan-TPP mass ratio showed a size minimum at the intermediate ratio of 7. *Ràzga et al.* confirmed that the smallest

particles were measured at chitosan/TPP=7 w/w [525]. Also, *Antoniou et al.* found the NPs' minimal size at ratios of 6 and 9. The balance of electrostatic attraction and steric hindrance may have an optimal equilibrium point at chitosan/TPP=7 w/w that results in the most compact structure [526]. Finally, I analyzed the effect of NaCl. Using a NaCl concentration of 50 mM, I reached the smallest NPs diameter I ever produced (140±25 nm). The tested concentrations went from 0 mM to 150 mM, which corresponded to NPs' sizes from 140 nm to over 300 nm. *Ràzga et al.* found a difference of just 30 nm for the same range of NaCl concentration tested, while *Antoniou et al.* registered a size increment of around 30% when the NaCl concentration went from 8.6 mM to 25.8 mM. Both studies are in substantial discordance with my results since I found much higher size variability and I identified the NPs' minimum size at a much higher sodium concentration than the other two studies. Other production parameters could have been tuned (stirring speed, rate of TPP/microRNA addiction to the chitosan solution, chitosan solution pH), and would have been, if an NPs' diameter of around 200nm would have not been reached tuning the four parameters initially chosen. However, it was also important to consider the general picture. This project is not focused on the description of chitosan-NPs, and how different production parameters can influence their features. Chitosan NPs should be functional to reach the final aim: the development of a microRNA-functionalized scaffold for heart valve regeneration. Thus, the chitosan-NPs production protocol optimization aimed to produce NPs with satisfying and literature-backend characteristics - an NPs' diameter around 200nm – and it was limited to that.

Chitosan-NPs produced with the optimized protocol were measured by DLS and TEM. A relevant diameter difference was observed: 140±25 nm by DLS, and between 12nm and 20 nm by TEM. The discrepancy between the two measuring methods can be explained by the different conditions of the NPs at the measurement time. The transmission electron microscope measures the NPs after they have been exsiccated and coated with carbon. As additional proof of actual NPs formation, backscattered x-rays analysis determined a spheroid-like topological distribution of the NPs' crosslinker – the TPP.

5.2.2 *In-vitro* biological characterization of the chitosan vector: cytotoxicity, proliferation, and uptake

The strong point of chitosan is its biocompatibility and lack of toxicity. Oral administration to mice did not elicit any adverse effect up to 100 mg/kg [336]. To verify this in my application, I

tested the effect of chitosan-NPs administration in terms of cytotoxicity and potential proliferation impairment. The scope of the microRNA functionalization of the scaffold is to improve the scaffold endothelialization. Hence, I needed to be sure that the transfection vector was not having a negative effect on two of the most important cell properties for successful colonization: viability and proliferation. I compared chitosan-NPs with a commercial microRNA transfection agent (Invitrogen Lipofectamine RNAiMAX). At first, I did not include any microRNA. The cells used in this experiment were the commercial immortalized ECs (EA.hy926). Lipofectamine was incubated following the manufacturer's protocol, while chitosan-NPs were tested at different concentrations. I fixed the minimum chitosan-NPs concentration in line with published studies [527][346][345]. The other concentrations were around 5 and 10-fold the lower NPs concentration to investigate the cytotoxicity threshold. Only the highest dosage caused significant viability reduction – around 10%. Published data showed significant cytotoxicity at around 5 and 10-fold the maximum concentration that I tested [527][346]. The threshold discrepancy may be due to the different types of cells used. Regarding proliferation trends, only Lipofectamine limited it by almost 36%. Samples incubated with Lipofectamine had lower cell density. The reason for that is unclear, and it was impossible to investigate it due to time and funding limitations.

I then tested if the incorporation of a microRNA in non-toxic and non-antiproliferative chitosan-NPs could worsen the NPs' properties. In terms of viability, I observed the only sample under 80% viability was the one administered with microRNA at 10 nM combined with Lipofectamine. Also, the proliferation reduction was observed only on Lipofectamine-transfected samples. Research reported Lipofectamine cytotoxicity and proliferation impairment on coronary arterial ECs [528], mesenchymal stem cells [529], and embryonic stem cell-derived ECs [530]. In my experiments, chitosan proved to be a biocompatible transfection vector.

I finally tested the chitosan-NPs uptake potential. I synthesized FITC-conjugated chitosan to make NPs visible under a fluorescence microscope. I calculated that one or more chitosan-NP was inside 82.4±9.2% of cells. This was a satisfying percentage of positive cells, aligned with or outperforming other non-viral vectors [531]. In terms of the amount of uptaken NPs, some vectors do better, like pullulan[532]. Serum present in culture media and blood, which would wet the construct I am designing in its final location, can constitute an issue. Indeed, transfected cells go down to 49.4±12.5% in media with 10% of FBS. A high number of chitosan-NPs was found in the culture media and in PBS used to wash cells at the end of the transfection. It is notorious that serum proteins tend to aggregate NPs into micrometric agglomerates, which then cannot enter the cells [533] [534]. This is not limited to chitosan-NPs, Lipofectamine is affected as well

[535] [536]. However, microRNA-NPs will be anchored on the scaffold in the final scaffold. Once released from it, they should not travel far to meet a cell to transfect, hence their likelihood to meet proteins and other particulates to aggregate with may be reduced.

5.2.3   Chitosan vector microRNA loading and transfection efficiency

Knowing the amount of loaded microRNA in the NPs is essential. Any transfection protocol requires incubating a precise amount of microRNA with cells, which will be then correlated with its effect on cell function and expression [537][538].

RT-qPCR is an extremely sensitive technique that allows the detection of minimal amounts of RNA. It could have been a suitable way to measure the microRNA amount embedded in the chitosan-NPs [539]. However, chitosan causes problems either during total RNA extraction or the RT-qPCR stage. Polysaccharides (like chitosan) are abundant in plant samples, and they cause issues with RNA extraction [540][541]. To amend the problem, RNA extraction kits were specifically designed for polysaccharides-rich samples. There are also specific extraction buffers designed for such samples, like CTAB-based buffers [542]. I tested both, but they were not beneficial for microRNA amount estimation in chitosan-NPs. The total RNA yield was less than the yield from the same samples extracted with the general-purpose Qiagen RNeasy micro kit. Disappointingly, even the most efficient method could extract only a small fraction of the microRNA embedded in the chitosan-NPs – around 24%.

In several publications, microRNA loading efficiency is calculated by measuring the amount of free-floating microRNA in the supernatant after NPs suspension centrifugation [543][544]. I tried to separate chitosan-NPs from free microRNA by centrifugation. However, I could not isolate chitosan-NPs on a tube bottom without breaking them. In that condition, part of the measured microRNA could have come from broken NPs. On the other hand, very slow centrifugation speeds left NPs floating in suspension. I basically could not find the right centrifugation speed to concentrate all chitosan-NPs on the vial bottom without crushing them. Chitosan-NPs are highly hydrated nanogels, thus they may be too soft to withstand the impact with the tube bottom surface during centrifugation. Hence, I tested a less mechanically stressful method to separate embedded from non-embedded microRNA, the dialysis. It is often used to separate compounds in a very gentle way [545][546]. The osmotic pressure is the only driver of the separation. Unfortunately, I realized that microRNA could not cross the dialysis membrane, although its pores were designed to allow membrane crossing by 30-fold larger compounds. Although

dialysis has been used to prepare NPs for short ncRNA delivery [547]–[549], it gave utterly unsatisfying results in my experiments. The causes of the failure are not clear to me. The microRNA size compared to the membrane MWCO is not the issue; the dialysis membrane pores were sufficiently large in theory. Given these results, I abandoned the use of dialysis membranes to estimate the amount of embedded microRNA.

As just discussed, I could not optimize a protocol to assay chitosan-NPs microRNA loading efficiency. As initially mentioned, free microRNA degrades within minutes if incubate with serum. Hence, instead of separating embedded from non-embedded microRNA, I exposed the microRNA-loaded NPs to a serum solution for 1h. Usually, transfecting agents manufacturers indicate a transfection time of no less than 4 hours. Thus, I assumed that the microRNA that does not withstand 1 hour in contact with serum nucleases is not likely to be transfected in cells. Thus, the amount of remaining microRNA is an approximate estimation of the microRNA that cells could internalize during the transfection. Still, RT-qPCR sensitivity was impaired by the presence of chitosan in the samples – see above. The selective enzymatic digestion of chitosan with chitosanase could have helped to increase RT-qPCR sensitivity when analyzing samples with chitosan, as shown in published works [424]–[426]. Chitosan enzymatic digestion by chitosanase allowed to raise the amount of extracted microRNA out of chitosan-NPs samples from 24% to 75%. Nevertheless, estimation of chitosan-NPs-loaded microRNA amount after exposition to FBS was still not possible. All microRNA freed from within chitosan-NPs by chitosanase would have been degraded as soon as it was getting in contact with the serum in the suspension. To avoid this, the final experimental protocol included the presence of an RNAse inhibitor during the chitosan digestion. After verifying that the RNAse inhibitor was not hindering the chitosanase activity, I finally managed to develop a protocol to estimate the quantity of microRNA that could reasonably be uptaken by cells when microRNA-loaded chitosan-NPs were administered. This was not an exact measurement of all microRNA complexed with chitosan, but an evaluation of the amount of microRNA that was receiving enough protection to be safely transfected to cells. The result of this measured with this protocol was not satisfying, though. Just 3% of initially embedded microRNA survived a 1-hour incubation with serum. Such a low amount would mean that 97% of expensive microRNA would be degraded and not achieve its target. In addition to the enormous waste of expensive material, the remaining microRNA may have not been enough to achieve a therapeutic effect. There are several studies showing microRNA-loading efficiency above 80% [550][551][552]. Thus, I tried to improve the chitosan-NPs loading efficiency by changing the chitosan and microRNA concentration, but I did not get improvements. The increase of chitosan concentration during the NPs production did not improve the microRNA

protection against FBS nucleases, nor increasing the microRNA initial amount resulted in a higher quantity of microRNA surviving FBS exposition. Perhaps, loading saturation - maximum microRNA that can be uploaded into NPs – was reached. The only beneficial modification was the elimination of the NaCl addition during the NPs fabrication. The increase of microRNA loading from 3% to around 18% reinforced my suspicion that NaCl ions were reducing the electrostatic attraction between chitosan and microRNA, although NaCl is used in published NPs fabrication protocols to reduce NPs' dimension variability [553]–[555].

Despite all the optimization work done and the promising literature, my experiments revealed that chitosan-NPs were not able to transfect microRNA to aortic ECs. I found no traces of the embedded microRNA in the RNA extract from the transfected cells. Chitosan may be still a good candidate for microRNA transfection with some modification. Nevertheless, given the scholarship remaining time and the ambitious objective of this project, I had to look for a different transfection vector and abandon chitosan.

5.3   Selection of alternative transfection vectors

As briefly outlined at the beginning of the discussion, many are the transfection vectors used in medical research. Chitosan was chosen because of its high biocompatibility, non-solubility at neutral pH, and good transfection performance reported in the literature. TMC is a chitosan derivative. The main difference between the two is that TMC is constantly positively charged and its charge does not depend on the environmental pH, as for chitosan. This may help to create a more stable bond with the microRNA [556]. TMC showed transfection potential when combined with pDNA [557] and siRNA [558]. However, it did not transfect microRNA to aortic ECs during my screening tests. Noteworthy, ECs are not the simplest cell type to transfect. Several publications report low transfection efficiency with non-viral vectors [559][560][561].

PEI was one of the first and most used transfection vectors. It also inspired commercial transfection agents such as JetPEI (Polyplus, France) [316]. The PEI's ability to permeabilize cell membranes could be the cause of its alleged cytotoxicity [562][563]. Despite its toxicity, the PEI's ability to transfect genetic material was not overlooked. Indeed, countless PEI derivatives were developed to exploit its transfection ability and try to mitigate its cytotoxicity [564] [565]. PEI-g-PEG was realized expressively to amend PEI cytotoxicity and increase its systemic circulation time [566][567]. PEI-g-PEG showed transfection potential in my experiments. However, the levels of transfected microRNA were not stable. PEI-g-PEG was more transfection efficient at

high concentrations. Noteworthy, the cell monolayers did not look healthy, gaps and round-shaped cells (a sign of poor cell health) were more frequent as PEI-g-PEG was increased. As outlined in the following paragraph, PEI showed higher transfection efficiency and no cytotoxicity in the concentration employed. Considering the limited time, I could not carry on with all the tested transfection materials to the next stages of the project. Thus, I choose the most performant, the PEI.

5.3.1 PEI as transfection vector

PEI is extremely transfection-efficient [568][569]. In my experiments it outperformed Lipofectamine by 2- to 3-fold, depending on the concentration. The PEI cytotoxicity threshold is extensively debated in the literature and it depends on different circumstances [570]. Regrettably, PEI cytotoxicity is positively correlated with its transfection efficiency, as it seems to be correlated with the charge density which is also the reason for its good transfection. *Wagner et al.* fixed the threshold at 360 $\mu g/mL^{-1}$ [571][572][325]. However, the amount employed in my experiments was 423 ng/mL at most - around 850-fold less. Since membrane permeabilization is a reason for PEI toxicity, I assayed potential membrane damages with an LDH assay. I noticed that there was no lactate leakage in samples treated with PEI or Lipofectamine, nor viability decreased. *Fisher et al.* found a relevant amount of LDH in culture media after fibroblasts were incubated with 10 $\mu g/mL$ [573]. *Hall et al.* showed some LDH leakage when branched-PEI with an Mw of 25 kDa (the same used in my experiments) was incubated with lung cancer cells at a concentration of 2 $\mu g/mL$ [574]. In both cases, PEI was not complexed with any genetic material, a state in which PEI is more cytotoxic [575]. Since I have used lower concentrations of PEI-microRNA complexes, which makes PEI less cytotoxic, my LDH assay data are reasonable. Also, no issues were noticed in the viability assay, viable cells were always equal to or more than 94%. Safety-wise the PEI-NPs did not seem to cause any concern. Highly likely, the limited amount used contributed to PEI tolerability. PLGA and PEI-g-PEG especially seemed promising as microRNA vectors, but a choice was mandatory as carrying forward all these materials in parallel was not feasible. Therefore, PEI was prioritized given its superior transfection efficacy.

5.3.2 Regenerative potential of the PEI-microRNA complex

After having proved the transfection potential of PEI-NPs, its functional effects were tested. Repeated trials gave unexpected results. Cell migration seemed faster when microRNA negative control was embedded in PEI-NPs. Also, proliferative cells had the same trend. The suspect of an unspecific effect of the microRNA negative control made me repeat the experiment with an additional negative control from a different manufacturer. The proliferation assay has clearly shown that only the lipofectamine-has-miR-132-3p complex had an enhancing effect, while migration assay results were inconclusive. Enhanced cell migration of PEI transfected samples and lipofectamine-has-miR-132-3p appeared only at the latest time point. The possible effect of the PEI material only was considered as well. However, PEI material only did not have any functional effect. In the light of these results, I tested gene regulation and I discovered none of the considered genes were downregulated in samples transfected with PEI-has-miR-132-3p. The gene regulation outcomes matched with the proliferation and migrations assays. The absence of downregulation of genes that reduce migration and proliferation speed by PEI-mediated transfection is likely a cause of no downstream effect – i.e. the lack of migration and proliferation acceleration in PEI-mediated hsa-mir-132-3p-transfected HAoECs. On the other hand, hsa-miR-132-3p-transfected HAoECs using Lipofectamine showed downregulation of genes that are known to slow down migration and proliferation. This observation at the translational level matches with the cell proliferation enhancement (functional level). I could not conclude the same for migration. MicroRNA transfection to HAoECs with PEI (both scramble and microRNA-132) resulted in faster migration compared with control. I could not give a reasonable justification for this. The enhanced migration could not be ascribed to the PEI material only, since HAoECs incubate with PEI and no microRNA did not have the same behaviour. Effective transfection of short non-coding microRNA by branched-PEI 25 kDa (used in this study) at polyethylenimine/RNA ratios similar to the ones employed in this study was already demonstrated [325] [318]. The silencing potential of the branched-PEI 25 kDa vector (used in this study) was also demonstrated in mesenchymal stem cells [324], neuroblastoma cells [318], and cervical cancer (HeLa cells) [576]. A specific characteristic of aortic ECs may be behind my negative results in the use of PEI, which are in contrast with published works.

Eventually, the only vector able to actuate gene silencing among the ones I tested was the Lipofectamine. That was the vector I utilized to functionalize the scaffold under development with microRNA, although it is expensive and its claimed cytotoxicity is stopping clinical use [577].

5.4   MicroRNA-bearing scaffold design

After testing different materials, it became clear that the only vector enabling microRNA to regulate gene expression in HAoECs was the commercial Lipofectamine RNAiMAX. The use of lipofectamine as a vector for the microRNA integration in the scaffold was dictated by the failure to regulate gene expression by RNA interference by the other tested vectors. Despite those vectors being previously proven to be working – see paragraph 1.5.5, the specificity of my application and/or my inexperience made Lipofectamine the only choice. It is not the best solution because it is an extremely expensive material (producing a 36 cm^2 of scaffold requires some £150 of lipofectamine), and its cytotoxicity [578]–[580], even though there are studies supporting the low cytotoxicity of Lipofectamine thesis [581], [582].

A general indication to support tissue regeneration is to create scaffolds with a high surface-volume ratio, highly porous, and interconnected pores. Electrospinning can produce construct with these characteristics made of several materials. Its mild process conditions (no extreme temperature or pressures) allow integration of different biomolecules, provided their compatibility with the production solvents [583]. Electrospun tissue-engineered valve substitutes were just proven to be feasible in animal models [584].

A key part of regenerative tissue engineering is that, eventually, no exogenous material remains, only autologously generated tissues. GL is biodegradable and possesses anchoring peptides like the RGD sequence which is recognized by cell integrins. Its suitability for tissue engineering does not surprise, since GL is the product of collagen denaturation, the most abundant protein in the body. GL is less antigenic than collagen, thus suitable for tissue engineering [585][586]. The scaffold I designed is constituted of three layers: 2 GL coatings and a core layer of blended PCL/GL. GL was crosslinked by GPTMS, which increases its duration in wet environments. Initially, the GL was dissolved in an NMP/water mixture to maintain the solution in the liquid state at RT and neutral pH – see paragraph 2.3. The use of NMP posed an additional issue. NMP is toxic so it must be removed from the scaffold after the electrospinning. However, its boiling point is at 202°C under atmospheric pressure, meaning it does not evaporate. Using a pressure-temperature nomograph, it is possible to see that the NMP boiling point is 0°C at 293 mbar. Thus, it was mandatory to dry the scaffold in a custom-made vacuum oven – see paragraph 3.6.2.2. Chemical analysis should have been carried out to measure potential residues of NMP after the solvent evaporation. However, time and costs limitations did not allow me to do so. Therefore, I add to rely on the goodness of published protocols at this stage [458]–[461]. The use of GL electrospun mat as a tissue engineering support was previously tested, and good cell colonisation was achieved [587]. Pore size was always well below average cell diameter – around

10 μm. However, I cannot exclude that cells would penetrate the scaffold as its colonization progresses. Long-term in-vivo experiments could be carried out to observe the dynamic of colonization in future developments of this project. Unfortunately, the scaffold's GL layer fabricated from a solution in NMP/water was not crosslinking. In my experience with GPTMS-crosslinked GL scaffolds, I did not have this problem when I used water/acetic acid 40/60 v/v or water only as a solvent. Thus, I hypothesized that NMP was interfering with the crosslinking of GL by GPTMS. I tried to verify my hypothesis in the literature, but I could not find examples of GPTMS-crosslinked gelatin scaffolds produced using NMP as a solvent. I only found examples with water/acetic acid mixes [588]. All non-experimented (or not reported) solvents could have unexpected interactions with GPTMS. That could have dragged me into an endless series of trials, so I decided that the GL layer would have been produced with water only as a solvent [589]. However, the issue that convinced me to avoid using water only in the first place was again blocking my path towards completing the project: water cannot keep GL in the liquid state at RT. The solution was to fit the electrospinning system with a climate control device that regulates temperature and relative humidity. The temperature must be kept above 35°C to have the GL solution in a liquid state. Moreover, when the electrospinning cabinet is heated up, the humidity decreases dramatically, and the GL dries on the needle tip. This creates a clot and prevents electrospinning. Thus, relative humidity must be kept under control. In my experiments, electrospinning is possible between 50 and 70% of relative humidity. As NMP/water was substituted with water only, the GL crosslinking by GPTMS was restored.

The NPs were localized on the GL layer by SEM and fluorescence microscopy. In SEM imaging, scaffolds with microRNA-vector complexes embedded in the GL layer showed bulging spheroids which were absent in scaffolds without microRNA-vector complexes. Additionally, NPs were functionalized with FITC before being added to the GL solution for scaffold production. Fluorescence functionalization of NPs has been already employed to determine whether NPs were embedded in electrospun scaffolds [590]. As a result, the scaffold with FITC-NPs showed a dotted fluorescent pattern distribution that can be ascribed to the embedding of fluorescent NPs. These assays cannot measure the fraction of NPs embedded inside the GL fibers and the one adsorbed on the fibers' surface. However, it has been shown that the NPs are integrated with the scaffold.

PCL mechanical properties and durability were considered by several research groups involved in valve regeneration [591][592][593]. It seemed to be a good candidate as a support material because of its mechanical support layer, biocompatibility, and durability [403]–[405]. In particular, its degradation time is between 2 and 4 years [406], the time during which the host

organism should regenerate the explanted valve. PCL's hydrophobicity reduces cell colonization, thus it is often used in combination with a hydrophilic material [594]. In this project, I blended it with GL. That resulted mandatory because the scaffold produced with the initial formulation – pure PCL core and GL coatings - was delaminating. PCL layer was separating from the GL one in wet conditions. That is likely due to GL's and PCL's different nature. PCL is hydrophobic while GL is hydrophilic. PCL tends to minimize its contact with water, while the GL layer swells as soon as it gets in contact with water. The GL mat microscopical aspect changes dramatically in wet conditions. As from SEM analysis, GL fibers become thicker and the mat pores almost disappear. Macroscopically, the contact with a water-based solution causes a dimensional rearrangement, the lateral dimensions are reduced by 14,8%, and the thickness increases by 90,8% [499]. It was not possible to perform SEM imaging of wet the PCL layer. However, it does not change its macroscopic dimensions. This different behavior in wet conditions may be the cause of the delamination. Since the bond between the materials is already weak because of the materials' different nature, the two opposite forces that kick in when the scaffold gets in contact with water may be sufficient to cause delamination. Delamination risk is not acceptable for heart valve scaffolds; thus, the scaffold manufacturing protocol was changed. After literature research, a GL/PCL blend in TFE - one of the few solvents of both materials - was tested. As GL is constituting the scaffold coating, a GL fraction in the core layer may improve the bond between the layers. Moreover, the PCL/GL blend is hydrophilic, and this reduced the difference in reaction to wet conditions of the scaffold layers [412], [413]. Eventually, this scaffold formulation did not suffer from delamination. Moreover, the addition of GL to the core layer may make it more suitable for cell colonization, in the event of cell penetration in the scaffold bulk.

The approach adopted to design this scaffold allowed two requirements to be decoupled: providing the scaffold with enough durability to allow the regeneration of the valve tissue, and embedding the microRNA in a material with sufficient degradation speed to allow the substantial release of microRNA for therapeutic purposes. Also, it should be possible to tune the microRNA-functionalized layer's degradation speed without concerning about general scaffold failure. Regrettably, I was not able to carry out mechanical tests on the scaffold due to time limitations, but several studies affirm that the use of PCL nears the scaffold's mechanical properties to the native valve's ones. *Ravishankar et al.* produced an electrospun blend of PCL and GL embedded in a glycosaminoglycan hydrogel to resemble the heart valve microstructure. They reached native valve-like mechanical properties together with a favorable environment for VICs [595].

The production of a pre-formed substitute could ease surgeons' job. Also, the combination of medical images and 3d-printing technologies can allow the personalization of a valve prosthesis avoiding possible mismatch of standardized prostheses [410][596][597]. In my project, I developed a pipeline that starts from a 3d model and reaches the deposition of the scaffold material on the 3d model-shaped physical collector. The development was interrupted by a technical problem - the need for an unstick surface for the collector. However, the project may be resumed with the help of a multidisciplinary team with chemistry expertise.

The microRNA-vector complex should be released to colonizing cells while the GL layer is degraded. Published work can be divided into two categories in this regard: studies in which the microRNA is adsorbed on the scaffold surface, and studies in which the microRNA is included inside the scaffold material. The former offers a microRNA released concentrated in the first period after the scaffold implantation; while the latter provides a more gradual release, which follows the scaffold degradation [377]. Considering the GL durability, I found the incorporation of the microRNA in the GL more appropriate. GL crosslinked with GPTMS degrades in around 18-21 days [400]. As the scaffold is implanted, the GL layer will degrade and microRNA-vector complexes will be released, becoming available to nearby cells. Hence, the microRNA administration could last the whole degradation period, promoting endothelialization for a prolonged time. Once microRNA is depleted, cells should return to their normal gene expression pattern, as microRNA-driven RNAi is transient [598]. Theoretically, this is desirable in tissue engineering as the final goal is to restore a patient's tissue or organ, which eventually should acquire a state of physiological function. Therefore, gene expression should not be permanently altered. In the second instance, the scaffold is not fully colonized as soon as it is implanted. Therefore, if the microRNA was just adsorbed on the surface, it may be depleted before a substantial number of cells could reach all the areas of the scaffold. Finally, serum nucleases are aggressive toward microRNA. Thus, microRNA would be degraded soon even if protected by a vector. Vectors are able to protect the microRNA for a limited time[599][600]. In the case of microRNA incorporation in the material bulk, the microRNA-vector complexes would be attacked by nucleases only when GL above them is degraded, i.e. days later depending on the complexes' position within the fibers. *Zhou et al.* incorporated the microRNA in the scaffold material, obtaining a sustained release for 56 days. The EC-covered scaffold surface was double in the microRNA-functionalized scaffold compared with the non-microRNA-functionalized one at 8 weeks [377].

Cell detachment from scaffolds is a non-standardized task; instead, it needs to be optimized according to the specific scaffold and cell type in use. To find a detachment protocol that yielded

enough cells for RT-qPCR analysis of RNA, I tested different dislodging agents and found that TrypLE combined with a pre-incubation with EDTA gave the best result. Pre-incubation with EDTA has the role of chelate Ca^{2+} and Mg^{2+} which are essential for cell adhesion. Since a porous electrospun scaffold can absorb relevant amounts of them, EDTA pre-incubation facilitated the duty of the dislodging enzymes. For every three replicates, 30 ng of RNA/µL was extracted, which was sufficient for RT-PCR analysis. From my experience with cellularized scaffolds, it is a fair amount. Obviously, it is possible to increment the extracted RNA using a larger scaffold, but I had to consider that microRNA-functionalized scaffolds are quite expensive, and I preferred to preserve my resources to repeat the experiment if needed.

In this work, the microRNA embedded in the scaffold (cel-miR-39-3p) was found on HAoECs cells 3 and 6 days after seeding. A longer cell incubation was not possible due to time limitations, but microRNA release data suggest that transfection could carry on for several more days. I observed microRNA release for up to 18 days in my release study. The release curve was far from linear. There was an initial burst of some 40% in the first three days. This may be an indication that a large part of microRNA was located on the surface or nearby it. Noteworthy, cells were cultured in standard culture media during the whole culture time. That means that cells underwent a prolonged microRNA transfection without perturbation of their environment. Typical transfection stresses, such as frequent media changes and lack of essential nutrients because of reduced serum media needed during transfection were avoided. Also, it is possible to study the effects of prolonged microRNA administration using this platform. A lipofectamine-functionalized scaffold has been already proposed. *Chin et al.* developed a PCL electrospun scaffold with lipofectamine-based complexes adsorbed on the surface achieving transfection [601]. Similarly, *Chooi et al.* produced their scaffold with Lipofectamine-siRNA adsorbed on the surface, reaching higher cell differentiation compared with the control [602].

6 Study limitations and future prospective

This project was focused on the design of a microRNA-functionalized scaffold for aortic valve regeneration.

As a general consideration, I must acknowledge that the number of replicates in each experiment was low. This was due to the complexity of the project which determined a constant struggle against time from the beginning. The idea was to add repetitions once a good part of the project would have been completed within an acceptable time. Unfortunately, this never happened, thus I limited the experimental replicates in the effort to complete the project. However, this is definitely one of the weakest points of this project that should be mended in the future.

The first study's problem arose with the difficulties found in selecting a proper vector for the application. Chitosan-NPs were supposed to be the vector of choice thanks to their biocompatibility, transfection efficacy, and water-insolubility. The latter specification is connected to the scaffold fabrication, which needed vector-microRNA complexes that do not dissolve in water solution. From the safety point of view, chitosan fulfilled the requirements. However, the chitosan loading efficiency was low, and, eventually, it was not able to transfect microRNA to HAoECs. My inexperience in non-viral vector production may have been the cause of the negative transfection outcomes with vectors approved in the literature. The search for a suitable transfection vector slowed down the whole project. After the tests I conducted, only the Lipofectamine turned out to be acceptable, as it was the only one able to allow the microRNA to regulate its target genes. Lipofectamine has been employed for scaffold functionalization in a few publications [601] [602]. So far, it is deemed too toxic for clinical application, and lipofectamine's commercial price is so high that may shy off scientists focused on the development of scaffolds with RNA interference ability. The reduction of economic costs is also essential for the healthcare system. Thus, the use of cheaper vectors is important for the transition of such a product to clinical application. There is intense research on lipid-based non-viral vectors. In futures developments, the test of non-patented liposome formulations may represent a valid solution. Positively charged phospholipids are extensively employed in experimental formulations of liposomes as they can hold genetic material by electrostatic attraction. Also, their charge and lipid nature facilitate the plasma membrane crossing [603]. However, the release of microRNA in the cytoplasm may be hampered due to the difficulty to overcome the lipid-RNA electrostatic attraction. For this reason, positively charged phospholipids are usually combined with ionizable lipids. These compounds help the formation

of microRNA-lipid complexes as they are positively charged at acidic pH. Their overall charge becomes neutral at physiological pH, facilitating the microRNA release and action [604]. Interesting results have been achieved on the use of these materials as non-viral vectors, and they may be suitable for integration in the scaffold designed in this project. Obviously, the employment of non-ready-to-use vectors will require appropriate chemical expertise. Moreover, the vector could be designed to target ECs, using specific antigens for instance. Poly(lactide-co-glycolide)-based and lipid-based vectors can be modified and shown to acquire target specificity. For instance, vectors functionalized with the REDV peptides are almost exclusively uptaken by ECs [484][273], [605].

After a few problems with the scaffold design, I found a good solution to create a material with theoretically good mechanical properties and the ability to administer microRNA. However, I was not able to perform mechanical tests to verify that the construct mechanical properties are similar to the native-valve ones. I can only rely on published data that show that similar scaffolds have suitable mechanical properties [591][593]. Single and biaxial tensile tests, and durability tests must be done to provide a mechanical characterization of the scaffold [606]. The use of pulse duplicators and high-frequency durability test machines will be a mandatory step for the development of this product. If the PCL/GL layer will not provide the scaffold with the mechanical requirements, blends with other materials could be explored. PGS, collagen, and PLLA are some of the materials used to blend with PCL for scaffold fabrication [607]–[609]. Otherwise, PCL could be substituted with materials with superior performances, such as polyurethanes (PU and PEUU), which have already proven to possess good mechanical properties and resistance to cyclic stress [610]–[613].

It is important to verify if hsa-mir-132-3p incorporated in the scaffold can downregulate the selected genes and enhance cell proliferation as shown after a common transfection on a cell monolayer. This is perhaps the most important test to demonstrate the feasibility of this proof of concept. This test should be done on cells cultured on the scaffold in static and dynamic conditions. Dynamic culture testing in a bioreactor is important to understand if cells could be transfected by the microRNA-functionalized scaffold in an environment where the vector-microRNA complexes are washed away as soon as they completely detach from the scaffold.

Other microRNAs have been shown to stimulate ECs' proliferation, such as microRNA-126 [377]. They could substitute hsa-mir-132-3p or be combined with it in an effort to speed up the endothelialization of the scaffold. The addition of VEGF may multiply the effect of microRNA-132 transfection [614].

The microRNA release study suggested that a large part of microRNA-vector complexes were on the GL fibers' surface or close to it. A study on the complexes distribution within the GL fibers should be carried out. Specific expertise on how to image the bulk of a single fiber should be sought beforehand. If the complexes distribution within the fibers required to be correct, coaxial electrospinning may represent the solution. Coaxial electrospinning allows the creation of nanofibers out of a fluid stream that is constituted by 2, 3, or even 4 separated solutions arranged in a coaxial fashion. Determined aliquots of microRNA would be confined in each fiber's layer. The microRNA release dynamic could be modified by allocating fractions of the total embedded microRNA closer or farther from the fibers' surface.

Whether in the construct developed in this project or as a coating of an already existing valve prosthesis (e.g. bioprostheses), functionalization with microRNA may help construct endothelialization speed and outcome, minimizing the risk of degenerative immune reactions and thromboembolism. Therefore, the possibility of coating valves currently employed in medical practice with a microRNA-functionalized GL layer should be explored.

In-vivo experiments in animal models would be important to observe the construct evolution, potential degeneration, and if microRNA functionalization increases the speed and outcome of the scaffold endothelialization. Leaflet thickening and degeneration are common issues in tissue-engineered valves and bioprostheses. Hence, *in-vivo* experiments should investigate if this construct is subjected to them as well. If so, the scaffold functionalization could be enriched and modified by combining different microRNA, siRNA, and growth factors. The functionalization could be layered to stimulate the formation of an EC lining on the surface, and the development of a VIC population in the scaffold bulk. Through the stimulation of the endothelial-to-mesenchymal transition with biochemical cues, like transforming growth factor-β [615], ECs and endothelial progenitor cells could acquire the VIC phenotype. The interstitial cells would develop a proper valvular microstructure and will maintain it. Also, the scaffold composition can be modified to avoid degeneration since it was shown that the VICs' phenotype is influenced by the matrix properties, e.g. the stiffness [616][617].

7   Conclusive remarks

This study aimed to create a tissue engineering-inspired solution for aortic valve regeneration since the current solutions are flawed. MicroRNA characteristics, such as transient transfection and the ability to influence theoretically all aspects of cell function make it ideal for regenerative medicine applications. Non-viral vectors have cargo capacity that allows them to carry high amounts of combinations of microRNA, growth factors, and drug molecules. Moreover, they can be limited to a specific body district and they can be functionalized to target specific receptors. Scaffolds for regenerative medicine are biodegradable constructs implanted in the target location, it can bear therapeutic molecules while supporting regeneration. These three elements could join to create the next generation of regenerative supports. In this project, I focused on the creation of a microRNA-functionalized scaffold able to stimulate the formation of an endothelial lining. Several unexpected obstacles prevented me to arrive where I programmed. The vector is not ideal to be integrated into this application, the scaffold's mechanical properties were not tested, and the scaffold's ability to stimulate endothelialization was not tested either. However, the feasibility of the product had an initial demonstration with the sustained transfection of microRNA to colonizing cells for up to 6 days. The scaffold's coating layer degradation releases the microRNA as expected and seeded cells picked it up. Longer studies in static and dynamic culture are required to establish the maximum duration of the microRNA administration, the effect on the scaffold endothelialization, and the scaffold's ability to maintain the required mechanical properties. The recently published studies confirmed the advantages that this type of regenerative support may provide compared to a passive scaffold. The product presents a high degree of complexity; different requirements and constraints intersect in a single device. Therefore, the future development and validation of this construct will require more work from a large team of collaborators with different expertise. However, the feasibility of this approach could open a new line of research consisting of the use of RNA interference in a local and sustained fashion as a potential tool to go beyond the limits of current therapeutical approaches.

8 References

[1]   R. J. Milne, D. Lennon, J. M. Stewart, S. vander Hoorn, and P. A. Scuffham, "Mortality and hospitalisation costs of rheumatic fever and rheumatic heart disease in New Zealand," *Journal of Paediatrics and Child Health*, vol. 48, no. 8, pp. 692–697, Aug. 2012, doi: 10.1111/j.1440-1754.2012.02446.x.

[2]   S. Coffey, B. J. Cairns, and B. Iung, "The modern epidemiology of heart valve disease," *Heart*, vol. 102, no. 1, pp. 75–85, Jan. 2016, doi: 10.1136/heartjnl-2014-307020.

[3]   R. A. Nishimura *et al.*, "2017 AHA/ACC Focused Update of the 2014 AHA/ACC Guideline for the Management of Patients With Valvular Heart Disease: A Report of the American College of Cardiology/American Heart Association Task Force on Clinical Practice Guidelines," *Circulation*, vol. 135, no. 25, Jun. 2017, doi: 10.1161/CIR.0000000000000503.

[4]   M. Andrejak and C. Tribouilloy, "Drug-induced valvular heart disease: An update," *Archives of Cardiovascular Diseases*, vol. 106, no. 5, pp. 333–339, May 2013, doi: 10.1016/j.acvd.2013.02.003.

[5]   *Principles of Heart Valve Engineering*. Elsevier, 2019. doi: 10.1016/C2017-0-00983-7.

[6]   C. Bonow and R. Otto, *Valvular Heart Disease: A Companion to Braunwald's Heart Disease 5th Edition*. Elsevier, 2020.

[7]   P. G. Supino, J. S. Borer, J. Preibisz, and A. Bornstein, "The Epidemiology of Valvular Heart Disease: a Growing Public Health Problem," *Heart Failure Clinics*, vol. 2, no. 4, pp. 379–393, Oct. 2006, doi: 10.1016/j.hfc.2006.09.010.

[8]   "Underlying Cause of Death 1999-2017 on CDC WONDER Online Database," 2018.

[9]   A. Marciniak, K. Glover, and R. Sharma, "Cohort profile: prevalence of valvular heart disease in community patients with suspected heart failure in UK," *BMJ Open*, vol. 7, no. 1, p. e012240, Jan. 2017, doi: 10.1136/bmjopen-2016-012240.

[10]   J. L. d'Arcy *et al.*, "Large-scale community echocardiographic screening reveals a major burden of undiagnosed valvular heart disease in older people: the OxVALVE Population Cohort Study," *European Heart Journal*, vol. 37, no. 47, pp. 3515–3522, Dec. 2016, doi: 10.1093/eurheartj/ehw229.

[11]   M. Lindroos, M. Kupari, J. Heikkilä, and R. Tilvis, "Prevalence of aortic valve abnormalities in the elderly: An echocardiographic study of a random population sample," *J Am Coll Cardiol*, vol. 21, no. 5, pp. 1220–1225, Apr. 1993, doi: 10.1016/0735-1097(93)90249-Z.

[12]   E. Jover, M. Fagnano, G. Angelini, and P. Madeddu, "Cell Sources for Tissue Engineering Strategies to Treat Calcific Valve Disease," *Frontiers in Cardiovascular Medicine*, vol. 5, Nov. 2018, doi: 10.3389/fcvm.2018.00155.

[13]   J. Leal, R. Luengo-Fernández, A. Gray, S. Petersen, and M. Rayner, "Economic burden of cardiovascular diseases in the enlarged European Union," *European Heart Journal*, vol. 27, no. 13, pp. 1610–1619, Jul. 2006, doi: 10.1093/eurheartj/ehi733.

[14]   "Estimating Expenditure by Disease, Age and Gender." [Online]. Available: https://www.oecd.org/els/health-systems/estimating-expenditure-by-disease-age-and-gender.htm

[15]   I. Ben-Dor *et al.*, "Correlates and Causes of Death in Patients With Severe Symptomatic Aortic Stenosis Who Are Not Eligible to Participate in a Clinical Trial of Transcatheter Aortic Valve Implantation," *Circulation*, vol. 122, no. 11_suppl_1, pp. S37–S42, Sep. 2010, doi: 10.1161/CIRCULATIONAHA.109.926873.

[16]   J. TURINA, O. HESS, F. SEPULCRI, and H. P. KRAYENBUEHL, "Spontaneous course of aortic valve disease," *European Heart Journal*, vol. 8, no. 5, pp. 471–483, May 1987, doi: 10.1093/oxfordjournals.eurheartj.a062307.

[17]   M. B. Leon *et al.*, "Transcatheter Aortic-Valve Implantation for Aortic Stenosis in Patients Who Cannot Undergo Surgery," *New England Journal of Medicine*, vol. 363, no. 17, pp. 1597–1607, Oct. 2010, doi: 10.1056/NEJMoa1008232.

[18]   K. S. Dujardin, M. Enriquez-Sarano, H. v. Schaff, K. R. Bailey, J. B. Seward, and A. J. Tajik, "Mortality and Morbidity of Aortic Regurgitation in Clinical Practice," *Circulation*, vol. 99, no. 14, pp. 1851–1857, Apr. 1999, doi: 10.1161/01.CIR.99.14.1851.

[19]   R. B. Singer, "Comparative mortality in medically treated aortic regurgitation.," *J Insur Med*, vol. 36, no. 1, pp. 10–5, 2004, [Online]. Available: http://www.ncbi.nlm.nih.gov/pubmed/15104025

[20]   J. A. Barreto-Filho *et al.*, "Trends in Aortic Valve Replacement for Elderly Patients in the United States, 1999-2011," *JAMA*, vol. 310, no. 19, p. 2078, Nov. 2013, doi: 10.1001/jama.2013.282437.

[21]   C. M. Otto *et al.*, "2020 ACC/AHA Guideline for the Management of Patients With Valvular Heart Disease: A Report of the American College of Cardiology/American Heart Association Joint Committee on Clinical Practice Guidelines," *Circulation*, vol. 143, no. 5, Feb. 2021, doi: 10.1161/CIR.0000000000000923.

[22]   L. Gaede *et al.*, "Trends in aortic valve replacement in Germany in 2015: transcatheter versus isolated surgical aortic valve repair," *Clinical Research in Cardiology*, vol. 106, no. 6, pp. 411–419, Jun. 2017, doi: 10.1007/s00392-016-1070-1.

[23]   "Heart and Circulatory Disease Statistics 2020," 2020.

[24]   G. H. Bevan, D. A. Zidar, R. A. Josephson, and S. G. Al-Kindi, "Mortality Due to Aortic Stenosis in the United States, 2008-2017," *JAMA*, vol. 321, no. 22, p. 2236, Jun. 2019, doi: 10.1001/jama.2019.6292.

[25]   "Surgical replacement of aortic valves offers good long-term survival," May 2017. doi: 10.3310/signal-000418.

[26]   N. Glaser, M. Persson, V. Jackson, M. J. Holzmann, A. Franco-Cereceda, and U. Sartipy, "Loss in Life Expectancy After Surgical Aortic Valve Replacement," *J Am Coll Cardiol*, vol. 74, no. 1, pp. 26–33, Jul. 2019, doi: 10.1016/j.jacc.2019.04.053.

[27]   D. Hernandez-Vaquero *et al.*, "Life expectancy of patients undergoing surgical aortic valve replacement compared with that of the general population," *Interactive CardioVascular and Thoracic Surgery*, vol. 30, no. 3, pp. 394–399, Mar. 2020, doi: 10.1093/icvts/ivz268.

[28]   M. T. A. Sharabiani, F. Fiorentino, G. D. Angelini, and N. N. Patel, "Long-term survival after surgical aortic valve replacement among patients over 65 years of age," *Open Heart*, vol. 3, no. 1, p. e000338, Mar. 2016, doi: 10.1136/openhrt-2015-000338.

[29]   E. S. Fioretta, P. E. Dijkman, M. Y. Emmert, and S. P. Hoerstrup, "The future of heart valve replacement: recent developments and translational challenges for heart valve tissue engineering," *Journal of Tissue Engineering and Regenerative Medicine*, vol. 12, no. 1, pp. e323–e335, Jan. 2018, doi: 10.1002/term.2326.

[30]   C. A. HUFNAGEL and W. P. HARVEY, "The surgical correction of aortic regurgitation preliminary report.," *Bull Georgetown Univ Med Cent*, vol. 6, no. 3, pp. 60–1, Jan. 1953, [Online]. Available: http://www.ncbi.nlm.nih.gov/pubmed/12997885

[31]   O. L. Gödje, T. Fischlein, K. Adelhard, G. Nollert, W. Klinner, and B. Reichart, "Thirty-Year Results of Starr-Edwards Prostheses in the Aortic and Mitral Position," *The Annals of Thoracic Surgery*, vol. 63, no. 3, pp. 613–619, Mar. 1997, doi: 10.1016/S0003-4975(96)00945-9.

[32]   P. Saxena, C. R. Bonnichsen, and K. L. Greason, "Starr–Edwards aortic valve: Forty-four years old and still working!," *The Journal of Thoracic and Cardiovascular Surgery*, vol. 146, no. 4, pp. e21–e22, Oct. 2013, doi: 10.1016/j.jtcvs.2013.05.034.

[33]   M. Amrane, G. Soulat, A. Carpentier, and J. Jouan, "Starr–Edwards aortic valve: 50+ years and still going strong: a case report," *European Heart Journal - Case Reports*, vol. 1, no. 2, Dec. 2017, doi: 10.1093/ehjcr/ytx014.

[34]   D. Bouchard *et al.*, "Twenty-Year Experience With the CarboMedics Mechanical Valve Prosthesis," *The Annals of Thoracic Surgery*, vol. 97, no. 3, pp. 816–823, Mar. 2014, doi: 10.1016/j.athoracsur.2013.09.098.

[35]   T. Suezawa, T. Morimoto, T. Jinno, and M. Tago, "Forty-Year Survival With Smeloff-Cutter and Starr-Edwards Prostheses," *The Annals of Thoracic Surgery*, vol. 85, no. 3, pp. e14–e16, Mar. 2008, doi: 10.1016/j.athoracsur.2007.12.007.

[36]   G. J. van Nooten *et al.*, "Twenty-Year Single-Center Experience With the Medtronic Open Pivot Mechanical Heart Valve," *The Annals of Thoracic Surgery*, vol. 97, no. 4, pp. 1306–1313, Apr. 2014, doi: 10.1016/j.athoracsur.2013.11.035.

[37]   M. D. Silver and G. J. Wilson, "The pathology of wear in the Beall model 104 heart valve prosthesis.," *Circulation*, vol. 56, no. 4, pp. 617–622, Oct. 1977, doi: 10.1161/01.CIR.56.4.617.

[38]   L. F. Hiratzka, N. T. Kouchoukos, G. L. Grunkemeier, D. C. Miller, H. E. Scully, and A. S. Wechsler, "Outlet strut fracture of the Björk-Shiley 60 ° Convexo-Concave valve: Current information and recommendations for patient care," *J Am Coll Cardiol*, vol. 11, no. 5, pp. 1130–1137, May 1988, doi: 10.1016/S0735-1097(98)90075-4.

[39]   D. Bouchard *et al.*, "Twenty-Year Experience With the CarboMedics Mechanical Valve Prosthesis," *The Annals of Thoracic Surgery*, vol. 97, no. 3, pp. 816–823, Mar. 2014, doi: 10.1016/j.athoracsur.2013.09.098.

[40]   G. J. van Nooten *et al.*, "Twenty-Year Single-Center Experience With the Medtronic Open Pivot Mechanical Heart Valve," *The Annals of Thoracic Surgery*, vol. 97, no. 4, pp. 1306–1313, Apr. 2014, doi: 10.1016/j.athoracsur.2013.11.035.

[41]   R. W. Emery *et al.*, "The St. Jude Medical Cardiac Valve Prosthesis: A 25-Year Experience With Single Valve Replacement," *The Annals of Thoracic Surgery*, vol. 79, no. 3, pp. 776–782, Mar. 2005, doi: 10.1016/j.athoracsur.2004.08.047.

[42]   S. MacIsaac, I. H. Jaffer, E. P. Belley-Côté, G. R. McClure, J. W. Eikelboom, and R. P. Whitlock, "How Did We Get Here?: A Historical Review and Critical Analysis of Anticoagulation Therapy Following Mechanical Valve Replacement," *Circulation*, vol. 140, no. 23, pp. 1933–1942, Dec. 2019, doi: 10.1161/CIRCULATIONAHA.119.041105.

[43] J. Hirsh, V. Fuster, J. Ansell, and J. L. Halperin, "American Heart Association/American College of Cardiology Foundation Guide to Warfarin Therapy," *Circulation*, vol. 107, no. 12, pp. 1692–1711, Apr. 2003, doi: 10.1161/01.CIR.0000063575.17904.4E.

[44] R. Tadros and S. Shakib, "Warfarin--indications, risks and drug interactions.," *Aust Fam Physician*, vol. 39, no. 7, pp. 476–9, Jul. 2010, [Online]. Available: http://www.ncbi.nlm.nih.gov/pubmed/20628660

[45] A. D. Waterman, P. E. Milligan, L. Bayer, G. A. Banet, S. K. Gatchel, and B. F. Gage, "Effect of warfarin nonadherence on control of the International Normalized Ratio," *American Journal of Health-System Pharmacy*, vol. 61, no. 12, pp. 1258–1264, Jun. 2004, doi: 10.1093/ajhp/61.12.1258.

[46] R. C. Wiggins, B. N. Bouma, C. G. Cochrane, and J. H. Griffin, "Role of high-molecular-weight kininogen in surface-binding and activation of coagulation Factor XI and prekallikrein.," *Proceedings of the National Academy of Sciences*, vol. 74, no. 10, pp. 4636–4640, Oct. 1977, doi: 10.1073/pnas.74.10.4636.

[47] M. B. Gorbet and M. v. Sefton, "Biomaterial-associated thrombosis: roles of coagulation factors, complement, platelets and leukocytes," *Biomaterials*, vol. 25, no. 26, pp. 5681–5703, Nov. 2004, doi: 10.1016/j.biomaterials.2004.01.023.

[48] T. A. Horbett, "Chapter 13 Principles underlying the role of adsorbed plasma proteins in blood interactions with foreign materials," *Cardiovascular Pathology*, vol. 2, no. 3, pp. 137–148, Jul. 1993, doi: 10.1016/1054-8807(93)90054-6.

[49] R. Roudaut, K. Serri, and S. Lafitte, "Thrombosis of prosthetic heart valves: diagnosis and therapeutic considerations," *Heart*, vol. 93, no. 1, pp. 137–142, Jan. 2007, doi: 10.1136/hrt.2005.071183.

[50] V. L. Gott and R. L. Daggett, "Serendipity and the development of heparin and carbon surfaces," *The Annals of Thoracic Surgery*, vol. 68, no. 3, pp. S19–S22, Sep. 1999, doi: 10.1016/S0003-4975(99)00817-6.

[51] F. Oveissi, S. Naficy, A. Lee, D. S. Winlaw, and F. Dehghani, "Materials and manufacturing perspectives in engineering heart valves: a review," *Materials Today Bio*, vol. 5, p. 100038, Jan. 2020, doi: 10.1016/j.mtbio.2019.100038.

[52] S. Forti *et al.*, "Hemocompatibility of pyrolytic carbon in comparison with other biomaterials," *Diamond and Related Materials*, vol. 20, no. 5–6, pp. 762–769, May 2011, doi: 10.1016/j.diamond.2011.03.026.

[53] M. S. Slaughter, B. Pederson, J. D. Graham, M. A. Sobieski, and S. C. Koenig, "Evaluation of new Forcefield technology: Reducing platelet adhesion and cell coverage of pyrolytic

carbon surfaces," *The Journal of Thoracic and Cardiovascular Surgery*, vol. 142, no. 4, pp. 921–925, Oct. 2011, doi: 10.1016/j.jtcvs.2011.01.012.

[54]   S. J. Phillips, "Thrombogenic Influence of Biomaterials in Patients with the Omni Series Heart Valve: Pyrolytic Carbon Versus Titanium," *ASAIO Journal*, vol. 47, no. 5, pp. 429–431, Sep. 2001, doi: 10.1097/00002480-200109000-00002.

[55]   W. R. E. Jamieson, "St Jude Medical Trifecta aortic prosthesis: Considerations for implantation," *The Journal of Thoracic and Cardiovascular Surgery*, vol. 149, no. 6, pp. 1576–1577, Jun. 2015, doi: 10.1016/j.jtcvs.2015.03.034.

[56]   S. Gelsomino, R. Frassani, L. Porreca, G. Morocutti, A. Morelli, and U. Livi, "Early and midterm results of model 300 CryoLife O'Brien stentless porcine aortic bioprosthesis," *The Annals of Thoracic Surgery*, vol. 71, no. 5, pp. S297–S301, May 2001, doi: 10.1016/S0003-4975(01)02526-7.

[57]   R. Tavakoli *et al.*, "Biological aortic valve replacement: advantages and optimal indications of stentless compared to stented valve substitutes. A review," *General Thoracic and Cardiovascular Surgery*, vol. 66, no. 5, pp. 247–256, May 2018, doi: 10.1007/s11748-018-0884-3.

[58]   T. Sénage *et al.*, "Early Structural Valve Deterioration of Mitroflow Aortic Bioprosthesis," *Circulation*, vol. 130, no. 23, pp. 2012–2020, Dec. 2014, doi: 10.1161/CIRCULATIONAHA.114.010400.

[59]   J. F. Obermiller, J. P. Hodde, C. S. McAlexander, K. Kokini, and S. F. Badylak, "A comparison of suture retention strengths for three biomaterials.," *Med Sci Monit*, vol. 10, no. 1, pp. PI1-5, Jan. 2004, [Online]. Available: http://www.ncbi.nlm.nih.gov/pubmed/14704643

[60]   R. Tavakoli *et al.*, "Biological aortic valve replacement: advantages and optimal indications of stentless compared to stented valve substitutes. A review," *General Thoracic and Cardiovascular Surgery*, vol. 66, no. 5, pp. 247–256, May 2018, doi: 10.1007/s11748-018-0884-3.

[61]   J. A. Funder *et al.*, "Aortic root distensibility and cross-sectional areas in stented and subcoronary stentless bioprostheses in pigs☆," *Interactive CardioVascular and Thoracic Surgery*, vol. 10, no. 6, pp. 976–980, Jun. 2010, doi: 10.1510/icvts.2009.230771.

[62]   S. J. Head, M. Çelik, and A. P. Kappetein, "Mechanical versus bioprosthetic aortic valve replacement," *European Heart Journal*, vol. 38, no. 28, pp. 2183–2191, Jul. 2017, doi: 10.1093/eurheartj/ehx141.

[63]   S. H. Rahimtoola, "Choice of Prosthetic Heart Valve in Adults," *J Am Coll Cardiol*, vol. 55, no. 22, pp. 2413–2426, Jun. 2010, doi: 10.1016/j.jacc.2009.10.085.

[64] M. W. A. van Geldorp *et al.*, "Patient outcome after aortic valve replacement with a mechanical or biological prosthesis: Weighing lifetime anticoagulant-related event risk against reoperation risk," *The Journal of Thoracic and Cardiovascular Surgery*, vol. 137, no. 4, pp. 881-886.e5, Apr. 2009, doi: 10.1016/j.jtcvs.2008.09.028.

[65] L. Ran, W. Wang, F. Secchi, Y. Xiang, W. Shi, and W. Huang, "Percutaneous pulmonary valve implantation in patients with right ventricular outflow tract dysfunction: a systematic review and meta-analysis," *Therapeutic Advances in Chronic Disease*, vol. 10, p. 204062231985763, Jan. 2019, doi: 10.1177/2040622319857635.

[66] P. Pibarot and J. G. Dumesnil, "Prosthetic Heart Valves," *Circulation*, vol. 119, no. 7, pp. 1034–1048, Feb. 2009, doi: 10.1161/CIRCULATIONAHA.108.778886.

[67] Tillquist, Tillquist, and T. Maddox, "Cardiac crossroads: deciding between mechanical or bioprosthetic heart valve replacement," *Patient Preference and Adherence*, p. 91, Feb. 2011, doi: 10.2147/PPA.S16420.

[68] R. Philip, T. K. S. Kumar, B. R. Waller, M. McCoy, and C. J. Knott-Craig, "Near Catastrophic Accelerated Structural Degeneration of the Perimount Magna Pericardial Bioprosthesis in Children," *The Annals of Thoracic Surgery*, vol. 102, no. 1, pp. 308–311, Jul. 2016, doi: 10.1016/j.athoracsur.2015.09.088.

[69] R. A. Manji, A. H. Menkis, B. Ekser, and D. K. C. Cooper, "Porcine bioprosthetic heart valves: The next generation," *American Heart Journal*, vol. 164, no. 2, pp. 177–185, Aug. 2012, doi: 10.1016/j.ahj.2012.05.011.

[70] S. F. Saleeb *et al.*, "Accelerated Degeneration of a Bovine Pericardial Bioprosthetic Aortic Valve in Children and Young Adults," *Circulation*, vol. 130, no. 1, pp. 51–60, Jul. 2014, doi: 10.1161/CIRCULATIONAHA.114.009835.

[71] G. Golomb, F. J. Schoen, M. S. Smith, J. Linden, M. Dixon, and R. J. Levy, "The role of glutaraldehyde-induced cross-links in calcification of bovine pericardium used in cardiac valve bioprostheses.," *Am J Pathol*, vol. 127, no. 1, pp. 122–30, Apr. 1987, [Online]. Available: http://www.ncbi.nlm.nih.gov/pubmed/3105321

[72] D. Zhu, L. Jin, X. Wang, L. Xu, and T. Liu, "Combined anticalcification treatment of bovine pericardium with decellularization and hyaluronic acid derivative," *Bio-Medical Materials and Engineering*, vol. 24, no. 1, pp. 741–749, 2014, doi: 10.3233/BME-130862.

[73] P. M. Taylor, P. Batten, N. J. Brand, P. S. Thomas, and M. H. Yacoub, "The cardiac valve interstitial cell," *The International Journal of Biochemistry & Cell Biology*, vol. 35, no. 2, pp. 113–118, Feb. 2003, doi: 10.1016/S1357-2725(02)00100-0.

[74] R. Shetty *et al.*, "Lipid-mediated inflammation and degeneration of bioprosthetic heart valves," *European Journal of Clinical Investigation*, vol. 39, no. 6, pp. 471–480, Jun. 2009, doi: 10.1111/j.1365-2362.2009.02132.x.

[75] P. K. Schaefermeier *et al.*, "Potential Cell Sources for Tissue Engineering of Heart Valves in Comparison With Human Pulmonary Valve Cells," *ASAIO Journal*, vol. 55, no. 1, pp. 86–92, Jan. 2009, doi: 10.1097/MAT.0b013e31818f54e4.

[76] E. S. Fioretta *et al.*, "Next-generation tissue-engineered heart valves with repair, remodelling and regeneration capacity," *Nature Reviews Cardiology*, vol. 18, no. 2, pp. 92–116, Feb. 2021, doi: 10.1038/s41569-020-0422-8.

[77] F. J. O'Brien, "Biomaterials & scaffolds for tissue engineering," *Materials Today*, vol. 14, no. 3, pp. 88–95, Mar. 2011, doi: 10.1016/S1369-7021(11)70058-X.

[78] W. J. Wells, H. Arroyo, R. M. Bremner, J. Wood, and V. A. Starnes, "Homograft conduit failure in infants is not due to somatic outgrowth," *The Journal of Thoracic and Cardiovascular Surgery*, vol. 124, no. 1, pp. 88–96, Jul. 2002, doi: 10.1067/mtc.2002.121158.

[79] A. Mookhoek *et al.*, "European multicenter experience with valve-sparing reoperations after the Ross procedure," *The Journal of Thoracic and Cardiovascular Surgery*, vol. 150, no. 5, pp. 1132–1137, Nov. 2015, doi: 10.1016/j.jtcvs.2015.08.043.

[80] E. Rabkin-Aikawa *et al.*, "Clinical pulmonary autograft valves: Pathologic evidence of adaptive remodeling in the aortic site," *The Journal of Thoracic and Cardiovascular Surgery*, vol. 128, no. 4, pp. 552–561, Oct. 2004, doi: 10.1016/j.jtcvs.2004.04.016.

[81] E. S. Fioretta, P. E. Dijkman, M. Y. Emmert, and S. P. Hoerstrup, "The future of heart valve replacement: recent developments and translational challenges for heart valve tissue engineering," *Journal of Tissue Engineering and Regenerative Medicine*, vol. 12, no. 1, pp. e323–e335, Jan. 2018, doi: 10.1002/term.2326.

[82] A. H. Chester and K. J. Grande-Allen, "Which Biological Properties of Heart Valves Are Relevant to Tissue Engineering?," *Frontiers in Cardiovascular Medicine*, vol. 7, Apr. 2020, doi: 10.3389/fcvm.2020.00063.

[83] M. H. Yacoub, P. J. Kilner, E. J. Birks, and M. Misfeld, "The aortic outflow and root: a tale of dynamism and crosstalk," *The Annals of Thoracic Surgery*, vol. 68, no. 3, pp. S37–S43, Sep. 1999, doi: 10.1016/S0003-4975(99)00745-6.

[84] C. S. Peskin and D. M. McQueen, "Mechanical equilibrium determines the fractal fiber architecture of aortic heart valve leaflets," *American Journal of Physiology-Heart and*

Circulatory Physiology, vol. 266, no. 1, pp. H319–H328, Jan. 1994, doi: 10.1152/ajpheart.1994.266.1.H319.

[85]   D. Simionescu, J. Chen, M. Jaeggli, B. Wang, and J. Liao, "Form Follows Function: Advances in Trilayered Structure Replication for Aortic Heart Valve Tissue Engineering," *Journal of Healthcare Engineering*, vol. 3, no. 2, pp. 179–202, Jun. 2012, doi: 10.1260/2040-2295.3.2.179.

[86]   J.-H. Chen and C. A. Simmons, "Cell–Matrix Interactions in the Pathobiology of Calcific Aortic Valve Disease," *Circulation Research*, vol. 108, no. 12, pp. 1510–1524, Jun. 2011, doi: 10.1161/CIRCRESAHA.110.234237.

[87]   J. Sohier, I. Carubelli, P. Sarathchandra, N. Latif, A. H. Chester, and M. H. Yacoub, "The potential of anisotropic matrices as substrate for heart valve engineering," *Biomaterials*, vol. 35, no. 6, pp. 1833–1844, Feb. 2014, doi: 10.1016/j.biomaterials.2013.10.061.

[88]   X. Zhang *et al.*, "Integrating valve-inspired design features into poly(ethylene glycol) hydrogel scaffolds for heart valve tissue engineering," *Acta Biomaterialia*, vol. 14, pp. 11–21, Mar. 2015, doi: 10.1016/j.actbio.2014.11.042.

[89]   H. Tseng *et al.*, "Anisotropic Poly(Ethylene Glycol)/Polycaprolactone Hydrogel–Fiber Composites for Heart Valve Tissue Engineering," *Tissue Engineering Part A*, vol. 20, no. 19–20, pp. 2634–2645, Oct. 2014, doi: 10.1089/ten.tea.2013.0397.

[90]   N. T. Saidy *et al.*, "Biologically Inspired Scaffolds for Heart Valve Tissue Engineering via Melt Electrowriting," *Small*, vol. 15, no. 24, p. 1900873, Jun. 2019, doi: 10.1002/smll.201900873.

[91]   S. Jana, B. J. Tefft, D. B. Spoon, and R. D. Simari, "Scaffolds for tissue engineering of cardiac valves," *Acta Biomaterialia*, vol. 10, no. 7, pp. 2877–2893, Jul. 2014, doi: 10.1016/j.actbio.2014.03.014.

[92]   A. Rutkovskiy *et al.*, "Valve Interstitial Cells: The Key to Understanding the Pathophysiology of Heart Valve Calcification," *J Am Heart Assoc*, vol. 6, no. 9, Sep. 2017, doi: 10.1161/JAHA.117.006339.

[93]   I. El-Hamamsy *et al.*, "Endothelium-Dependent Regulation of the Mechanical Properties of Aortic Valve Cusps," *J Am Coll Cardiol*, vol. 53, no. 16, pp. 1448–1455, Apr. 2009, doi: 10.1016/j.jacc.2008.11.056.

[94]   A. H. Chester, I. El-Hamamsy, J. T. Butcher, N. Latif, S. Bertazzo, and M. H. Yacoub, "The living aortic valve: From molecules to function," *Global Cardiology Science and Practice*, vol. 2014, no. 1, p. 11, Jan. 2014, doi: 10.5339/gcsp.2014.11.

[95] D. Bourboulia and W. G. Stetler-Stevenson, "Matrix metalloproteinases (MMPs) and tissue inhibitors of metalloproteinases (TIMPs): Positive and negative regulators in tumor cell adhesion," *Seminars in Cancer Biology*, vol. 20, no. 3, pp. 161–168, Jun. 2010, doi: 10.1016/j.semcancer.2010.05.002.

[96] O. Fondard *et al.*, "Extracellular matrix remodelling in human aortic valve disease: the role of matrix metalloproteinases and their tissue inhibitors," *European Heart Journal*, vol. 26, no. 13, pp. 1333–1341, Jul. 2005, doi: 10.1093/eurheartj/ehi248.

[97] S. R. van Doren, "Matrix metalloproteinase interactions with collagen and elastin," *Matrix Biology*, vol. 44–46, pp. 224–231, May 2015, doi: 10.1016/j.matbio.2015.01.005.

[98] A. H. Chester and P. M. Taylor, "Molecular and functional characteristics of heart-valve interstitial cells," *Philosophical Transactions of the Royal Society B: Biological Sciences*, vol. 362, no. 1484, pp. 1437–1443, Aug. 2007, doi: 10.1098/rstb.2007.2126.

[99] E. Rabkin, M. Aikawa, J. R. Stone, Y. Fukumoto, P. Libby, and F. J. Schoen, "Activated Interstitial Myofibroblasts Express Catabolic Enzymes and Mediate Matrix Remodeling in Myxomatous Heart Valves," *Circulation*, vol. 104, no. 21, pp. 2525–2532, Nov. 2001, doi: 10.1161/hc4601.099489.

[100] N. J. Brand, A. Roy, G. Hoare, A. Chester, and M. H. Yacoub, "Cultured interstitial cells from human heart valves express both specific skeletal muscle and non-muscle markers," *The International Journal of Biochemistry & Cell Biology*, vol. 38, no. 1, pp. 30–42, Jan. 2006, doi: 10.1016/j.biocel.2005.06.018.

[101] A. C. Liu, V. R. Joag, and A. I. Gotlieb, "The Emerging Role of Valve Interstitial Cell Phenotypes in Regulating Heart Valve Pathobiology," *The American Journal of Pathology*, vol. 171, no. 5, pp. 1407–1418, Nov. 2007, doi: 10.2353/ajpath.2007.070251.

[102] J. Richards *et al.*, "Side-Specific Endothelial-Dependent Regulation of Aortic Valve Calcification," *The American Journal of Pathology*, vol. 182, no. 5, pp. 1922–1931, May 2013, doi: 10.1016/j.ajpath.2013.01.037.

[103] G. Pompilio *et al.*, "Endothelial-Dependent Dynamic and Antithrombotic Properties of Porcine Aortic and Pulmonary Valves," *The Annals of Thoracic Surgery*, vol. 65, no. 4, pp. 986–992, Apr. 1998, doi: 10.1016/S0003-4975(98)00075-7.

[104] M. W. Radomski, R. M. J. Palmer, and S. Moncada, "The anti-aggregating properties of vascular endothelium: interactions between prostacyclin and nitric oxide," *British Journal of Pharmacology*, vol. 92, no. 3, pp. 639–646, Nov. 1987, doi: 10.1111/j.1476-5381.1987.tb11367.x.

[105] C. M. Otto, J. Kuusisto, D. D. Reichenbach, A. M. Gown, and K. D. O'Brien, "Characterization of the early lesion of 'degenerative' valvular aortic stenosis. Histological and immunohistochemical studies.," *Circulation*, vol. 90, no. 2, pp. 844–853, Aug. 1994, doi: 10.1161/01.CIR.90.2.844.

[106] J. T. Butcher and R. M. Nerem, "Valvular Endothelial Cells Regulate the Phenotype of Interstitial Cells in Co-culture: Effects of Steady Shear Stress," *Tissue Engineering*, vol. 12, no. 4, pp. 905–915, Apr. 2006, doi: 10.1089/ten.2006.12.905.

[107] D. D. Ku, J. M. Nelson, J. B. Caulfield, and M. J. Winn, "Release of Endothelium-Derived Relaxing Factors from Canine Cardiac Valves," *Journal of Cardiovascular Pharmacology*, vol. 16, no. 2, pp. 212–218, Aug. 1990, doi: 10.1097/00005344-199008000-00006.

[108] E. S. Fioretta, L. von Boehmer, S. E. Motta, V. Lintas, S. P. Hoerstrup, and M. Y. Emmert, "Cardiovascular tissue engineering: From basic science to clinical application," *Experimental Gerontology*, no. March, pp. 0–1, 2018, doi: 10.1016/j.exger.2018.03.022.

[109] M. E. Tedder, A. Simionescu, J. Chen, J. Liao, and D. T. Simionescu, "Assembly and Testing of Stem Cell-Seeded Layered Collagen Constructs for Heart Valve Tissue Engineering," *Tissue Engineering Part A*, vol. 17, no. 1–2, pp. 25–36, Jan. 2011, doi: 10.1089/ten.tea.2010.0138.

[110] J. Mosier, N. Nguyen, K. Parker, and C. L. Simpson, "Calcification of Biomaterials and Diseased States," in *Biomaterials - Physics and Chemistry - New Edition*, InTech, 2018. doi: 10.5772/intechopen.71594.

[111] E. S. Fioretta, P. E. Dijkman, M. Y. Emmert, and S. P. Hoerstrup, "The future of heart valve replacement: recent developments and translational challenges for heart valve tissue engineering," *Journal of Tissue Engineering and Regenerative Medicine*, vol. 12, no. 1, pp. e323–e335, Jan. 2018, doi: 10.1002/term.2326.

[112] M. Yang, Y.-H. Lin, W.-P. Shi, H.-C. Shi, Y. J. Gu, and Y.-S. Shu, "Surface heparin treatment of the decellularized porcine heart valve: Effect on tissue calcification," *Journal of Biomedical Materials Research Part B: Applied Biomaterials*, vol. 105, no. 2, pp. 400–405, Feb. 2017, doi: 10.1002/jbm.b.33490.

[113] P. Aguiari *et al.*, "In vitro comparative assessment of decellularized bovine pericardial patches and commercial bioprosthetic heart valves," *Biomedical Materials*, vol. 12, no. 1, p. 015021, Feb. 2017, doi: 10.1088/1748-605X/aa5644.

[114] F. W. H. Sutherland *et al.*, "From Stem Cells to Viable Autologous Semilunar Heart Valve," *Circulation*, vol. 111, no. 21, pp. 2783–2791, May 2005, doi: 10.1161/CIRCULATIONAHA.104.498378.

[115] S. P. Hoerstrup *et al.*, "Functional Living Trileaflet Heart Valves Grown In Vitro," *Circulation*, vol. 102, no. Supplement 3, pp. III-44-III–49, Nov. 2000, doi: 10.1161/01.CIR.102.suppl_3.III-44.

[116] P. E. Dijkman, A. Driessen-Mol, L. Frese, S. P. Hoerstrup, and F. P. T. Baaijens, "Decellularized homologous tissue-engineered heart valves as off-the-shelf alternatives to xeno- and homografts," *Biomaterials*, vol. 33, no. 18, pp. 4545–4554, Jun. 2012, doi: 10.1016/j.biomaterials.2012.03.015.

[117] Z. H. Syedain, L. A. Meier, M. T. Lahti, S. L. Johnson, and R. T. Tranquillo, "Implantation of Completely Biological Engineered Grafts Following Decellularization into the Sheep Femoral Artery," *Tissue Engineering Part A*, vol. 20, no. 11–12, pp. 1726–1734, Jun. 2014, doi: 10.1089/ten.tea.2013.0550.

[118] V. Lintas *et al.*, "Development of a Novel Human Cell-Derived Tissue-Engineered Heart Valve for Transcatheter Aortic Valve Replacement: an In Vitro and In Vivo Feasibility Study," *Journal of Cardiovascular Translational Research*, vol. 11, no. 6, pp. 470–482, Dec. 2018, doi: 10.1007/s12265-018-9821-1.

[119] P. Poggio *et al.*, "Noggin attenuates the osteogenic activation of human valve interstitial cells in aortic valve sclerosis," *Cardiovascular Research*, vol. 98, no. 3, pp. 402–410, Jun. 2013, doi: 10.1093/cvr/cvt055.

[120] S. Jana, R. T. Tranquillo, and A. Lerman, "Cells for tissue engineering of cardiac valves," *Journal of Tissue Engineering and Regenerative Medicine*, vol. 10, no. 10, pp. 804–824, Oct. 2016, doi: 10.1002/term.2010.

[121] H. Okano *et al.*, "Steps Toward Safe Cell Therapy Using Induced Pluripotent Stem Cells," *Circulation Research*, vol. 112, no. 3, pp. 523–533, Feb. 2013, doi: 10.1161/CIRCRESAHA.111.256149.

[122] S.-S. Kim *et al.*, "Tissue Engineering of Heart Valves In Vivo Using Bone Marrow-derived Cells," *Artificial Organs*, vol. 30, no. 7, pp. 554–557, Jul. 2006, doi: 10.1111/j.1525-1594.2006.00258.x.

[123] G. C. Engelmayr, V. L. Sales, J. E. Mayer, and M. S. Sacks, "Cyclic flexure and laminar flow synergistically accelerate mesenchymal stem cell-mediated engineered tissue formation: Implications for engineered heart valve tissues," *Biomaterials*, vol. 27, no. 36, pp. 6083–6095, Dec. 2006, doi: 10.1016/j.biomaterials.2006.07.045.

[124] J. E. Jordan, J. K. Williams, S.-J. Lee, D. Raghavan, A. Atala, and J. J. Yoo, "Bioengineered self-seeding heart valves," *The Journal of Thoracic and Cardiovascular Surgery*, vol. 143, no. 1, pp. 201–208, Jan. 2012, doi: 10.1016/j.jtcvs.2011.10.005.

[125] J. Bischoff and E. Aikawa, "Progenitor Cells Confer Plasticity to Cardiac Valve Endothelium," *Journal of Cardiovascular Translational Research*, vol. 4, no. 6, pp. 710–719, Dec. 2011, doi: 10.1007/s12265-011-9312-0.

[126] A. Hilfiker, C. Kasper, R. Hass, and A. Haverich, "Mesenchymal stem cells and progenitor cells in connective tissue engineering and regenerative medicine: is there a future for transplantation?," *Langenbeck's Archives of Surgery*, vol. 396, no. 4, pp. 489–497, Apr. 2011, doi: 10.1007/s00423-011-0762-2.

[127] T. I. Croll *et al.*, "Modelling oxygen diffusion and cell growth in a porous, vascularising scaffold for soft tissue engineering applications," *Chemical Engineering Science*, vol. 60, no. 17, pp. 4924–4934, Sep. 2005, doi: 10.1016/j.ces.2005.03.051.

[128] E. Wernike, Z. Li, M. Alini, and S. Grad, "Effect of reduced oxygen tension and long-term mechanical stimulation on chondrocyte-polymer constructs.," *Cell Tissue Res*, vol. 331, no. 2, pp. 473–83, Feb. 2008, doi: 10.1007/s00441-007-0500-9.

[129] E. Volkmer *et al.*, "Hypoxia in Static and Dynamic 3D Culture Systems for Tissue Engineering of Bone," *Tissue Engineering Part A*, vol. 14, no. 8, pp. 1331–1340, Aug. 2008, doi: 10.1089/ten.tea.2007.0231.

[130] G. Aleksieva *et al.*, "Use of a special bioreactor for the cultivation of a new flexible polyurethane scaffold for aortic valve tissue engineering," *BioMedical Engineering OnLine*, vol. 11, no. 1, p. 92, 2012, doi: 10.1186/1475-925X-11-92.

[131] S. P. Hoerstrup *et al.*, "Tissue engineering of functional trileaflet heart valves from human marrow stromal cells.," *Circulation*, vol. 106, no. 12 Suppl 1, pp. I143-50, Sep. 2002, [Online]. Available: http://www.ncbi.nlm.nih.gov/pubmed/12354724

[132] D. Schmidt *et al.*, "Minimally-Invasive Implantation of Living Tissue Engineered Heart Valves," *J Am Coll Cardiol*, vol. 56, no. 6, pp. 510–520, Aug. 2010, doi: 10.1016/j.jacc.2010.04.024.

[133] G. C. Engelmayr, V. L. Sales, J. E. Mayer, and M. S. Sacks, "Cyclic flexure and laminar flow synergistically accelerate mesenchymal stem cell-mediated engineered tissue formation: Implications for engineered heart valve tissues," *Biomaterials*, vol. 27, no. 36, pp. 6083–6095, Dec. 2006, doi: 10.1016/j.biomaterials.2006.07.045.

[134] S. Ramaswamy *et al.*, "The role of organ level conditioning on the promotion of engineered heart valve tissue development in-vitro using mesenchymal stem cells," *Biomaterials*, vol. 31, no. 6, pp. 1114–1125, Feb. 2010, doi: 10.1016/j.biomaterials.2009.10.019.

[135] E. E. Buse, S. L. Hilbert, R. A. Hopkins, and G. L. Converse, "Pulse Duplicator Hydrodynamic Testing of Bioengineered Biological Heart Valves," *Cardiovascular Engineering and Technology*, vol. 7, no. 4, pp. 352–362, Dec. 2016, doi: 10.1007/s13239-016-0275-9.

[136] D. Schmidt *et al.*, "Prenatally Fabricated Autologous Human Living Heart Valves Based on Amniotic Fluid Derived Progenitor Cells as Single Cell Source," *Circulation*, vol. 116, no. 11_suppl, pp. I-64-I–70, Sep. 2007, doi: 10.1161/CIRCULATIONAHA.106.681494.

[137] P. E. Dijkman, A. Driessen-Mol, L. Frese, S. P. Hoerstrup, and F. P. T. Baaijens, "Decellularized homologous tissue-engineered heart valves as off-the-shelf alternatives to xeno- and homografts," *Biomaterials*, vol. 33, no. 18, pp. 4545–4554, Jun. 2012, doi: 10.1016/j.biomaterials.2012.03.015.

[138] T. C. Flanagan *et al.*, "In Vivo Remodeling and Structural Characterization of Fibrin-Based Tissue-Engineered Heart Valves in the Adult Sheep Model," *Tissue Engineering Part A*, vol. 15, no. 10, pp. 2965–2976, Oct. 2009, doi: 10.1089/ten.tea.2009.0018.

[139] Z. H. Syedain *et al.*, "Implantation of a Tissue-engineered Heart Valve from Human Fibroblasts Exhibiting Short Term Function in the Sheep Pulmonary Artery," *Cardiovascular Engineering and Technology*, vol. 2, no. 2, pp. 101–112, Jun. 2011, doi: 10.1007/s13239-011-0039-5.

[140] T. Mizutani, H. Haga, and K. Kawabata, "Cellular stiffness response to external deformation: tensional homeostasis in a single fibroblast.," *Cell Motil Cytoskeleton*, vol. 59, no. 4, pp. 242–8, Dec. 2004, doi: 10.1002/cm.20037.

[141] P. S. Robinson, S. L. Johnson, M. C. Evans, V. H. Barocas, and R. T. Tranquillo, "Functional tissue-engineered valves from cell-remodeled fibrin with commissural alignment of cell-produced collagen.," *Tissue Eng Part A*, vol. 14, no. 1, pp. 83–95, Jan. 2008, doi: 10.1089/ten.a.2007.0148.

[142] M. A. A. van Vlimmeren, A. Driessen-Mol, C. W. J. Oomens, and F. P. T. Baaijens, "An in vitro model system to quantify stress generation, compaction, and retraction in engineered heart valve tissue.," *Tissue Eng Part C Methods*, vol. 17, no. 10, pp. 983–91, Oct. 2011, doi: 10.1089/ten.TEC.2011.0070.

[143] B. Sanders *et al.*, "Improved Geometry of Decellularized Tissue Engineered Heart Valves to Prevent Leaflet Retraction," *Annals of Biomedical Engineering*, vol. 44, no. 4, pp. 1061–1071, Apr. 2016, doi: 10.1007/s10439-015-1386-4.

[144] M. A. A. van Vlimmeren, A. Driessen-Mol, C. W. J. Oomens, and F. P. T. Baaijens, "Passive and active contributions to generated force and retraction in heart valve tissue

engineering," *Biomechanics and Modeling in Mechanobiology*, vol. 11, no. 7, pp. 1015–1027, Sep. 2012, doi: 10.1007/s10237-011-0370-7.

[145] J. L. Balestrini and K. L. Billiar, "Magnitude and Duration of Stretch Modulate Fibroblast Remodeling," *Journal of Biomechanical Engineering*, vol. 131, no. 5, May 2009, doi: 10.1115/1.3049527.

[146] M. Y. Emmert *et al.*, "Computational modeling guides tissue-engineered heart valve design for long-term in vivo performance in a translational sheep model," *Science Translational Medicine*, vol. 10, no. 440, p. eaan4587, May 2018, doi: 10.1126/scitranslmed.aan4587.

[147] P. M. Dohmen *et al.*, "Mid-Term Clinical Results Using a Tissue-Engineered Pulmonary Valve to Reconstruct the Right Ventricular Outflow Tract During the Ross Procedure," *The Annals of Thoracic Surgery*, vol. 84, no. 3, pp. 729–736, Sep. 2007, doi: 10.1016/j.athoracsur.2007.04.072.

[148] E. S. Fioretta *et al.*, "Next-generation tissue-engineered heart valves with repair, remodelling and regeneration capacity," *Nature Reviews Cardiology*, vol. 18, no. 2, pp. 92–116, Feb. 2021, doi: 10.1038/s41569-020-0422-8.

[149] P. M. Dohmen, A. Lembcke, S. Holinski, A. Pruss, and W. Konertz, "Ten Years of Clinical Results With a Tissue-Engineered Pulmonary Valve," *The Annals of Thoracic Surgery*, vol. 92, no. 4, pp. 1308–1314, Oct. 2011, doi: 10.1016/j.athoracsur.2011.06.009.

[150] E. S. Fioretta *et al.*, "Next-generation tissue-engineered heart valves with repair, remodelling and regeneration capacity," *Nature Reviews Cardiology*, vol. 18, no. 2, pp. 92–116, Jan. 2021, doi: 10.1038/s41569-020-0422-8.

[151] A. H. Chester and K. J. Grande-Allen, "Which Biological Properties of Heart Valves Are Relevant to Tissue Engineering?," *Frontiers in Cardiovascular Medicine*, vol. 7, Jan. 2020, doi: 10.3389/fcvm.2020.00063.

[152] T. B. Wissing, V. Bonito, C. V. C. Bouten, and A. I. P. M. Smits, "Biomaterial-driven in situ cardiovascular tissue engineering—a multi-disciplinary perspective," *npj Regenerative Medicine*, vol. 2, no. 1, p. 18, Dec. 2017, doi: 10.1038/s41536-017-0023-2.

[153] C. V. C. Bouten, A. I. P. M. Smits, and F. P. T. Baaijens, "Can We Grow Valves Inside the Heart? Perspective on Material-based In Situ Heart Valve Tissue Engineering," *Frontiers in Cardiovascular Medicine*, vol. 5, May 2018, doi: 10.3389/fcvm.2018.00054.

[154] J. Kluin *et al.*, "In situ heart valve tissue engineering using a bioresorbable elastomeric implant – From material design to 12 months follow-up in sheep," *Biomaterials*, vol. 125, pp. 101–117, May 2017, doi: 10.1016/j.biomaterials.2017.02.007.

[155] G. Bennink *et al.*, "A novel restorative pulmonary valved conduit in a chronic sheep model: Mid-term hemodynamic function and histologic assessment," *The Journal of Thoracic and Cardiovascular Surgery*, vol. 155, no. 6, pp. 2591-2601.e3, Jun. 2018, doi: 10.1016/j.jtcvs.2017.12.046.

[156] N. Krishnamoorthy *et al.*, "A Strategy to Enhance Secretion of Extracellular Matrix Components by Stem Cells: Relevance to Tissue Engineering," *Tissue Engineering Part A*, vol. 24, no. 1–2, pp. 145–156, Jan. 2018, doi: 10.1089/ten.tea.2017.0060.

[157] U. Hersel, C. Dahmen, and H. Kessler, "RGD modified polymers: biomaterials for stimulated cell adhesion and beyond," *Biomaterials*, vol. 24, no. 24, pp. 4385–4415, Nov. 2003, doi: 10.1016/S0142-9612(03)00343-0.

[158] J. Zhou *et al.*, "Promotion of adhesion and proliferation of endothelial progenitor cells on decellularized valves by covalent incorporation of RGD peptide and VEGF," *Journal of Materials Science: Materials in Medicine*, vol. 27, no. 9, p. 142, Sep. 2016, doi: 10.1007/s10856-016-5750-1.

[159] X. Dong *et al.*, "RGD-modified acellular bovine pericardium as a bioprosthetic scaffold for tissue engineering," *Journal of Materials Science: Materials in Medicine*, vol. 20, no. 11, pp. 2327–2336, Nov. 2009, doi: 10.1007/s10856-009-3791-4.

[160] J. Shi, N. Dong, and Z. Sun, "Immobilization of decellularized valve scaffolds with Arg-Gly-Asp-containing peptide to promote myofibroblast adhesion," *Journal of Huazhong University of Science and Technology [Medical Sciences]*, vol. 29, no. 4, pp. 503–507, Aug. 2009, doi: 10.1007/s11596-009-0422-8.

[161] J. Zhu, P. He, L. Lin, D. R. Jones, and R. E. Marchant, "Biomimetic Poly(ethylene glycol)-Based Hydrogels as Scaffolds for Inducing Endothelial Adhesion and Capillary-Like Network Formation," *Biomacromolecules*, vol. 13, no. 3, pp. 706–713, Mar. 2012, doi: 10.1021/bm201596w.

[162] G. Neufeld, T. Cohen, S. Gengrinovitch, and Z. Poltorak, "Vascular endothelial growth factor (VEGF) and its receptors.," *FASEB J*, vol. 13, no. 1, pp. 9–22, Jan. 1999, [Online]. Available: http://www.ncbi.nlm.nih.gov/pubmed/9872925

[163] J. Zhou *et al.*, "Promotion of adhesion and proliferation of endothelial progenitor cells on decellularized valves by covalent incorporation of RGD peptide and VEGF," *Journal of Materials Science: Materials in Medicine*, vol. 27, no. 9, p. 142, Sep. 2016, doi: 10.1007/s10856-016-5750-1.

[164] M. L. W. Knetsch and L. H. Koole, "VEGF-E enhances endothelialization and inhibits thrombus formation on polymeric surfaces," *Journal of Biomedical Materials Research Part A*, vol. 9999A, p. NA-NA, 2009, doi: 10.1002/jbm.a.32538.

[165] Y. H. Shen, M. S. Shoichet, and M. Radisic, "Vascular endothelial growth factor immobilized in collagen scaffold promotes penetration and proliferation of endothelial cells," *Acta Biomaterialia*, vol. 4, no. 3, pp. 477–489, May 2008, doi: 10.1016/j.actbio.2007.12.011.

[166] D. B. Rifkin and D. Moscatelli, "Recent developments in the cell biology of basic fibroblast growth factor.," *Journal of Cell Biology*, vol. 109, no. 1, pp. 1–6, Jul. 1989, doi: 10.1083/jcb.109.1.1.

[167] K. Doi and T. Matsuda, "Enhanced vascularization in a microporous polyurethane graft impregnated with basic fibroblast growth factor and heparin," *Journal of Biomedical Materials Research*, vol. 34, no. 3, pp. 361–370, Mar. 1997, doi: 10.1002/(SICI)1097-4636(19970305)34:3<361::AID-JBM11>3.0.CO;2-J.

[168] P. T. Thevenot, A. M. Nair, J. Shen, P. Lotfi, C.-Y. Ko, and L. Tang, "The effect of incorporation of SDF-1α into PLGA scaffolds on stem cell recruitment and the inflammatory response," *Biomaterials*, vol. 31, no. 14, pp. 3997–4008, May 2010, doi: 10.1016/j.biomaterials.2010.01.144.

[169] S. E. Motta *et al.*, "Development of an Off-the-Shelf Tissue-Engineered Sinus Valve for Transcatheter Pulmonary Valve Replacement: a Proof-of-Concept Study," *Journal of Cardiovascular Translational Research*, vol. 11, no. 3, pp. 182–191, Jun. 2018, doi: 10.1007/s12265-018-9800-6.

[170] E. S. Fioretta *et al.*, "Next-generation tissue-engineered heart valves with repair, remodelling and regeneration capacity," *Nature Reviews Cardiology*, vol. 18, no. 2, pp. 92–116, Feb. 2021, doi: 10.1038/s41569-020-0422-8.

[171] S. Shimoni, I. Bar, V. Meledin, E. Derazne, G. Gandelman, and J. George, "Circulating Endothelial Progenitor Cells and Clinical Outcome in Patients with Aortic Stenosis," *PLOS ONE*, vol. 11, no. 2, p. e0148766, Feb. 2016, doi: 10.1371/journal.pone.0148766.

[172] D. A. Ingram, N. M. Caplice, and M. C. Yoder, "Unresolved questions, changing definitions, and novel paradigms for defining endothelial progenitor cells," *Blood*, vol. 106, no. 5, pp. 1525–1531, Sep. 2005, doi: 10.1182/blood-2005-04-1509.

[173] A. J. Melchiorri *et al.*, "Contrasting Biofunctionalization Strategies for the Enhanced Endothelialization of Biodegradable Vascular Grafts," *Biomacromolecules*, vol. 16, no. 2, pp. 437–446, Feb. 2015, doi: 10.1021/bm501853s.

[174] V. L. Sales, "Transforming Growth Factor- 1 Modulates Extracellular Matrix Production, Proliferation, and Apoptosis of Endothelial Progenitor Cells in Tissue-Engineering Scaffolds," *Circulation*, vol. 114, no. 1_suppl, pp. I-193-I–199, Jul. 2006, doi: 10.1161/CIRCULATIONAHA.105.001628.

[175] V. L. Sales *et al.*, "Protein Precoating of Elastomeric Tissue-Engineering Scaffolds Increased Cellularity, Enhanced Extracellular Matrix Protein Production, and Differentially Regulated the Phenotypes of Circulating Endothelial Progenitor Cells," *Circulation*, vol. 116, no. 11_suppl, pp. I-55-I–63, Sep. 2007, doi: 10.1161/CIRCULATIONAHA.106.6806637.

[176] A. H. Zaidi *et al.*, "Preliminary experience with porcine intestinal submucosa (CorMatrix) for valve reconstruction in congenital heart disease: Histologic evaluation of explanted valves," *The Journal of Thoracic and Cardiovascular Surgery*, vol. 148, no. 5, pp. 2216-2225.e1, Nov. 2014, doi: 10.1016/j.jtcvs.2014.02.081.

[177] H. Spriestersbach *et al.*, "First percutaneous implantation of a completely tissue-engineered self-expanding pulmonary heart valve prosthesis using a newly developed delivery system: a feasibility study in sheep," *Cardiovascular Intervention and Therapeutics*, vol. 32, no. 1, pp. 36–47, Jan. 2017, doi: 10.1007/s12928-016-0396-y.

[178] A. Driessen-Mol *et al.*, "Transcatheter implantation of homologous 'off-the-shelf' tissue-engineered heart valves with self-repair capacity: Long-term functionality and rapid in vivo remodeling in sheep," *J Am Coll Cardiol*, vol. 63, no. 13, pp. 1320–1329, 2014, doi: 10.1016/j.jacc.2013.09.082.

[179] B. Weber *et al.*, "Off-the-shelf human decellularized tissue-engineered heart valves in a non-human primate model," *Biomaterials*, vol. 34, no. 30, pp. 7269–7280, Oct. 2013, doi: 10.1016/j.biomaterials.2013.04.059.

[180] J. D. Roh *et al.*, "Tissue-engineered vascular grafts transform into mature blood vessels via an inflammation-mediated process of vascular remodeling," *Proceedings of the National Academy of Sciences*, vol. 107, no. 10, pp. 4669–4674, Mar. 2010, doi: 10.1073/pnas.0911465107.

[181] J. W. van Rijswijk *et al.*, "Failure of decellularized porcine small intestinal submucosa as a heart valved conduit," *The Journal of Thoracic and Cardiovascular Surgery*, vol. 160, no. 4, pp. e201–e215, Oct. 2020, doi: 10.1016/j.jtcvs.2019.09.164.

[182] P. Simon, "Early failure of the tissue engineered porcine heart valve SYNERGRAFT™ in pediatric patients," *European Journal of Cardio-Thoracic Surgery*, vol. 23, no. 6, pp. 1002–1006, Jun. 2003, doi: 10.1016/S1010-7940(03)00094-0.

[183] M. Hofmann *et al.*, "Congenital aortic valve repair using CorMatrix ® : A histologic evaluation," *Xenotransplantation*, vol. 24, no. 6, p. e12341, Nov. 2017, doi: 10.1111/xen.12341.

[184] Z. Mosala Nezhad, P. Baldin, A. Poncelet, and G. el Khoury, "Calcific Degeneration of CorMatrix 4 Years After Bicuspidization of Unicuspid Aortic Valve," *The Annals of Thoracic Surgery*, vol. 104, no. 6, pp. e431–e433, Dec. 2017, doi: 10.1016/j.athoracsur.2017.07.040.

[185] N. Filippo, A. Paola, and I. Laura, "Biocompatibility Evaluation Criteria for Novel Xenograft Materials: Distribution and Quantification of Remnant Nucleic Acid and Alpha-Gal Epitope," *Journal of Stem Cell Research & Therapy*, vol. 01, no. S6, 2013, doi: 10.4172/2157-7633.S6-009.

[186] G. BaoLin and P. X. Ma, "Synthetic biodegradable functional polymers for tissue engineering: a brief review.," *Sci China Chem*, vol. 57, no. 4, pp. 490–500, Apr. 2014, doi: 10.1007/s11426-014-5086-y.

[187] S. Ravi and E. L. Chaikof, "Biomaterials for vascular tissue engineering," *Regenerative Medicine*, vol. 5, no. 1, pp. 107–120, Jan. 2010, doi: 10.2217/rme.09.77.

[188] J. Leijten, J. Rouwkema, Y. S. Zhang, A. Nasajpour, M. R. Dokmeci, and A. Khademhosseini, "Advancing Tissue Engineering: A Tale of Nano-, Micro-, and Macroscale Integration," *Small*, vol. 12, no. 16, pp. 2130–2145, Apr. 2016, doi: 10.1002/smll.201501798.

[189] A. Atala, S. B. Bauer, S. Soker, J. J. Yoo, and A. B. Retik, "Tissue-engineered autologous bladders for patients needing cystoplasty," *The Lancet*, vol. 367, no. 9518, pp. 1241–1246, Apr. 2006, doi: 10.1016/S0140-6736(06)68438-9.

[190] J. A. Gastel, W. R. Muirhead, J. T. Lifrak, P. D. Fadale, M. J. Hulstyn, and D. P. Labrador, "Meniscal tissue regeneration using a collagenous biomaterial derived from porcine small intestine submucosa," *Arthroscopy: The Journal of Arthroscopic & Related Surgery*, vol. 17, no. 2, pp. 151–159, Feb. 2001, doi: 10.1053/jars.2001.20959.

[191] A. K. Capulli *et al.*, "JetValve: Rapid manufacturing of biohybrid scaffolds for biomimetic heart valve replacement," *Biomaterials*, vol. 133, pp. 229–241, Jul. 2017, doi: 10.1016/j.biomaterials.2017.04.033.

[192] X. Liu, L. A. Smith, J. Hu, and P. X. Ma, "Biomimetic nanofibrous gelatin/apatite composite scaffolds for bone tissue engineering," *Biomaterials*, vol. 30, no. 12, pp. 2252–2258, Apr. 2009, doi: 10.1016/j.biomaterials.2008.12.068.

[193] E. Alsberg, K. W. Anderson, A. Albeiruti, R. T. Franceschi, and D. J. Mooney, "Cell-interactive Alginate Hydrogels for Bone Tissue Engineering," *Journal of Dental Research*, vol. 80, no. 11, pp. 2025–2029, Nov. 2001, doi: 10.1177/00220345010800111501.

[194] T. Zachos, A. Diggs, S. Weisbrode, J. Bartlett, and A. Bertone, "Mesenchymal Stem Cell-mediated Gene Delivery of Bone Morphogenetic Protein-2 in an Articular Fracture Model," *Molecular Therapy*, vol. 15, no. 8, pp. 1543–1550, Aug. 2007, doi: 10.1038/sj.mt.6300192.

[195] S. H. Park *et al.*, "An injectable, click-crosslinked, cytomodulin-modified hyaluronic acid hydrogel for cartilage tissue engineering," *NPG Asia Materials*, vol. 11, no. 1, p. 30, Dec. 2019, doi: 10.1038/s41427-019-0130-1.

[196] M. Movahedi, A. Asefnejad, M. Rafienia, and M. T. Khorasani, "Potential of novel electrospun core-shell structured polyurethane/starch (hyaluronic acid) nanofibers for skin tissue engineering: In vitro and in vivo evaluation," *International Journal of Biological Macromolecules*, vol. 146, pp. 627–637, Mar. 2020, doi: 10.1016/j.ijbiomac.2019.11.233.

[197] R. L. Mauck *et al.*, "Functional Tissue Engineering of Articular Cartilage Through Dynamic Loading of Chondrocyte-Seeded Agarose Gels," *Journal of Biomechanical Engineering*, vol. 122, no. 3, pp. 252–260, Jun. 2000, doi: 10.1115/1.429656.

[198] D. Y. Lewitus *et al.*, "Biohybrid Carbon Nanotube/Agarose Fibers for Neural Tissue Engineering," *Advanced Functional Materials*, vol. 21, no. 14, pp. 2624–2632, Jul. 2011, doi: 10.1002/adfm.201002429.

[199] N. Boucard *et al.*, "The use of physical hydrogels of chitosan for skin regeneration following third-degree burns," *Biomaterials*, vol. 28, no. 24, pp. 3478–3488, Aug. 2007, doi: 10.1016/j.biomaterials.2007.04.021.

[200] N. Iwasaki *et al.*, "Feasibility of Polysaccharide Hybrid Materials for Scaffolds in Cartilage Tissue Engineering: Evaluation of Chondrocyte Adhesion to Polyion Complex Fibers Prepared from Alginate and Chitosan," *Biomacromolecules*, vol. 5, no. 3, pp. 828–833, May 2004, doi: 10.1021/bm0400067.

[201] B. Weber *et al.*, "Injectable living marrow stromal cell-based autologous tissue engineered heart valves: first experiences with a one-step intervention in primates," *European Heart Journal*, vol. 32, no. 22, pp. 2830–2840, Nov. 2011, doi: 10.1093/eurheartj/ehr059.

[202] X. Hu, W. Lui, L. Cui, M. Wang, and Y. Cao, "Tissue Engineering of Nearly Transparent Corneal Stroma," *Tissue Engineering*, vol. 11, no. 11–12, pp. 1710–1717, Nov. 2005, doi: 10.1089/ten.2005.11.1710.

[203] X. Zhou *et al.*, "Fabrication of polylactic acid (PLA)-based porous scaffold through the combination of traditional bio-fabrication and 3D printing technology for bone regeneration," *Colloids and Surfaces B: Biointerfaces*, vol. 197, p. 111420, Jan. 2021, doi: 10.1016/j.colsurfb.2020.111420.

[204] N. Hibino *et al.*, "Late-term results of tissue-engineered vascular grafts in humans," *The Journal of Thoracic and Cardiovascular Surgery*, vol. 139, no. 2, pp. 431-436.e2, Feb. 2010, doi: 10.1016/j.jtcvs.2009.09.057.

[205] Y. Lai *et al.*, "Osteogenic magnesium incorporated into PLGA/TCP porous scaffold by 3D printing for repairing challenging bone defect," *Biomaterials*, vol. 197, pp. 207–219, Mar. 2019, doi: 10.1016/j.biomaterials.2019.01.013.

[206] F. S. Tabatabaei Mirakabad *et al.*, "PLGA-Based Nanoparticles as Cancer Drug Delivery Systems," *Asian Pacific Journal of Cancer Prevention*, vol. 15, no. 2, pp. 517–535, Jan. 2014, doi: 10.7314/APJCP.2014.15.2.517.

[207] Z. Wang *et al.*, "Differences in the performance of PCL-based vascular grafts as abdominal aorta substitutes in healthy and diabetic rats," *Biomaterials Science*, vol. 4, no. 10, pp. 1485–1492, 2016, doi: 10.1039/C6BM00178E.

[208] Y. Wu *et al.*, "Fabrication of dentin-like scaffolds through combined 3D printing and bio-mineralisation," *Cogent Engineering*, vol. 3, no. 1, p. 1222777, Dec. 2016, doi: 10.1080/23311916.2016.1222777.

[209] L. van Hoof *et al.*, "Support of the aortic wall: a histological study in sheep comparing a macroporous mesh with low-porosity vascular graft of the same polyethylene terephthalate material," *Interactive CardioVascular and Thoracic Surgery*, vol. 25, no. 1, pp. 89–95, Jul. 2017, doi: 10.1093/icvts/ivx009.

[210] M. H. Hassan *et al.*, "The Potential of Polyethylene Terephthalate Glycol as Biomaterial for Bone Tissue Engineering," *Polymers (Basel)*, vol. 12, no. 12, p. 3045, Dec. 2020, doi: 10.3390/polym12123045.

[211] J.-Y. Park, J.-H. Lee, C.-H. Kim, and Y.-J. Kim, "Fabrication of polytetrafluoroethylene nanofibrous membranes for guided bone regeneration," *RSC Advances*, vol. 8, no. 60, pp. 34359–34369, 2018, doi: 10.1039/C8RA05637D.

[212] S. Matsuura *et al.*, "A Radiation-Crosslinked Gelatin Hydrogel That Promotes Tissue Incorporation of an Expanded Polytetrafluoroethylene Vascular Graft in Rats," *Biomolecules*, vol. 11, no. 8, p. 1105, Jul. 2021, doi: 10.3390/biom11081105.

[213] S. Ranganathan, K. Balagangadharan, and N. Selvamurugan, "Chitosan and gelatin-based electrospun fibers for bone tissue engineering," *International Journal of Biological Macromolecules*, vol. 133, pp. 354–364, Jul. 2019, doi: 10.1016/j.ijbiomac.2019.04.115.

[214] S. Gorgieva and V. Kokol, "Collagen- vs. Gelatine-Based Biomaterials and Their Biocompatibility: Review and Perspectives," in *Biomaterials Applications for Nanomedicine*, InTech, 2011. doi: 10.5772/24118.

[215] A. Duconseille, D. Andueza, F. Picard, V. Santé-Lhoutellier, and T. Astruc, "Variability in pig skin gelatin properties related to production site: A near infrared and fluorescence spectroscopy study," *Food Hydrocolloids*, vol. 63, pp. 108–119, Feb. 2017, doi: 10.1016/j.foodhyd.2016.08.001.

[216] A. Y. Kim, Y. Kim, S. H. Lee, Y. Yoon, W.-H. Kim, and O.-K. Kweon, "Effect of Gelatin on Osteogenic Cell Sheet Formation Using Canine Adipose-Derived Mesenchymal Stem Cells," *Cell Transplantation*, vol. 26, no. 1, pp. 115–123, Jan. 2017, doi: 10.3727/096368916X693338.

[217] R. M. H. Raja Nhari, Y. Che Man, A. Ismail, and N. Anuar, "Chemical and functional properties of bovine and porcine skin gelatin," *International Food Research Journal*, vol. 817, pp. 813–817, 2011, [Online]. Available: http://ifrj.upm.edu.my/18 (02) 2011/(48) IFRJ-2010-159.pdf

[218] S. O. A. Koskinen *et al.*, "Serum concentrations of collagen degrading enzymes and their inhibitors after downhill running," *Scandinavian Journal of Medicine & Science in Sports*, vol. 11, no. 1, pp. 9–15, Feb. 2001, doi: 10.1034/j.1600-0838.2001.011001009.x.

[219] B. Mohanty and H. B. Bohidar, "Microscopic structure of gelatin coacervates," *International Journal of Biological Macromolecules*, vol. 36, no. 1–2, pp. 39–46, Jul. 2005, doi: 10.1016/j.ijbiomac.2005.03.012.

[220] D. P. Speer, M. Chvapil, C. D. Eskelson, and J. Ulreich, "Biological effects of residual glutaraldehyde in glutaraldehyde-tanned collagen biomaterials," *Journal of Biomedical Materials Research*, vol. 14, no. 6, pp. 753–764, Nov. 1980, doi: 10.1002/jbm.820140607.

[221] E. M. Masutani, C. K. Kinoshita, T. T. Tanaka, A. K. D. Ellison, and B. A. Yoza, "Increasing Thermal Stability of Gelatin by UV-Induced Cross-Linking with Glucose," *International Journal of Biomaterials*, vol. 2014, pp. 1–9, 2014, doi: 10.1155/2014/979636.

[222] A. Bigi, G. Cojazzi, S. Panzavolta, N. Roveri, and K. Rubini, "Stabilization of gelatin films by crosslinking with genipin," *Biomaterials*, vol. 23, no. 24, pp. 4827–4832, Dec. 2002, doi: 10.1016/S0142-9612(02)00235-1.

[223] C. Tonda-Turo *et al.*, "Comparative analysis of gelatin scaffolds crosslinked by genipin and silane coupling agent," *International Journal of Biological Macromolecules*, vol. 49, no. 4, pp. 700–706, Nov. 2011, doi: 10.1016/j.ijbiomac.2011.07.002.

[224] C. Tonda-Turo *et al.*, "Crosslinked gelatin nanofibres: Preparation, characterisation and in vitro studies using glial-like cells," *Materials Science and Engineering: C*, vol. 33, no. 5, pp. 2723–2735, Jul. 2013, doi: 10.1016/j.msec.2013.02.039.

[225] H. Aoki, H. Miyoshi, and Y. Yamagata, "Electrospinning of gelatin nanofiber scaffolds with mild neutral cosolvents for use in tissue engineering," *Polymer Journal*, vol. 47, no. 3, pp. 267–277, Mar. 2015, doi: 10.1038/pj.2014.94.

[226] P. A. Maroju, P. Tata, A. Balapure, J. Ray Dutta, and R. Ganesan, "Lactobacillus amylovorus derived lipase-mediated silver derivatization over poly(ε-caprolactone) towards antimicrobial coatings," *Enzyme and Microbial Technology*, vol. 150, p. 109888, Oct. 2021, doi: 10.1016/j.enzmictec.2021.109888.

[227] A. M. Martins *et al.*, "The Role of Lipase and α-Amylase in the Degradation of Starch/Poly(ε-Caprolactone) Fiber Meshes and the Osteogenic Differentiation of Cultured Marrow Stromal Cells," *Tissue Engineering Part A*, vol. 15, no. 2, pp. 295–305, Feb. 2009, doi: 10.1089/ten.tea.2008.0025.

[228] E. Díaz, I. Sandonis, and M. B. Valle, "In Vitro Degradation of Poly(caprolactone)/nHA Composites," *Journal of Nanomaterials*, vol. 2014, pp. 1–8, 2014, doi: 10.1155/2014/802435.

[229] N. Bölgen, Y. Z. Menceloğlu, K. Acatay, İ. Vargel, and E. Pişkin, "In vitro and in vivo degradation of non-woven materials made of poly(ε-caprolactone) nanofibers prepared by electrospinning under different conditions," *Journal of Biomaterials Science, Polymer Edition*, vol. 16, no. 12, pp. 1537–1555, Jan. 2005, doi: 10.1163/156856205774576655.

[230] J. H. Ashton *et al.*, "Polymeric endoaortic paving: Mechanical, thermoforming, and degradation properties of polycaprolactone/polyurethane blends for cardiovascular applications," *Acta Biomaterialia*, vol. 7, no. 1, pp. 287–294, Jan. 2011, doi: 10.1016/j.actbio.2010.09.004.

[231] E. Malikmammadov, T. E. Tanir, A. Kiziltay, V. Hasirci, and N. Hasirci, "PCL and PCL-based materials in biomedical applications," *Journal of Biomaterials Science, Polymer Edition*, vol. 29, no. 7–9, pp. 863–893, Jun. 2018, doi: 10.1080/09205063.2017.1394711.

[232] N. Siddiqui, S. Asawa, B. Birru, R. Baadhe, and S. Rao, "PCL-Based Composite Scaffold Matrices for Tissue Engineering Applications," *Molecular Biotechnology*, vol. 60, no. 7, pp. 506–532, Jul. 2018, doi: 10.1007/s12033-018-0084-5.

[233] T. Lou *et al.*, "Bi-Layer Scaffold of Chitosan/PCL-Nanofibrous Mat and PLLA-Microporous Disc for Skin Tissue Engineering," *Journal of Biomedical Nanotechnology*, vol. 10, no. 6, pp. 1105–1113, Jun. 2014, doi: 10.1166/jbn.2014.1793.

[234] C. Murphy, K. Kolan, W. Li, J. Semon, D. Day, and M. Leu, "3D bioprinting of stem cells and polymer/bioactive glass composite scaffolds for tissue engineering," *International Journal of Bioprinting*, vol. 3, no. 1, Jan. 2017, doi: 10.18063/IJB.2017.01.005.

[235] Y. S. Cho *et al.*, "Fabrication of dual-pore scaffolds using SLUP (salt leaching using powder) and WNM (wire-network molding) techniques," *Materials Science and Engineering: C*, vol. 45, pp. 546–555, Dec. 2014, doi: 10.1016/j.msec.2014.10.009.

[236] Z. Fereshteh, M. Fathi, A. Bagri, and A. R. Boccaccini, "Preparation and characterization of aligned porous PCL/zein scaffolds as drug delivery systems via improved unidirectional freeze-drying method," *Materials Science and Engineering: C*, vol. 68, pp. 613–622, Nov. 2016, doi: 10.1016/j.msec.2016.06.009.

[237] X. Jing, H.-Y. Mi, and L.-S. Turng, "Comparison between PCL/hydroxyapatite (HA) and PCL/halloysite nanotube (HNT) composite scaffolds prepared by co-extrusion and gas foaming," *Materials Science and Engineering: C*, vol. 72, pp. 53–61, Mar. 2017, doi: 10.1016/j.msec.2016.11.049.

[238] X. Qin and D. Wu, "Effect of different solvents on poly(caprolactone) (PCL) electrospun nonwoven membranes," *Journal of Thermal Analysis and Calorimetry*, vol. 107, no. 3, pp. 1007–1013, Mar. 2012, doi: 10.1007/s10973-011-1640-4.

[239] C. M. Crews, "Targeting the Undruggable Proteome: The Small Molecules of My Dreams," *Chemistry & Biology*, vol. 17, no. 6, pp. 551–555, Jun. 2010, doi: 10.1016/j.chembiol.2010.05.011.

[240] X. Chen, L. S. Mangala, C. Rodriguez-Aguayo, X. Kong, G. Lopez-Berestein, and A. K. Sood, "RNA interference-based therapy and its delivery systems," *Cancer and Metastasis Reviews*, vol. 37, no. 1, pp. 107–124, Mar. 2018, doi: 10.1007/s10555-017-9717-6.

[241] R. Brown, E. Curry, L. Magnani, C. S. Wilhelm-Benartzi, and J. Borley, "Poised epigenetic states and acquired drug resistance in cancer," *Nature Reviews Cancer*, vol. 14, no. 11, pp. 747–753, Nov. 2014, doi: 10.1038/nrc3819.

[242] A.-M. Yu, C. Jian, A. H. Yu, and M.-J. Tu, "RNA therapy: Are we using the right molecules?," *Pharmacology & Therapeutics*, vol. 196, pp. 91–104, Apr. 2019, doi: 10.1016/j.pharmthera.2018.11.011.

[243] M. Kellis *et al.*, "Defining functional DNA elements in the human genome," *Proceedings of the National Academy of Sciences*, vol. 111, no. 17, pp. 6131–6138, Apr. 2014, doi: 10.1073/pnas.1318948111.

[244] J. S. Mattick, "RNA regulation: a new genetics?," *Nature Reviews Genetics*, vol. 5, no. 4, pp. 316–323, Apr. 2004, doi: 10.1038/nrg1321.

[245] J. S. Mattick, "Non-coding RNAs: the architects of eukaryotic complexity," *EMBO Rep*, vol. 2, no. 11, pp. 986–991, Nov. 2001, doi: 10.1093/embo-reports/kve230.

[246] F. Rashid, A. Shah, and G. Shan, "Long Non-coding RNAs in the Cytoplasm," *Genomics, Proteomics & Bioinformatics*, vol. 14, no. 2, pp. 73–80, Apr. 2016, doi: 10.1016/j.gpb.2016.03.005.

[247] C. M. Curtin, I. M. Castaño, and F. J. O'Brien, "Scaffold-Based microRNA Therapies in Regenerative Medicine and Cancer," *Advanced Healthcare Materials*, vol. 7, no. 1, p. 1700695, Jan. 2018, doi: 10.1002/adhm.201700695.

[248] M. J. Marzi *et al.*, "Degradation dynamics of microRNAs revealed by a novel pulse-chase approach," *Genome Research*, vol. 26, no. 4, pp. 554–565, Apr. 2016, doi: 10.1101/gr.198788.115.

[249] J. K. W. Lam, M. Y. T. Chow, Y. Zhang, and S. W. S. Leung, "siRNA Versus miRNA as Therapeutics for Gene Silencing," *Molecular Therapy - Nucleic Acids*, vol. 4, p. e252, 2015, doi: 10.1038/mtna.2015.23.

[250] C. V. C. Bouten, A. I. P. M. Smits, and F. P. T. Baaijens, "Can We Grow Valves Inside the Heart? Perspective on Material-based In Situ Heart Valve Tissue Engineering," *Frontiers in Cardiovascular Medicine*, vol. 5, May 2018, doi: 10.3389/fcvm.2018.00054.

[251] S. M. Elbashir, J. Harborth, W. Lendeckel, A. Yalcin, K. Weber, and T. Tuschl, "Duplexes of 21-nucleotide RNAs mediate RNA interference in cultured mammalian cells," *Nature*, vol. 411, no. 6836, pp. 494–498, May 2001, doi: 10.1038/35078107.

[252] X. Chen, L. S. Mangala, C. Rodriguez-Aguayo, X. Kong, G. Lopez-Berestein, and A. K. Sood, "RNA interference-based therapy and its delivery systems," *Cancer and Metastasis Reviews*, vol. 37, no. 1, pp. 107–124, Mar. 2018, doi: 10.1007/s10555-017-9717-6.

[253] S. E. J. Fischer, "RNA Interference and MicroRNA-Mediated Silencing," *Current Protocols in Molecular Biology*, vol. 112, no. 1, Oct. 2015, doi: 10.1002/0471142727.mb2601s112.

[254] M. S. Beg *et al.*, "Phase I study of MRX34, a liposomal miR-34a mimic, administered twice weekly in patients with advanced solid tumors," *Investigational New Drugs*, vol. 35, no. 2, pp. 180–188, Apr. 2017, doi: 10.1007/s10637-016-0407-y.

[255] F. Stelma *et al.*, "Immune phenotype and function of natural killer and T cells in chronic hepatitis C patients who received a single dose of anti-MicroRNA-122, RG-101," *Hepatology*, vol. 66, no. 1, pp. 57–68, Jul. 2017, doi: 10.1002/hep.29148.

[256] C. Boada, R. Sukhovershin, R. Pettigrew, and J. P. Cooke, "RNA therapeutics for cardiovascular disease," *Current Opinion in Cardiology*, vol. 36, no. 3, pp. 256–263, May 2021, doi: 10.1097/HCO.0000000000000850.

[257] M. Caputo, J. Saif, C. Rajakaruna, M. Brooks, G. D. Angelini, and C. Emanueli, "MicroRNAs in vascular tissue engineering and post-ischemic neovascularization," *Advanced Drug Delivery Reviews*, vol. 88, pp. 78–91, Jul. 2015, doi: 10.1016/j.addr.2015.05.003.

[258] J. Chen *et al.*, "mir-17–92 Cluster Is Required for and Sufficient to Induce Cardiomyocyte Proliferation in Postnatal and Adult Hearts," *Circulation Research*, vol. 112, no. 12, pp. 1557–1566, Jun. 2013, doi: 10.1161/CIRCRESAHA.112.300658.

[259] Y. Zhuang, H. Peng, V. Mastej, and W. Chen, "MicroRNA Regulation of Endothelial Junction Proteins and Clinical Consequence," *Mediators of Inflammation*, vol. 2016, pp. 1–6, 2016, doi: 10.1155/2016/5078627.

[260] S. P. Srivastava, A. F. Hedayat, K. Kanasaki, and J. E. Goodwin, "microRNA Crosstalk Influences Epithelial-to-Mesenchymal, Endothelial-to-Mesenchymal, and Macrophage-to-Mesenchymal Transitions in the Kidney," *Frontiers in Pharmacology*, vol. 10, Aug. 2019, doi: 10.3389/fphar.2019.00904.

[261] P. Nammian, V. Razban, S. M. B. Tabei, and S.-L. Asadi-Yousefabad, "MicroRNA-126: Dual Role in Angiogenesis Dependent Diseases," *Current Pharmaceutical Design*, vol. 26, no. 38, pp. 4883–4893, Oct. 2020, doi: 10.2174/1381612826666200504120737.

[262] S. Biswas and S. Chakrabarti, "Increased Extracellular Matrix Protein Production in Chronic Diabetic Complications: Implications of Non-Coding RNAs," *Non-Coding RNA*, vol. 5, no. 1, p. 30, Mar. 2019, doi: 10.3390/ncrna5010030.

[263] E. R. Porrello *et al.*, "Regulation of neonatal and adult mammalian heart regeneration by the miR-15 family," *Proceedings of the National Academy of Sciences*, vol. 110, no. 1, pp. 187–192, Jan. 2013, doi: 10.1073/pnas.1208863110.

[264] A. Tiwari, B. Mukherjee, and M. Dixit, "MicroRNA Key to Angiogenesis Regulation: MiRNA Biology and Therapy," *Current Cancer Drug Targets*, vol. 18, no. 3, pp. 266–277, Feb. 2018, doi: 10.2174/1568009617666170630142725.

[265] S. Wang and E. N. Olson, "AngiomiRs—Key regulators of angiogenesis," *Current Opinion in Genetics & Development*, vol. 19, no. 3, pp. 205–211, Jun. 2009, doi: 10.1016/j.gde.2009.04.002.

[266] R. Menghini *et al.*, "MicroRNA 217 Modulates Endothelial Cell Senescence via Silent Information Regulator 1," *Circulation*, vol. 120, no. 15, pp. 1524–1532, Oct. 2009, doi: 10.1161/CIRCULATIONAHA.109.864629.

[267] M. K. Nguyen, O. Jeon, M. D. Krebs, D. Schapira, and E. Alsberg, "Sustained localized presentation of RNA interfering molecules from in situ forming hydrogels to guide stem cell osteogenic differentiation," *Biomaterials*, vol. 35, no. 24, pp. 6278–6286, Aug. 2014, doi: 10.1016/j.biomaterials.2014.04.048.

[268] C. M. Curtin, I. M. Castaño, and F. J. O'Brien, "Scaffold-Based microRNA Therapies in Regenerative Medicine and Cancer," *Advanced Healthcare Materials*, vol. 7, no. 1, pp. 1–22, 2018, doi: 10.1002/adhm.201700695.

[269] Y. Li *et al.*, "The promotion of bone regeneration through positive regulation of angiogenic–osteogenic coupling using microRNA-26a," *Biomaterials*, vol. 34, no. 21, pp. 5048–5058, Jul. 2013, doi: 10.1016/j.biomaterials.2013.03.052.

[270] M. G. Monaghan *et al.*, "Exogenous miR-29B Delivery Through a Hyaluronan-Based Injectable System Yields Functional Maintenance of the Infarcted Myocardium," *Tissue Engineering Part A*, vol. 24, no. 1–2, pp. 57–67, Jan. 2018, doi: 10.1089/ten.tea.2016.0527.

[271] H. J. Diao, W. C. Low, Q. R. Lu, and S. Y. Chew, "Topographical effects on fiber-mediated microRNA delivery to control oligodendroglial precursor cells development," *Biomaterials*, vol. 70, pp. 105–114, Nov. 2015, doi: 10.1016/j.biomaterials.2015.08.029.

[272] E. N. James, A. M. Delany, and L. S. Nair, "Post-transcriptional regulation in osteoblasts using localized delivery of miR-29a inhibitor from nanofibers to enhance extracellular matrix deposition," *Acta Biomaterialia*, vol. 10, no. 8, pp. 3571–3580, Aug. 2014, doi: 10.1016/j.actbio.2014.04.026.

[273] F. Zhou *et al.*, "Targeted delivery of microRNA-126 to vascular endothelial cells via REDV peptide modified PEG-trimethyl chitosan," *Biomater. Sci.*, pp. 10–12, 2016, doi: 10.1039/C5BM00629E.

[274] S. Zhang *et al.*, "Gelatin nanofibrous membrane fabricated by electrospinning of aqueous gelatin solution for guided tissue regeneration," *Journal of Biomedical Materials Research Part A*, vol. 90A, no. 3, pp. 671–679, Sep. 2009, doi: 10.1002/jbm.a.32136.

[275] M. Séon-Lutz, A.-C. Couffin, S. Vignoud, G. Schlatter, and A. Hébraud, "Electrospinning in water and in situ crosslinking of hyaluronic acid / cyclodextrin nanofibers: Towards wound dressing with controlled drug release," *Carbohydrate Polymers*, vol. 207, pp. 276–287, Mar. 2019, doi: 10.1016/j.carbpol.2018.11.085.

[276] C. Yang, X. Wu, Y. Zhao, L. Xu, and S. Wei, "Nanofibrous scaffold prepared by electrospinning of poly(vinyl alcohol)/gelatin aqueous solutions," *Journal of Applied Polymer Science*, vol. 121, no. 5, pp. 3047–3055, Sep. 2011, doi: 10.1002/app.33934.

[277] R. Katare *et al.*, "Transplantation of human pericyte progenitor cells improves the repair of infarcted heart through activation of an angiogenic program involving micro-RNA-132," *Circulation Research*, vol. 109, no. 8, pp. 894–906, 2011, doi: 10.1161/CIRCRESAHA.111.251546.

[278] S. Anand *et al.*, "MicroRNA-132–mediated loss of p120RasGAP activates the endothelium to facilitate pathological angiogenesis," *Nature Medicine*, vol. 16, no. 8, pp. 909–914, Aug. 2010, doi: 10.1038/nm.2186.

[279] S. Singh, J. Johnson, and S. Chellappan, "Small molecule regulators of Rb–E2F pathway as modulators of transcription," *Biochimica et Biophysica Acta (BBA) - Gene Regulatory Mechanisms*, vol. 1799, no. 10–12, pp. 788–794, Oct. 2010, doi: 10.1016/j.bbagrm.2010.07.004.

[280] C. Boscher, V. Gaonac'h-Lovejoy, C. Delisle, and J.-P. Gratton, "Polarization and sprouting of endothelial cells by angiopoietin-1 require PAK2 and paxillin-dependent Cdc42 activation," *Molecular Biology of the Cell*, vol. 30, no. 17, pp. 2227–2239, Aug. 2019, doi: 10.1091/mbc.E18-08-0486.

[281] S. Wang *et al.*, "The Endothelial-Specific MicroRNA miR-126 Governs Vascular Integrity and Angiogenesis," *Developmental Cell*, vol. 15, no. 2, pp. 261–271, Aug. 2008, doi: 10.1016/j.devcel.2008.07.002.

[282] E. Jover *et al.*, "Human adventitial pericytes provide a unique source of anti-calcific cells for cardiac valve engineering: Role of microRNA-132-3p," *Free Radical Biology and Medicine*, vol. 165, pp. 137–151, Mar. 2021, doi: 10.1016/j.freeradbiomed.2021.01.029.

[283] K. Gong *et al.*, "MiR-132 regulates osteogenic differentiation via downregulating Sirtuin1 in a peroxisome proliferator-activated receptor β/δ–dependent manner," *Biochemical and Biophysical Research Communications*, vol. 478, no. 1, pp. 260–267, Sep. 2016, doi: 10.1016/j.bbrc.2016.07.057.

[284] X. Shu *et al.*, "MicroRNA-93 regulates angiogenesis in peripheral arterial disease by targeting CDKN1A," *Molecular Medicine Reports*, Apr. 2019, doi: 10.3892/mmr.2019.10196.

[285] J. Devalliere *et al.*, "Sustained delivery of proangiogenic microRNA-132 by nanoparticle transfection improves endothelial cell transplantation," *The FASEB Journal*, vol. 28, no. 2, pp. 908–922, Feb. 2014, doi: 10.1096/fj.13-238527.

[286] Z. YANG *et al.*, "In vitro and in vivo characterization of silk fibroin/gelatin composite scaffolds for liver tissue engineering," *Journal of Digestive Diseases*, vol. 13, no. 3, pp. 168–178, Mar. 2012, doi: 10.1111/j.1751-2980.2011.00566.x.

[287] K. A. Whitehead, R. Langer, and D. G. Anderson, "Knocking down barriers: advances in siRNA delivery," *Nature Reviews Drug Discovery*, vol. 8, no. 2, pp. 129–138, Feb. 2009, doi: 10.1038/nrd2742.

[288] S. M. Sarett, K. v. Kilchrist, M. Miteva, and C. L. Duvall, "Conjugation of palmitic acid improves potency and longevity of siRNA delivered via endosomolytic polymer nanoparticles," *Journal of Biomedical Materials Research Part A*, vol. 103, no. 9, pp. 3107–3116, Sep. 2015, doi: 10.1002/jbm.a.35413.

[289] R. P. Hickerson *et al.*, "Stability Study of Unmodified siRNA and Relevance to Clinical Use," *Oligonucleotides*, vol. 18, no. 4, pp. 345–354, Dec. 2008, doi: 10.1089/oli.2008.0149.

[290] V. Bitko, A. Musiyenko, O. Shulyayeva, and S. Barik, "Inhibition of respiratory viruses by nasally administered siRNA," *Nature Medicine*, vol. 11, no. 1, pp. 50–55, Jan. 2005, doi: 10.1038/nm1164.

[291] N. Li *et al.*, "Small interfering RNA targeting NF-κB attenuates lipopolysaccharide-induced acute lung injury in rats," *BMC Physiology*, vol. 16, no. 1, p. 7, Dec. 2016, doi: 10.1186/s12899-016-0027-y.

[292] A. G. Rosas-Taraco, D. M. Higgins, J. Sánchez-Campillo, E. J. Lee, I. M. Orme, and M. González-Juarrero, "Intrapulmonary Delivery of XCL1-Targeting Small Interfering RNA in Mice Chronically Infected with Mycobacterium tuberculosis," *American Journal of Respiratory Cell and Molecular Biology*, vol. 41, no. 2, pp. 136–145, Aug. 2009, doi: 10.1165/rcmb.2008-0363OC.

[293] J. Gottlieb *et al.*, "ALN-RSV01 for prevention of bronchiolitis obliterans syndrome after respiratory syncytial virus infection in lung transplant recipients," *The Journal of Heart and Lung Transplantation*, vol. 35, no. 2, pp. 213–221, Feb. 2016, doi: 10.1016/j.healun.2015.08.012.

[294] J. DeVincenzo *et al.*, "A randomized, double-blind, placebo-controlled study of an RNAi-based therapy directed against respiratory syncytial virus," *Proceedings of the National Academy of Sciences*, vol. 107, no. 19, pp. 8800–8805, May 2010, doi: 10.1073/pnas.0912186107.

[295] Y. Qiu, M. Y. T. Chow, W. Liang, W. W. Y. Chung, J. C. W. Mak, and J. K. W. Lam, "From Pulmonary Surfactant, Synthetic KL4 Peptide as Effective siRNA Delivery Vector for

Pulmonary Delivery," *Molecular Pharmaceutics*, vol. 14, no. 12, pp. 4606–4617, Dec. 2017, doi: 10.1021/acs.molpharmaceut.7b00725.

[296] K. A. Whitehead, R. Langer, and D. G. Anderson, "Knocking down barriers: advances in siRNA delivery," *Nature Reviews Drug Discovery*, vol. 8, no. 2, pp. 129–138, Feb. 2009, doi: 10.1038/nrd2742.

[297] M. Kato and R. Natarajan, "MicroRNAs in diabetic nephropathy: functions, biomarkers, and therapeutic targets," *Ann N Y Acad Sci*, vol. 1353, no. 1, pp. 72–88, Sep. 2015, doi: 10.1111/nyas.12758.

[298] D. Schiroli *et al.*, "Effective In Vivo Topical Delivery of siRNA and Gene Silencing in Intact Corneal Epithelium Using a Modified Cell-Penetrating Peptide," *Molecular Therapy - Nucleic Acids*, vol. 17, pp. 891–906, Sep. 2019, doi: 10.1016/j.omtn.2019.07.017.

[299] D. Peng *et al.*, "miR-142-3p suppresses uveal melanoma by targeting CDC25C, TGFβR1, GNAQ, WASL, and RAC1," *Cancer Management and Research*, vol. Volume 11, pp. 4729–4742, May 2019, doi: 10.2147/CMAR.S206461.

[300] L. Chen *et al.*, "Overexpression of the Oral Mucosa-Specific microRNA-31 Promotes Skin Wound Closure," *International Journal of Molecular Sciences*, vol. 20, no. 15, p. 3679, Jul. 2019, doi: 10.3390/ijms20153679.

[301] S. A. Shorter, A. S. Gollings, M. A. M. Gorringe-Pattrick, J. E. Coakley, P. D. R. Dyer, and S. C. W. Richardson, "The potential of toxin-based drug delivery systems for enhanced nucleic acid therapeutic delivery," *Expert Opinion on Drug Delivery*, vol. 14, no. 5, pp. 685–696, May 2017, doi: 10.1080/17425247.2016.1227781.

[302] G. Sailaja, H. HogenEsch, A. North, J. Hays, and S. K. Mittal, "Encapsulation of recombinant adenovirus into alginate microspheres circumvents vector-specific immune response," *Gene Therapy*, vol. 9, no. 24, pp. 1722–1729, Dec. 2002, doi: 10.1038/sj.gt.3301858.

[303] A. Breen, P. Strappe, A. Kumar, T. O'Brien, and A. Pandit, "Optimization of a fibrin scaffold for sustained release of an adenoviral gene vector," *Journal of Biomedical Materials Research Part A*, vol. 78A, no. 4, pp. 702–708, Sep. 2006, doi: 10.1002/jbm.a.30735.

[304] S. Laufs *et al.*, "Lentiviral vector integration sites in human NOD/SCID repopulating cells," *The Journal of Gene Medicine*, vol. 8, no. 10, pp. 1197–1207, Oct. 2006, doi: 10.1002/jgm.958.

[305] M. B. Mowa, C. Crowther, and P. Arbuthnot, "Therapeutic potential of adenoviral vectors for delivery of expressed RNAi activators," *Expert Opinion on Drug Delivery*, vol. 7, no. 12, pp. 1373–1385, Dec. 2010, doi: 10.1517/17425247.2010.533655.

[306] X. Chen, L. S. Mangala, C. Rodriguez-Aguayo, X. Kong, G. Lopez-Berestein, and A. K. Sood, "RNA interference-based therapy and its delivery systems," *Cancer and Metastasis Reviews*, vol. 37, no. 1, pp. 107–124, Mar. 2018, doi: 10.1007/s10555-017-9717-6.

[307] M. Rezaee, R. K. Oskuee, H. Nassirli, and B. Malaekeh-Nikouei, "Progress in the development of lipopolyplexes as efficient non-viral gene delivery systems," *Journal of Controlled Release*, vol. 236, pp. 1–14, Aug. 2016, doi: 10.1016/j.jconrel.2016.06.023.

[308] K. Buyens *et al.*, "Liposome based systems for systemic siRNA delivery: Stability in blood sets the requirements for optimal carrier design," *Journal of Controlled Release*, vol. 158, no. 3, pp. 362–370, Mar. 2012, doi: 10.1016/j.jconrel.2011.10.009.

[309] Z. Li *et al.*, "Lipofectamine 2000/siRNA complexes cause endoplasmic reticulum unfolded protein response in human endothelial cells," *Journal of Cellular Physiology*, vol. 234, no. 11, pp. 21166–21181, Nov. 2019, doi: 10.1002/jcp.28719.

[310] J. L. Santos, D. Pandita, J. Rodrigues, A. P. Pego, P. L. Granja, and H. Tomas, "Non-Viral Gene Delivery to Mesenchymal Stem Cells: Methods, Strategies and Application in Bone Tissue Engineering and Regeneration," *Current Gene Therapy*, vol. 11, no. 1, pp. 46–57, Feb. 2011, doi: 10.2174/156652311794520102.

[311] C. Tros de Ilarduya, Y. Sun, and N. Düzgüneş, "Gene delivery by lipoplexes and polyplexes," *European Journal of Pharmaceutical Sciences*, vol. 40, no. 3, pp. 159–170, Jun. 2010, doi: 10.1016/j.ejps.2010.03.019.

[312] A. Akinc, M. Thomas, A. M. Klibanov, and R. Langer, "Exploring polyethylenimine-mediated DNA transfection and the proton sponge hypothesis," *The Journal of Gene Medicine*, vol. 7, no. 5, pp. 657–663, May 2005, doi: 10.1002/jgm.696.

[313] A. Schroeder, C. G. Levins, C. Cortez, R. Langer, and D. G. Anderson, "Lipid-based nanotherapeutics for siRNA delivery," *Journal of Internal Medicine*, vol. 267, no. 1, pp. 9–21, Jan. 2010, doi: 10.1111/j.1365-2796.2009.02189.x.

[314] A. E. Labatut and G. Mattheolabakis, "Non-viral based miR delivery and recent developments," *European Journal of Pharmaceutics and Biopharmaceutics*, vol. 128, pp. 82–90, Jul. 2018, doi: 10.1016/j.ejpb.2018.04.018.

[315] A. Mokhtarzadeh *et al.*, "Biodegradable nano-polymers as delivery vehicles for therapeutic small non-coding ribonucleic acids," *Journal of Controlled Release*, vol. 245, pp. 116–126, Jan. 2017, doi: 10.1016/j.jconrel.2016.11.017.

[316] V. Iranpur Mobarakeh *et al.*, "Optimization of chitosan nanoparticles as an anti-HIV siRNA delivery vehicle," *International Journal of Biological Macromolecules*, vol. 129, pp. 305–315, May 2019, doi: 10.1016/j.ijbiomac.2019.02.036.

[317] O. Boussif *et al.*, "A versatile vector for gene and oligonucleotide transfer into cells in culture and in vivo: polyethylenimine.," *Proceedings of the National Academy of Sciences*, vol. 92, no. 16, pp. 7297–7301, Aug. 1995, doi: 10.1073/pnas.92.16.7297.

[318] A. Kwok and S. L. Hart, "Comparative structural and functional studies of nanoparticle formulations for DNA and siRNA delivery," *Nanomedicine: Nanotechnology, Biology and Medicine*, vol. 7, no. 2, pp. 210–219, Apr. 2011, doi: 10.1016/j.nano.2010.07.005.

[319] Y. Zhang, Z. Wang, and R. A. Gemeinhart, "Progress in microRNA delivery," *Journal of Controlled Release*, vol. 172, no. 3, pp. 962–974, Dec. 2013, doi: 10.1016/j.jconrel.2013.09.015.

[320] A. F. Ibrahim, U. Weirauch, M. Thomas, A. Grünweller, R. K. Hartmann, and A. Aigner, "MicroRNA Replacement Therapy for miR-145 and miR-33a Is Efficacious in a Model of Colon Carcinoma," *Cancer Research*, vol. 71, no. 15, pp. 5214–5224, Aug. 2011, doi: 10.1158/0008-5472.CAN-10-4645.

[321] B. Urban-Klein, S. Werth, S. Abuharbeid, F. Czubayko, and A. Aigner, "RNAi-mediated gene-targeting through systemic application of polyethylenimine (PEI)-complexed siRNA in vivo," *Gene Therapy*, vol. 12, no. 5, pp. 461–466, Mar. 2005, doi: 10.1038/sj.gt.3302425.

[322] M. Grzelinski *et al.*, "RNA Interference-Mediated Gene Silencing of Pleiotrophin Through Polyethylenimine-Complexed Small Interfering RNAs In Vivo Exerts Antitumoral Effects in Glioblastoma Xenografts," *Human Gene Therapy*, vol. 17, no. 7, pp. 751–766, Jul. 2006, doi: 10.1089/hum.2006.17.751.

[323] Y. Li, J. Zhang, B. Wang, Y. Shen, and A. Ouahab, "Co-delivery of siRNA and hypericin into cancer cells by hyaluronic acid modified PLGA-PEI nanoparticles," *Drug Development and Industrial Pharmacy*, vol. 42, no. 5, pp. 737–746, May 2016, doi: 10.3109/03639045.2015.1091469.

[324] L. C. Herrera and V. P. Shastri, "Silencing of GFP expression in human mesenchymal stem cells using quaternary polyplexes of siRNA-PEI with glycosaminoglycans and albumin," *Acta Biomaterialia*, vol. 99, pp. 397–411, Nov. 2019, doi: 10.1016/j.actbio.2019.09.006.

[325] M. Wagner, A. C. Rinkenauer, A. Schallon, and U. S. Schubert, "Opposites attract: influence of the molar mass of branched poly(ethylene imine) on biophysical characteristics of siRNA-based polyplexese," *RSC Advances*, vol. 3, no. 31, p. 12774, 2013, doi: 10.1039/c3ra42069h.

[326] V. Kafil and Y. Omidi, "Cytotoxic impacts of linear and branched polyethylenimine nanostructures in a431 cells.," *Bioimpacts*, vol. 1, no. 1, pp. 23–30, 2011, doi: 10.5681/bi.2011.004.

[327] B. I. Florea, C. Meaney, H. E. Junginger, and G. Borchard, "Transfection efficiency and toxicity of polyethylenimine in differentiated Calu-3 and nondifferentiated COS-1 cell cultures," *AAPS PharmSci*, vol. 4, no. 3, pp. 1–11, Sep. 2002, doi: 10.1208/ps040312.

[328] Y. Liu *et al.*, "PEG–PEI/siROCK2 Protects Against Aβ42-Induced Neurotoxicity in Primary Neuron Cells for Alzheimer Disease," *Cellular and Molecular Neurobiology*, vol. 35, no. 6, pp. 841–848, Aug. 2015, doi: 10.1007/s10571-015-0178-6.

[329] G.-Y. Chiou *et al.*, "Cationic polyurethanes-short branch PEI-mediated delivery of Mir145 inhibited epithelial–mesenchymal transdifferentiation and cancer stem-like properties and in lung adenocarcinoma," *Journal of Controlled Release*, vol. 159, no. 2, pp. 240–250, Apr. 2012, doi: 10.1016/j.jconrel.2012.01.014.

[330] D. Jere *et al.*, "Chitosan-graft-polyethylenimine for Akt1 siRNA delivery to lung cancer cells," *International Journal of Pharmaceutics*, vol. 378, no. 1–2, pp. 194–200, Aug. 2009, doi: 10.1016/j.ijpharm.2009.05.046.

[331] X. Zhang *et al.*, "Poly(ethylene glycol)-block-polyethylenimine copolymers as carriers for gene delivery: Effects of PEG molecular weight and PEGylation degree," *Journal of Biomedical Materials Research Part A*, vol. 84A, no. 3, pp. 795–804, Mar. 2008, doi: 10.1002/jbm.a.31343.

[332] M. Glodde, S. R. Sirsi, and G. J. Lutz, "Physiochemical Properties of Low and High Molecular Weight Poly(ethylene glycol)-Grafted Poly(ethylene imine) Copolymers and Their Complexes with Oligonucleotides," *Biomacromolecules*, vol. 7, no. 1, pp. 347–356, Jan. 2006, doi: 10.1021/bm050726t.

[333] H. Katas and C. Mui Wen, "Preparation and Characterisation of Highly Loaded Fluorescent Chitosan Nanoparticles," *ISRN Pharmaceutics*, vol. 2011, pp. 1–5, Nov. 2011, doi: 10.5402/2011/246162.

[334] T. Sato, T. Ishii, and Y. Okahata, "In vitro gene delivery mediated by chitosan. Effect of pH, serum, and molecular mass of chitosan on the transfection efficiency," *Biomaterials*, vol. 22, no. 15, pp. 2075–2080, Aug. 2001, doi: 10.1016/S0142-9612(00)00385-9.

[335] H. Katas and H. O. Alpar, "Development and characterisation of chitosan nanoparticles for siRNA delivery," *Journal of Controlled Release*, vol. 115, no. 2, pp. 216–225, Oct. 2006, doi: 10.1016/j.jconrel.2006.07.021.

[336] K. Sonaje, Y.-H. Lin, J.-H. Juang, S.-P. Wey, C.-T. Chen, and H.-W. Sung, "In vivo evaluation of safety and efficacy of self-assembled nanoparticles for oral insulin delivery," *Biomaterials*, vol. 30, no. 12, pp. 2329–2339, Apr. 2009, doi: 10.1016/j.biomaterials.2008.12.066.

[337] T. Kean and M. Thanou, "Biodegradation, biodistribution and toxicity of chitosan," *Advanced Drug Delivery Reviews*, vol. 62, no. 1, pp. 3–11, Jan. 2010, doi: 10.1016/j.addr.2009.09.004.

[338] M. Huang, C.-W. Fong, E. Khor, and L.-Y. Lim, "Transfection efficiency of chitosan vectors: Effect of polymer molecular weight and degree of deacetylation," *Journal of Controlled Release*, vol. 106, no. 3, pp. 391–406, Sep. 2005, doi: 10.1016/j.jconrel.2005.05.004.

[339] T. Sato, T. Ishii, and Y. Okahata, "In vitro gene delivery mediated by chitosan. Effect of pH, serum, and molecular mass of chitosan on the transfection efficiency," *Biomaterials*, vol. 22, no. 15, pp. 2075–2080, Aug. 2001, doi: 10.1016/S0142-9612(00)00385-9.

[340] Y. Cao, Y. F. Tan, Y. S. Wong, M. W. J. Liew, and S. Venkatraman, "Recent Advances in Chitosan-Based Carriers for Gene Delivery," *Marine Drugs*, vol. 17, no. 6, p. 381, Jun. 2019, doi: 10.3390/md17060381.

[341] K. A. Howard *et al.*, "RNA Interference in Vitro and in Vivo Using a Novel Chitosan/siRNA Nanoparticle System," *Molecular Therapy*, vol. 14, no. 4, pp. 476–484, Oct. 2006, doi: 10.1016/j.ymthe.2006.04.010.

[342] K. Azuma *et al.*, "Chitin, Chitosan, and Its Derivatives for Wound Healing: Old and New Materials," *Journal of Functional Biomaterials*, vol. 6, no. 1, pp. 104–142, Mar. 2015, doi: 10.3390/jfb6010104.

[343] X. Liu *et al.*, "The influence of polymeric properties on chitosan/siRNA nanoparticle formulation and gene silencing," *Biomaterials*, vol. 28, no. 6, pp. 1280–1288, Feb. 2007, doi: 10.1016/j.biomaterials.2006.11.004.

[344] E. E. Esmaeilzadeh Gharehdaghi *et al.*, "Chitosan Nanoparticles for siRNA Delivery: Optimization of Processing/Formulation Parameters," *Nucleic Acid Therapeutics*, vol. 24, no. 6, pp. 420–427, Dec. 2014, doi: 10.1089/nat.2014.0484.

[345] K. A. Howard *et al.*, "RNA Interference in Vitro and in Vivo Using a Novel Chitosan/siRNA Nanoparticle System," *Molecular Therapy*, vol. 14, no. 4, pp. 476–484, Oct. 2006, doi: 10.1016/j.ymthe.2006.04.010.

[346] M. Alameh *et al.*, "siRNA Delivery with Chitosan: Influence of Chitosan Molecular Weight, Degree of Deacetylation, and Amine to Phosphate Ratio on in Vitro Silencing Efficiency,

Hemocompatibility, Biodistribution, and in Vivo Efficacy," *Biomacromolecules*, vol. 19, no. 1, pp. 112–131, Jan. 2018, doi: 10.1021/acs.biomac.7b01297.

[347] H. Katas and H. O. Alpar, "Development and characterisation of chitosan nanoparticles for siRNA delivery," *Journal of Controlled Release*, vol. 115, no. 2, pp. 216–225, Oct. 2006, doi: 10.1016/j.jconrel.2006.07.021.

[348] H.-D. Lu, H.-Q. Zhao, K. Wang, and L.-L. Lv, "Novel hyaluronic acid–chitosan nanoparticles as non-viral gene delivery vectors targeting osteoarthritis," *International Journal of Pharmaceutics*, vol. 420, no. 2, pp. 358–365, Nov. 2011, doi: 10.1016/j.ijpharm.2011.08.046.

[349] M. Huang, C.-W. Fong, E. Khor, and L.-Y. Lim, "Transfection efficiency of chitosan vectors: Effect of polymer molecular weight and degree of deacetylation," *Journal of Controlled Release*, vol. 106, no. 3, pp. 391–406, Sep. 2005, doi: 10.1016/j.jconrel.2005.05.004.

[350] M. Huang, E. Khor, and L.-Y. Lim, "Uptake and Cytotoxicity of Chitosan Molecules and Nanoparticles: Effects of Molecular Weight and Degree of Deacetylation," *Pharmaceutical Research*, vol. 21, no. 2, pp. 344–353, Feb. 2004, doi: 10.1023/B:PHAM.0000016249.52831.a5.

[351] S. Maiz-Fernández, L. Pérez-Álvarez, U. Silván, J. L. Vilas-Vilela, and S. Lanceros-Méndez, "pH-Induced 3D Printable Chitosan Hydrogels for Soft Actuation," *Polymers (Basel)*, vol. 14, no. 3, p. 650, Feb. 2022, doi: 10.3390/polym14030650.

[352] C. He, L. Yin, C. Tang, and C. Yin, "Trimethyl Chitosan-Cysteine Nanoparticles for Systemic Delivery of TNF-α siRNA via Oral and Intraperitoneal Routes," *Pharmaceutical Research*, vol. 30, no. 10, pp. 2596–2606, Oct. 2013, doi: 10.1007/s11095-013-1086-4.

[353] P. Eivazy *et al.*, "The impact of the codelivery of drug-siRNA by trimethyl chitosan nanoparticles on the efficacy of chemotherapy for metastatic breast cancer cell line (MDA-MB-231)," *Artificial Cells, Nanomedicine, and Biotechnology*, vol. 45, no. 5, pp. 889–896, Jul. 2017, doi: 10.1080/21691401.2016.1185727.

[354] M. Mir, N. Ahmed, and A. ur Rehman, "Recent applications of PLGA based nanostructures in drug delivery," *Colloids and Surfaces B: Biointerfaces*, vol. 159, pp. 217–231, Nov. 2017, doi: 10.1016/j.colsurfb.2017.07.038.

[355] F. Alexis, "Factors affecting the degradation and drug-release mechanism of poly(lactic acid) and poly[(lactic acid)-co-(glycolic acid)]," *Polymer International*, vol. 54, no. 1, pp. 36–46, Jan. 2005, doi: 10.1002/pi.1697.

[356] A. Rothen-Weinhold, K. Besseghir, and R. Gurny, "Analysis of the influence of polymer characteristics and core loading on the in vivo release of a somatostatin analogue,"

European Journal of Pharmaceutical Sciences, vol. 5, no. 6, pp. 303–313, Nov. 1997, doi: 10.1016/S0928-0987(97)00022-5.

[357] S. Y. Jeon *et al.*, "Co-delivery of Cbfa-1-targeting siRNA and SOX9 protein using PLGA nanoparticles to induce chondrogenesis of human mesenchymal stem cells," *Biomaterials*, vol. 35, no. 28, pp. 8236–8248, Sep. 2014, doi: 10.1016/j.biomaterials.2014.05.092.

[358] S.-J. Gwak, Y. Yun, D. H. Yoon, K. N. Kim, and Y. Ha, "Therapeutic Use of 3β-[N-(N',N'-Dimethylaminoethane) Carbamoyl] Cholesterol-Modified PLGA Nanospheres as Gene Delivery Vehicles for Spinal Cord Injury," *PLOS ONE*, vol. 11, no. 1, p. e0147389, Jan. 2016, doi: 10.1371/journal.pone.0147389.

[359] D. K. Jensen *et al.*, "Design of an inhalable dry powder formulation of DOTAP-modified PLGA nanoparticles loaded with siRNA," *Journal of Controlled Release*, vol. 157, no. 1, pp. 141–148, Jan. 2012, doi: 10.1016/j.jconrel.2011.08.011.

[360] Q. Li *et al.*, "Multifunctional REDV-G-TAT-G-NLS-Cys peptide sequence conjugated gene carriers to enhance gene transfection efficiency in endothelial cells," *Colloids and Surfaces B: Biointerfaces*, vol. 184, p. 110510, Dec. 2019, doi: 10.1016/j.colsurfb.2019.110510.

[361] A. O'Donnell *et al.*, "Intranasal and intravenous administration of octa-arginine modified poly(lactic-co-glycolic acid) nanoparticles facilitates central nervous system delivery of loperamide," *Journal of Pharmacy and Pharmacology*, vol. 67, no. 4, pp. 525–536, Mar. 2015, doi: 10.1111/jphp.12347.

[362] D. W. Hutmacher, "Scaffold design and fabrication technologies for engineering tissues--state of the art and future perspectives.," *J Biomater Sci Polym Ed*, vol. 12, no. 1, pp. 107–24, 2001, doi: 10.1163/156856201744489.

[363] B. Subia, J. Kundu, and S. C., "Biomaterial Scaffold Fabrication Techniques for Potential Tissue Engineering Applications," *Tissue Engineering*, no. 3, 2010, doi: 10.5772/8581.

[364] T. Lu, Y. Li, and T. Chen, "Techniques for fabrication and construction of three-dimensional scaffolds for tissue engineering," *International Journal of Nanomedicine*, p. 337, Jan. 2013, doi: 10.2147/IJN.S38635.

[365] M. Rahmati *et al.*, "Electrospinning for tissue engineering applications," *Progress in Materials Science*, vol. 117, p. 100721, Apr. 2021, doi: 10.1016/j.pmatsci.2020.100721.

[366] J. Xue, T. Wu, Y. Dai, and Y. Xia, "Electrospinning and Electrospun Nanofibers: Methods, Materials, and Applications," *Chemical Reviews*, vol. 119, no. 8, pp. 5298–5415, Apr. 2019, doi: 10.1021/acs.chemrev.8b00593.

[367] M. Heidari, S. H. Bahrami, M. Ranjbar-Mohammadi, and P. B. Milan, "Smart electrospun nanofibers containing PCL/gelatin/graphene oxide for application in nerve tissue engineering," *Materials Science and Engineering: C*, vol. 103, p. 109768, Oct. 2019, doi: 10.1016/j.msec.2019.109768.

[368] T. Jiang, E. J. Carbone, K. W.-H. Lo, and C. T. Laurencin, "Electrospinning of polymer nanofibers for tissue regeneration," *Progress in Polymer Science*, vol. 46, pp. 1–24, Jul. 2015, doi: 10.1016/j.progpolymsci.2014.12.001.

[369] Y.-N. Jiang, H.-Y. Mo, and D.-G. Yu, "Electrospun drug-loaded core–sheath PVP/zein nanofibers for biphasic drug release," *International Journal of Pharmaceutics*, vol. 438, no. 1–2, pp. 232–239, Nov. 2012, doi: 10.1016/j.ijpharm.2012.08.053.

[370] S. Bae *et al.*, "Heparin-Eluting Electrospun Nanofiber Yarns for Antithrombotic Vascular Sutures," *ACS Applied Materials & Interfaces*, vol. 10, no. 10, pp. 8426–8435, Mar. 2018, doi: 10.1021/acsami.7b14888.

[371] M. Rahmati *et al.*, "Electrospinning for tissue engineering applications," *Progress in Materials Science*, vol. 117, p. 100721, Apr. 2021, doi: 10.1016/j.pmatsci.2020.100721.

[372] D. Radke *et al.*, "Tissue Engineering at the Blood-Contacting Surface: A Review of Challenges and Strategies in Vascular Graft Development," *Advanced Healthcare Materials*, vol. 7, no. 15, p. 1701461, Aug. 2018, doi: 10.1002/adhm.201701461.

[373] K. N. Ekdahl *et al.*, "Innate immunity activation on biomaterial surfaces: A mechanistic model and coping strategies," *Advanced Drug Delivery Reviews*, vol. 63, no. 12, pp. 1042–1050, Sep. 2011, doi: 10.1016/j.addr.2011.06.012.

[374] X. Ren *et al.*, "Surface modification and endothelialization of biomaterials as potential scaffolds for vascular tissue engineering applications," *Chemical Society Reviews*, vol. 44, no. 15, pp. 5680–5742, 2015, doi: 10.1039/C4CS00483C.

[375] S. J. Phillips, "Thrombogenic Influence of Biomaterials in Patients with the Omni Series Heart Valve: Pyrolytic Carbon Versus Titanium," *ASAIO Journal*, vol. 47, no. 5, pp. 429–431, Sep. 2001, doi: 10.1097/00002480-200109000-00002.

[376] F. Zhou *et al.*, "Nanofiber-mediated microRNA-126 delivery to vascular endothelial cells for blood vessel regeneration," *Acta Biomaterialia*, vol. 43, pp. 303–313, Oct. 2016, doi: 10.1016/j.actbio.2016.07.048.

[377] F. Zhou *et al.*, "Electrospun membranes of PELCL/PCL-REDV loading with miRNA-126 for enhancement of vascular endothelial cell adhesion and proliferation," *Materials Science and Engineering C*, vol. 85, no. June 2017, pp. 37–46, 2018, doi: 10.1016/j.msec.2017.12.005.

[378] M. S. Hulshoff, G. del Monte-Nieto, J. Kovacic, and G. Krenning, "Non-coding RNA in endothelial-to-mesenchymal transition," *Cardiovascular Research*, vol. 115, no. 12, pp. 1716–1731, Oct. 2019, doi: 10.1093/cvr/cvz211.

[379] A. Martello *et al.*, "Phenotypic miRNA Screen Identifies miR-26b to Promote the Growth and Survival of Endothelial Cells," *Molecular Therapy - Nucleic Acids*, vol. 13, pp. 29–43, Dec. 2018, doi: 10.1016/j.omtn.2018.08.006.

[380] R. P. Hickerson *et al.*, "Stability Study of Unmodified siRNA and Relevance to Clinical Use," *Oligonucleotides*, vol. 18, no. 4, pp. 345–354, Dec. 2008, doi: 10.1089/oli.2008.0149.

[381] P. Calvo, C. Remunàn-Lòpez, J. L. Vila-Jato, and M. J. Alonso, "Novel hydrophilic chitosan-polyethylene oxide nanoparticles as protein carriers," *Journal of Applied Polymer Science*, vol. 63, no. 1, pp. 125–132, Jan. 1997, doi: 10.1002/(SICI)1097-4628(19970103)63:1<125::AID-APP13>3.0.CO;2-4.

[382] F. Rázga, D. Vnuková, V. Némethová, P. Mazancová, and I. Lacík, "Preparation of chitosan-TPP sub-micron particles: Critical evaluation and derived recommendations," *Carbohydrate Polymers*, vol. 151, pp. 488–499, Oct. 2016, doi: 10.1016/j.carbpol.2016.05.092.

[383] P. Erbacher, S. Zou, T. Bettinger, A. M. Steffan, and J. S. Remy, "Chitosan-based vector/DNA complexes for gene delivery: biophysical characteristics and transfection ability.," *Pharm Res*, vol. 15, no. 9, pp. 1332–9, Sep. 1998, doi: 10.1023/a:1011981000671.

[384] H. Katas and H. O. Alpar, "Development and characterisation of chitosan nanoparticles for siRNA delivery," *Journal of Controlled Release*, vol. 115, no. 2, pp. 216–225, Oct. 2006, doi: 10.1016/j.jconrel.2006.07.021.

[385] M. P. Lisanti *et al.*, "Characterization of caveolin-rich membrane domains isolated from an endothelial-rich source: implications for human disease.," *Journal of Cell Biology*, vol. 126, no. 1, pp. 111–126, Jul. 1994, doi: 10.1083/jcb.126.1.111.

[386] P. M. Azizi *et al.*, "Clathrin-dependent entry and vesicle-mediated exocytosis define insulin transcytosis across microvascular endothelial cells," *Molecular Biology of the Cell*, vol. 26, no. 4, pp. 740–750, Feb. 2015, doi: 10.1091/mbc.E14-08-1307.

[387] I. Ricard, M. D. Payet, and G. Dupuis, "VCAM-1 is internalized by a clathrin-related pathway in human endothelial cells but its α4β1 integrin counter-receptor remains associated with the plasma membrane in human T lymphocytes," *European Journal of Immunology*, vol. 28, no. 5, pp. 1708–1718, May 1998, doi: 10.1002/(SICI)1521-4141(199805)28:05<1708::AID-IMMU1708>3.0.CO;2-Y.

201

[388] E. Tkachenko, E. Lutgens, R.-V. Stan, and M. Simons, "Fibroblast growth factor 2 endocytosis in endothelial cells proceed via syndecan-4-dependent activation of Rac1 and a Cdc42-dependent macropinocytic pathway," *Journal of Cell Science*, vol. 117, no. 15, pp. 3189–3199, Jul. 2004, doi: 10.1242/jcs.01190.

[389] S. Bhattacharya, D. Roxbury, X. Gong, D. Mukhopadhyay, and A. Jagota, "DNA Conjugated SWCNTs Enter Endothelial Cells via Rac1 Mediated Macropinocytosis," *Nano Letters*, vol. 12, no. 4, pp. 1826–1830, Apr. 2012, doi: 10.1021/nl204058u.

[390] M. Tamaru, H. Akita, T. Fujiwara, K. Kajimoto, and H. Harashima, "Leptin-derived peptide, a targeting ligand for mouse brain-derived endothelial cells via macropinocytosis," *Biochemical and Biophysical Research Communications*, vol. 394, no. 3, pp. 587–592, Apr. 2010, doi: 10.1016/j.bbrc.2010.03.024.

[391] K. Y. Fung, C. Wang, S. Nyegaard, B. Heit, G. D. Fairn, and W. L. Lee, "SR-BI Mediated Transcytosis of HDL in Brain Microvascular Endothelial Cells Is Independent of Caveolin, Clathrin, and PDZK1," *Frontiers in Physiology*, vol. 8, Oct. 2017, doi: 10.3389/fphys.2017.00841.

[392] A. L. Zhou *et al.*, "Apolipoprotein A-I Crosses the Blood-Brain Barrier through Clathrin-Independent and Cholesterol-Mediated Endocytosis," *Journal of Pharmacology and Experimental Therapeutics*, vol. 369, no. 3, pp. 481–488, Jun. 2019, doi: 10.1124/jpet.118.254201.

[393] C. Aslan, N. Çelebi, İ. T. Değim, A. Atak, and Ç. Özer, "Development of Interleukin-2 Loaded Chitosan-Based Nanogels Using Artificial Neural Networks and Investigating the Effects on Wound Healing in Rats," *AAPS PharmSciTech*, vol. 18, no. 4, pp. 1019–1030, May 2017, doi: 10.1208/s12249-016-0662-4.

[394] J. Antoniou, F. Liu, H. Majeed, J. Qi, W. Yokoyama, and F. Zhong, "Physicochemical and morphological properties of size-controlled chitosan–tripolyphosphate nanoparticles," *Colloids and Surfaces A: Physicochemical and Engineering Aspects*, vol. 465, pp. 137–146, Jan. 2015, doi: 10.1016/j.colsurfa.2014.10.040.

[395] F. Rázga, D. Vnuková, V. Némethová, P. Mazancová, and I. Lacík, "Preparation of chitosan-TPP sub-micron particles: Critical evaluation and derived recommendations," *Carbohydrate Polymers*, vol. 151, pp. 488–499, Oct. 2016, doi: 10.1016/j.carbpol.2016.05.092.

[396] H. Katas and H. O. Alpar, "Development and characterisation of chitosan nanoparticles for siRNA delivery," *Journal of Controlled Release*, vol. 115, no. 2, pp. 216–225, Oct. 2006, doi: 10.1016/j.jconrel.2006.07.021.

[397] X. Chen *et al.*, "Nanoparticle delivery of stable miR-199a-5p agomir improves the osteogenesis of human mesenchymal stem cells via the HIF1a pathway," *Biomaterials*, vol. 53, pp. 239–250, Jun. 2015, doi: 10.1016/j.biomaterials.2015.02.071.

[398] A. Rampino, M. Borgogna, P. Blasi, B. Bellich, and A. Cesàro, "Chitosan nanoparticles: Preparation, size evolution and stability," *International Journal of Pharmaceutics*, vol. 455, no. 1–2, pp. 219–228, Oct. 2013, doi: 10.1016/j.ijpharm.2013.07.034.

[399] M. Huang, C.-W. Fong, E. Khor, and L.-Y. Lim, "Transfection efficiency of chitosan vectors: Effect of polymer molecular weight and degree of deacetylation," *Journal of Controlled Release*, vol. 106, no. 3, pp. 391–406, Sep. 2005, doi: 10.1016/j.jconrel.2005.05.004.

[400] M. Carrabba, "Novel approaches of scaffold fabrication for vascular tissue engineering," 2019.

[401] J. He, Y. Liang, M. Shi, and B. Guo, "Anti-oxidant electroactive and antibacterial nanofibrous wound dressings based on poly(ε-caprolactone)/quaternized chitosan-graft-polyaniline for full-thickness skin wound healing," *Chemical Engineering Journal*, vol. 385, p. 123464, Apr. 2020, doi: 10.1016/j.cej.2019.123464.

[402] A. Cipitria, A. Skelton, T. R. Dargaville, P. D. Dalton, and D. W. Hutmacher, "Design, fabrication and characterization of PCL electrospun scaffolds—a review," *Journal of Materials Chemistry*, vol. 21, no. 26, p. 9419, 2011, doi: 10.1039/c0jm04502k.

[403] C. del Gaudio, M. Grigioni, A. Bianco, and G. de Angelis, "Electrospun Bioresorbable Heart Valve Scaffold for Tissue Engineering," *The International Journal of Artificial Organs*, vol. 31, no. 1, pp. 68–75, Jan. 2008, doi: 10.1177/039139880803100110.

[404] M. A. Woodruff and D. W. Hutmacher, "The return of a forgotten polymer—Polycaprolactone in the 21st century," *Progress in Polymer Science*, vol. 35, no. 10, pp. 1217–1256, Oct. 2010, doi: 10.1016/j.progpolymsci.2010.04.002.

[405] C. del Gaudio, A. Bianco, and M. Grigioni, "Electrospun bioresorbable trileaflet heart valve prosthesis for tissue engineering: in vitro functional assessment of a pulmonary cardiac valve design.," *Annali dell'Istituto superiore di sanita*, vol. 44, no. 2, pp. 178–86, 2008, [Online]. Available: http://www.ncbi.nlm.nih.gov/pubmed/18660567

[406] J. C. Middleton and A. J. Tipton, "Synthetic biodegradable polymers as orthopedic devices," *Biomaterials*, vol. 21, no. 23, pp. 2335–2346, Dec. 2000, doi: 10.1016/S0142-9612(00)00101-0.

[407] A. L. Y. Nachlas *et al.*, "A multilayered valve leaflet promotes cell-laden collagen type I production and aortic valve hemodynamics," *Biomaterials*, vol. 240, p. 119838, May 2020, doi: 10.1016/j.biomaterials.2020.119838.

[408] J. Zakko *et al.*, "Development of Tissue Engineered Heart Valves for Percutaneous Transcatheter Delivery in a Fetal Ovine Model," *JACC: Basic to Translational Science*, vol. 5, no. 8, pp. 815–828, Aug. 2020, doi: 10.1016/j.jacbts.2020.06.009.

[409] B. Feng, H. Tu, H. Yuan, H. Peng, and Y. Zhang, "Acetic-Acid-Mediated Miscibility toward Electrospinning Homogeneous Composite Nanofibers of GT/PCL," *Biomacromolecules*, vol. 13, no. 12, pp. 3917–3925, Dec. 2012, doi: 10.1021/bm3009389.

[410] R. Bilkhu, M. Jahangiri, and C. M. Otto, "Patient-prosthesis mismatch following aortic valve replacement," *Heart*, vol. 105, no. Suppl 2, pp. s28–s33, Mar. 2019, doi: 10.1136/heartjnl-2018-313515.

[411] H. Aoki, H. Miyoshi, and Y. Yamagata, "Electrospinning of gelatin nanofiber scaffolds with mild neutral cosolvents for use in tissue engineering," *Polymer Journal*, vol. 47, no. 3, pp. 267–277, Mar. 2015, doi: 10.1038/pj.2014.94.

[412] Y. Zhang, H. Ouyang, C. T. Lim, S. Ramakrishna, and Z.-M. Huang, "Electrospinning of gelatin fibers and gelatin/PCL composite fibrous scaffolds," *Journal of Biomedical Materials Research*, vol. 72B, no. 1, pp. 156–165, Jan. 2005, doi: 10.1002/jbm.b.30128.

[413] W. Fu *et al.*, "Electrospun gelatin/PCL and collagen/PLCL scaffolds for vascular tissue engineering," *International Journal of Nanomedicine*, p. 2335, May 2014, doi: 10.2147/IJN.S61375.

[414] V. V. Alvino *et al.*, "In Vitro and In Vivo Preclinical Testing of Pericyte-Engineered Grafts for the Correction of Congenital Heart Defects," *J Am Heart Assoc*, vol. 9, no. 4, Feb. 2020, doi: 10.1161/JAHA.119.014214.

[415] M. TAKEICHI and T. OKADA, "Roles of magnesium and calcium ions in cell-to-substrate adhesion," *Experimental Cell Research*, vol. 74, no. 1, pp. 51–60, Sep. 1972, doi: 10.1016/0014-4827(72)90480-6.

[416] C.-J. S. Edgell *et al.*, "Endothelium specific Weibel-Palade bodies in a continuous human cell line, EA.hy926," *In Vitro Cellular & Developmental Biology*, vol. 26, no. 12, pp. 1167–1172, Dec. 1990, doi: 10.1007/BF02623694.

[417] K. Ahn, S. Pan, K. Beningo, and D. Hupe, "A permanent human cell line (EA.hy926) preserves the characteristics of endothelin converting enzyme from primary human umbilical vein endothelial cells," *Life Sciences*, vol. 56, no. 26, pp. 2331–2341, May 1995, doi: 10.1016/0024-3205(95)00227-W.

[418] F. Cardarelli *et al.*, "The intracellular trafficking mechanism of Lipofectamine-based transfection reagents and its implication for gene delivery," *Scientific Reports*, vol. 6, no. 1, p. 25879, Sep. 2016, doi: 10.1038/srep25879.

[419] P. Han, D. Hanlon, O. Sobolev, R. Chaudhury, and R. L. Edelson, "Ex vivo dendritic cell generation—A critical comparison of current approaches," 2019, pp. 251–307. doi: 10.1016/bs.ircmb.2019.10.003.

[420] M. Bauer *et al.*, "Toxic Effects of Lipid-Mediated Gene Transfer in Ventral Mesencephalic Explant Cultures," *Basic <html_ent glyph="@amp;" ascii="&"/> Clinical Pharmacology <html_ent glyph="@amp;" ascii="&"/> Toxicology*, vol. 98, no. 4, pp. 395–400, Apr. 2006, doi: 10.1111/j.1742-7843.2006.pto_310.x.

[421] S. Brodie *et al.*, "The novel long non-coding RNA TALNEC2, regulates tumor cell growth and the stemness and radiation response of glioma stem cells," *Oncotarget*, vol. 8, no. 19, pp. 31785–31801, May 2017, doi: 10.18632/oncotarget.15991.

[422] K. Ouyang, J. Li, H. Huang, Q. Que, P. Li, and X. Chen, "A simple method for RNA isolation from various tissues of the tree Neolamarckia cadamba," *Biotechnology & Biotechnological Equipment*, vol. 28, no. 6, pp. 1008–1013, Nov. 2014, doi: 10.1080/13102818.2014.981086.

[423] L. Wang and J. P. Stegemann, "Extraction of high quality RNA from polysaccharide matrices using cetlytrimethylammonium bromide," *Biomaterials*, vol. 31, no. 7, pp. 1612–1618, Mar. 2010, doi: 10.1016/j.biomaterials.2009.11.024.

[424] A. Merzouki, "Chitosanase-based method for RNA isolation from cells transfected with chitosan/siRNA nanocomplexes for real-time RT-PCR in gene silencing," *International Journal of Nanomedicine*, p. 473, Jul. 2010, doi: 10.2147/IJN.S10879.

[425] H.-Q. Mao *et al.*, "Chitosan-DNA nanoparticles as gene carriers: synthesis, characterization and transfection efficiency," *Journal of Controlled Release*, vol. 70, no. 3, pp. 399–421, Feb. 2001, doi: 10.1016/S0168-3659(00)00361-8.

[426] A. Almalik, P. J. Day, and N. Tirelli, "HA-Coated Chitosan Nanoparticles for CD44-Mediated Nucleic Acid Delivery," *Macromolecular Bioscience*, vol. 13, no. 12, pp. 1671–1680, Dec. 2013, doi: 10.1002/mabi.201300302.

[427] J. K. W. Lam, M. Y. T. Chow, Y. Zhang, and S. W. S. Leung, "siRNA Versus miRNA as Therapeutics for Gene Silencing," *Molecular Therapy - Nucleic Acids*, vol. 4, p. e252, 2015, doi: 10.1038/mtna.2015.23.

[428] B. P. Lewis, C. B. Burge, and D. P. Bartel, "Conserved Seed Pairing, Often Flanked by Adenosines, Indicates that Thousands of Human Genes are MicroRNA Targets," *Cell*, vol. 120, no. 1, pp. 15–20, Jan. 2005, doi: 10.1016/j.cell.2004.12.035.

[429] M. Pomaznoy, B. Ha, and B. Peters, "GOnet: a tool for interactive Gene Ontology analysis," *BMC Bioinformatics*, vol. 19, no. 1, p. 470, Dec. 2018, doi: 10.1186/s12859-018-2533-3.

[430] J. Antoniou, F. Liu, H. Majeed, J. Qi, W. Yokoyama, and F. Zhong, "Physicochemical and morphological properties of size-controlled chitosan–tripolyphosphate nanoparticles," *Colloids and Surfaces A: Physicochemical and Engineering Aspects*, vol. 465, pp. 137–146, Jan. 2015, doi: 10.1016/j.colsurfa.2014.10.040.

[431] A. Fàbregas *et al.*, "Impact of physical parameters on particle size and reaction yield when using the ionic gelation method to obtain cationic polymeric chitosan–tripolyphosphate nanoparticles," *International Journal of Pharmaceutics*, vol. 446, no. 1–2, pp. 199–204, Mar. 2013, doi: 10.1016/j.ijpharm.2013.02.015.

[432] S. D. Conner and S. L. Schmid, "Regulated portals of entry into the cell," *Nature*, vol. 422, no. 6927, pp. 37–44, Mar. 2003, doi: 10.1038/nature01451.

[433] J. Dausend *et al.*, "Uptake Mechanism of Oppositely Charged Fluorescent Nanoparticles in HeLa Cells," *Macromolecular Bioscience*, vol. 8, no. 12, pp. 1135–1143, Dec. 2008, doi: 10.1002/mabi.200800123.

[434] J. A. Swanson and C. Watts, "Macropinocytosis," *Trends in Cell Biology*, vol. 5, no. 11, pp. 424–428, Nov. 1995, doi: 10.1016/S0962-8924(00)89101-1.

[435] J. Zhu *et al.*, "Size-dependent cellular uptake efficiency, mechanism, and cytotoxicity of silica nanoparticles toward HeLa cells," *Talanta*, vol. 107, pp. 408–415, Mar. 2013, doi: 10.1016/j.talanta.2013.01.037.

[436] F. Lu, S.-H. Wu, Y. Hung, and C.-Y. Mou, "Size Effect on Cell Uptake in Well-Suspended, Uniform Mesoporous Silica Nanoparticles," *Small*, vol. 5, no. 12, pp. 1408–1413, Jun. 2009, doi: 10.1002/smll.200900005.

[437] K. Yin Win and S.-S. Feng, "Effects of particle size and surface coating on cellular uptake of polymeric nanoparticles for oral delivery of anticancer drugs," *Biomaterials*, vol. 26, no. 15, pp. 2713–2722, May 2005, doi: 10.1016/j.biomaterials.2004.07.050.

[438] T. Sato, T. Ishii, and Y. Okahata, "In vitro gene delivery mediated by chitosan. Effect of pH, serum, and molecular mass of chitosan on the transfection efficiency," *Biomaterials*, vol. 22, no. 15, pp. 2075–2080, Aug. 2001, doi: 10.1016/S0142-9612(00)00385-9.

[439] M. Huang, E. Khor, and L.-Y. Lim, "Uptake and Cytotoxicity of Chitosan Molecules and Nanoparticles: Effects of Molecular Weight and Degree of Deacetylation," *Pharmaceutical Research*, vol. 21, no. 2, pp. 344–353, Feb. 2004, doi: 10.1023/B:PHAM.0000016249.52831.a5.

[440] X. Zhang *et al.*, "Poly(ethylene glycol)-block-polyethylenimine copolymers as carriers for gene delivery: Effects of PEG molecular weight and PEGylation degree," *Journal of Biomedical Materials Research Part A*, vol. 84A, no. 3, pp. 795–804, Jan. 2008, doi: 10.1002/jbm.a.31343.

[441] F. Hu *et al.*, "The exogenous delivery of microRNA-449b-5p using spermidine-PLGA nanoparticles efficiently decreases hepatic injury," *RSC Advances*, vol. 9, no. 60, pp. 35135–35144, 2019, doi: 10.1039/C9RA06129K.

[442] K. A. Woodrow, Y. Cu, C. J. Booth, J. K. Saucier-Sawyer, M. J. Wood, and W. Mark Saltzman, "Intravaginal gene silencing using biodegradable polymer nanoparticles densely loaded with small-interfering RNA," *Nature Materials*, vol. 8, no. 6, pp. 526–533, Jun. 2009, doi: 10.1038/nmat2444.

[443] F. Hu *et al.*, "The exogenous delivery of microRNA-449b-5p using spermidine-PLGA nanoparticles efficiently decreases hepatic injury," *RSC Advances*, vol. 9, no. 60, pp. 35135–35144, 2019, doi: 10.1039/C9RA06129K.

[444] R. Devulapally, K. Foygel, T. v Sekar, J. K. Willmann, and R. Paulmurugan, "Gemcitabine and Antisense-microRNA Co-encapsulated PLGA–PEG Polymer Nanoparticles for Hepatocellular Carcinoma Therapy," *ACS Applied Materials & Interfaces*, vol. 8, no. 49, pp. 33412–33422, Dec. 2016, doi: 10.1021/acsami.6b08153.

[445] G. Liang *et al.*, "PLGA-based gene delivering nanoparticle enhance suppression effect of miRNA in HePG2 cells," *Nanoscale Research Letters*, vol. 6, no. 1, p. 447, 2011, doi: 10.1186/1556-276X-6-447.

[446] O. Germershaus, S. Mao, J. Sitterberg, U. Bakowsky, and T. Kissel, "Gene delivery using chitosan, trimethyl chitosan or polyethylenglycol-graft-trimethyl chitosan block copolymers: Establishment of structure–activity relationships in vitro," *Journal of Controlled Release*, vol. 125, no. 2, pp. 145–154, Jan. 2008, doi: 10.1016/j.jconrel.2007.10.013.

[447] N. Brodusch *et al.*, "Scanning Electron Microscopy versus Transmission Electron Microscopy for Material Characterization: A Comparative Study on High-Strength Steels," *Scanning*, vol. 2021, pp. 1–19, May 2021, doi: 10.1155/2021/5511618.

[448] M. Winey, J. B. Meehl, E. T. O'Toole, and T. H. Giddings, "Conventional transmission electron microscopy," *Molecular Biology of the Cell*, vol. 25, no. 3, pp. 319–323, Feb. 2014, doi: 10.1091/mbc.e12-12-0863.

[449] A. Rosenauer, F. F. Krause, K. Müller, M. Schowalter, and T. Mehrtens, "Conventional Transmission Electron Microscopy Imaging beyond the Diffraction and Information

Limits," *Physical Review Letters*, vol. 113, no. 9, p. 096101, Aug. 2014, doi: 10.1103/PhysRevLett.113.096101.

[450] R. J. Keyse, A. J. Garratt-Reed, P. J. Goodhew, and G. W. Lorimer, *Introduction to Scanning Transmission Electron Microscopy*. Routledge, 2018. doi: 10.1201/9780203749890.

[451] N. R. Lugg, G. Kothleitner, N. Shibata, and Y. Ikuhara, "On the quantitativeness of EDS STEM," *Ultramicroscopy*, vol. 151, pp. 150–159, Apr. 2015, doi: 10.1016/j.ultramic.2014.11.029.

[452] A. Mendelovits, T. Prat, Y. Gonen, and G. Rytwo, "Improved Colorimetric Determination of Chitosan Concentrations by Dye Binding," *Applied Spectroscopy*, vol. 66, no. 8, pp. 979–982, Aug. 2012, doi: 10.1366/12-06591a.

[453] G. Wu *et al.*, "Improving the osteogenesis of rat mesenchymal stem cells by chitosan-based-microRNA nanoparticles," *Carbohydrate Polymers*, vol. 138, pp. 49–58, Mar. 2016, doi: 10.1016/j.carbpol.2015.11.044.

[454] X. Chen *et al.*, "Nanoparticle delivery of stable miR-199a-5p agomir improves the osteogenesis of human mesenchymal stem cells via the HIF1a pathway," *Biomaterials*, vol. 53, pp. 239–250, Jun. 2015, doi: 10.1016/j.biomaterials.2015.02.071.

[455] P. T. Sharpe, "Centrifugation," in *Methods of Cell Separation*, Elsevier Science, 1988, pp. 18–69.

[456] S. Ramakrishna, K. Fujihara, W.-E. Teo, and Z. Ma, *An Introduction to Electrospinning and Nanofibers*. Singapore: World Scientific Publishing Co Pte Ltd, 2005.

[457] W.-P. Dow, M.-Y. Yen, W.-B. Lin, and S.-W. Ho, "Influence of Molecular Weight of Polyethylene Glycol on Microvia Filling by Copper Electroplating," *Journal of The Electrochemical Society*, vol. 152, no. 11, p. C769, 2005, doi: 10.1149/1.2052019.

[458] S. Gee, B. Johnson, and A. L. Smith, "Optimizing electrospinning parameters for piezoelectric PVDF nanofiber membranes," *Journal of Membrane Science*, vol. 563, pp. 804–812, Oct. 2018, doi: 10.1016/j.memsci.2018.06.050.

[459] H. Jiang, Y. Hu, P. Zhao, Y. Li, and K. Zhu, "Modulation of protein release from biodegradable core–shell structured fibers prepared by coaxial electrospinning," *Journal of Biomedical Materials Research Part B: Applied Biomaterials*, vol. 79B, no. 1, pp. 50–57, Oct. 2006, doi: 10.1002/jbm.b.30510.

[460] S. Xu, J. Zhang, A. He, J. Li, H. Zhang, and C. C. Han, "Electrospinning of native cellulose from nonvolatile solvent system," *Polymer (Guildf)*, vol. 49, no. 12, pp. 2911–2917, Jun. 2008, doi: 10.1016/j.polymer.2008.04.046.

[461] H. Jiang, Y. Hu, Y. Li, P. Zhao, K. Zhu, and W. Chen, "A facile technique to prepare biodegradable coaxial electrospun nanofibers for controlled release of bioactive agents," *Journal of Controlled Release*, vol. 108, no. 2–3, pp. 237–243, Nov. 2005, doi: 10.1016/j.jconrel.2005.08.006.

[462] C. Webb *et al.*, "The Impact of Solvent Selection: Strategies to Guide the Manufacturing of Liposomes Using Microfluidics," *Pharmaceutics*, vol. 11, no. 12, p. 653, Dec. 2019, doi: 10.3390/pharmaceutics11120653.

[463] R. N. Rowland and J. F. Woodley, "The stability of liposomes in vitro to pH, bile salts and pancreatic lipase," *Biochimica et Biophysica Acta (BBA) - Lipids and Lipid Metabolism*, vol. 620, no. 3, pp. 400–409, Dec. 1980, doi: 10.1016/0005-2760(80)90131-9.

[464] K. Wang *et al.*, "Three-Layered PCL Grafts Promoted Vascular Regeneration in a Rabbit Carotid Artery Model," *Macromolecular Bioscience*, vol. 16, no. 4, pp. 608–618, Apr. 2016, doi: 10.1002/mabi.201500355.

[465] C. X. F. Lam, D. W. Hutmacher, J.-T. Schantz, M. A. Woodruff, and S. H. Teoh, "Evaluation of polycaprolactone scaffold degradation for 6 months in vitro and in vivo," *Journal of Biomedical Materials Research Part A*, vol. 90A, no. 3, pp. 906–919, Sep. 2009, doi: 10.1002/jbm.a.32052.

[466] Y. Pan *et al.*, "Small-diameter hybrid vascular grafts composed of polycaprolactone and polydioxanone fibers," *Scientific Reports*, vol. 7, no. 1, p. 3615, Dec. 2017, doi: 10.1038/s41598-017-03851-1.

[467] J. Hahn, S. F. J. Wickham, W. M. Shih, and S. D. Perrault, "Addressing the Instability of DNA Nanostructures in Tissue Culture," *ACS Nano*, vol. 8, no. 9, pp. 8765–8775, Sep. 2014, doi: 10.1021/nn503513p.

[468] T. J. McKee and S. v. Komarova, "Is it time to reinvent basic cell culture medium?," *American Journal of Physiology-Cell Physiology*, vol. 312, no. 5, pp. C624–C626, May 2017, doi: 10.1152/ajpcell.00336.2016.

[469] Y. Huang, Y. Cai, and Y. Lapitsky, "Factors affecting the stability of chitosan/tripolyphosphate micro- and nanogels: resolving the opposing findings," *Journal of Materials Chemistry B*, vol. 3, no. 29, pp. 5957–5970, 2015, doi: 10.1039/C5TB00431D.

[470] R. Pecora, "Dynamic Light Scattering Measurement of Nanometer Particles in Liquids," *Journal of Nanoparticle Research*, vol. 2, no. 2, pp. 123–131, 2000, doi: 10.1023/A:1010067107182.

[471] T. Czepkowshi and W. Słówko, "Some limitations of surface profile reconstruction in scanning electron microscopy," *Scanning*, vol. 18, no. 6, pp. 433–446, Dec. 2006, doi: 10.1002/sca.1996.4950180606.

[472] O. P. Choudhary and P. ka, "Scanning Electron Microscope: Advantages and Disadvantages in Imaging Components," *International Journal of Current Microbiology and Applied Sciences*, vol. 6, no. 5, pp. 1877–1882, May 2017, doi: 10.20546/ijcmas.2017.605.207.

[473] W. Fan, W. Yan, Z. Xu, and H. Ni, "Formation mechanism of monodisperse, low molecular weight chitosan nanoparticles by ionic gelation technique," *Colloids and Surfaces B: Biointerfaces*, vol. 90, pp. 21–27, Feb. 2012, doi: 10.1016/j.colsurfb.2011.09.042.

[474] T. López-León, E. L. S. Carvalho, B. Seijo, J. L. Ortega-Vinuesa, and D. Bastos-González, "Physicochemical characterization of chitosan nanoparticles: electrokinetic and stability behavior," *Journal of Colloid and Interface Science*, vol. 283, no. 2, pp. 344–351, Mar. 2005, doi: 10.1016/j.jcis.2004.08.186.

[475] M. TSAI, S. BAI, and R. CHEN, "Cavitation effects versus stretch effects resulted in different size and polydispersity of ionotropic gelation chitosan–sodium tripolyphosphate nanoparticle," *Carbohydrate Polymers*, vol. 71, no. 3, pp. 448–457, Feb. 2008, doi: 10.1016/j.carbpol.2007.06.015.

[476] D. B. Williams and C. B. Carter, "The Transmission Electron Microscope," in *Transmission Electron Microscopy*, Boston, MA: Springer US, 1996, pp. 3–17. doi: 10.1007/978-1-4757-2519-3_1.

[477] K. A. Howard *et al.*, "RNA Interference in Vitro and in Vivo Using a Novel Chitosan/siRNA Nanoparticle System," *Molecular Therapy*, vol. 14, no. 4, pp. 476–484, Oct. 2006, doi: 10.1016/j.ymthe.2006.04.010.

[478] J. Steven Leeder, H.-M. Dosch, and S. P. Spielberg, "Cellular toxicity of sulfamethoxazole reactive metabolites—I," *Biochemical Pharmacology*, vol. 41, no. 4, pp. 567–574, Feb. 1991, doi: 10.1016/0006-2952(91)90629-J.

[479] J. Li *et al.*, "Selectively Inducing Cancer Cell Death by Intracellular Enzyme-Instructed Self-Assembly (EISA) of Dipeptide Derivatives," *Advanced Healthcare Materials*, vol. 6, no. 15, p. 1601400, Aug. 2017, doi: 10.1002/adhm.201601400.

[480] X. Xu, R. M. Capito, and M. Spector, "Plasmid size influences chitosan nanoparticle mediated gene transfer to chondrocytes," *Journal of Biomedical Materials Research Part A*, vol. 84A, no. 4, pp. 1038–1048, Mar. 2008, doi: 10.1002/jbm.a.31479.

[481] J. Nuutila and E.-M. Lilius, "Flow cytometric quantitative determination of ingestion by phagocytes needs the distinguishing of overlapping populations of binding and ingesting cells," *Cytometry Part A*, vol. 65A, no. 2, pp. 93–102, Jun. 2005, doi: 10.1002/cyto.a.20139.

[482] F. Nadiya, N. Anjali, A. Gangaprasad, and K. K. Sabu, "High-quality RNA extraction from small cardamom tissues rich in polysaccharides and polyphenols," *Analytical Biochemistry*, vol. 485, pp. 25–27, Sep. 2015, doi: 10.1016/j.ab.2015.05.017.

[483] P. W. Inglis, M. de C. R. Pappas, L. v. Resende, and D. Grattapaglia, "Fast and inexpensive protocols for consistent extraction of high quality DNA and RNA from challenging plant and fungal samples for high-throughput SNP genotyping and sequencing applications," *PLOS ONE*, vol. 13, no. 10, p. e0206085, Oct. 2018, doi: 10.1371/journal.pone.0206085.

[484] Y. Byeon *et al.*, "CD44-targeted PLGA nanoparticles incorporating paclitaxel and FAK siRNA overcome chemoresistance in epithelial ovarian cancer," *Cancer Research*, p. canres.3871.2017, Aug. 2018, doi: 10.1158/0008-5472.CAN-17-3871.

[485] F. Li, F. Wang, C. Zhu, Q. Wei, T. Zhang, and Y. L. Zhou, "miR-221 suppression through nanoparticle-based miRNA delivery system for hepatocellular carcinoma therapy and its diagnosis as a potential biomarker," *International Journal of Nanomedicine*, vol. Volume 13, pp. 2295–2307, Apr. 2018, doi: 10.2147/IJN.S157805.

[486] Y. Cui, X. Li, K. Zeljic, S. Shan, Z. Qiu, and Z. Wang, "Effect of PEGylated Magnetic PLGA-PEI Nanoparticles on Primary Hippocampal Neurons: Reduced Nanoneurotoxicity and Enhanced Transfection Efficiency with Magnetofection," *ACS Applied Materials & Interfaces*, vol. 11, no. 41, pp. 38190–38204, Oct. 2019, doi: 10.1021/acsami.9b15014.

[487] C. F. Windisch, G. D. Maupin, and B. P. McGrail, "Ultraviolet (UV) Raman Spectroscopy Study of the Soret Effect in High-Pressure CO_2–Water Solutions," *Applied Spectroscopy*, vol. 66, no. 7, pp. 731–739, Jul. 2012, doi: 10.1366/12-06591.

[488] L. Guo and P. H. Santschi, "Ultrafiltration and its Applications to Sampling and Characterisation of Aquatic Colloids," in *Environmental Colloids and Particles*, Chichester, UK: John Wiley & Sons, Ltd, 2007, pp. 159–221. doi: 10.1002/9780470024539.ch4.

[489] A. K. Varkouhi, T. Lammers, R. M. Schiffelers, M. J. van Steenbergen, W. E. Hennink, and G. Storm, "Gene silencing activity of siRNA polyplexes based on biodegradable polymers," *European Journal of Pharmaceutics and Biopharmaceutics*, vol. 77, no. 3, pp. 450–457, Apr. 2011, doi: 10.1016/j.ejpb.2010.11.016.

[490] K. Sharma, S. Somavarapu, A. Colombani, N. Govind, and K. M. G. Taylor, "Nebulised siRNA encapsulated crosslinked chitosan nanoparticles for pulmonary delivery,"

International Journal of Pharmaceutics, vol. 455, no. 1–2, pp. 241–247, Oct. 2013, doi: 10.1016/j.ijpharm.2013.07.024.

[491] S. Techaarpornkul, S. Wongkupasert, P. Opanasopit, A. Apirakaramwong, J. Nunthanid, and U. Ruktanonchai, "Chitosan-Mediated siRNA Delivery In Vitro: Effect of Polymer Molecular Weight, Concentration and Salt Forms," *AAPS PharmSciTech*, vol. 11, no. 1, pp. 64–72, Mar. 2010, doi: 10.1208/s12249-009-9355-6.

[492] S. Anand *et al.*, "MicroRNA-132–mediated loss of p120RasGAP activates the endothelium to facilitate pathological angiogenesis," *Nature Medicine*, vol. 16, no. 8, pp. 909–914, Aug. 2010, doi: 10.1038/nm.2186.

[493] R. Katare *et al.*, "Transplantation of Human Pericyte Progenitor Cells Improves the Repair of Infarcted Heart Through Activation of an Angiogenic Program Involving Micro-RNA-132," *Circulation Research*, vol. 109, no. 8, pp. 894–906, Sep. 2011, doi: 10.1161/CIRCRESAHA.111.251546.

[494] T. Ma *et al.*, "MicroRNA-132, Delivered by Mesenchymal Stem Cell-Derived Exosomes, Promote Angiogenesis in Myocardial Infarction," *Stem Cells International*, vol. 2018, pp. 1–11, Sep. 2018, doi: 10.1155/2018/3290372.

[495] S. Singh, J. Johnson, and S. Chellappan, "Small molecule regulators of Rb–E2F pathway as modulators of transcription," *Biochimica et Biophysica Acta (BBA) - Gene Regulatory Mechanisms*, vol. 1799, no. 10–12, pp. 788–794, Oct. 2010, doi: 10.1016/j.bbagrm.2010.07.004.

[496] C. Boscher, V. Gaonac'h-Lovejoy, C. Delisle, and J.-P. Gratton, "Polarization and sprouting of endothelial cells by angiopoietin-1 require PAK2 and paxillin-dependent Cdc42 activation," *Molecular Biology of the Cell*, vol. 30, no. 17, pp. 2227–2239, Aug. 2019, doi: 10.1091/mbc.E18-08-0486.

[497] S. Wang *et al.*, "The Endothelial-Specific MicroRNA miR-126 Governs Vascular Integrity and Angiogenesis," *Developmental Cell*, vol. 15, no. 2, pp. 261–271, Aug. 2008, doi: 10.1016/j.devcel.2008.07.002.

[498] X. Shu *et al.*, "MicroRNA-93 regulates angiogenesis in peripheral arterial disease by targeting CDKN1A," *Molecular Medicine Reports*, Apr. 2019, doi: 10.3892/mmr.2019.10196.

[499] M. Fagnano, "Tubular scaffolds and proangiogenic 3D matrices as alternative strategies in vascular tissue engineering," 2017.

[500] S. MacIsaac, I. H. Jaffer, E. P. Belley-Côté, G. R. McClure, J. W. Eikelboom, and R. P. Whitlock, "How Did We Get Here?: A Historical Review and Critical Analysis of

Anticoagulation Therapy Following Mechanical Valve Replacement," *Circulation*, vol. 140, no. 23, pp. 1933–1942, Dec. 2019, doi: 10.1161/CIRCULATIONAHA.119.041105.

[501] S. F. Saleeb *et al.*, "Accelerated Degeneration of a Bovine Pericardial Bioprosthetic Aortic Valve in Children and Young Adults," *Circulation*, vol. 130, no. 1, pp. 51–60, Jul. 2014, doi: 10.1161/CIRCULATIONAHA.114.009835.

[502] J. Zhou *et al.*, "Development of Decellularized Aortic Valvular Conduit Coated by Heparin–SDF-1α Multilayer," *The Annals of Thoracic Surgery*, vol. 99, no. 2, pp. 612–618, Feb. 2015, doi: 10.1016/j.athoracsur.2014.09.001.

[503] J. E. Jordan, J. K. Williams, S.-J. Lee, D. Raghavan, A. Atala, and J. J. Yoo, "Bioengineered self-seeding heart valves," *The Journal of Thoracic and Cardiovascular Surgery*, vol. 143, no. 1, pp. 201–208, Jan. 2012, doi: 10.1016/j.jtcvs.2011.10.005.

[504] M. Schleicher, H. P. Wendel, O. Fritze, and U. A. Stock, "In vivo tissue engineering of heart valves: evolution of a novel concept," *Regenerative Medicine*, vol. 4, no. 4, pp. 613–619, Jul. 2009, doi: 10.2217/rme.09.22.

[505] J. I. Rotmans *et al.*, "In Vivo Cell Seeding With Anti-CD34 Antibodies Successfully Accelerates Endothelialization but Stimulates Intimal Hyperplasia in Porcine Arteriovenous Expanded Polytetrafluoroethylene Grafts," *Circulation*, vol. 112, no. 1, pp. 12–18, Jul. 2005, doi: 10.1161/CIRCULATIONAHA.104.504407.

[506] R. J. Smith, M. T. Koobatian, A. Shahini, D. D. Swartz, and S. T. Andreadis, "Capture of endothelial cells under flow using immobilized vascular endothelial growth factor," *Biomaterials*, vol. 51, pp. 303–312, May 2015, doi: 10.1016/j.biomaterials.2015.02.025.

[507] A. Sen, K. O'Malley, Z. Wang, G. v. Raj, D. B. DeFranco, and S. R. Hammes, "Paxillin Regulates Androgen- and Epidermal Growth Factor-induced MAPK Signaling and Cell Proliferation in Prostate Cancer Cells*," *Journal of Biological Chemistry*, vol. 285, no. 37, pp. 28787–28795, Sep. 2010, doi: 10.1074/jbc.M110.134064.

[508] X. Shu *et al.*, "MicroRNA-93 regulates angiogenesis in peripheral arterial disease by targeting CDKN1A," *Molecular Medicine Reports*, Apr. 2019, doi: 10.3892/mmr.2019.10196.

[509] M. Wen *et al.*, "Local Delivery of Dual MicroRNAs in Trilayered Electrospun Grafts for Vascular Regeneration," *ACS Applied Materials & Interfaces*, vol. 12, no. 6, pp. 6863–6875, Feb. 2020, doi: 10.1021/acsami.9b19452.

[510] F. Zhou *et al.*, "Nanofiber-mediated microRNA-126 delivery to vascular endothelial cells for blood vessel regeneration," *Acta Biomaterialia*, vol. 43, pp. 303–313, Oct. 2016, doi: 10.1016/j.actbio.2016.07.048.

[511] X. Chen, L. S. Mangala, C. Rodriguez-Aguayo, X. Kong, G. Lopez-Berestein, and A. K. Sood, "RNA interference-based therapy and its delivery systems," *Cancer and Metastasis Reviews*, vol. 37, no. 1, pp. 107–124, Mar. 2018, doi: 10.1007/s10555-017-9717-6.

[512] *The Biochemistry of the Nucleic Acids*. Elsevier, 1972. doi: 10.1016/B978-0-12-205350-4.X5002-1.

[513] X. Chen, L. S. Mangala, C. Rodriguez-Aguayo, X. Kong, G. Lopez-Berestein, and A. K. Sood, "RNA interference-based therapy and its delivery systems," *Cancer and Metastasis Reviews*, vol. 37, no. 1, pp. 107–124, Mar. 2018, doi: 10.1007/s10555-017-9717-6.

[514] E. Fernández Fernández, B. Santos-Carballal, W.-M. Weber, and F. M. Goycoolea, "Chitosan as a non-viral co-transfection system in a cystic fibrosis cell line," *International Journal of Pharmaceutics*, vol. 502, no. 1–2, pp. 1–9, Apr. 2016, doi: 10.1016/j.ijpharm.2016.01.083.

[515] S. Chen, H. Yan, B. Sun, A. Zuo, and D. Liang, "Subretinal transfection of chitosan-loaded TLR3-siRNA for the treatment of experimental autoimmune uveitis," *European Journal of Pharmaceutics and Biopharmaceutics*, vol. 85, no. 3, pp. 726–735, Nov. 2013, doi: 10.1016/j.ejpb.2013.09.005.

[516] T. Sato, T. Ishii, and Y. Okahata, "In vitro gene delivery mediated by chitosan. Effect of pH, serum, and molecular mass of chitosan on the transfection efficiency," *Biomaterials*, vol. 22, no. 15, pp. 2075–2080, Aug. 2001, doi: 10.1016/S0142-9612(00)00385-9.

[517] Y. Ysrafil *et al.*, "MicroRNA-155-5p Diminishes in Vitro Ovarian Cancer Cell Viability by Targeting HIF1α Expression," *Advanced Pharmaceutical Bulletin*, vol. 10, no. 4, pp. 630–637, Aug. 2020, doi: 10.34172/apb.2020.076.

[518] Z. Huang *et al.*, "Low-molecular weight chitosan/vascular endothelial growth factor short hairpin RNA for the treatment of hepatocellular carcinoma," *Life Sciences*, vol. 91, no. 23–24, pp. 1207–1215, Dec. 2012, doi: 10.1016/j.lfs.2012.09.015.

[519] S. Gordon, "Phagocytosis: An Immunobiologic Process," *Immunity*, vol. 44, no. 3, pp. 463–475, Mar. 2016, doi: 10.1016/j.immuni.2016.02.026.

[520] S. D. Conner and S. L. Schmid, "Regulated portals of entry into the cell," *Nature*, vol. 422, no. 6927, pp. 37–44, Mar. 2003, doi: 10.1038/nature01451.

[521] J. Zhang *et al.*, "Intracellular distribution and internalization pathways of guanidinylated bioresponsive poly(amido amine)s in gene delivery," *Asian Journal of Pharmaceutical Sciences*, vol. 13, no. 4, pp. 360–372, Jul. 2018, doi: 10.1016/j.ajps.2018.02.008.

[522] P. G. Frank, S. E. Woodman, D. S. Park, and M. P. Lisanti, "Caveolin, Caveolae, and Endothelial Cell Function," *Arteriosclerosis, Thrombosis, and Vascular Biology*, vol. 23, no. 7, pp. 1161–1168, Jul. 2003, doi: 10.1161/01.ATV.0000070546.16946.3A.

[523] S. Mazumdar, D. Chitkara, and A. Mittal, "Exploration and insights into the cellular internalization and intracellular fate of amphiphilic polymeric nanocarriers," *Acta Pharmaceutica Sinica B*, vol. 11, no. 4, pp. 903–924, Apr. 2021, doi: 10.1016/j.apsb.2021.02.019.

[524] C. Aslan, N. Çelebi, İ. T. Değim, A. Atak, and Ç. Özer, "Development of Interleukin-2 Loaded Chitosan-Based Nanogels Using Artificial Neural Networks and Investigating the Effects on Wound Healing in Rats," *AAPS PharmSciTech*, vol. 18, no. 4, pp. 1019–1030, May 2017, doi: 10.1208/s12249-016-0662-4.

[525] F. Rázga, D. Vnuková, V. Némethová, P. Mazancová, and I. Lacík, "Preparation of chitosan-TPP sub-micron particles: Critical evaluation and derived recommendations," *Carbohydrate Polymers*, vol. 151, pp. 488–499, Oct. 2016, doi: 10.1016/j.carbpol.2016.05.092.

[526] J. Antoniou, F. Liu, H. Majeed, J. Qi, W. Yokoyama, and F. Zhong, "Physicochemical and morphological properties of size-controlled chitosan–tripolyphosphate nanoparticles," *Colloids and Surfaces A: Physicochemical and Engineering Aspects*, vol. 465, pp. 137–146, Jan. 2015, doi: 10.1016/j.colsurfa.2014.10.040.

[527] M. Huang, E. Khor, and L.-Y. Lim, "Uptake and Cytotoxicity of Chitosan Molecules and Nanoparticles: Effects of Molecular Weight and Degree of Deacetylation," *Pharmaceutical Research*, vol. 21, no. 2, pp. 344–353, Feb. 2004, doi: 10.1023/B:PHAM.0000016249.52831.a5.

[528] P. L. Michael, Y. T. Lam, J. Hung, R. P. Tan, M. Santos, and S. G. Wise, "Comprehensive Evaluation of the Toxicity and Biosafety of Plasma Polymerized Nanoparticles," *Nanomaterials*, vol. 11, no. 5, p. 1176, Apr. 2021, doi: 10.3390/nano11051176.

[529] R. M. Raftery *et al.*, "Highly versatile cell-penetrating peptide loaded scaffold for efficient and localised gene delivery to multiple cell types: From development to application in tissue engineering," *Biomaterials*, vol. 216, p. 119277, Sep. 2019, doi: 10.1016/j.biomaterials.2019.119277.

[530] H. Yang *et al.*, "An in Vivo miRNA Delivery System for Restoring Infarcted Myocardium," *ACS Nano*, vol. 13, no. 9, pp. 9880–9894, Sep. 2019, doi: 10.1021/acsnano.9b03343.

[531] V. Pandey, T. Haider, A. R. Chandak, A. Chakraborty, S. Banerjee, and V. Soni, "Surface modified silk fibroin nanoparticles for improved delivery of doxorubicin: Development,

characterization, in-vitro studies," *International Journal of Biological Macromolecules*, vol. 164, pp. 2018–2027, Dec. 2020, doi: 10.1016/j.ijbiomac.2020.07.326.

[532] M. F. Bostanudin, A. Lalatsa, D. C. Górecki, and E. Barbu, "Engineering butylglyceryl-modified polysaccharides towards nanomedicines for brain drug delivery," *Carbohydrate Polymers*, vol. 236, p. 116060, May 2020, doi: 10.1016/j.carbpol.2020.116060.

[533] K. Ozturk, F. B. Arslan, E. Tavukcuoglu, G. Esendagli, and S. Calis, "Aggregation of chitosan nanoparticles in cell culture: Reasons and resolutions," *International Journal of Pharmaceutics*, vol. 578, p. 119119, Mar. 2020, doi: 10.1016/j.ijpharm.2020.119119.

[534] M.-H. Ki *et al.*, "Chitosan-Based Hybrid Nanocomplex for siRNA Delivery and Its Application for Cancer Therapy," *Pharmaceutical Research*, vol. 31, no. 12, pp. 3323–3334, Dec. 2014, doi: 10.1007/s11095-014-1422-3.

[535] J. Kim, Y. Kang, S. Y. Tzeng, and J. J. Green, "Synthesis and application of poly(ethylene glycol)-co-poly(β-amino ester) copolymers for small cell lung cancer gene therapy," *Acta Biomaterialia*, vol. 41, pp. 293–301, Sep. 2016, doi: 10.1016/j.actbio.2016.05.040.

[536] Z. Wang, H. Zou, Z. Wang, J. Wu, Z. Xia, and M. Feng, "Highly stable polyglutamate derivatives/siRNA polyplex efficiently down-relegate survivin expression and augment the efficacy of cisplatin," *International Journal of Pharmaceutics*, vol. 505, no. 1–2, pp. 24–34, May 2016, doi: 10.1016/j.ijpharm.2016.03.062.

[537] E. Esmaeilzadeh Gharehdaghi *et al.*, "Chitosan Nanoparticles for siRNA Delivery: Optimization of Processing/Formulation Parameters," *Nucleic Acid Therapeutics*, vol. 24, no. 6, pp. 420–427, Dec. 2014, doi: 10.1089/nat.2014.0484.

[538] X. Yuan, B. A. Shah, N. K. Kotadia, J. Li, H. Gu, and Z. Wu, "The Development and Mechanism Studies of Cationic Chitosan-Modified Biodegradable PLGA Nanoparticles for Efficient siRNA Drug Delivery," *Pharmaceutical Research*, vol. 27, no. 7, pp. 1285–1295, Jul. 2010, doi: 10.1007/s11095-010-0103-0.

[539] H. Wang *et al.*, "microRNA-21 promotes breast cancer proliferation and metastasis by targeting LZTFL1," *BMC Cancer*, vol. 19, no. 1, p. 738, Dec. 2019, doi: 10.1186/s12885-019-5951-3.

[540] K. Gasic, A. Hernandez, and S. S. Korban, "RNA extraction from different apple tissues rich in polyphenols and polysaccharides for cDNA library construction," *Plant Molecular Biology Reporter*, vol. 22, no. 4, pp. 437–438, Dec. 2004, doi: 10.1007/BF02772687.

[541] L. Wang and J. P. Stegemann, "Extraction of high quality RNA from polysaccharide matrices using cetlytrimethylammonium bromide," *Biomaterials*, vol. 31, no. 7, pp. 1612–1618, Mar. 2010, doi: 10.1016/j.biomaterials.2009.11.024.

[542] L. Wang and J. P. Stegemann, "Extraction of high quality RNA from polysaccharide matrices using cetlytrimethylammonium bromide," *Biomaterials*, vol. 31, no. 7, pp. 1612–1618, Mar. 2010, doi: 10.1016/j.biomaterials.2009.11.024.

[543] X. Chen *et al.*, "Nanoparticle delivery of stable miR-199a-5p agomir improves the osteogenesis of human mesenchymal stem cells via the HIF1a pathway," *Biomaterials*, vol. 53, pp. 239–250, Jun. 2015, doi: 10.1016/j.biomaterials.2015.02.071.

[544] H. Katas and H. O. Alpar, "Development and characterisation of chitosan nanoparticles for siRNA delivery," *Journal of Controlled Release*, vol. 115, no. 2, pp. 216–225, Oct. 2006, doi: 10.1016/j.jconrel.2006.07.021.

[545] N. Kimura *et al.*, "Development of a Microfluidic-Based Post-Treatment Process for Size-Controlled Lipid Nanoparticles and Application to siRNA Delivery," *ACS Applied Materials & Interfaces*, vol. 12, no. 30, pp. 34011–34020, Jul. 2020, doi: 10.1021/acsami.0c05489.

[546] A. D. Tagalakis *et al.*, "A method for concentrating lipid peptide DNA and siRNA nanocomplexes that retains their structure and transfection efficiency," *International Journal of Nanomedicine*, p. 2673, Apr. 2015, doi: 10.2147/IJN.S78935.

[547] Y. Peng, X. Zhu, and L. Qiu, "Electroneutral composite polymersomes self-assembled by amphiphilic polyphosphazenes for effective miR-200c in vivo delivery to inhibit drug resistant lung cancer," *Biomaterials*, vol. 106, pp. 1–12, Nov. 2016, doi: 10.1016/j.biomaterials.2016.08.001.

[548] J. A. Kulkarni *et al.*, "Fusion-dependent formation of lipid nanoparticles containing macromolecular payloads," *Nanoscale*, vol. 11, no. 18, pp. 9023–9031, 2019, doi: 10.1039/C9NR02004G.

[549] R. Mihaila *et al.*, "Lipid nanoparticle purification by Spin Centrifugation–Dialysis (SCD): A facile and high-throughput approach for small scale preparation of siRNA–lipid complexes," *International Journal of Pharmaceutics*, vol. 420, no. 1, pp. 118–121, Nov. 2011, doi: 10.1016/j.ijpharm.2011.08.017.

[550] H. Shali *et al.*, "Co-delivery of insulin-like growth factor 1 receptor specific siRNA and doxorubicin using chitosan-based nanoparticles enhanced anticancer efficacy in A549 lung cancer cell line," *Artificial Cells, Nanomedicine, and Biotechnology*, vol. 46, no. 2, pp. 293–302, Feb. 2018, doi: 10.1080/21691401.2017.1307212.

[551] E. Esmaeilzadeh Gharehdaghi *et al.*, "Chitosan Nanoparticles for siRNA Delivery: Optimization of Processing/Formulation Parameters," *Nucleic Acid Therapeutics*, vol. 24, no. 6, pp. 420–427, Dec. 2014, doi: 10.1089/nat.2014.0484.

[552] C. Carrillo *et al.*, "Chitosan nanoparticles as non-viral gene delivery systems: Determination of loading efficiency," *Biomedicine & Pharmacotherapy*, vol. 68, no. 6, pp. 775–783, Jul. 2014, doi: 10.1016/j.biopha.2014.07.009.

[553] H. Lu, L. Lv, Y. Dai, G. Wu, H. Zhao, and F. Zhang, "Porous Chitosan Scaffolds with Embedded Hyaluronic Acid/Chitosan/Plasmid-DNA Nanoparticles Encoding TGF-β1 Induce DNA Controlled Release, Transfected Chondrocytes, and Promoted Cell Proliferation," *PLoS ONE*, vol. 8, no. 7, p. e69950, Jul. 2013, doi: 10.1371/journal.pone.0069950.

[554] A. Bozkir and O. M. Saka, "Chitosan Nanoparticles for Plasmid DNA Delivery: Effect of Chitosan Molecular Structure on Formulation and Release Characteristics," *Drug Delivery*, vol. 11, no. 2, pp. 107–112, Jan. 2004, doi: 10.1080/10717540490280705.

[555] N. Sawtarie, Y. Cai, and Y. Lapitsky, "Preparation of chitosan/tripolyphosphate nanoparticles with highly tunable size and low polydispersity," *Colloids and Surfaces B: Biointerfaces*, vol. 157, pp. 110–117, Sep. 2017, doi: 10.1016/j.colsurfb.2017.05.055.

[556] P. Eivazy *et al.*, "The impact of the codelivery of drug-siRNA by trimethyl chitosan nanoparticles on the efficacy of chemotherapy for metastatic breast cancer cell line (MDA-MB-231)," *Artificial Cells, Nanomedicine, and Biotechnology*, vol. 45, no. 5, pp. 889–896, Jul. 2017, doi: 10.1080/21691401.2016.1185727.

[557] O. Germershaus, S. Mao, J. Sitterberg, U. Bakowsky, and T. Kissel, "Gene delivery using chitosan, trimethyl chitosan or polyethylenglycol-graft-trimethyl chitosan block copolymers: Establishment of structure–activity relationships in vitro," *Journal of Controlled Release*, vol. 125, no. 2, pp. 145–154, Jan. 2008, doi: 10.1016/j.jconrel.2007.10.013.

[558] P. Eivazy *et al.*, "The impact of the codelivery of drug-siRNA by trimethyl chitosan nanoparticles on the efficacy of chemotherapy for metastatic breast cancer cell line (MDA-MB-231)," *Artificial Cells, Nanomedicine, and Biotechnology*, vol. 45, no. 5, pp. 889–896, Jul. 2017, doi: 10.1080/21691401.2016.1185727.

[559] A. T. Kovala, K. A. Harvey, P. Mcglynn, G. Boguslawski, J. G. N. Garcia, and D. English, "High-efficiency transient transfection of endothelial cells for functional analysis," *The FASEB Journal*, vol. 14, no. 15, pp. 2486–2494, Dec. 2000, doi: 10.1096/fj.00-0147com.

[560] J. L. Hernandez, T. Coll, and C. J. Ciudad, "A highly efficient electroporation method for the transfection of endothelial cells," *Angiogenesis*, vol. 7, no. 3, pp. 235–241, 2004, doi: 10.1007/s10456-004-4180-8.

[561] J. Yang *et al.*, "Multitargeting Gene Delivery Systems for Enhancing the Transfection of Endothelial Cells," *Macromolecular Rapid Communications*, vol. 37, no. 23, pp. 1926–1931, Dec. 2016, doi: 10.1002/marc.201600345.

[562] I. M. Helander, H.-L. Alakomi, K. Latva-Kala, and P. Koski, "Polyethyleneimine is an effective permeabilizer of Gram-negative bacteria," *Microbiology (N Y)*, vol. 143, no. 10, pp. 3193–3199, Oct. 1997, doi: 10.1099/00221287-143-10-3193.

[563] N. OKU, N. YAMAGUCHI, N. YAMAGUCHI, S. SHIBAMOTO, F. ITO, and M. NANGO, "The Fusogenic Effect of Synthetic Polycations on Negatively Charged Lipid Bilayers1," *The Journal of Biochemistry*, vol. 100, no. 4, pp. 935–944, Oct. 1986, doi: 10.1093/oxfordjournals.jbchem.a121806.

[564] C.-F. Wang, Y.-X. Lin, T. Jiang, F. He, and R.-X. Zhuo, "Polyethylenimine-grafted polycarbonates as biodegradable polycations for gene delivery," *Biomaterials*, vol. 30, no. 27, pp. 4824–4832, Sep. 2009, doi: 10.1016/j.biomaterials.2009.05.053.

[565] M. A. Islam *et al.*, "Major degradable polycations as carriers for DNA and siRNA," *Journal of Controlled Release*, vol. 193, pp. 74–89, Nov. 2014, doi: 10.1016/j.jconrel.2014.05.055.

[566] X. Zhang *et al.*, "Poly(ethylene glycol)-block-polyethylenimine copolymers as carriers for gene delivery: Effects of PEG molecular weight and PEGylation degree," *Journal of Biomedical Materials Research Part A*, vol. 84A, no. 3, pp. 795–804, Mar. 2008, doi: 10.1002/jbm.a.31343.

[567] A. Malek, F. Czubayko, and A. Aigner, "PEG grafting of polyethylenimine (PEI) exerts different effects on DNA transfection and siRNA-induced gene targeting efficacy," *Journal of Drug Targeting*, vol. 16, no. 2, pp. 124–139, Jan. 2008, doi: 10.1080/10611860701849058.

[568] C. Y. M. Hsu and H. Uludağ, "A simple and rapid nonviral approach to efficiently transfect primary tissue–derived cells using polyethylenimine," *Nature Protocols*, vol. 7, no. 5, pp. 935–945, May 2012, doi: 10.1038/nprot.2012.038.

[569] C. Malloggi *et al.*, "Comparative evaluation and optimization of off-the-shelf cationic polymers for gene delivery purposes," *Polymer Chemistry*, vol. 6, no. 35, pp. 6325–6339, 2015, doi: 10.1039/C5PY00915D.

[570] F. P. Seib, A. T. Jones, and R. Duncan, "Comparison of the endocytic properties of linear and branched PEIs, and cationic PAMAM dendrimers in B16f10 melanoma cells," *Journal of Controlled Release*, vol. 117, no. 3, pp. 291–300, Feb. 2007, doi: 10.1016/j.jconrel.2006.10.020.

[571]   D. Fischer, Y. Li, B. Ahlemeyer, J. Krieglstein, and T. Kissel, "In vitro cytotoxicity testing of polycations: influence of polymer structure on cell viability and hemolysis," *Biomaterials*, vol. 24, no. 7, pp. 1121–1131, Mar. 2003, doi: 10.1016/S0142-9612(02)00445-3.

[572]   M. Neu, D. Fischer, and T. Kissel, "Recent advances in rational gene transfer vector design based on poly(ethylene imine) and its derivatives," *The Journal of Gene Medicine*, vol. 7, no. 8, pp. 992–1009, Aug. 2005, doi: 10.1002/jgm.773.

[573]   D. Fischer, Y. Li, B. Ahlemeyer, J. Krieglstein, and T. Kissel, "In vitro cytotoxicity testing of polycations: influence of polymer structure on cell viability and hemolysis," *Biomaterials*, vol. 24, no. 7, pp. 1121–1131, Mar. 2003, doi: 10.1016/S0142-9612(02)00445-3.

[574]   A. Hall *et al.*, "Polyethylenimine architecture-dependent metabolic imprints and perturbation of cellular redox homeostasis," *Biochimica et Biophysica Acta (BBA) - Bioenergetics*, vol. 1847, no. 3, pp. 328–342, Mar. 2015, doi: 10.1016/j.bbabio.2014.12.002.

[575]   J. Y. Cherng, P. van de Wetering, H. Talsma, D. J. Crommelin, and W. E. Hennink, "Effect of size and serum proteins on transfection efficiency of poly ((2-dimethylamino)ethyl methacrylate)-plasmid nanoparticles.," *Pharm Res*, vol. 13, no. 7, pp. 1038–42, Jul. 1996, doi: 10.1023/a:1016054623543.

[576]   A. C. Richards Grayson, A. M. Doody, and D. Putnam, "Biophysical and Structural Characterization of Polyethylenimine-Mediated siRNA Delivery in Vitro," *Pharmaceutical Research*, vol. 23, no. 8, pp. 1868–1876, Aug. 2006, doi: 10.1007/s11095-006-9009-2.

[577]   S. He *et al.*, "Down-regulation of GP130 signaling sensitizes bladder cancer to cisplatin by impairing Ku70 DNA repair signaling and promoting apoptosis," *Cellular Signalling*, vol. 81, p. 109931, May 2021, doi: 10.1016/j.cellsig.2021.109931.

[578]   C. Chen *et al.*, "EGFP-EGF1-Conjugated PLGA Nanoparticles for Targeted Delivery of siRNA into Injured Brain Microvascular Endothelial Cells for Efficient RNA Interference," *PLoS ONE*, vol. 8, no. 4, p. e60860, Apr. 2013, doi: 10.1371/journal.pone.0060860.

[579]   J. Cui *et al.*, "Ex vivo pretreatment of human vessels with siRNA nanoparticles provides protein silencing in endothelial cells," *Nature Communications*, vol. 8, no. 1, p. 191, Dec. 2017, doi: 10.1038/s41467-017-00297-x.

[580]   Z. Li *et al.*, "Lipofectamine 2000/siRNA complexes cause endoplasmic reticulum unfolded protein response in human endothelial cells," *Journal of Cellular Physiology*, vol. 234, no. 11, pp. 21166–21181, Nov. 2019, doi: 10.1002/jcp.28719.

[581]   Y. Arthanari, A. Pluen, R. Rajendran, H. Aojula, and C. Demonacos, "Delivery of therapeutic shRNA and siRNA by Tat fusion peptide targeting bcr–abl fusion gene in

Chronic Myeloid Leukemia cells," *Journal of Controlled Release*, vol. 145, no. 3, pp. 272–280, Aug. 2010, doi: 10.1016/j.jconrel.2010.04.011.

[582] T. Wang, L. Larcher, L. Ma, and R. Veedu, "Systematic Screening of Commonly Used Commercial Transfection Reagents towards Efficient Transfection of Single-Stranded Oligonucleotides," *Molecules*, vol. 23, no. 10, p. 2564, Oct. 2018, doi: 10.3390/molecules23102564.

[583] T. Jiang, E. J. Carbone, K. W.-H. Lo, and C. T. Laurencin, "Electrospinning of polymer nanofibers for tissue regeneration," *Progress in Polymer Science*, vol. 46, pp. 1–24, Jul. 2015, doi: 10.1016/j.progpolymsci.2014.12.001.

[584] G. N. Coyan *et al.*, "In vivo functional assessment of a novel degradable metal and elastomeric scaffold-based tissue engineered heart valve," *The Journal of Thoracic and Cardiovascular Surgery*, vol. 157, no. 5, pp. 1809–1816, May 2019, doi: 10.1016/j.jtcvs.2018.09.128.

[585] A. O. Elzoghby, W. M. Samy, and N. A. Elgindy, "Protein-based nanocarriers as promising drug and gene delivery systems," *Journal of Controlled Release*, vol. 161, no. 1, pp. 38–49, Jul. 2012, doi: 10.1016/j.jconrel.2012.04.036.

[586] K. Su and C. Wang, "Recent advances in the use of gelatin in biomedical research," *Biotechnology Letters*, vol. 37, no. 11, pp. 2139–2145, Nov. 2015, doi: 10.1007/s10529-015-1907-0.

[587] D. C. Ardila, E. Tamimi, T. Doetschman, W. R. Wagner, and J. P. vande Geest, "Modulating smooth muscle cell response by the release of TGFβ2 from tubular scaffolds for vascular tissue engineering," *Journal of Controlled Release*, vol. 299, pp. 44–52, Apr. 2019, doi: 10.1016/j.jconrel.2019.02.024.

[588] M. Carrabba *et al.*, "Design, fabrication and perivascular implantation of bioactive scaffolds engineered with human adventitial progenitor cells for stimulation of arteriogenesis in peripheral ischemia," *Biofabrication*, vol. 8, no. 1, p. 015020, Mar. 2016, doi: 10.1088/1758-5090/8/1/015020.

[589] C. Tonda-Turo *et al.*, "Crosslinked gelatin nanofibres: Preparation, characterisation and in vitro studies using glial-like cells," *Materials Science and Engineering: C*, vol. 33, no. 5, pp. 2723–2735, Jul. 2013, doi: 10.1016/j.msec.2013.02.039.

[590] M. Chen *et al.*, "Chitosan/siRNA Nanoparticles Encapsulated in PLGA Nanofibers for siRNA Delivery," *ACS Nano*, vol. 6, no. 6, pp. 4835–4844, Jun. 2012, doi: 10.1021/nn300106t.

[591] S. Jana, A. Bhagia, and A. Lerman, "Optimization of polycaprolactone fibrous scaffold for heart valve tissue engineering," *Biomedical Materials*, vol. 14, no. 6, p. 065014, Oct. 2019, doi: 10.1088/1748-605X/ab3d24.

[592] M. van Lieshout, G. Peters, M. Rutten, and F. Baaijens, "A Knitted, Fibrin-Covered Polycaprolactone Scaffold for Tissue Engineering of the Aortic Valve," *Tissue Engineering*, vol. 12, no. 3, pp. 481–487, Mar. 2006, doi: 10.1089/ten.2006.12.481.

[593] H. Tseng *et al.*, "Anisotropic Poly(Ethylene Glycol)/Polycaprolactone Hydrogel–Fiber Composites for Heart Valve Tissue Engineering," *Tissue Engineering Part A*, vol. 20, no. 19–20, pp. 2634–2645, Oct. 2014, doi: 10.1089/ten.tea.2013.0397.

[594] S. Sant, C. M. Hwang, S.-H. Lee, and A. Khademhosseini, "Hybrid PGS-PCL microfibrous scaffolds with improved mechanical and biological properties," *Journal of Tissue Engineering and Regenerative Medicine*, vol. 5, no. 4, pp. 283–291, Apr. 2011, doi: 10.1002/term.313.

[595] P. Ravishankar, A. Ozkizilcik, A. Husain, and K. Balachandran, "Anisotropic Fiber-Reinforced Glycosaminoglycan Hydrogels for Heart Valve Tissue Engineering," *Tissue Engineering Part A*, vol. 27, no. 9–10, pp. 513–525, May 2021, doi: 10.1089/ten.tea.2020.0118.

[596] P. Pibarot and J. G. Dumesnil, "Hemodynamic and clinical impact of prosthesis–patient mismatch in the aortic valve position and its prevention," *J Am Coll Cardiol*, vol. 36, no. 4, pp. 1131–1141, Oct. 2000, doi: 10.1016/S0735-1097(00)00859-7.

[597] K. M. Farooqi *et al.*, "3D Printing and Heart Failure," *JACC: Heart Failure*, vol. 7, no. 2, pp. 132–142, Feb. 2019, doi: 10.1016/j.jchf.2018.09.011.

[598] C.-I. AN, A. SAWADA, E. FUKUSAKI, and A. KOBAYASHI, "A Transient RNA Interference Assay System Using Arabidopsis Protoplasts," *Bioscience, Biotechnology, and Biochemistry*, vol. 67, no. 12, pp. 2674–2677, Jan. 2003, doi: 10.1271/bbb.67.2674.

[599] J. Lee and H. J. Ahn, "PEGylated DC-Chol/DOPE cationic liposomes containing KSP siRNA as a systemic siRNA delivery Carrier for ovarian cancer therapy," *Biochemical and Biophysical Research Communications*, vol. 503, no. 3, pp. 1716–1722, Sep. 2018, doi: 10.1016/j.bbrc.2018.07.104.

[600] S. Taetz *et al.*, "Hyaluronic Acid-Modified DOTAP/DOPE Liposomes for the Targeted Delivery of Anti-Telomerase siRNA to CD44-Expressing Lung Cancer Cells," *Oligonucleotides*, vol. 19, no. 2, pp. 103–116, Jun. 2009, doi: 10.1089/oli.2008.0168.

[601] J. S. Chin, W. H. Chooi, H. Wang, W. Ong, K. W. Leong, and S. Y. Chew, "Scaffold-mediated non-viral delivery platform for CRISPR/Cas9-based genome editing," *Acta Biomaterialia*, vol. 90, pp. 60–70, May 2019, doi: 10.1016/j.actbio.2019.04.020.

[602] W. H. Chooi, W. Ong, A. Murray, J. Lin, D. Nizetic, and S. Y. Chew, "Scaffold mediated gene knockdown for neuronal differentiation of human neural progenitor cells," *Biomaterials Science*, vol. 6, no. 11, pp. 3019–3029, 2018, doi: 10.1039/C8BM01034J.

[603] A. Lechanteur, V. Sanna, A. Duchemin, B. Evrard, D. Mottet, and G. Piel, "Cationic Liposomes Carrying siRNA: Impact of Lipid Composition on Physicochemical Properties, Cytotoxicity and Endosomal Escape," *Nanomaterials*, vol. 8, no. 5, p. 270, Apr. 2018, doi: 10.3390/nano8050270.

[604] S. Kimura, I. A. Khalil, Y. H. A. Elewa, and H. Harashima, "Novel lipid combination for delivery of plasmid DNA to immune cells in the spleen," *Journal of Controlled Release*, vol. 330, pp. 753–764, Feb. 2021, doi: 10.1016/j.jconrel.2021.01.005.

[605] Q. Li *et al.*, "Multifunctional REDV-G-TAT-G-NLS-Cys peptide sequence conjugated gene carriers to enhance gene transfection efficiency in endothelial cells," *Colloids and Surfaces B: Biointerfaces*, vol. 184, p. 110510, Dec. 2019, doi: 10.1016/j.colsurfb.2019.110510.

[606] A. Rassoli, N. Fatouraee, R. Guidoin, and Z. Zhang, "Comparison of tensile properties of xenopericardium from three animal species and finite element analysis for bioprosthetic heart valve tissue," *Artificial Organs*, vol. 44, no. 3, pp. 278–287, Mar. 2020, doi: 10.1111/aor.13552.

[607] A. Hasan, S. Soliman, F. el Hajj, Y.-T. Tseng, H. C. Yalcin, and H. E. Marei, "Fabrication and In Vitro Characterization of a Tissue Engineered PCL-PLLA Heart Valve," *Scientific Reports*, vol. 8, no. 1, p. 8187, Dec. 2018, doi: 10.1038/s41598-018-26452-y.

[608] S. Sant and A. Khademhosseini, "Fabrication and characterization of tough elastomeric fibrous scaffolds for tissue engineering applications," in *2010 Annual International Conference of the IEEE Engineering in Medicine and Biology*, Aug. 2010, pp. 3546–3548. doi: 10.1109/IEMBS.2010.5627486.

[609] B. W. Tillman, S. K. Yazdani, S. J. Lee, R. L. Geary, A. Atala, and J. J. Yoo, "The in vivo stability of electrospun polycaprolactone-collagen scaffolds in vascular reconstruction," *Biomaterials*, vol. 30, no. 4, pp. 583–588, Feb. 2009, doi: 10.1016/j.biomaterials.2008.10.006.

[610] Y. Xue, V. Sant, J. Phillippi, and S. Sant, "Biodegradable and biomimetic elastomeric scaffolds for tissue-engineered heart valves," *Acta Biomaterialia*, vol. 48, pp. 2–19, Jan. 2017, doi: 10.1016/j.actbio.2016.10.032.

[611] A. D'Amore *et al.*, "Heart valve scaffold fabrication: Bioinspired control of macro-scale morphology, mechanics and micro-structure," *Biomaterials*, vol. 150, pp. 25–37, Jan. 2018, doi: 10.1016/j.biomaterials.2017.10.011.

[612] J. Kucinska-Lipka, I. Gubanska, H. Janik, and M. Sienkiewicz, "Fabrication of polyurethane and polyurethane based composite fibres by the electrospinning technique for soft tissue engineering of cardiovascular system," *Materials Science and Engineering: C*, vol. 46, pp. 166–176, Jan. 2015, doi: 10.1016/j.msec.2014.10.027.

[613] W. D. Merryman, G. C. Engelmayr, J. Liao, and M. S. Sacks, "Defining biomechanical endpoints for tissue engineered heart valve leaflets from native leaflet properties," *Progress in Pediatric Cardiology*, vol. 21, no. 2, pp. 153–160, Mar. 2006, doi: 10.1016/j.ppedcard.2005.11.001.

[614] S. Pramanik, C. Saha, S. Chowdhury, C. Bose, N. P. Bhattacharyya, and L. K. Mondal, "Decreased Levels of miR-126 and miR-132 in Plasma and Vitreous Humor of Non-Proliferative Diabetic Retinopathy Among Subjects with Type-2 Diabetes Mellitus," *Diabetes, Metabolic Syndrome and Obesity: Targets and Therapy*, vol. Volume 15, pp. 345–358, Feb. 2022, doi: 10.2147/DMSO.S346097.

[615] V. L. Sales, "Transforming Growth Factor- 1 Modulates Extracellular Matrix Production, Proliferation, and Apoptosis of Endothelial Progenitor Cells in Tissue-Engineering Scaffolds," *Circulation*, vol. 114, no. 1_suppl, pp. I-193-I–199, Jul. 2006, doi: 10.1161/CIRCULATIONAHA.105.001628.

[616] A. M. T. Quinlan and K. L. Billiar, "Investigating the role of substrate stiffness in the persistence of valvular interstitial cell activation," *Journal of Biomedical Materials Research Part A*, p. n/a-n/a, 2012, doi: 10.1002/jbm.a.34162.

[617] K. Wyss, C. Y. Y. Yip, Z. Mirzaei, X. Jin, J.-H. Chen, and C. A. Simmons, "The elastic properties of valve interstitial cells undergoing pathological differentiation," *Journal of Biomechanics*, vol. 45, no. 5, pp. 882–887, Mar. 2012, doi: 10.1016/j.jbiomech.2011.11.030.